Investigations into the mechanisms behind the antagonistic effects and phage resistance of probiotic *Escherichia coli* strain Nissle 1917

Untersuchungen der Mechanismen des antagonistischen Effekts und der Phagenresistenz des probiotischen *Escherichia coli*-Stammes Nissle 1917

Doctoral thesis for a doctoral degree
at the Graduate School of Life Sciences,
Julius-Maximilians-Universität Würzburg

Section: Infection and Immunity

submitted by

Manonmani Soundararajan

from
Coimbatore, India

Würzburg, 2020

Submitted on: ……..……..

Office stamp

Members of the Thesis Committee

Chairperson: Prof. Dr. Thomas Dandekar

Primary Supervisor: Dr. Tobias Ölschläger

Supervisor (Second): Prof. Dr. Roy Gross

Supervisor (Third): Dr. Rudolf von Bünau

Supervisor (Fourth): Prof. Dr. Konrad Förstner

Date of Public Defence: ……..……

Date of Receipt of Certificates: …….

Affidavit

I hereby confirm that my thesis entitled “ Investigations into the mechanisms behind the antagonistic effects and phage resistance of probiotic *Escherichia coli* strain Nissle 1917” is the result of my own work. I did not receive any help or support from commercial consultants. All source and/or materials applied are listed and specified in the thesis.

Furthermore, I confirm that this thesis has not yet been submitted as part of another examination process neither in identical nor in similar form.

Würzburg,

Eidesstattliche Erklärung

Hiermit erkläre ich an Eides statt, die Dissertation " Untersuchungen der Mechanismen des antagonistischen Effekts und der Phagenresistenz des probiotischen *Escherichia coli*-Stammes Nissle 1917" eigenständig, d. h. insbesondere selbstständig und ohne Hilfe eines kommerziellen Promotionsberaters, angefertigt und keine anderen als die von mir angegebenen Quellen und Hilfsmittel verwendet zu haben.

Ich erkläre außerdem, dass die Dissertation weder in gleicher noch in ähnlicher Form bereits in einem anderen Prüfungsverfahren vorgelegen hat.

Würzbzrg,

This dissertation is dedicated to

my family and friends

Acknowledgement

I wish to thank the following people whose assistance was a milestone in the completion of this project. First and foremost, I would like to express my deepest gratitude to my primary supervisor (Doctor-father), Dr Tobias Ölschläger (*Institute for Molecular Infection Biology, University of Wuerzburg*) for providing me with an opportunity to pursue my PhD in a very interesting topic. I am very much grateful for all his support, encouragement, guidance and the interesting discussions we had which enriched my research experience. In addition, he made it possible for me to participate in several national and international conferences, where I was able to exchange ideas with other experts in the field and was also able to develop my presentation skills.

I would like to thank Prof. Dr Roy Gross (*Chair of Microbiology, Biocenter, University of Wuerzburg*) and Dr Rudolf von Bünau (*Pharma-Zentrale GmbH, Herdecke*) for their support as my second and third supervisor. Especially, for their professional guidance regarding the continuation of my project and for their valuable technical inputs. I would like to acknowledge Prof. Dr Konrad Förstner for inspiring my interest in the transcriptomics, Dr Richa Barti and all the members of *Core Unit Systemmedizin, Würzburg* for their technical support.

I am very much thankful to Pharma-Zentrale GmbH and Ardeypharm GmbH for their financial support. Special mention to Dr Rudolf von Bünau, Dr Birgit Klinikert and Ms Silke Dubbert for their valuable inputs during the review sessions which were of great importance in the progress of the work and for the friendly dinners. Also, I am very much thankful to Graduate School of Life Science (GSLS) for organizing the graduate program and providing the opportunity to participate in varied workshops in particular to Dr Gabriele Blum-Oehler, who has been a huge support throughout my master and PhD phase.

Special thanks to Prof. Dr Georg Krohne and Mrs Claudia Gehrig-Höhn (*Zentrale Abteilung für Mikroskopie - Imaging Core Facility,University of Wuerzburg)* for their guidance and support in electron microscopy. I would also like to thank Ms Hilde Merkert (*IT support - Lab management, Institute for Molecular Infection Biology*) for taking care of a variety of problems and for constant support.

My research partner, Dr Susanne Bury, was instrumental in the progress of my thesis, for which, I am extremely grateful. Also for being my moral support, best friend and to have made my life in Wuerzburg fun and comfortable. I also thank my loving and caring lab mates Srikkanth, Rebekka and all the former members of the Ölschläger lab for the many moments (dinners, home parties, movies, drinks, mensa time etc) which made my time as a doctoral student an extraordinarily beautiful experience.

My heartfelt thanks go to my husband, Dr Mohindar Murugesh Karunakaran for all his love, care and moral support without whom this thesis would have not been possible. I also thank my dear friends in Wuerzburg (Ravi, Abishek, Rahul, Ashwin, Aparna and Radhika) who were my home away from home and their support and encouragement was a great motivation to me. I express my thanks to my classmates of FOKUS Life Science (Jonathan, Xidi and David) for their love and affection over all these years in Germany. Love and support from my girls from home (MaChMuLiPiKeReMoSh) was a huge motivation to pursue my career. Lots of love to my dear friend Priya who not only contributed to proof-reading this thesis but also has been my pillar of support since I met her.

Last but not least, I would like to thank my family and in-law family for their love, affection and understanding especially my parents who always believed in me no matter what.

Table of contents

Summary 11
Zusammenfassung 13
1 Introduction 16
1.1. Gut microbiota 16
1.2. Probiotics 17
1.3. *E. coli* Nissle 1917 (EcN) 17
1.4. Molecular characterisation of EcN 18
1.5. Enterohaemorrhagic *E. coli* (EHEC) strains 20
1.5.1. Influence of EcN on EHEC strains 21
1.6. Phages in gut microbiota 22
1.7. Bacteriophage infection cycles 23
1.8. Bacteriophage receptors 24
1.9. Bacteriophage resistance mechanisms 26
1.10. Aim of the thesis 29
2 Materials 30
2.1 List of equipment 30
2.2 Chemicals 32
2.3 DNA and protein markers 34
2.4 Bacterial strains and phages 35
2.5 Oligonucleotides 36
2.6 Bacterial growth media and solutions 38
2.7 Commercially available assay kits 39
2.8 Column preparation for caesium-chloride (CsCl) density centrifugation 39
3 Methods 40
3.1 Microbiological methods 40
3.1.1 Overnight culture cultivation 40
3.1.2 Bacterial stock preparation and storage 40
3.1.3 *E. coli* strain identification 40
3.1.4 Bacterial growth 41
3.1.5 Phage propagation 41
3.1.6 Purification of phages 42
3.1.7 Coincubation conditions 43
3.1.8 Phage-Plaque-Assay (PPA) 43
3.1.9 Lambda lysogeny detection in *E. coli* samples incubated with lambda phages 44
3.1.10 Verotoxin ELISA 45
3.1.11 Processing of *E. coli* culture and supernatants 45

3.1.11.1 Heat killing (HK) or 1 % formaldehyde treatment (FA): 45
3.1.11.2 Proteinase K (PK) or sodium meta periodate (SMP) treatment 46
3.1.11.3 Supernatant preparation 46
3.1.11.4 Polymyxin B (PMB) treatment 47
3.1.12 LPS isolation 48
3.1.13 Testing the T4 phage adsorption to *E. coli* 49
3.2 Molecular biological methods 49
3.2.1 Polymerase Chain Reaction (PCR) 49
3.2.2 Localization of T4 phage DNA by T4 specific PCR 50
3.2.3 Agarose gel electrophoresis 51
3.2.4 Purification of PCR amplicons 52
3.2.5 Gel extraction 52
3.2.6 Sequencing 52
3.2.7 RNA isolation 53
3.2.8 Quantitative Real-Time PCR (qRT-PCR) 54
3.2.9 Two-step RT-PCR 55
3.2.10 qRT-PCR data analysis 56
3.2.11 SDS gel electrophoresis and LPS specific staining 57
3.3 Microscopic methods 58
3.3.1 Confocal microscopic examination of T4 phage and *E. coli* interaction 58
3.3.2 Transmission electron microscopic examination of EcN after incubation with T4 phages 58
3.4 Transcriptomics experimental setup 58
3.4.1 Single culture: fermenter and LB culture set up 59
3.4.2 Coculture: Transwell assay set up 59
3.5 Bioinformatic analysis 60
3.5.1 RNA library preparation for transcriptome analysis 60
3.5.2 Analysis of deep sequencing data 61
3.5.3 Functional prediction 61
3.6 Statistical analysis 62
4 Results 63
4.1. *E. coli* strain identification 63
4.1.1. Testing the purity of *E. coli* strains with ECC plates 63
4.1.2. Strain identification by PCR 64
4.1.3. EcN mutant verification using PCR 66
4.2. Transcriptomic response of EcN in different culturing conditions 69
4.2.1. Enhanced expression of fitness factors of EcN in fermenter culture condition 70

4.3. Transcriptomic response of EcN coincubated with pathogenic *E. coli* strain EHEC EDL933 and non-pathogenic *E. coli* K-12 strain MG1655 74
4.3.1. Shiga toxin reduction by EcN in a Transwell system 75
4.3.2. Time point-based RNA isolation from EcN coincubated with EDL933 and MG1655 77
4.3.3. Transcriptomic response of EcN towards EDL933 and MG1655 79
4.4. Lambdoid phage resistance of EcN 91
4.4.1. Testing the lambda lysogeny in EcN cells incubated with lambda phages 91
4.4.2. Role of a lambdoid prophage gene of EcN: the "phage repressor (*pr*)" gene and its role in EcN's lambda phage resistance 93
4.4.3. Determination of lambda phage titer reduction by EcN 98
4.4.4. Impact of EcN mutants on lambda phage inactivation 99
4.4.5. Investigation of lambda phage inactivating mechanism(s) of EcN 101
4.4.6. Impact of other *E. coli* strains on lambda phage inactivation 103
4.5. Lytic phage resistance of EcN 106
4.5.1. T4 phage plaque assay 107
4.5.2. Microscopic examination of *E. coli* and T4 phage coincubation 107
4.5.3. T4 phage DNA localization by PCR 109
4.5.4. Role of EcN's K5 capsule in its T4 phage resistance 110
4.5.5. T4 phage inactivation by EcN 111
4.5.6. Transcriptomic analysis of EcN in the presence of T4 phages 117
4.5.7. Biochemical studies to investigate the T4 phage inactivating factor in EcN 119
4.5.8. Impact of other *E. coli* strains on T4 phages 127
5. Discussion 130
5.1. Expression of probiotic factors in EcN fermenter culture 130
5.2. EcN shows a discriminative response towards pathogenic and non-pathogenic *E. coli* 132
5.3. Effect of EcN on lysogenic lambda phages 135
5.4. Investigation of EcN's lambda phage resistance/defence mechanism 140
5.5. Capsule mediated T4 phage defence in EcN 141
5.6. Effect of EcN on lytic T4 phages 142
5.7. EcN's LPS inactivated T4 phages 144
6. Conclusion 147
7. References 150
8. Annexure 164
Annexure 1: Details of deletion mutants of EcN used in this study 164
Annexure 2: Regulation of ferrous iron transport system (EfeUOB) in the EcN fermenter cultures 165

Annexure 3: Details of up and downregulated genes in EcN when coincubated with EDL933 for 3 h and their functional predictions* 165

Annexure 4: Functional details of up and down-regulated genes in EcN when incubated with T4 phages for 2 h* 165

Annexure 5: Alignment of the amino acid sequence of the lambda phage receptors (LamB) of EcN and MG1655 166

9. Abbreviations 167

10. List of Figures 170

11. List of tables 173

12. Curriculum Vitae 174

Summary

Gastrointestinal infections account for high morbidity and mortality in humans every year across the globe. The increasing emergence of antibiotic resistance among the gastrointestinal pathogens and the induction of virulence factors by antibiotics makes it highly risky to only depend on antibiotic therapy for intestinal infections. Most of these infections are associated with an imbalance in the gut microbial population whereas the restoration of the balance with probiotic supplements can result in an improvement of the health condition. Probiotics are therefore considered as successful support in the treatment of gastrointestinal infections.

E. coli Nissle 1917 (EcN) is the active component of the probiotic medication Mutaflor® and has been used in the treatment of various gastrointestinal disorders for more than 100 years. Several studies have reported antagonistic effects of EcN against enterohemorrhagic *E. coli* (EHEC) *in vitro* and *in vivo*. However, detailed investigations on the probiotic mechanisms and safety aspects of EcN are a pre-requisite, for administering EcN to treat EHEC infected patients or to use EcN as a prophylactic for the patient's close contacts.

In this regard, the first part of the study aimed to understand the nature and behaviour of EcN in the presence of pathogenic or non-pathogenic *E. coli* strains. Transcriptomic analysis was deployed to this end. We investigated the changes in EcN's transcriptome after different time points of coculture with the EHEC strain EDL933 or the K-12 strain MG1655. The transcriptome data reported a strain-specific response in EcN at all the investigated time points (3 h, 5 h, 7 h and 8 h) of coincubation. The alterations in gene regulation of EcN were highly pronounced in initial timepoints (3 h and 5 h) of coincubation with EDL933, which gradually decreased over time. In the presence of MG1655, the alterations were strongly differentially regulated only at later time points (7 h and 8 h). The unique transcriptional response of EcN towards two different *E. coli* strains, that are genetically more than 98 % identical, was startling.

More importantly, this can be considered as a beneficial trait of EcN over a chemical-pharmaceutical preparation like an antibiotic that might act identically on all target cells.

Bacteriophages are one of the most abundant members of gut microbiota. On the one hand, the infection of a probiotic strain by a lysogenic phage could transfer genetic material coding for pathogenic factors or antibiotic resistance into an otherwise beneficial probiotic bacterium and thereby converting it into a virulent pathogenic bacterium. On the other hand, infection by a lytic phage could result in bacterial lysis and prevent the bacterium from exerting its probiotic effect. Thus, in order to successfully establish and colonise the gut, it is crucial for any probiotic to be resistant against phage infections. To address this, in the second part of the study, we investigated the phage resistance of EcN towards the lysogenic lambda and the lytic T4 phage.

EcN showed complete resistance against tested phages and was also able to inactivate these phages upon coincubation. In the case of lambda phages, the resistance was attributed to the presence of a lambdoid prophage (prophage 3) in the genome of EcN. In addition, the overexpression of one of the early genes of EcN's prophage 3 (i.e. phage repressor gene *pr*) in the phage sensitive MG1655 conferred partial protection against lambda phage infection. Moreover, the inactivation was mediated by binding of lambda phages to its receptor LamB. Experiments with lytic T4 phages revealed that the EcN's K5 polysaccharide capsule was crucial for its T4 phage resistance, while its lipopolysaccharide (LPS) inactivated the T4 phages. Apart from protecting itself, EcN displayed even a protective role for the tested K-12 strains, by interfering with the lysogeny and lysis by these phages.

In summary, this work highlights two novel positive traits of the probiotic strain EcN: i) the strain-specific response that was evident from the global transcriptome analysis of EcN when incubated with other *E. coli* strains, and ii) lytic and lysogenic phage resistance. Both these traits are additional safety aspects for a well-characterised probiotic strain and encourage its application in therapeutics.

Zusammenfassung

Gastrointestinale Infektionen sind jedes Jahr weltweit für eine hohe Morbidität und Mortalität beim Menschen verantwortlich. Das zunehmende Auftreten von Antibiotikaresistenzen bei gastrointestinalen Pathogenen und die Induktion von Virulenzfaktoren durch Antibiotika machen es hoch riskant Darminfektionen ausschließlich mit Antibiotika zu behandeln. Die meisten gastrointestinalen Infektionen sind mit einem Ungleichgewicht in der mikrobiellen Darmpopulation verbunden, während die Wiederherstellung des Gleichgewichts mit Probiotika zu einer Verbesserung des Gesundheitszustands führen kann. Daher gelten Probiotika als hilfreiche Unterstützung bei der Behandlung von Magen-Darm-Infektionen.

E. coli Nissle 1917 (EcN) ist der aktive Bestandteil des probiotischen Medikaments Mutaflor® und wird seit mehr als 100 Jahren zur Behandlung verschiedener gastrointestinaler Erkrankungen eingesetzt. Mehrere Studien haben über die antagonistische Wirkung von EcN gegenüber enterohämorrhagischer *E. coli* (EHEC) sowohl *in vitro* als auch *in vivo* berichtet. Detaillierte Untersuchungen zu den probiotischen Mechanismen und Sicherheitsaspekten von EcN sind jedoch Voraussetzung für eine mögliche Verabreichung von EcN zur Behandlung von EHEC-infizierten Patienten oder für die Verwendung von EcN als Prophylaxe für den engsten Umkreis der infizierten Patienten.

In dieser Hinsicht zielte der erste Teil dieser Studie darauf ab, die Natur und das Verhalten von EcN in Gegenwart von pathogenen oder nicht-pathogenen Bakterienstämmen zu verstehen. Zu diesem Zweck wurden die Veränderungen im Transkriptom von EcN nach verschiedenen Zeitpunkten der Co-Kultur mit dem EHEC-Stamm EDL933 oder dem K-12 Stamm MG1655 untersucht. Die Transkriptomdaten zeigten eine stammspezifische Reaktion von EcN zu allen untersuchten Zeitpunkten (3 h, 5 h, 7 h und 8 h) der Co-Inkubation. Die Veränderungen in der Genregulation von EcN waren zu den primären Zeitpunkten der Co-Kultur mit EDL933 (3 h und 5 h) sehr ausgeprägt und nahmen im Laufe der Zeit allmählich ab. Während der Co-Kultur

mit MG1655 hingegen, kam es erst zu späteren Zeitpunkten zu einer starken Veränderung in der Genregulation (7 h und 8 h). Diese einzigartige transkriptionelle Reaktion von EcN auf zwei verschiedene *E. coli* Stämme, die genetisch zu mehr als 98 % identisch sind, war verblüffend. Diese Eigenschaft von EcN kann als vorteilhaft gegenüber einem chemisch-pharmazeutischen Präparat wie einem Antibiotikum angesehen werden, welches auf alle Zielzellen identisch wirken könnte.

Bakteriophagen sind einer der häufigsten Bestandteile der Darm Mikrobiota. Durch die Infektion eines probiotischen Stammes mit einem lysogenen Phagen ist es möglich, dass genetisches Material, das für pathogene Faktoren oder Antibiotikaresistenzen kodiert, übertragen wird und das Probiotikum dadurch zu einem virulent pathogenen Bakterium umgewandelt wird. Darüber hinaus könnte die Infektion durch einen lytischen Phagen zur Lyse des Probiotikums führen wodurch seine probiotische Wirkung unterbunden werden würde. Für eine erfolgreiche Besiedlung des Darms ist es daher für Probiotika entscheidend gegenüber Phagen Infektionen resistent zu sein. Um dieses Problem anzugehen, wurde im zweiten Teil der Studie die Phagen Resistenz von EcN gegenüber dem lysogenen Phagen Lambda und dem lytischen Phagen T4 untersucht.

EcN zeigte eine vollständige Resistenz gegenüber den getesteten Phagen und konnte darüber hinaus die Phagen während der Co-Inkubation inaktivieren. Bei den Lambda-Phagen konnte die Resistenz auf das Vorhandensein eines Lambda-Prophagen (Prophage 3) im Genom von EcN zurückgeführt werden. Dies wurde durch das Ergebnis, dass die Überexpression eines der frühen Gene von EcNs Prophagen 3 (dem Phagen-Repressor *pr*) im Phagen sensitiven K-12 Stamm MG1655 zu einem partiellen Schutz gegenüber einer Lambda-Phagen Infektion führte, gestützt. Die Inaktivierung der Lambda-Phagen hingegen wurde durch die Bindung der Phagen an EcNs Rezeptor LamB vermittelt. Experimente mit lytischen T4-Phagen konnten aufzeigen, dass die K5-Polysaccharid Kapsel von EcN entscheidend für seine T4-Phagenresistenz ist,

EcNs Lipopolysaccharid (LPS) wiederum die T4-Phagen inaktiviert. Abgesehen davon, dass EcN sich selbst vor Phagen Infektionen schützt, konnte gezeigt werden, dass EcN eine Phagen initiierte Lysogenie oder Lyse der getesteten K-12-Stämme verhindert.

Zusammenfassend hebt diese Arbeit zwei neue positive Eigenschaften des probiotischen Stammes EcN hervor: i) die stammspezifische Reaktion, die sich aus der globalen Transkriptomanalyse von EcN während der Inkubation mit anderen *E. coli*-Stämmen ergab, und ii) die lytische und lysogene Phagenresistenz. Beide Merkmale sind zusätzliche Sicherheitsaspekte eines bereits gut charakterisierten probiotischen Stammes und unterstützen seine therapeutische Anwendung.

1 Introduction

1.1. Gut microbiota

Intestinal microbiota plays an important role in human health. The number of microorganisms inhabiting the gastrointestinal (GI) tract has been estimated to be $\sim 10^{13}$ to 10^{14} microbial cells, with around 1:1 bacterium to human cell ratio (Sender et al., 2016;Kho and Lal, 2018). However, this estimate doesn't take the fungi and viruses present in the gut into consideration. The dominant members of the "bacterial core microbiome" are Firmicutes, Bacteroidetes, Actinobacteria, Verrucomicrobia, Fusobacteria, and Proteobacteria, with the two phyla Firmicutes and Bacteroidetes representing 90% of the gut microbiota (Arumugam et al., 2011;Hollister et al., 2014). An infant's gut microbiota is established immediately after birth and is affected by several factors such as delivery mode, breast milk vs. formula feeding, antibiotic usage, and timing of the introduction of solid foods and cessation of milk feeding (Francino, 2014;Tanaka and Nakayama, 2017). These alterations continue until three years of age and, subsequently, humans acquire stable gut microbiota (Yatsunenko et al., 2012)

Imbalances in the gut microbial population termed as dysbiosis are often associated with disease conditions (Belizario and Faintuch, 2018). For instance, some studies suggest that the ratio of Firmicutes:Bacteroidetes can be used to determine the susceptibility to obesity and other metabolic syndromes (Ley et al., 2006;Xu et al., 2012). In addition, the phylum Proteobacteria generally constitutes for only a small proportion of the gut microbiota in healthy individuals, but often account for higher proportions in patients with GI diseases (Chen et al., 2011;Pflughoeft and Versalovic, 2012). Usage of antibiotics, psychological and physical stress, and certain dietary components have been found to contribute to intestinal dysbiosis (Hawrelak and Myers, 2004). Overall, the gut microbiome research has established a complex bi-directional link between the intestinal microbiome and the host which is significant for human health as well as implicated in disease pathogenesis.

1.2. **Probiotics**

The World Health Organization defines probiotics as “live microorganisms which when administered in adequate amounts confer a health benefit on the host” (WHO, 2001). Owing to the side-effects of antibiotic therapy such as antibiotic resistance and destruction of beneficial bacteria in the gut, probiotics are considered as a safe alternative for treating gastrointestinal infections (Trafalska and Grzybowska, 2004). Usage of probiotics to treat infections dates back to the early 19th century when the Russian scientist Elie Metchnikoff theorized that consumption of “soured milk” with lactic-acid bacteria suppressed the growth of proteolytic bacteria (Vaughan, 1965;Podolsky, 2012;Mackowiak, 2013). Alongside, Henry Tissier of the Pasteur Institute noticed that the *Bifidobacterium* conferred clinical benefits when used to treat diarrhoea in babies (Tissier, 1906). Health benefits have mainly been demonstrated for specific probiotic strains of the following genera: *Lactobacillus*, *Bifidobacterium*, *Saccharomyces*, *Streptococcus*, *Enterococcus*, *Escherichia*, and *Bacillus* (Fijan, 2014). The nature of colonization of the human gut by probiotics is strain-specific and depends on the individual’s microbiota and gastrointestinal tract region (Zmora et al., 2018). As mentioned earlier, gastrointestinal disorders often are linked with an imbalance in the gut microbial population and manipulation of the microbiome was one of the successful therapeutic strategies to treat dysbiosis. In this line, studies have reported that administration of probiotic bacteria supersede potentially pathogenic bacteria and boost the rebuilding of the gut microbiota (Gareau et al., 2010;Oelschlaeger, 2010;Raman et al., 2013;Lievin-Le Moal and Servin, 2014).

1.3. ***E. coli* Nissle 1917 (EcN)**

E. coli belongs to the phylum Proteobacteria and is a very common inhabitant of the lower intestine (Fijan, 2014). The probiotic effect of *E. coli* was first demonstrated in 1917, during a shigellosis outbreak. German professor Alfred Nissle isolated a strain of *E. coli* from a soldier who was not affected by the disease (Nissle, 1918). This strain of serotype O6:K5:H1 was later

named after him as "*E. coli* Nissle 1917 (EcN)" and was registered as a licensed probiotic medication known as Mutaflor®. Since its serendipitous discovery, EcN has been employed in the treatment of various gastrointestinal disorders like inflammatory bowel disease, ulcerative colitis, colon cancer (Kruis et al., 2004;Henker et al., 2008;Kruis et al., 2012;Xia et al., 2013) and undoubtedly is one of the most extensively investigated probiotic strains (Wassenaar, 2016). Additionally, the reported antagonistic nature of EcN against the gastrointestinal pathogens such as *Listeria monocytogenes*, *Candida albicans*, *Shigella* and *Salmonella* promote its application in prophylaxis and therapy (Halbert, 1948;Altenhoefer et al., 2004;Sonnenborn and Schulze, 2009).

1.4. **Molecular characterisation of EcN**

EcN belongs to the serotype O6:K5:H1 which is typical for *E. coli* strains associated with urinary tract infections. However, EcN is completely non-pathogenic and lacks the prominent virulent genes when compared to its close relative UPEC strain CFT073 (Sonnenborn and Schulze, 2009). On the other hand, EcN exhibits several fitness factors that contribute to its colonization efficiency and survival within the host (Grozdanov et al., 2004). Genome analysis of EcN showed that EcN possesses three fimbrial determinants: curli, type 1 and F1C fimbriae which are required for biofilm formation, adherence to epithelial cells, intestinal colonization, and persistence in the gut of infant mice (Stentebjerg-Olesen et al., 1999;Lasaro et al., 2009;Schierack et al., 2011;Kleta et al., 2014;Staudova et al., 2015). The O6 antigen determinant of EcN's LPS has a point mutation introducing a stop codon in the gene for the O6 antigen polymerase. This mutation makes the O6 polysaccharide side chain very short, consisting of only one single "repeating unit" of the O6 antigen. This special characteristic of EcN's LPS is responsible for its semi-rough phenotype and also contributes to its serum sensitivity (Grozdanov et al., 2002). This modification in LPS also plays a role in immunomodulating properties exhibited by EcN (Guttsches et al., 2012). Another interesting

feature of EcN is the presence of an extracellular polysaccharide capsule of the K5 serotype. The K5-kind of capsule is present only in 1 % of *E. coli* isolates and in EcN, it is involved in modulating the immune interactions with intestinal epithelial cells (Hafez et al., 2010;Nzakizwanayo et al., 2015). The H1-type flagella of EcN are responsible for mucin binding and inducing human beta-defensins (Schlee et al., 2007;Troge et al., 2012). The most striking factor of EcN is that it harbours several iron-uptake and transport systems which have reported to assist in efficient colonization and out-competing other pathogenic bacteria in the gut (Grosse et al., 2006;Valdebenito et al., 2006;Deriu et al., 2013). The antagonistic nature of EcN can be attributed to the microcins H47 and M which are low-molecular-weight antimicrobial peptides. They display potent bactericidal activity against phylogenetically related bacteria that lack complementary immunity proteins (Patzer et al., 2003;Baquero et al., 2019). In addition to the above-mentioned fitness factors, EcN also possesses two small cryptic plasmids, termed pMUT1 and pMUT2 which are genetically stable and are not self-transmissible to other *E. coli* strains. The circular DNAs of these two strain-specific plasmids have been completely sequenced and do not carry any antibiotic resistance cassette (Blum-Oehler et al., 2003). **Figure 1. 1** collectively illustrates the various surface structures and strain-specific fitness characteristics of EcN discussed above.

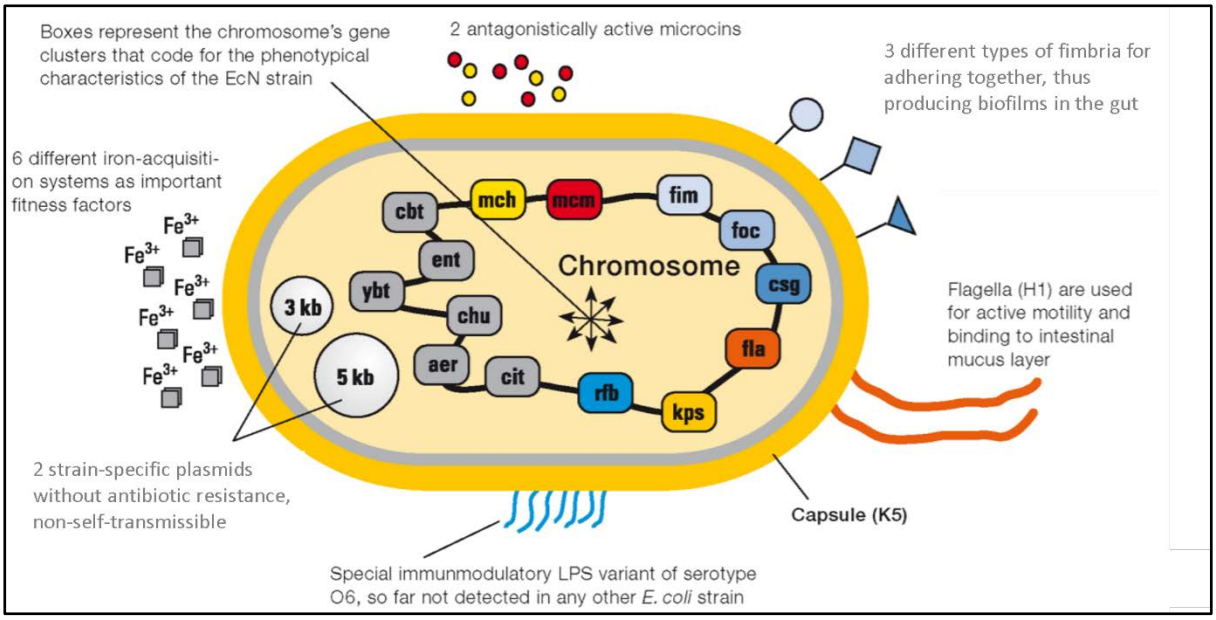

Figure 1. 1: Schematic representation of various factors in EcN that contribute to the fitness of the strain. Image modified from [https://www.mutaflor.com/e-coli-strain-nissle-1917-strain-specific-properties-and-mechanisms-of-action/molecular-mechanisms-of-action.html (Pharma-Zentrale GmbH)](https://www.mutaflor.com/e-coli-strain-nissle-1917-strain-specific-properties-and-mechanisms-of-action/molecular-mechanisms-of-action.html)

1.5. Enterohaemorrhagic *E. coli* (EHEC) strains

Enterohaemorrhagic *Escherichia coli* (EHEC) are pathogenic *E. coli* that cause bloody diarrhoea in humans, which might develop into haemolytic uremic syndrome (HUS). HUS is a life-threatening disease that causes kidney damage due to the production of shiga toxin (Stx) which is the main virulence factor of EHEC strains (Karpman et al., 2017). The genomic information for Stx1 and Stx2 are encoded on lambdoid prophages in the chromosome of EHEC strains known as *stx*-phages (O'Brien et al., 1984;Kruger and Lucchesi, 2015). The production of *stx*-phages is induced during an SOS response, which results in an increased Stx and *stx*-phage release that worsen the disease progression (Del Cogliano et al., 2018;Zhang et al., 2019). The Stx uses the globotriaosylceramide (Gb3) receptor of eukaryotic cells for cell entry (Melton-Celsa, 2014). So far, the intestinal tract of ruminants is the only known reservoir of EHEC and the absence of Gb3 receptor in ruminants makes them insensitive to Stx of these bacteria (Mainil, 1999;Pruimboom-Brees et al., 2000). EHEC infection of humans was due to the consumption of contaminated bovine products like undercooked meat, milk or dairy

products and fresh produce such as lettuce, bean sprouts and spinach (Armstrong et al., 1996;Hilborn et al., 1999;WHO, 2011;Gobin et al., 2018). EHEC outbreaks have also been waterborne, owing to faecal contaminated drinking-water (Olsen et al., 2002).

The 2011 EHEC outbreak in Germany was the biggest ever seen in Europe, and the second biggest ever reported worldwide, due to its size and severity. While previous outbreaks have often been attributed to EHEC strains of serotype O157:H7, in 2011, Germany was hit by the serotype O104:H4. The genome analysis of two isolates of O104:H4 strains from the 2011 outbreak revealed that the increased virulence and fitness of this serotype was due to a unique combination of genomic features from EHEC and entero-aggregative *E. coli* (EAEC) strains (Bohnlein et al., 2016). In particular, this serotype possesses an *stx*-phage typical for EHEC strains and an aggregative adhesion fimbria (AAF) operon, which is a distinguishing feature for EAEC strains (Brzuszkiewicz et al., 2011). In the outbreak from May to September 2011, approximately 3,816 EHEC cases were reported and 22 % (845) of the total number of patients developed HUS and unfortunately, the total death toll was 54 (Frank et al., 2011). In general, the differences observed with respect to the severity of the disease progression among the patients infected by EHEC strains could be attributed to the *stx*-phage infection of the commensal *E. coli* strains in their microbiota that produces more virulent and resistant pathogens.

1.5.1. **Influence of EcN on EHEC strains**

Treating the EHEC infected patients with antibiotics induces the release of *stx*-phages and results in an eventual increase in Stx release which emphasizes the need for alternative strategies (Zhang et al., 2000;Pacheco and Sperandio, 2012). The antagonistic effect of EcN against the EHEC strain EDL933 was first reported by (Reissbrodt et al., 2009) and since then several studies have reported the inhibition of growth, Stx production and biofilm formation of EHEC strains when cocultured with the probiotic EcN (Rund et al., 2013;Mohsin et al.,

2015;Bury, 2018;Fang et al., 2018). In particular, a former colleague of the lab, Dr Susanne Bury, investigated the influence of EcN on the “big five” EHEC strains and two isolates from the 2011 outbreak and her study revealed that the presence of EcN resulted in a reduction of the Stx level of about 90 % (Bury, 2018). In vivo studies, demonstrated that EcN exhibited a strong inhibitory effect on growth, *stx* gene expression (Sahar H. Ali, 2017) and served as a natural barrier for the intestine colonization of *E. coli* O157:H7 (Leatham et al., 2009). These results collectively support the application of EcN as a supplementary or an alternative therapeutic approach for EHEC infections.

1.6. Phages in gut microbiota

Bacteriophages (phages) are viruses that infect bacteria and are the most abundant replicating entities on the planet which flourish wherever their bacterial hosts exist. The presence of phages in the intestine was described by D’Herelle in 1917 and he observed their therapeutic potential in the stools of patients with dysentery (D'Herelle, 2007). Before the advent of the antibiotic era, phages have been employed to treat a variety of intestinal infections, mainly cholera and dysentery (D'Herelle, 1929;Babalova et al., 1968). However, the fluctuation in the success rate of these treatments paved the way for the antibiotic based therapy which was more efficient and cost-effective. With the rise of bacterial resistance to antibiotics, phage therapy has recently regained interest (Aminov, 2010;Kutter et al., 2010). Especially, the presence and role of phages in the intestinal microbiota are extensively studied in the recent decade. With the help of novel technologies that involve metagenomics approaches, there is a better assessment of the microbial diversity in the human intestine (Eckburg et al., 2005;Gill et al., 2006). Recent studies have estimated the ratio of phages to bacteria in a healthy human gut as 1:1 and these phages belong to the families: *Myoviridae*, *Podoviridae*, *Siphoviridae* and *Microviridae* (**Figure 1. 2**) (Carding et al., 2017;Mirzaei and Maurice, 2017;Shkoporov and Hill, 2019). Emerging views suggest intestinal phages as one of the major forces responsible for shaping the diversity and

composition of the gut bacterial community (Manrique et al., 2016;d'Humieres et al., 2019;Maurice, 2019).

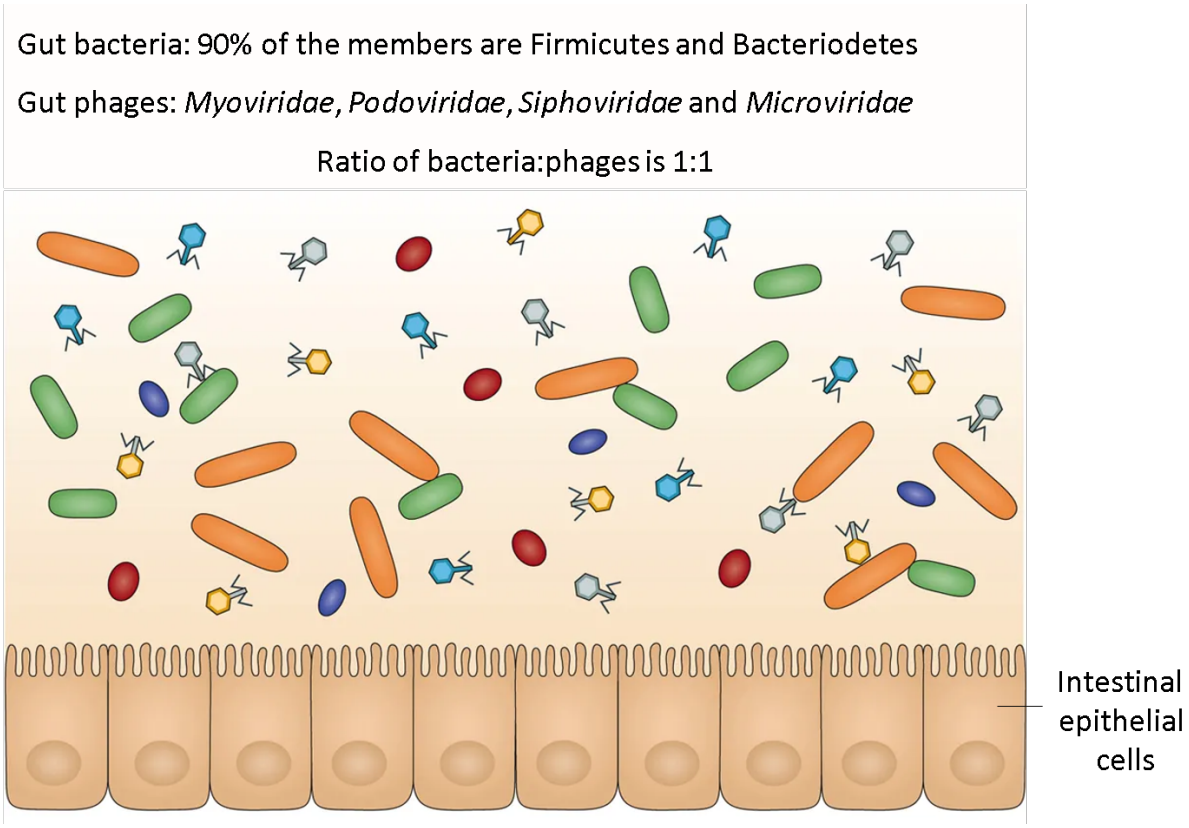

Figure 1. 2: Illustration of bacteria and bacteriophage communities in the healthy adult gut. Image modified from (Mirzaei and Maurice, 2017)

1.7. Bacteriophage infection cycles

In the intestine, just like in other environments, phages can be distinguished based on their life cycle into virulent and temperate phages. Virulent phages, upon infection, induce a "lytic cycle", which is followed by phage production and host cell lysis (Kaiser, 2014). Temperate phages, on the other hand, adopt the "lysogeny cycle" in which after the infection, the phage DNA integrates into the bacterial chromosome as a prophage (Howard-Varona et al., 2017). The prophage remains dormant and is replicated passively along with the bacterial genome until specific cues such as bacterial DNA damage by UV light or antibiotics, temperature shifts or oxidative stress, which induce the SOS response of the host leading to phage lytic cycle and subsequent death of the lysogenised bacteria (Monk and Kinross, 1975;Elespuru, 1984;Los et

al., 2010). In this context, when considering intestinal phages, one should take into account both free-lytic phages and lysogenised prophages. **Figure 1. 3** graphically illustrates the overview of bacterial lysis and lysogenization by bacteriophages.

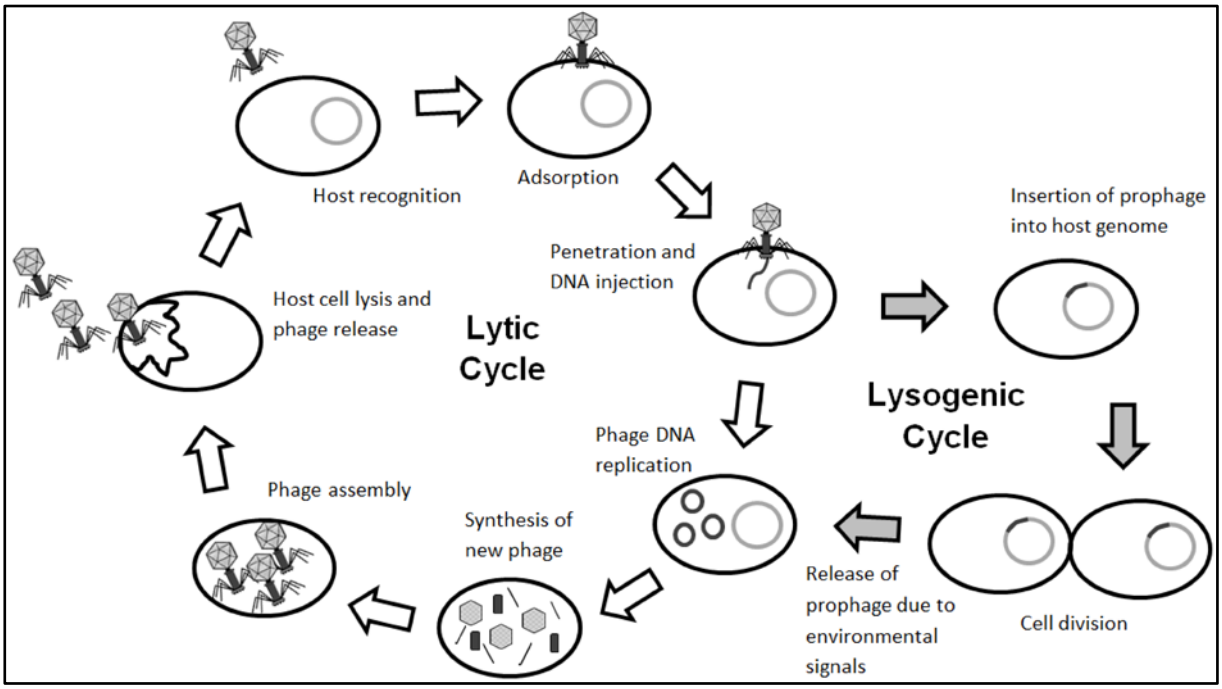

Figure 1. 3: Lytic and lysogenic cycle of bacteriophages. Stepwise illustration of lysis and lysogenisation of bacteria by virulent and temperate phages. Image modified from (Doss et al., 2017)

1.8. Bacteriophage receptors

Bacteriophages attach to the receptors on their host surface in order to inject their DNA into the host and this process of attachment is termed as adsorption (Letarov and Kulikov, 2017). A lot of cell surface structures of *E. coli* have been reported to function as phage receptors (Bertozzi Silva et al., 2016;Hantke, 2020). As, we have used the lysogenic lambda phages and lytic T4 phages in this study, the receptors and adsorption mechanism of these phages are discussed here briefly.

Lambda phages belong to the family of *Siphoviridae* and have a long non-contractile tail, and the tip of their tails is evolved to interact with specific porins in the membrane of the host to allow entry of its DNA (2012;Casjens and Hendrix, 2015). In *E. coli*, these phages use the "J

protein" in their tail tip to bind irreversibly to their specific receptor (Chatterjee and Rothenberg, 2012). The J protein interacts with the maltose porin LamB (the product of the *lamB* gene) in the outer membrane of *E. coli*, following which, the DNA passes through the mannose PTS permease sugar transporting system in the inner membrane, encoded by the *manXYZ* genes (**Figure 1. 4**) (Randall-Hazelbauer and Schwartz, 1973;Erni et al., 1987). Consecutively, the DNA is processed in the host cytoplasm to undergo the lytic or lysogenic cycle.

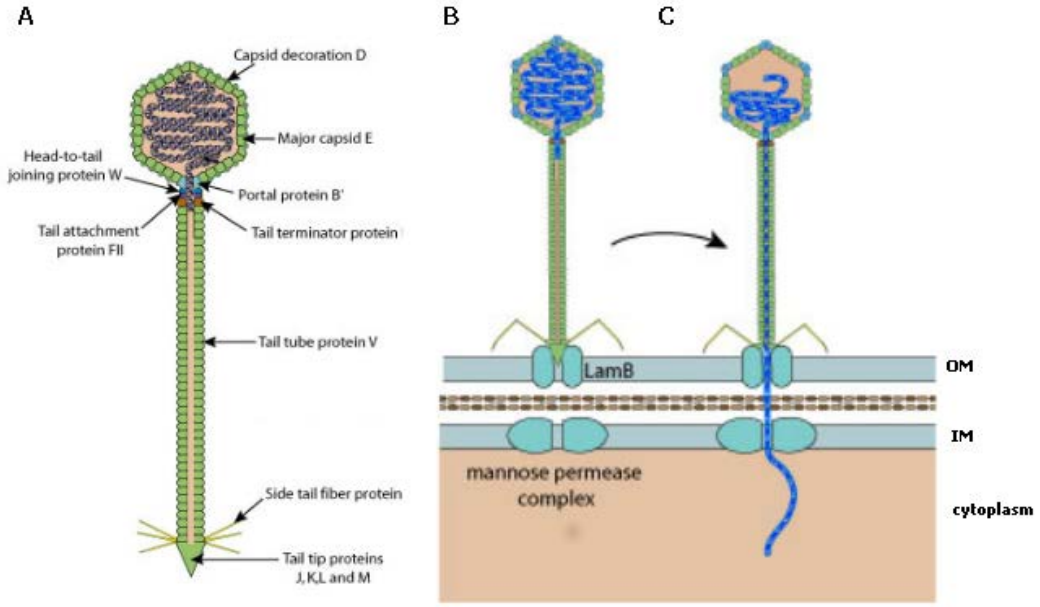

Figure 1. 4: Schematic representation of bacteriophage lambda attachment to *E. coli*. (**A**) Bacteriophage lambda; (**B**) Attachment of lambda phage tail protein (J) to LamB in *E. coli* outer membrane (OM); (**C**) Lambda phage DNA injection through the mannose permease complex in the *E. coli* inner membrane (IN) into the cytoplasm. Image modified from: (Viralzone, 2013)

T4 phage adsorption to *E. coli* is a two-step process, initially, a reversible attachment of its long tail fibres to the *E. coli* LPS followed by an irreversible anchoring of short tail fibres of the T4 base plate to the receptors on the host cell surface e.g. LPS or outer membrane proteins (Garen and Puck, 1951;Riede, 1987;Bertozzi Silva et al., 2016). The successful attachment of both the tail fibres to the host leads to a conformational change of the base plate which triggers the contraction of the outer tail sheath (Furukawa et al., 1983) that subsequently propels the inner tube

through the outer membrane, creating a channel for DNA ejection into the host cell (Leiman and Shneider, 2012;Hu et al., 2015) (**Figure 1. 5**). In this regard, the receptor specificity of the T4 long tail fibres is crucial for the successful host selection and infection. From various studies, it could be concluded that the long tail fibres of T4 specifically recognize the LPS with glucose residues at the distal end of the core oligosaccharide (e.g. *E. coli* B strain) (Wilson et al., 1970;Hantke, 2020). However, in *E. coli* K-12 strains since the glucose residue at the distal end is masked by heptose, the presence of an outer membrane protein C (Omp C) is additionally required for successful T4 phage adsorption (Mutoh et al., 1978;Washizaki et al., 2016).

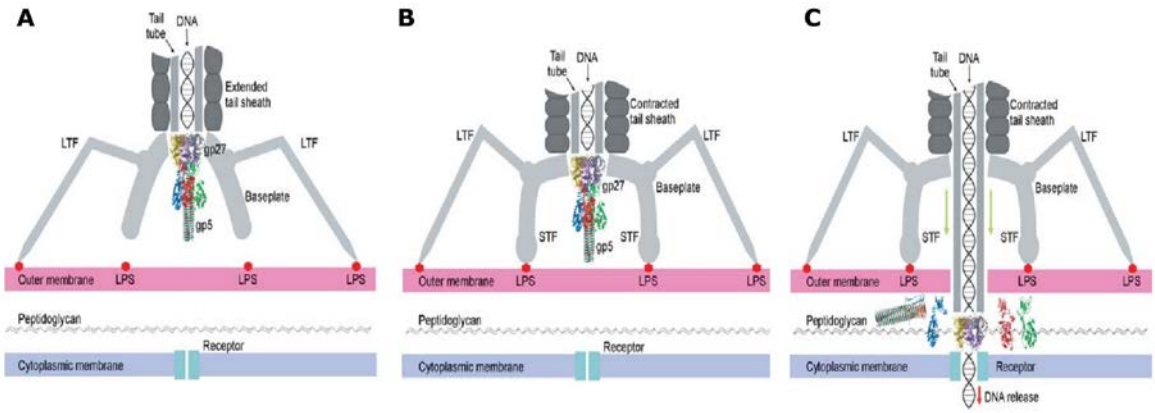

Figure 1. 5: Model depicting the interactions between T4 phage tail and *E. coli* cell surface receptors. (**A**) Attachment of T4 phage's long tail fibres (LTF) to LPS molecules and/or outer membrane proteins (OMP) of *E. coli*. (**B**) The short tail fibres (STF) are attached to the LPS molecules and/or OMP in the outer membrane. The T4 tail sheath has contracted, pushing the tail tube with its gp5 tail protein through the outer membrane. (**C**) The lysozyme domain of gp5 digests the peptidoglycan cell wall. The inner tail tube penetrates and allows the T4 DNA to enter the cytoplasm. Image modified from (Rossmann et al., 2007)

1.9. Bacteriophage resistance mechanisms

Phage - bacteria interactions in the gastrointestinal tract appear to be highly diverse and lead to interminable evolution of phages and bacteria (Weitz et al., 2005;Samson et al., 2013;Scanlan, 2017). Corresponding bacterial evolutions lead to the development of several bacterial defence mechanisms that help bacteria to survive in the gut by battling constant phage attacks (Labrie et al., 2010;Azam and Tanji, 2019). Bacterial strains adopt several strategies to modify their

surface structures which prevent the initial adsorption of phages and thereby escaping the infection. Firstly, they either alter their prospective phage receptors or inhibit their production, thus making them not recognized by phages (Picken and Beacham, 1977;Sijtsma et al., 1990;Mizoguchi et al., 2003;Chatterjee and Rothenberg, 2012). Secondly, bacteria acquire various barriers to inhibit phage adsorption by production of extracellular matrix (e.g. capsule, biofilm) (Kauffmann, 1945;Sapelli and Goebel, 1964;Scholl et al., 2005;Abedon, 2017;Vidakovic et al., 2018), or by production of competitive inhibitors that block the phage receptors (e.g.OMVs, protein A) (Manning and Kuehn, 2011;Reyes-Robles et al., 2018) (Nordstrom and Forsgren, 1974). The next popular approach adopted by bacteria to prevent the infection is by blocking the entry of phage DNA (e.g. superinfection exclusion system) (Lu and Henning, 1989;Hofer et al., 1995;Ali et al., 2014) or by degrading the injected phage DNA (e.g. restriction-modification (RM) systems - (Ershova et al., 2015), CRISPR-Cas - (Deveau et al., 2010;Szczepankowska, 2012). Finally, bacteria have also developed strategies to target and inhibit a crucial step of phage multiplication such as replication, transcription or translation, e.g. abortive infection system - (Emond et al., 1998;Dy et al., 2014). In abortive infection, the bacterium adopting this mechanism would undergo programmed cell death but the death of the infected cell protects the surrounding bacteria from phage infection. Certain bacteria evolve to possess phage-inducible chromosomal islands (PICIs) integrated into their genome, which interferes with the process of phage assembly (Penades and Christie, 2015;Fillol-Salom et al., 2018). **Figure 1. 6** graphically summarises the various phage resistance mechanisms developed by bacteria to inhibit phage infection.

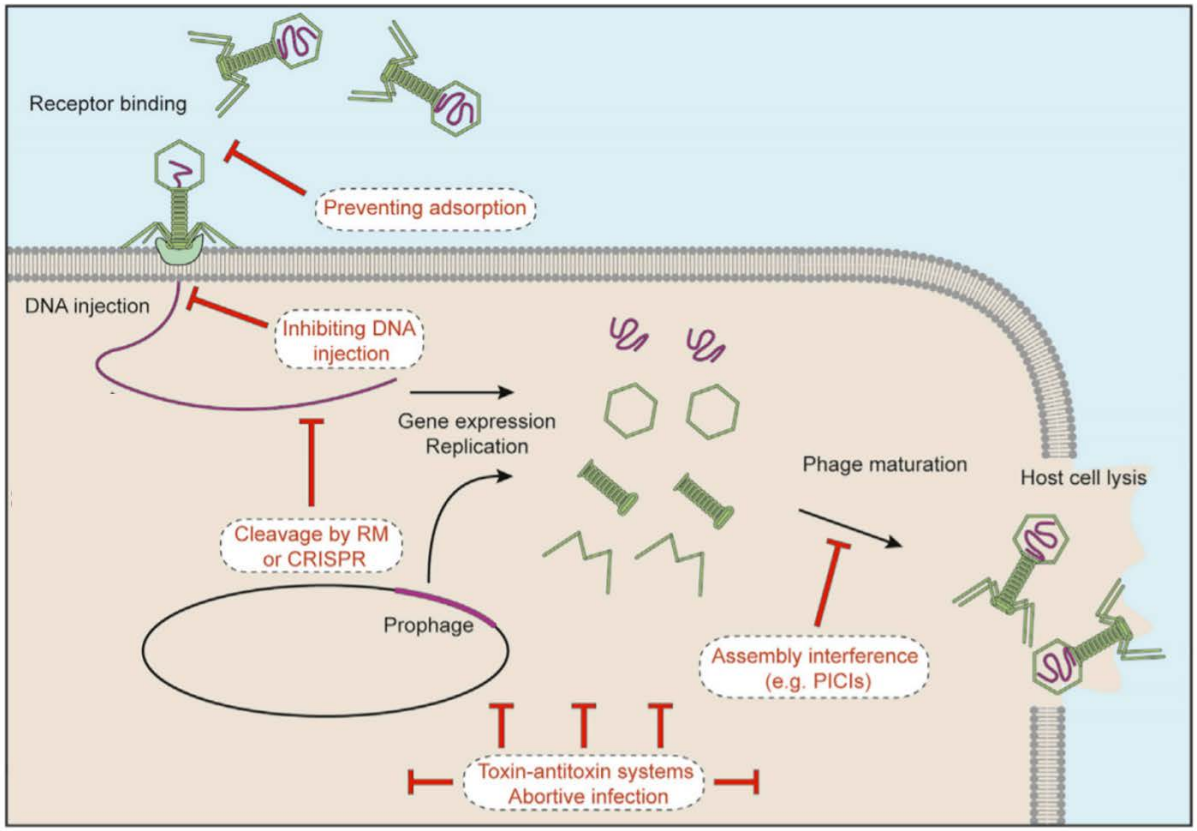

Figure 1. 6: Illustration of various stages of bacteriophage life cycle that are targeted by different phage resistance mechanisms. The stages of the phage life cycle are written in black and the corresponding resistance mechanisms targeting each step are written in red within a text box. Image modified from: (Rostol and Marraffini, 2019)

Apart from the above-mentioned widely investigated bacterial resistance mechanisms, there are also several novel mechanisms that have been identified and reported by research groups in the recent past e.g. BREX – blocks phage DNA replication in the host by methylation-dependent manner (Goldfarb et al., 2015), DISARM– defence islands that function similar to that of RM systems (Ofir et al., 2018), pAgos – targets invading nucleic acid (Sashital, 2017;Willkomm et al., 2018). Recently, microbial pangenome analysis (Doron et al., 2018) identified several previously unknown defence systems namely the Zorya system, Thoeris system, Druantia system, etc. Bacteriophage resistance mechanisms are driven by the endless antagonistic arms race between phages and bacteria, thus contributing to a fascinating field of research that must be explored indefinitely.

1.10. **Aim of the thesis**

For over a century, the probiotic *E. coli* strain Nissle has been successfully used in the treatment of various gastrointestinal diseases (Sonnenborn, 2016). EcN was shown to exhibit antagonistic activity against different pathogenic enterobacteria, both *in vivo* and *in vitro* (Sonnenborn and Schulze, 2009). Especially, it was identified to interfere with the Stx production of EHEC strains and pre-colonization of mice with EcN hindered the EHEC strain EDL933 from colonising the gut (Leatham et al., 2009;Reissbrodt et al., 2009;Rund et al., 2013). Therefore, the first part of the study aimed to have a closer observation of changes in EcN that were responsible for the observed effects on EHEC strain EDL933. Understanding and characterizing EcN's mechanism(s) behind the inhibition of Stx production is imperative for its application in the treatment of EHEC infections.

However, the antagonistic or beneficial nature of the ingested probiotic strain may not exert any long-lasting effect due to the selection/killing by intestinal phages (Ventura et al., 2011). Hence, the major part of the study was aimed to determine probable phage resistance of EcN towards two major classes of bacteriophages: lysogenic lambda phage and lytic T4 phage, and if there is such resistance, then to investigate it on the molecular level. The results of these studies were expected to add further knowledge and deeper insights into EcN's safety aspects and genome stability.

2 Materials

2.1 List of equipment

Table 2. 1: List of laboratory equipment used in this study

Equipment/ Material	Specifications	Company
- 80 °C freezer	HFU 686 Basic	Thermo Fisher Scientific (Bremen)
- 20 °C freezer	Premium NoFrost GN 3056	Liebherr (Ochsenhausen)
4 °C freezer	Öko Energiesparer	Privileg (Fuerth)
Analysis scale	JL-180	Chyo Balance Corporation (Japan)
Autoclave	Systec DX-200	Systec (Linden)
Centrifuge*	Heraeus Multifuge X1 centrifuge Rotor: Sorvall 75002000	Thermo Scientific (Erlangen)
Centrifuge (1 L)	Avanti J-26XP Rotor: JLA-8.1000	Beckman Coulter (Sinsheim)
Centrifuge bottles (1 L)	J-LITE Polypropylenflaschen-1000 ml (komplett)	Beckman Coulter (Sinsheim)
Confocal microscope	Leica microscope-TCS MP5	Leica Microsystems, Germany
Copper grid	Grid size 100 mesh x 250 µm pitch, copper	Sigma-Aldrich GmbH (Taufkirchen)
Culture tubes	13 mL	Sarstedt (Nuembrecht)
Electrophoresis chamber	Midi – large 460.000	Harnischmacher (Nottuln)
ELISA reader	Multiscan FC Microplate Photometer	Thermo Scientific (Erlangen)
Eppendorf tubes	1.5 mL, 2 mL	Sarstedt (Nuembrecht)
Falcon tubes	15 mL, 50 mL	Sarstedt (Nuembrecht)
Filter tips	10 µL, 100 µL, 1 mL	A. Hartenstein (Wuerzburg)
Gel documentation	INTAS® GDS	Intas (Goettingen)
Heating block	HX-2, PEQLAB	Biotechnologie GmbH (Erlangen)
Incubator (37 ˚C)	Function Line BB 16	Heraeus Holding GmbH (Hanau)
Laminar hood	Class II Type A/B3	Nuaire (Plymouth, MN, USA)
Microcentrifuge (tabletop)	Heraeus Pico 21	Heraeus (Hanau)

Microwave	8017	Privileg (Stuttgart)
NanoDrop	NanoDrop 2000c spectrophotometer	Thermo Scientific (Erlangen)
Needle	25 gauge, EU23	A. Hartenstein (Wuerzburg)
OD Cuvette	1.5 – 3 mL	Laborhaus Scheller (Euerbach)
Petri dish	92 x 16 mm	Nerbe Plus (Winsen)
pH meter	Inolab pH 720	WTW (Weilheim)
Pipet boy	Accu-Jet® Pro	Brand (Wertheim)
SDS PAGE electrophoresis system	Mini-PROTEAN Tetra cell	Bio-Rad GmbH (München)
Serological pipettes	5, 10, 25 mL	Greiner (Frickenhausen)
Slide-A-Lyzer mini dialysis cassette	2 KDa MWCO (Cat no: 69580)	Thermo Scientific (Erlangen)
Sonicator	Bandlein Sonoplus HD70	A. Hartenstein (Wuerzburg)
Spectrophotometer	Eppendorf Biophotometer	Eppendorf, Hamburg
Sterile filter	Acrodisc PES 0.2 µm, 32 mm, sterile (Article No. 514-4131)	PALL (Dreieich), VWR
Thermocycler	Flex Cycler	Analytik Jena AG (Jena)
Transwell insert	PET, 0.4 µm, 4.5 cm^2, 24 mm (Article No. 657640)	Greiner (Frickenhausen)
Transmission electron microscope	JEOL JEM-2100 TEM	JEOL (Freising)
Ultracentrifuge	Optima L-80 x p Rotor: SW40Ti	Beckman Coulter (Sinsheim)
Ultracentrifuge tubes	14 ml ultra-clear Beckman 40Ti	Beckman Coulter (Sinsheim)
Vivaspin	Vivaspin Turbo 15	Sartorius
Vortexer	Vortex Power Mix L46	Labinco (Breda, Niederlande)
Water bath	WB 20, P-D	Industriegesellschaft mbH (Dresden)
Well plates	6, 24, 96 (F-form)	Laborhaus Scheller (Euerbach)

*Unless otherwise mentioned, Heraeus Multifuge X1 centrifuge was usually used for centrifuging steps in the work.

2.2 **Chemicals**

Table 2. 2: Chemicals used in this study

Chemicals	Company
Acetic acid	Carl Roth GmbH & Co. KG (Karlsruhe)
Agar bacteriology grade	AppliChem (Darmstadt)
Agarose	Peqlab Biotechnologie GmbH (Erlangen)
Ampicillin	Carl Roth GmbH & Co. KG (Karlsruhe)
Chromogenic *E. coli* coliform agar (ECC)	Medco Diagnostica (Munich)
Disodium phosphate (Na_2HPO_4)	Carl Roth GmbH & Co. KG (Karlsruhe)
Dimethylsulfoxide (DMSO)	Thermo Fisher Scientific (Erlangen)
DNase I RNase-free	New England Biolabs (Frankfurt)
DNA loading dye 6x	Thermo Fisher Scientific (Erlangen)
Calcium chloride ($CaCl_2$)	Carl Roth GmbH & Co. KG (Karlsruhe)
Caesium chloride (CsCl)	Sigma-Aldrich GmbH (Taufkirchen)
Chloroform	Sigma-Aldrich GmbH (Taufkirchen)
Ethylenediaminetetraacetic acid (EDTA)	Carl Roth GmbH & Co. KG (Karlsruhe)
Ethanol (EtOH) 100 %	Carl Roth GmbH & Co. KG (Karlsruhe)
Ethidium bromide (EtBr)	Carl Roth GmbH & Co. KG (Karlsruhe)
Glacial acetic acid (100 %)	Carl Roth GmbH & Co. KG (Karlsruhe)
Glutaraldehyde	Sigma-Aldrich GmbH (Taufkirchen)
Glycerol (86%)	Carl Roth GmbH & Co. KG (Karlsruhe)
Glycol blue	Thermo Fisher Scientific (Erlangen)
Hydrogen chloride (HCl)	Carl Roth GmbH & Co. KG (Karlsruhe)
Isopropyl β-D-1-thiogalactopyranoside (IPTG)	Carl Roth GmbH & Co. KG (Karlsruhe)
Magnesium chloride ($MgCl_2$)	Carl Roth GmbH & Co. KG (Karlsruhe)
Magnesium sulphate ($MgSO_4$)	Carl Roth GmbH & Co. KG (Karlsruhe)
Methanol	Carl Roth GmbH & Co. KG (Karlsruhe)
Mitomycin C (MMC)	AppliChem (Darmstadt)

Monopotassium phosphate (KH_2PO_4)	Carl Roth GmbH & Co. KG (Karlsruhe)
Monosodium phosphate (NaH_2PO_4)	Carl Roth GmbH & Co. KG (Karlsruhe)
N-acetylglucosamine (GlcNAc)	Sigma-Aldrich GmbH (Taufkirchen)
Nucleoside triphosphate (dNTPs)	Thermo Fisher Scientific (Erlangen)
Polyethelene glycol 8000 (PEG 8000)	Sigma-Aldrich GmbH (Taufkirchen)
PCR master mix (2x)	Thermo Fisher Scientific (Erlangen)
Phenol liquified (90 %)	Sigma-Aldrich GmbH (Taufkirchen)
Phusion High-Fidelity DNA polymerase 2U/µL	Thermo Fisher Scientific (Erlangen)
Phusion 5x HF buffer	Thermo Fisher Scientific (Erlangen)
Polymyxin B sulfate	Sigma-Aldrich GmbH (Taufkirchen)
Potassium chloride (KCl)	Carl Roth GmbH & Co. KG (Karlsruhe)
Power SYBR® Green RNA-to-CT™ 1-Step kit	Thermo Fisher Scientific (Erlangen)
Proteinase K (RNA grade)	Qiagen (Hilden)
Proteinase K	Roche, Manheim
RNAprotect Bacteria Reagent	Qiagen (Hilden)
RNAse A	Sigma-Aldrich GmbH (Taufkirchen)
RNAse free water	Thermo Fisher Scientific (Erlangen)
RT-PCR enzyme mix	Thermo Fisher Scientific (Erlangen)
Sodium acetate 3 M	Carl Roth GmbH & Co. KG (Karlsruhe)
Sodium chloride (NaCl)	Carl Roth GmbH & Co. KG (Karlsruhe)
Sodium hydroxide (NaOH)	Carl Roth GmbH & Co. KG (Karlsruhe)
Tryptone	MP Biomedicals GmbH (Eschwege)
Tris (hydroxymethyl)aminomethane (Tris)	Carl Roth GmbH & Co. KG (Karlsruhe)
TruPAGE™ SDS running buffer (1x)	Sigma-Aldrich GmbH (Taufkirchen)
TruPAGE™ SDS sample buffer	Sigma-Aldrich GmbH (Taufkirchen)
Uranyl acetate	Science Services GmbH (Munich)
Yeast extract	MP Biomedicals GmbH (Eschwege)
β-Mercaptoethanol	Carl Roth GmbH & Co. KG (Karlsruhe)

2.3 DNA and protein markers

Table 2. 3: DNA and protein ladders used in this study

	Figure	Company
GeneRuler 100 bp DNA ladder	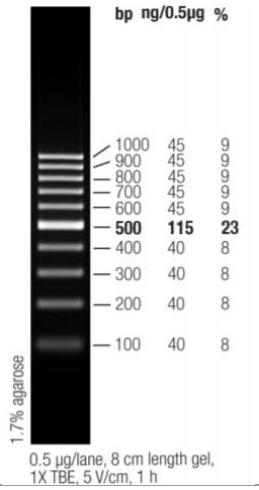	Thermo Fisher Scientific (Erlangen)
GeneRuler 1 kb DNA ladder	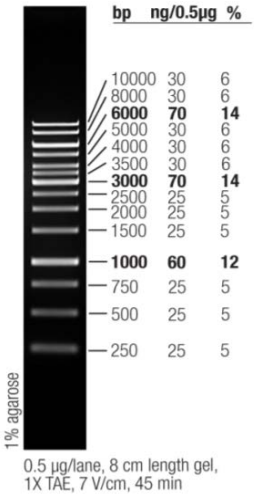	Thermo Fisher Scientific (Erlangen)
PageRuler prestained protein ladder	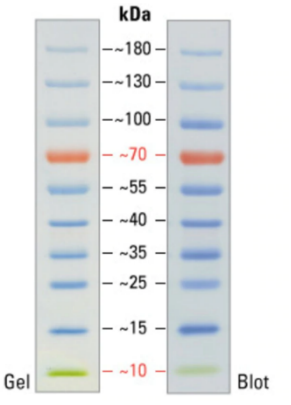 **SDS-PAGE band profile of the PageRuler Prestained Protein Ladder** Images are from a 4-20% Tris-glycine gel (SDS-PAGE) and subsequent transfer to membrane.	Thermo Fisher Scientific (Erlangen)

2.4 **Bacterial strains and phages**

Table 2. 4: List of *E. coli* strains used in this study. Unless otherwise mentioned, the source of the bacterial strains used in the study is the strain collection of the Institute for Molecular Infection Biology (IMIB), Wuerzburg.

***E. coli* strain**	**Serotype**	**Description**	**Strain collection Nr.**
***E. coli* Nissle 1917 (EcN)**	O6:K5:H1	non-pathogenic probiotic strain, pMUT1, pMUT2, microcins H47/M, F1C-fimbria, type 1 fimbria, curli source: Ardeypharm GmbH, Herdecke	464
***E. coli* K-12 MG1655**	O-:H48:K-	K-12 wildtype strain, F^-, λ^-, *ilvG*$^-$, *rfb-50*, *rph-1*	416
***E. coli* K-12 HB101**	O-:H48:K-	K-12 derivative; F^-, λ^-, *mcrB*, *mrr*, *hsdS20* (r_B^-, m_B^-), *recA13*, *leuB6*, *ara-14*, *proA2*, *lacY1*, *galK2*, *xyl-5*, *mtl-1*, *rpsL20* (Sm^R), *glnV44*	502
***E. coli* K-12 DH5α**	O-:H48:K-	K-12 derivative; F^-, *endA1*, *hsdR17* (*rk*$^-$, *mk*), *supE44*, *thi-1*, *recA1*, *gyrA*, *relA1*, λ^-, Δ(*lacZYA-argF*) U169, Φ80dlacZ ΔM15, *deoR*, *nupG*	278
***E. coli* SE11**	O152:H28	commensal strain isolated from healthy adult source: Japan Collection of Microorganisms (JCM 16574) (Oshima et al., 2008)	528
***E. coli* SE15**	O150:H5	commensal strain isolated from healthy adult source: Japan Collection of Microorganisms (JCM 16575) (Toh et al., 2010)	529
***E. coli* CFT073**	O6:K2:H1	uropathogenic *E. coli* strain, human isolate, hemolysin, type IV Pili, S and P fimbrial adhesins, a close relative to EcN	212
***E. coli* K-12 993 W lysogen**	not determined	K-12 strain harbouring lambda lysogen source: Klaus Hantke, Tuebingen	462
SK22D	O6:K5:H1	*a mchCDEF* deletion mutant of EcN (no microcins)	498
EcNΔ *k5*	O6:K5:H1	a *kps* deletion mutant of EcN which lacks the entire determinant spanning from *kpsF* to *kpsM* (17521 bp)	94
EcNΔ *csg*	O6:K5:H1	*csg* deletion mutant of EcN (no curli adhesin)	96
EcNΔ *bcs*	O6:K5:H1	*bcs* deletion mutant of EcN (no cellulose)	97

EcNΔ *fliC*	O6:K5:H1	*fliC* deletion mutant of EcN (no flagella)	260
MG1655R	OR:H48:K-	MG1655 harbouring the pUC19 plasmid (100 µg/ml Amp)	566
MG1655R*pr*	OR:H48:K-	MG1655 harbouring the pUC19 plasmid with the *phage repressor* (*pr*) (100 µg/ml Amp)	550
MG1655*sieB*	OR:H48:K-	MG1655 harbouring the pUC19 plasmid with the superinfection exclusion protein B (*sieB*) (100 µg/ml Amp)	549
MG1655_S	OR:H48:K-	MG1655 harbouring the pUC19 plasmid with the antisense transcript (1,104 bp) spanning over the *sieB* and antitermination protein N of EcN's prophage 3 in the sense orientation (100 µg/ml Amp)	569
MG1655_AS	OR:H48:K-	MG1655 harbouring the pUC19 plasmid with the antisense transcript (1,104 bp) spanning over the *sieB* and antitermination protein N of EcN's prophage 3 in the antisense orientation (100 µg/ml Amp)	567
MG1655_1772	OR:H48:K-	MG1655 harbouring the pUC19 plasmid with the gene: *EcN_1772* (100 µg/ml Amp)	639
***E. coli* EDL933**	O157:H7	*stx1, stx2* harbouring STEC strain source: Ulrich Dobrindt, Muenster	3 (S3 lab)

Table 2. 5: List of the phages used in this study.

Phages	Source
Shiga toxin-producing phages (*stx*-phages)	*stx*-phages were isolated and provided by Dr Susanne Bury
Lambda phages	lambda phages were isolated by inducing the strain *E. coli* K-12 993 W lysogen
T4 phages	IMIB, Wuerzburg
K5 capsule specific phages	Statens Serum Institute Cat No:60759

2.5 **Oligonucleotides**

Table 2. 6: Oligonucleotides used in this study. Unless otherwise mentioned, the oligonucleotides used in this study were self-designed. NA: no amplicon was expected.

Name/ ID in primer collection	Sequence (5'- 3')	Amplicon size (bp)	Amplification region
EcN_1L2	AATGAACCAGATCCGTGTGA	103	

EcN_1R2	CAGGTCCAAACGTAACAGTGC		EcN specific chromosomal region source: (Troge, 2012)
EcN_4L2	GGGCGATCGGAT TTAATCAT	186	
EcN_4R2	CGAGGACTCGGAGCTTACTG		
EcN_5L1	GCCTCTCGCAACTTAACGAC	232	
EcN_5R1	AGTTATCCAGCGTTGCCATC		
K-12 _F	ATCCTGCGCACCAATCAACAA	1,684	K-12 specific chromosomal region
K-12_R	TTCCCACGGACATGAAGACTA		
CFT_F	AAGAAAAGAGCAGAGCGAT	EcN: NA CFT073: 421	*hlyD* gene of CFT073 source: (Bury, 2018)
CFT_R	TAACAACCCCACCTTCAGTAT		
SE11 fwd	GGAATTACCCATCCACCTGTA	EcN: NA SE11: 257	SE11 specific region ECSE_4549 source: (Oshima et al., 2008)
SE11 rev	AAACCCCGTTTCACTAAC		
SE15 fwd	CCACTGATGTTGATAATGC	EcN: NA SE15: 540	SE15 specific fimbrial operon source:(Toh et al., 2010)
SE15 rev	TTAGTTCTTCTGGCATCG		
mchC_F	TGTCGAACACGTTTCCTGAG	EcN: 3,558 SK22D: 608	Screening of microcin (*mchC* to *mchF*) deletion in EcN source:(Patzer et al., 2003)
mchC_R	AAACGCGACTGGATATCACC		
K5_ext_F	AGTGAAGGAAGGCCCGGAAG	EcN: NA EcNΔ*k5*: 1,126	Screening of K5 (*kpsF* to *kpsM*) capsule deletion
K5_ext_R	ATCAATCGCGTGCGTTCTGG		
K5_int_F	GAACGGTGCGGCAGTCAACG	EcN: 1,032 EcNΔ*k5*: NA	Screening of K5 (*kpsF* to *kpsM*) capsule deletion
K5_int_R	GACGATGTCCCCACACGGCG		
csg_F	GCGGAAAACGGAGATTTAAAA	EcN: 1,322 EcNΔ*csg*: 345	Screening of curli (*csg*) deletion in EcN source: (Bury, 2018)
csg_R	CCCTTGCTGGGTCGTATT		
bcsA_F	CCACCATTGCCATCTGCT	EcN: NA EcNΔ*bcs*: 1,412	Screening of cellulose (*bcs*) deletion in EcN source: (Bury, 2018)
bcsA_R	ACCGACGAAATGCTCACAG		
fliC_F	GACGATTAGTGGGTGAAATGA	EcN: 2,184 EcNΔfliC:475	Screening the flagellin (*fliC*) deletion in EcN source: (Bury, 2018)
fliC_R	CGTCGACTAACAAAAAATGGC		
λ_Q_F	GGAGAAGGCGCATGAGACTC	624	

λ _Q_R	GCTGCTAACGTGTGACCGCAT		*Q* gene (late gene regulator) of lambda phage
ndd_T4_F	CCTCACTGGCGTCCGAAGAC	580	*ndd* gene of T4 phage
ndd_T4_R	TCATGCGGCCTTGGAGTAGAA		
pKD3_F	ACACGTCTTGAGCGATTGTG	1,098	Screening pKD3 plasmid that is used as an internal control in T4 specific PCR
pKD3_R	AGCCTCTCAAAGCAATTTTC		
lamB_RT_F	ATGTCTGCTCAGGCAATGC	EcN: 135	Real time PCR: *lamB* gene of EcN
lamB_RT_R	CACATTCGTTGCCAAGACGG		
Pr_RT_F	TCCGATTAGCAGGGCTTT	EcN: 59	Real-time PCR: *pr* gene of EcN
Pr_RT_R	CCGGGCGTTTTTTATTGGT		
hcaT_F	ACAAACGCAGGCCAGAAAG	EcN: 127	Real time PCR: reference gene *hcaT* of EcN source:(Zhou et al., 2011a)
hcaT_R	GCTGCTCGGCTTTCTCATC		
1290_fwd	CATCCTGTTGTTTTGCGTTAGC	not applicable	Real-time PCR: antisense strand of *sieB* gene of EcN
1290_rev	GCTACAGCGAATGCCAAAT		Real-time PCR: sense strand of *sieB* gene of EcN

2.6 **Bacterial growth media and solutions**

Table 2. 7: Different media composition used in this study

(i) **LB medium composition**

Contents	Amount
Yeast extract	5 g
NaCl	5 g
Tryptone	10 g
dH_2O	up to 1000 mL

(ii) **0.7 % LB soft agar composition**

Contents	Amount
Yeast extract	5 g
NaCl	5 g
Tryptone	10 g
Agar	7 g
dH_2O	up to 1000 mL

(iii) **1.5 % LB-Agar composition**

Contents	Amount
Yeast extract	5 g
NaCl	5 g
Tryptone	10 g
Agar	15 g
dH_2O	up to 1000 mL

(iv) **List of solutions used in this study**

Solutions	Composition
TAE buffer (50x)	24.2 % (w/v) Tris, 5.7 % (v/v) Acetic acid, 10 % (v/v) 0.5 M EDTA (pH 8.0)
PBS (10x)	8 % (w/v) NaCl, 0.2 % (w/v) KCl, 1.44 % (w/v) Na_2HPO4
SM buffer (1x)	100 mM NaCl, 10mM $MgSO_4$, 50mM Tris-HCl, pH 7.5

2.7 **Commercially available assay kits**

Table 2. 8: Kits used in this study

Assay kit	Company
RIDASCREEN® Verotoxin ELISA (C2201)	R-BioPharm AG (Darmstadt)
RNeasy® Mini Kit	Qiagen (Hilden)
QIAquick PCR purification kit	Qiagen (Hilden)
Pro-Q®Emerald 300 Lipopolysaccharide Gel Stain Kit (Cat no: P20495)	Thermo Fisher Scientific (Erlangen)
12 % TruPAGE™ Precast Gels (PCG2010-10EA)	Sigma-Aldrich GmbH (Taufkirchen)

2.8 **Column preparation for caesium-chloride (CsCl) density centrifugation**

Table 2. 9: Column preparation for CsCl density centrifugation

Density (ρ)	Weight of CsCl (g)/ 20 ml SM buffer	Loading volume/ Order*
1.3 g/ml	7.8	2 ml/ first
1.5 g/ml	13.4	2 ml/ second

1.8 g/ml	19	2 ml/ third

*the solutions were loaded in the given order into a 14 ml ultracentrifuge tube using a syringe with a long needle (25 gauge) by always inserting the needle until the bottom of the tube

3 Methods

3.1 Microbiological methods

3.1.1 Overnight culture cultivation

For the overnight culture cultivation, a single bacteria colony or a loop of bacterial culture or 20 µl of bacterial glycerol stock was added to 2 ml Luria-Bertani (LB) medium in a 13 ml sterile culture tube. The overnight culture (ONC) was incubated in a shaking incubator for 14 – 16 h at 37 ˚C, 200 rpm.

3.1.2 Bacterial stock preparation and storage

For long term storage, 2 ml ONC was centrifuged in a tabletop microcentrifuge at 13,000 x g for 5 mins at room temperature (RT). The pellet was thoroughly resuspended with 500 µl of 10 mM $MgCl_2$ after which, 1 ml of 86 % glycerol was added. After a brief vortex, the glycerol stocks were stored at either -20 ˚C or -80 ˚C.

3.1.3 *E. coli* strain identification

E. coli strains were tested for their identity and purity by selective chromogenic *E. coli* coliform agar (ECC) plates and polymerase chain reaction (PCR). ECC plates enable the differentiation among *E. coli* strains based on the enzymes they possess and their ability to metabolize lactose and ß-glucuronides. Some *E. coli* strains harbour only ß-D-galactosidase enzyme-producing pink to dark pink colonies. Whereas, the majority of *E. coli* strains additionally possess ß-D-glucuronidase enzyme and therefore producing blue to violet colonies. To test this, either a loop of bacterial ONC was streaked on an ECC plate or 100 µl of ONC was serially diluted in 0.9 % saline until 6^{th} dilution (10^{-6}) and 50 µl of the 6^{th} dilution was plated on an ECC plate using sterile L-rod and incubated upside-down, at 37 ˚C overnight (O/N), after which the colony

formation was observed. Further verification was performed by PCR where primers that amplify selective genes of the individual strains were used in the PCR reaction (3.2.1). Primers complementary to the flanking regions of the deleted genomic regions were employed in PCR to validate the EcN mutants used in the study. The binding regions of the screening primers used in this study are described in Annexure 1.

3.1.4 **Bacterial growth**

In various experimental setups, bacterial density was measured as optical density (OD) at a wavelength (λ) = 600 nm with a spectrophotometer. To determine the live bacterial count, the colony-forming units (CFUs/ml) were measured by plating the serial dilutions of bacterial culture on agar plates. Therefore, bacterial culture was diluted in 0.9 % saline and 100 µl of appropriate dilution was plated with glass beads on LB-Agar plates with or without suitable antibiotics or on an ECC plate. The plates were then incubated upside-down, at 37 ˚C, O/N, before the CFUs/ml were noted.

3.1.5 **Phage propagation**

a. Lambda phage cultivation and storage

The induction of the lambda phages was achieved by adding 1 µg/ml of mitomycin C (MMC) to mid-log growing phase (OD_{600} 0.3 - 0.5) *E. coli* K-12 993 W lysogen culture harbouring lambda lysogen. The culture was further incubated in the dark for 6 h at 37 °C in a rotary shaker (200 rpm) and centrifuged at 4,696 x g for 5 mins at RT. Finally, lambda phages were isolated by sterile filtering the supernatant with 0.2 µm sterile filters and stored at 4 °C for future experiments.

b. T4 phage cultivation and storage

For T4 phage production, either a single T4 phage plaque or 10^6 PFUs/ml T4 phage lysate was inoculated into a mid-log growing phase *E. coli* K-12 MG1655 culture and incubated at 37 °C in a rotary shaker (200 rpm) until clear lysis was observed (~ 6 h). The lysate was then

centrifuged at 4,696 x g for 5 mins at RT and T4 phages were isolated by sterile filtration of the supernatant with 0.2 µm sterile filters and were stored at 4 °C for future experiments. For long term storage, 2 % chloroform was added to the lysate, mixed well and stored at 4 °C.

3.1.6 **Purification of phages**

For microscopic experiments, pure T4 phage stock of high titer was produced by caesium chloride density centrifugation as described by (Zeng and Golding, 2011). For this purpose, T4 phage lysate was produced in a large volume (1,000 ml) as described in 3.1.5_b. Further, 2 % chloroform was added to the lysate, mixed well and incubated for 15 mins and centrifuged at 10,000 rpm for 15 mins, 4 °C in Avanti J-26XP centrifuge using 1 L Beckmann Coulter centrifuge bottles. The supernatant (lysate) was stored in a 1,000 ml flask to which DNAse1(1 µg/ml) and RNAse (1 µg/ml) were added and incubated for 1 h at RT. The phage lysate was subjected to 1 M NaCl treatment and incubated on ice for 3 h in a 1 L centrifuge bottle, followed by addition of 10 % polyethylene glycol (PEG 8000) until it was completely dissolved and incubated for 16 h at 4 ˚C which resulted in precipitation of phages along with PEG 8000. The lysate was then centrifuged in Avanti J-26XP centrifuge (10,000 rpm, 15 mins, 4°C) and the pellet (phage particles precipitated with PEG 8000) was dissolved in SM buffer (4 ml SM buffer per 250 ml of initial phage lysate) and incubated for 16 hr at 4°C with very mild shaking. The lysate (SM buffer with phage particles) was transferred into a 50 ml falcon tube, and an equal volume of chloroform was added to the lysate and centrifuged at 4,696 x g, 15 mins at 4°C. Later, the supernatant was subjected to caesium-chloride (CsCl) density centrifugation. 2 ml of three different densities (ρ) (1.3 g/ml, 1.5 g/ml and 1.7 g/ml) of CsCl solution were prepared as described in the Table 2. 9 and loaded in a 14 ml ultra-clear Beckman 40Ti ultracentrifuge tube at the order of 1.3 g/ml, 1.5 g/ml and 1.7 g/ml. Phage lysate (8 ml) was loaded on top of each tube and centrifuged in a Beckman SW40Ti rotor at 4 °C (24,000 rpm/ 4 h). The phage band which appeared between 1.3 g/ml and 1.5 g/ml CsCl/SM

layers (shown in **Figure 3. 1**) was carefully isolated with the help of a 25-gauge needle and a syringe. The phages were dialyzed against 1000-fold more SM buffer for 16 h (buffer was changed after 1 h, 4 h and 8 h) to get rid of the CsCl. The isolated phage stock was stored at 4 °C for further use.

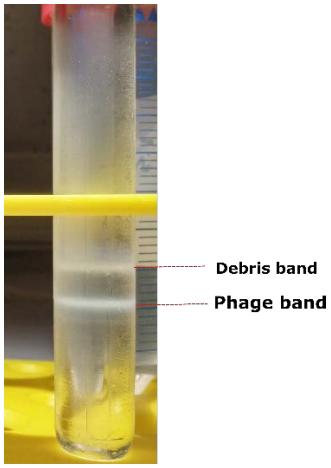

Figure 3. 1: Purified T4 phage band visible after CsCl density centrifugation

3.1.7 Coincubation conditions

In order to understand the influence of EcN on phages and phage infection of other sensitive strains, co-/ and tri-culture experiments were performed. For this, OD_{600} of bacterial ONCs were determined and the cells were collected by centrifugation at 4,696 x g for 10 mins at RT. The bacterial pellet was resuspended in LB medium to obtain ~10^9 CFUs/ml of *E. coli* strains and 100 µl of phage extract was used to set up mono-/co-/or tri-cultures with 100 µl of EcN and/or K-12 strains in a 24-well plate. Each well was adjusted to a final volume of 1 ml with LB medium. The plates were incubated in a static manner for the desired amount of time at 37 °C. The CFUs/ml were determined by plating serial dilutions in 0.9 % saline on LB agar plates or on ECC plates. The samples were sterile filtered for phage-plaque assay.

3.1.8 Phage-Plaque-Assay (PPA)

To determine the number of plaque-forming units (PFUs/ml) in the sample, a phage plaque assay was performed. For this, 200 µl of *E. coli* ONC (OD_{600} ~ 2.0 to 3.0) was mixed along

with 3 ml 0.7 % LB soft agar. In addition, 1.5 µg/ml mitomycin C (MMC) and 20 mM $CaCl_2$ were used for determination of PFUs/ml of lysogenic phages. After a brief vortex, 3 ml of 0.7 % LB soft agar was poured on 1.5 % LB agar plate. Once the plates were dried, phage samples were serially diluted in 0.9 % saline and 10 µl of the serially diluted phage samples were spotted on the plate. In the case of MG1655 recombinant strains harbouring a pUC19 plasmid with ampicillin (Amp) cassette, the strains were grown in 100 µg/ml Amp supplemented medium with 1 mM IPTG. When these strains were used as indicator strains in PPA, along with ONC, 100 µg/ml Amp + 1 mM IPTG were also used in 0.7 % LB agar. IPTG inductions were carried out for 2 h at RT before the phages were dropped on a plate. The plates were allowed to dry and incubated at 37 ˚C, O/N after which PFUs/ml were recorded.

3.1.9 **Lambda lysogeny detection in *E. coli* samples incubated with lambda phages**

In the case of lambda phage incubation with *E. coli* strains, the possible lysogeny was determined by two factors: i) genome integration of phage DNA, ii) bacterial lysis and phage production. Firstly, to determine the possible integration of phage DNA into the bacterial genome after incubation, a *lambda*- phage specific PCR was performed with λ_Q_F/R primer pair. For this, *E. coli* cells incubated with the phages for 24 h were serially diluted and plated on LB agar plates. After overnight incubation at 37 ˚C, all the colonies on the plate (~ 100 to 300) were collected using a sterile L-rod and further diluted to 1:1000 with 0.9 % saline. 2 µl of diluted *E. coli* cells were used as a template for PCR with 2x PCR Master Mix to screen for the lambda phage specific DNA (3.2.1). Secondly, to screen for the successful lysogeny in *E. coli* cells incubated with the lambda phages, the phage production was induced using MMC. In this experiment, the *E. coli* cells were incubated with lambda phages (10:1) for a longer incubation time to allow possible lysogeny until the phage titer in the supernatant reached zero (120 h). The cells were then washed with 0.9 % saline thrice by centrifuging in a tabletop microcentrifuge (13,000 x g, RT, 5 min) and pellets were suspended in 1 ml LB medium and

transferred to a 24 well plate to which 1 µg/ml MMC was added and incubated for 16 h at 37 ˚C, static in dark to induce the phage production followed by sterile filtration to isolate the produced phages. The phage signal was further amplified by adding 100 µl of MG1655 cells (~ 10^8 CFUs/ml) and the volume was adjusted to 1 ml with LB medium and incubated for 24 h at 37 ˚C, static. Finally, the supernatant of the incubation was collected by centrifugation and the phage titer in the sample was determined by PPA (3.1.8).

3.1.10 **Verotoxin ELISA**

The Stx level of the given sample was determined with the Ridascreen® Verotoxin ELISA kit in a 96-well microtiter plate, which is coated with a monoclonal antibody binding specifically to Stx1 and Stx2. Samples were diluted (1:10) in 0.9 % saline, mixed by vortex and 100 µl of the diluted samples were transferred to the provided 96-well microtiter plate. The ELISA was performed according to the manufacturer's instructions. The toxin concentrations in each well were measured with the Multiscan FC Microplate Photometer at the OD_{450}. The obtained values were multiplicated by 10. The control provided in the kit served as positive control and 0.9 % saline was used as the negative control.

3.1.11 **Processing of *E. coli* culture and supernatants**

To study the phage inactivation mechanism(s), *E. coli* cells and supernatants were subjected to different treatments as described below:

3.1.11.1 **Heat killing (HK) or 1 % formaldehyde (FA) treatment:**

10 ml of 24 h static cultures were pelleted at 4,696 x g for 10 mins at RT and washed twice with 500 µl of 0.9 % saline. The pellets were resuspended in LB medium to obtain 10^{10} CFUs/ml and 300 µl of EcN cells were transferred to 1.5 ml Eppendorf tubes and thereon heat-killed for 1 h at 100 °C (HK) or 300 µl of resuspended EcN cells were incubated in 1 % FA, O/N at 4 °C. The 1 % FA fixed *E. coli* were washed twice with 500 µl of 0.9 % saline (13,000 x g, 5 mins, RT) and resuspended in LB medium to reach 10^{10} CFUs/ml. Finally, 100 µl of the killed *E. coli*

were mixed with 100 µl of phages, adjusted to 1 ml with LB medium and incubated for 24 h at 37 °C in a 24 well system.

3.1.11.2 **Proteinase K (PK) or sodium meta periodate (SMP) treatment**

Both PK and SMP treatment of live *E. coli* cells led to only partial effect and always survivor *E. coli* cells were observed, hence for these experiments, the *E. coli* cells were first killed with heat and then further treatments were carried out.

Like heat-killing, the pellets of 24 h static cultures were resuspended in LB medium to obtain 10^{10} CFUs/ml and 300 µl was heat-killed for 1 h at 100 ˚C. For proteinase K treatment, proteinase K (PK) was added to the heat-killed cells at a final concentration of 1 mg/ml and incubated at 37 °C for 1 h, followed by an inactivation at 75 °C for 20 mins. After which, 100 µl of heat-killed and PK treated cells (HK + PK) were used in coincubation studies with 100 µl of phages in 1 ml LB medium for further studies. In case of SMP treatment, 300 µl of heat-killed cells were treated with SMP (40 mM) and incubated at RT for 1 h followed by washing with fresh LB medium twice. 100 µl of the sample was then used in coincubation studies.

3.1.11.3 **Supernatant preparation**

On the other hand, the supernatants of 10 ml, 24 h static culture were sterile filtered with 0.22 µm PALL sterile filter and concentrated approximately 10-fold (10x) with Vivaspin Turbo 15 (MWCO - 5 KDa) by centrifuging at 4,696 x g, RT for 20 mins. The flow-through from the centrifugation (S_FT) was also used in the coincubation in order to test the involvement of low molecular weight components of the supernatant in phage inactivation. 100 µl of concentrated supernatant (10x) was added to 100 µl of phages and the volume was made up to 1 ml with LB medium and incubated for 24 h at 37 °C in a 24 well system.

3.1.11.4 **Polymyxin B (PMB) treatment**

To understand the involvement of LPS in phage inactivation, heat-killed *E. coli* cultures (10^{10} CFUs/ml) or supernatants were incubated with PMB of a final concentration 25 µg/ml for 1 h at 37 ˚C. 100 µl of the PMB treated *E. coli* /supernatant was added to 100 µl of phages, to a final volume of 1 ml with LB medium and incubated for 24 h at 37 °C in a 24-well plate. For the experimental setup involving PMB treatment, 25 µg/ml PMB was used also in the coincubation set up in a 24 well plate.

The details of the coincubation setup made with samples subjected to the above-mentioned processing methods are described in **Table 3. 1** below.

Table 3. 1: Description of processed *E. coli* samples

Legend	Description (set up in a 24 well plate)
LB	Medium control 100 µl of ~10^9 PFUs/ml T4 phage lysate + 900 µl of LB medium
LB_S	Medium control (10x concentrated) 100 µl of ~10^9 PFUs/ml T4 phage lysate + 100 µl of 10x concentrated LB medium + 800 µl of LB medium
EcN	Live EcN cells 100 µl of ~10^9 PFUs/ml T4 phage lysate + 100 µl of ~10^9 EcN (overnight grown and washed) CFUs/ml + 800 µl of LB medium
EcN_S	EcN supernatant (10x concentrated) 100 µl of ~10^9 PFUs/ml T4 phage lysate + 100 µl of 10x concentrated EcN supernatant of overnight grown EcN cells + 800 µl of LB medium
MG_S	MG1655 supernatant (10x concentrated) 100 µl of ~10^9 PFUs/ml T4 phage lysate + 100 µl of 10x concentrated MG1655 supernatant of overnight grown MG1655 cells + 800 µl of LB medium
EcN_HK	Heat-killed EcN cells 100 µl of ~10^9 PFUs/ml T4 phage lysate + 100 µl of EcN heat-killed cells + 800 µl of LB medium
EcN + 1% FA	Formaldehyde-killed EcN cells 100 µl of ~10^9 PFUs/ml T4 phage lysate + 100 µl of formaldehyde-killed EcN cells + 800 µl of LB medium
HK_S	Supernatant of heat-killed EcN cells

	100 µl of ~10^9 PFUs/ml T4 phage lysate + 100 µl supernatant of heat-killed EcN cells + 800 µl of LB medium
EcN_S FT	Flow-through from EcN supernatant (< 5 KDa) 100 µl of ~10^9 PFUs/ml T4 phage lysate + 900 µl flow-through of EcN supernatant from Vivaspin Turbo 15 (MWCO < 5 KDa)
+ PK	Proteinase K (1 mg/ml) treated sample 100 µl of ~10^9 PFUs/ml T4 phage lysate + 100 µl of PK treated sample + 800 µl of LB medium
+ SMP	Sodium meta periodate (40 mM) treated sample 100 µl of ~10^9 PFUs/ml T4 phage lysate + 100 µl of PK treated sample + 800 µl of LB medium
+ PMB	Polymyxin B (25 µg/ml) treated sample 100 µl of ~10^9 PFUs/ml T4 phage lysate + 100 µl of PK treated sample + 785 µl of LB medium + 15 µl of 0.5 mg/ml PMB (25 µg/ml)

3.1.12 **LPS isolation**

To isolate LPS from *E. coli* strains, 20 ml cultures (OD_{600} ~ 0.5) were centrifuged at 10,000 × g for 5 mins. The pellets were washed twice in PBS and sonicated for 10 mins on ice (amplitude 60 %, 30 sec off/ 30 sec on) followed by treatment with 1 mg/ml proteinase K to the cell mixture and the tubes were incubated at 65 °C for an additional hour. The mixture was subsequently treated with RNAse (140 µg/mL) and DNAse (20 µg/mL) in the presence of 10 µl 20 % $MgSO_4$, 40 µl chloroform and incubated O/N at 37 °C. At the following day, an equal volume of hot 90 % phenol (65 – 70) ˚C was added to the sample followed by vigorous shaking at (65 – 70) ˚C for 15 mins. Suspensions were then cooled and centrifuged at 8,500 x g, 15 mins and the supernatants were transferred to 15 ml falcon tubes to which sodium acetate (0.5 M final concentration) and 10 volumes of 95 % ethanol were added. Samples were stored at -20 ˚C, overnight to precipitate. The next day, the tubes were centrifuged (2,000 x g, 10 mins, 4 ˚C) and the pellets were resuspended in 1 ml distilled water. Further, samples were dialyzed extensively against Millipore water at 4 ˚C. Finally, the purified LPS product was stored at - 20 ˚C until use.

3.1.13 **Testing the T4 phage adsorption to *E. coli***

To understand the T4 phage attachment to *E. coli*, T4 phages were added to 10 ml of a mid-log grown phase *E. coli* culture (OD_{600} - 0.5) at an MOI of 100 times more *E. coli* than phages. 500 µl of the culture was taken at different time points (0, 1, 3, 6, 9, 12 and 30 mins) after the addition of T4 phages and sterile filtered after which the PFUs/ml were determined by PPA.

3.2 **Molecular biological methods**

3.2.1 **Polymerase Chain Reaction (PCR)**

PCR is a basic molecular biology technique used for the exponential replication of a specific DNA segment, wherein the length of the DNA segment to be amplified is defined by the primer pair used. The amplification cycles consist of three steps which begins with denaturing the double-stranded (ds) DNA by heating it to a temperature between 95 ºC and 98 ºC so that the hydrogen bonds between the individual base pairs could be dissolved. In the second step, each primer of the pair binds to the complementary sequence of the single-stranded (ss) DNA segment at an optimal primer annealing temperature depending on its sequence. Finally, the elongation step takes place at 72 ºC in which DNA polymerase adds the nucleotides to the 3' end of the primer, thereby extending the DNA strand and the elongation time depends on the length of the amplicon. The number of amplification cycles depends on the type of polymerase or nucleotide concentration which is usually 30 to 35 cycles. Finally, an extended elongation phase for 10 mins was provided to complete the elongation of all the amplicons generated in every cycle. In this work, for standard PCR reactions, a Taq polymerase-based master mix, PCR Master Mix (2x) was used. The PCR conditions and temperature profiles were used according to the manufacturer's instructions which are listed in Table 3. 2. And for the experiments in which the PCR amplicons would be used in subsequent sequencing and cloning, Phusion High-Fidelity DNA polymerase was used. The PCR conditions and temperature profiles for Phusion Polymerase-based PCR reaction are listed in Table 3. 3. The optimal

annealing temperature was adapted according to the primer pair used. Unless otherwise mentioned, *E. coli* templates were prepared by incubating 100 µl of bacterial ONC in 1.5 ml Eppendorf tube for 10 mins at 100 ˚C or a colony was picked from LB agar plate and dissolved in 100 µl 0.9 % saline and incubated for 10 mins at 100 ˚C. For other specific PCRs used in the study, template preparation is explained in the respective method sections.

Table 3. 2:Taq polymerase-based PCR Master Mix (2x) reaction set up

PCR reaction mix	1x	PCR condition
2x PCR MM	12.5 µl	step 1: 95 ˚C for 5 mins step 2: 95 ˚C for 30 sec *step 3: X ˚C for 1 mins step 4: 72 ˚C for 1 mins/kb step 2 to 4 – 35 cycles step 5: 72 ˚C for 10 mins step 6: hold at 4 ˚C
Forward primer (10 µM)	1.25 µl (0.5 µM)	
Reverse primer (10 µM)	1.25 µl (0.5 µM)	
Template	2 µl (Plasmid DNA – 20 to 30 ng) (Genomic DNA – 100 ng)	
Millipore water	Up to 25 µl	

*The annealing temperature in step 3 (X ˚C) was calculated according to the primers used

Table 3. 3: Phusion High-Fidelity DNA polymerase -based PCR reaction set up

PCR reaction mix	1x	PCR condition
5X Phusion HF Buffer	10 µl	step 1: 98 ˚C for 45 sec step 2: 98 ˚C for 10 sec *step 3: X ˚C for 30 sec step 4: 72 ˚C for 15–30 sec/kb step 2 to 4 – 35 cycles step 5: 72 ˚C for 10 mins step 6: hold at 4 ˚C
10 mM dNTPs	1 µl	
Forward primer (10 µM)	2.5 µl (0.5 µM)	
Reverse primer (10 µM)	2.5 µl (0.5 µM)	
100 % DMSO	1.5 µl (3 %)	
Template	(Plasmid DNA – 20 to 30 ng) (Genomic DNA – 100 ng)	
Phusion DNA Polymerase	0.5 µl	
Millipore water	Up to 50 µl	

*The annealing temperature in step 3 (X ˚C) was calculated according to the primers used

3.2.2 Localization of T4 phage DNA by T4 specific PCR

T4 specific PCR was adopted to check whether the T4 phages are bound to EcN or localized in the supernatant after coincubation. For this, 1 ml of *E. coli* cells incubated with T4 phages at an MOI of 1:1 for 24 h, static at 37 °C were centrifuged at 4,696 x g for 10 mins at RT. The

pellets were washed twice with 0.9 % saline (13,000 x g, RT, 5 mins) and were then resuspended in 1 ml of fresh LB medium. Similarly, the supernatant from coincubation was sterile filtered. In this PCR, the *ndd* gene, specific for T4 phages was screened with T4_*ndd*_F/R primer pair. As an internal control, 1 µl of plasmid pKD3 was used along with primer pair pKD3_F/R in each PCR reaction and 2 µl of EcN pellet and supernatant samples were used as a template for PCR with 2x PCR Master Mix as described in the **Table 3. 4**.

Table 3. 4: PCR conditions for localization of T4 phage DNA by T4 specific PCR

PCR reaction mix	1x	PCR condition
2x PCR MM	12.5 µl	step 1: 95 ˚C for 5 min step 2: 95 ˚C for 30 sec step 3: 55 ˚C for 1 min step 4: 72 ˚C for 2 min step 2 to 4 – 35 cycles step 5: 72 ˚C for 10 min step 6: hold at 4 ˚C
T4_*ndd*_F	1.25 µl	
T4_*ndd*_R	1.25 µl	
Plasmid pKD3	1 µl (30 ng)	
pKD3_F	1.25 µl	
pKD3_R	1.25 µl	
Template	2 µl	
Water	Up to 25 µl	

3.2.3 **Agarose gel electrophoresis**

For visualization of the PCR amplicons, 2 % agarose gel was prepared. For this, 3 g of agarose was melted in 150 ml 1x TAE buffer in a 250 ml Erlenmeyer flask until the agarose was completely dissolved. The agarose solution was then carefully poured into a gel casting chamber with 26-well comb and left until it was completely hardened. The gel was then carefully shifted into the electrophoresis chamber and the comb was removed. The sample to be visualized on the gel was mixed with 6x DNA loading dye and 10 µl of the mixture was loaded into gel pocket. For the DNA size control, 7 µl of DNA ladder with appropriate DNA length was loaded. The DNA ladders used in this are mentioned in **Table 2. 3**. The DNA was separated by size during electrophoresis at 150 V, 500 mA for 1 h in 1x TAE bath. After the electrophoresis, the gel was carefully transferred to an ethidium bromide (EtBr) bath and incubated for 20 mins to allow inter-chelation. Unbound EtBr was washed off with distilled

water and then DNA chelated by EtBr was visualized at the INTAS Gel documentation system at 300 nm (EtBr absorbance maximum). The visualized picture was saved as “TIFF” file and used for further analysis and the gel pictures were processed with ImageJ 1.50i.

3.2.4 **Purification of PCR amplicons**

The PCR amplicons which were further employed in cloning experiments or needed to be sequenced were purified with QIAquick PCR Purification Kit according to the manufacturer’s instruction. Using QIAquick spin columns provided in this kit, any PCR amplicons ranging from 100 bp to 10 kb can be purified from unused primers, nucleotides, polymerases, and salts. After the purification, the amplicon was again tested on 2 % agarose gel by electrophoresis and also the concentration of the PCR product was determined with NanoDrop 2000c spectrophotometer at an absorbance of 260/280 nm and 260/230 nm.

3.2.5 **Gel extraction**

QIAquick Gel Extraction Kit was used for isolating the DNA fragments from agarose gels by removing the agarose, salt and ethidium bromide contamination which could hinder their downstream application. The extraction was performed according to manufacturer’s instruction after which the fragment was again tested on 2 % agarose gel by electrophoresis and also the concentration of the DNA was determined with NanoDrop 2000c spectrophotometer at an absorbance of 260/280 nm and 260/230.

3.2.6 **Sequencing**

The PCR product was sent for sequencing to LGC genomics after either PCR purification or gel extraction. The concentration of the sample sent for sequencing was determined according to the instruction from the company which was based on the length of the DNA fragment to be sequenced. Generally, for one sample to be sequenced, 10 µl of the sample (made up to the concentration suggested by the company) was mixed with either 4 µl of the forward primer or 4 µl of the reverse primer and 2 x 14 µl samples were sent for sequencing.

3.2.7 **RNA isolation**

To understand the transcriptomic response of EcN at different culturing conditions or towards coincubation with phages or other *E. coli* strains, RNA was isolated from EcN cultures that were grown in different culturing conditions (3.4.1) or from EcN that was incubated with phages as described in 3.1.7 or with other *E. coli* strains in a Transwell system as described in 3.4.2. EcN cultures incubated at a specific condition were pooled as one replication, and for each condition, RNA was isolated from three replicates. The 3 ml culture was then transferred into a 15 ml falcon tube containing 6 ml of RNAprotect® Bacteria Reagent and incubated for 5 mins at RT followed by centrifugation for 10 mins at 4,696 x g. Total bacterial RNA was isolated from the pellet using the RNAeasy Mini Kit according to the manufacturer's instructions. Contaminating DNA was removed by DNase (2 U/ml) digestion for 10 mins at 37 °C. The remaining RNA was further purified by ethanol precipitation for which the isolated RNA was pipetted to a 1.5 ml Eppendorf tube and adjusted to a final volume of 180 µl with RNase free water. 18 µl of 3 M sodium acetate and 1.33 µl of 15 mg/ml GlycoBlue were added and the sample was gently vortexed. 600 µl of 100 % EtOH was added and the solution was incubated at -20 °C overnight. The next day, the RNA was collected by pelleting it at 13,000 x g for 30 mins at 4 °C in a tabletop microcentrifuge. The resulting pellet (blue colour can be seen) was cleaned in a double washing step with 250 µl 70 % ice-cold EtOH (13,000 x g, 5 mins, 4 °C). After air-drying of the pellet to remove residual ethanol, the RNA was dissolved in 25 µl of RNase free water. The RNA content was determined by measuring the absorbance at 260 nm and 230 nm at the NanoDrop 2000c spectrophotometer. The total RNA quality was also assessed by Core Unit SystemMedicin (SysMed) with an Agilent 2100 Bioanalyzer (Agilent, CA). RNA integrity numbers of all samples were ~8.0 or more.

3.2.8 **Quantitative Real-Time PCR (qRT-PCR)**

qRT-PCR is a tool used to quantify the RNA and thereby analysing the transcript level and gene expression of any organism at a certain time point. Unlike the conventional PCR, it monitors the amplification of a specific DNA molecule during the PCR and reports the kinetics of amplification and hence referred to as real-time. The initial step is reverse transcription where the reverse transcriptase enzyme transcribes mRNA into cDNA which is used as a template in qRT-PCR. After the initial denaturation and primer annealing, dsDNA amplicons are produced. The quantification is done by detecting the signal from the fluorescent dye SYBR green in the qRT-PCR mix, which can only bind to the minor groove of dsDNA and thereby quantifying the transcript level. The amplification curve obtained by qRT-PCR can be subdivided into three phases: (i) the baseline phase in which the DNA concentration and hence, the level of bound fluorescent dye is too low to be detected, (ii) the exponential phase in which the amplification of the template proceeds and the fluorescence dye exceeds a certain threshold and from this time point, the DNA amplification can be tracked at a wavelength of 510 nm (iii) the last plateau phase, in which the DNA amplification has reached its maximum as the number of free enzymes is too low to continue the amplification. In our study, the qRT-PCR method was used to validate the results of the transcriptomic analysis which indicated upregulation of certain genes in EcN in presence of phages and to quantify the expression of l*amB* gene in EcN upon induction with maltose. Primers which amplify specific DNA fragments were designed and the optimal concentration was determined. The isolated RNA was diluted to 40 ng/µl with RNase free water. 1 µl of the RNA was used as a template in the Power SYBR™ Green RNA-to-CT™ 1-Step Kit. Following thermal cycler conditions were applied:

48 °C/30 mins - 95 °C/10 mins - [95 °C/15 sec - 60 °C/1 min] 40x

Reverse transcription - Activation of the polymerase - [Denaturation - Annealing/Elongation]

The constantly expressed *E. coli* gene *hcaT* was used as the reference gene (Zhou et al., 2011a).

3.2.9 **Two-step RT-PCR**

Although the above-mentioned one-step RT-PCR method is very quick and reliable, in case of issues with antisense regulations it would be ideal to do a two-step RT-PCR where PCR is performed after cDNA synthesis. Elaborately, in one-step RT-PCR, during cDNA synthesis step there is a possibility that both sense and antisense cDNA could be synthesized. For e.g. the forward primer would bind to the complementary strand of the sense strand and will synthesize cDNA and this cDNA synthesized will be based on the number of antisense transcript available. In the same case, there is also a possibility that the reverse primer of the forward strand acting as a forward primer for the complementary strand and synthesizing cDNA of sense transcripts. Hence when there was a need, to identify if the regulation was from particularly from sense or antisense strand, we synthesized cDNA in the first step with an appropriate gene-specific primer and then do the PCR in the next step. For understanding the regulation of antisense transcript of *sieB* gene in EcN a forward primer (1290_fwd) was used, and to understand the sense regulation a reverse primer (1290_rev) was used in the preparation of cDNA reaction master mix I as described in **Table 3. 5** and then 100 ng of RNA sample was added to master mix and RNA was denatured at 65 °C for 5 mins after which 7 µl of master mix II prepared as described in **Table 3. 6** was added. The reaction mixture was incubated for cDNA synthesis at 50 °C for 10 mins and then inactivation was carried out at 80 °C for 10 mins. Finally, in the second step, the PCR was performed by adding 1 µl of synthesized cDNA or water to 9 µl PCR master mix prepared as described in **Table 3. 7** and the following thermal cycler conditions were applied similar to one-step RT-PCR (3.2.8).

95 °C/10 mins - [95 °C/15 sec - 60 °C/1 min] 40x

Activation of the polymerase - [Denaturation - Annealing/Elongation]

The constantly expressed *E. coli* gene *hcaT* was used as reverence gene (Zhou et al., 2011a).

Table 3. 5: cDNA synthesis master mix I for step 1 of two-step RT PCR

Master mix I	1x (µl)
10mM dNTP mix	1
Primer (1290_fwd/1290_rev)	1
Nuclease free H_2O	8

Table 3. 6: cDNA synthesis master mix II for step 1 of two-step RT PCR

Master mix II	1x (µl)
5x SSIV RT buffer	4
100 mM DTT	1
RNAse OUT inhibitor	1
SSIV RT enzyme	1

Table 3. 7: PCR master mix for step 2 of two-step RT PCR

PCR master mix	1x (µl)
SyBr green PCR mix	5
1290_fwd (200 nM)	1
1290_rev (200 nM)	1
dH_2O	2

3.2.10 **qRT-PCR data analysis**

The cDNAs threshold cycle (Ct) values, obtained by qRT-PCR, were analysed through the comparative ΔΔCT method (Giulietti et al., 2001). For each gene-targeted, this method compares the Ct value of the test samples with the Ct value of the reference sample. For each target gene expression, Ct values are normalized according to the values of the housekeeping gene. The relative expression of the target genes in the different samples were calculated according to the following formula: ΔCt = Ct (target gene) - Ct (housekeeping gene) where Ct (target gene) indicates the value of the threshold cycle for the gene of interest, and Ct (housekeeping gene) indicates the value of the threshold cycle for the housekeeping gene used as normalizer. Subsequently, the relative expression of all samples in comparison with the Ct

values obtained from the corresponding control was calculated as follows: RE = 2-ΔΔCt, where ΔΔCt = ΔCt (sample) – ΔCt (control) and RE indicates the relative expression, ΔCt (sample) indicates the difference between Ct values of the target gene and the housekeeping gene(s) calculated for the test sample, ΔCt (control) indicates the difference between the Ct values of the target gene and the Ct values of the housekeeping gene obtained from the control.

3.2.11 **SDS gel electrophoresis and LPS specific staining**

The isolated LPS samples were visualized on 12 % TruPAGE™ Precast Gels following the manufacturer's instruction. Briefly, the isolated LPS samples (32.5 µl) were mixed with 5 µl of 10 % ß-mercaptoethanol and 12.5 µl of SDS sample loading buffer (TruPAGE™ SDS sample buffer) and samples were heated at 70 °C for 10 mins, after which 20 µl was loaded on to the 12 % TruPAGE™ Precast Gels assembled on the Mini-PROTEAN Tetra cell SDS PAGE system and 1x TruPAGE™ SDS running buffer was used and electrophoresis was carried out at 180 V for 1 h. After electrophoresis, the gel was subjected to LPS specific staining with the help of Pro-Q® Emerald 300 LPS gel stain kit. The procedure involves initial fixation of the gel in a fixation solution containing 50 % methanol and 5 % acetic acid followed by oxidation with a solution of periodic acid and 3 % acetic acid. The gel was carefully washed with a solution of 3 % glacial acetic acid in between every step and finally the gel was stained with freshly prepared Pro-Q® Emerald 300 Staining Solution. The staining solution stock and periodic acid were provided in the kit and a detailed protocol was provided by the manufacturer along with the kit and also available online (https://assets.thermofisher.com/TFS-Assets/LSG/manuals/mp20495.pdf). Finally, the stained gel was visualized using INTAS Gel documentation system at 300 nm and the picture was saved as "TIFF" file for further analysis.

3.3 Microscopic methods

3.3.1 Confocal microscopic examination of T4 phage and *E. coli* interaction

For the confocal microscopy, the bacteria-phage infection method was adapted from (Zeng and Golding, 2011) and modified for T4 phages as described here: T4 phages (~10^{11} PFUs/ml) were stained with 0.5 µg/ml DAPI and incubated for10 mins at room RT in dark. The excess DAPI was removed by dialyzing the phages using Slide-A-Lyzer mini dialysis cassette (2 KDa MWCO) against 100-fold LB medium in a 50 ml falcon tube (4 h, 4 °C, rolling). Meanwhile, the LB agarose slabs were prepared as described in (Zeng and Golding, 2011) and following the dialysis, 100 µl of DAPI stained T4 phages were mixed with 500 µl of mid-log growing phase *E. coli* and was incubated for 30 mins on ice and subsequently, the mixture was moved to 37 °C for 5 mins. The samples were immediately pelleted down (8,000 x g, 5 mins) in a tabletop microcentrifuge and the pellets were resuspended in 50 µl LB medium and 2 µl of the phage-bacteria mixture was placed on the agarose slab and it was covered with a coverslip (24 x 50 mm). After a minute the slide was carefully mounted on the microscope stage and imaging was done at high magnification (100x objective) by Leica microscope-TCS MP5.

3.3.2 Transmission electron microscopic examination of EcN after incubation with T4 phages

For negative staining, T4 phages were incubated with EcN at an MOI (multiplicity of infection) of 100 (EcN:T4 – 100:1) for 1 h at 37 °C and the samples were then fixed with 0.5 % glutaraldehyde and stained with 0.5 % uranyl acetate on a copper grid. The image was captured in JEOL JEM-2100 TEM at Zentrale Abteilung für Mikroskopie, Biocentre, Universität Würzburg.

3.4 Transcriptomics experimental setup

E. coli is economical, and we believe, the factors influencing its effects are produced only when necessary. Hence, to study the mechanism(s) behind EcN's probiotic effect and its antagonistic

effect on the other *E. coli* strains (e.g. inhibition of shiga toxin production in EHEC) we isolated RNA from EcN that was under different experimental setup and performed RNA sequencing followed by transcriptome analysis to understand the gene regulations.

3.4.1 Single culture: fermenter and LB culture set up

EcN was grown under different culturing conditions such as fermenter-grown and LB-overnight grown. For the fermenter grown condition, the EcN cell pellets from two different time points of stationary phase were obtained from Ardeypharm GmbH, Herdecke. The schematic representation **(Figure 3. 2)** depicts the timeline of the fermentation process and the timepoints at which the samples were obtained. For the LB-overnight grown condition, 3 ml of LB medium was inoculated with 20 µl of EcN glycerol stock in a sterile culture tube and incubated overnight at 37 ˚C, 180 rpm in a shaker.

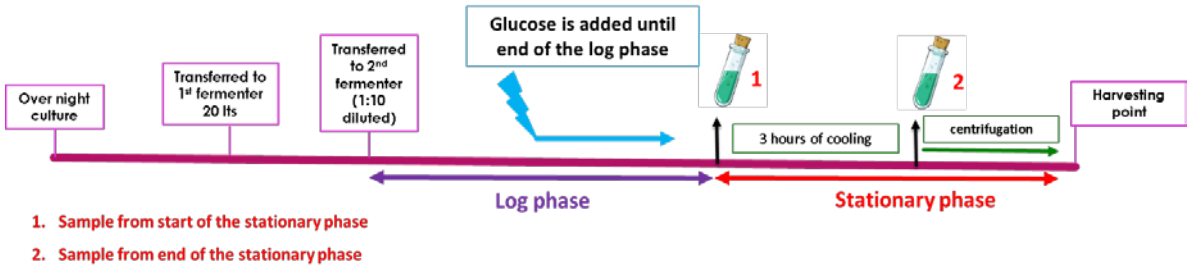

Figure 3. 2: Schematic representation of the Mutaflor fermentation process. EcN samples were obtained from starting (1) and ending (2) of the stationary phase from Ardeypharm GmbH, Herdecke

3.4.2 Coculture: Transwell assay set up

A Transwell system was used to coculture the *E. coli* strains to understand the transcriptomic response of EcN towards the other strain. In this approach, the bacterial strains were separated by a ThinCertTM Cell Culture Insert with a pore size of 0.4 µm, which allowed the diffusion of all secreted substrates but kept the strains separated. As described in (3.1.7), the bacterial strains were centrifuged and diluted to the mentioned OD_{600} values. 250 µl of the prepared EcN culture was added to the well (lower compartment) and 250 µl of *E. coli* EDL933 or MG1655

culture was added to the insert (upper compartment) in a 6 well plate and each compartment was adjusted to a final volume of 2.5 ml LB medium.

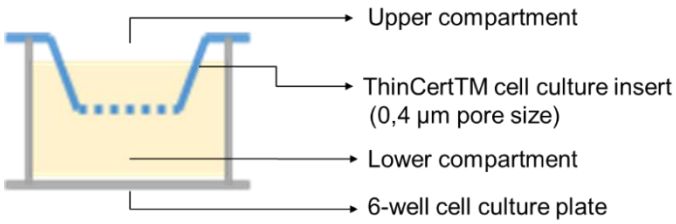

Figure 3. 3: Illustration of a typical Transwell system used in this study.

Figure 3. 3 is the graphical depiction of a Transwell system used in this study. The plates were then sealed with parafilm and incubated for the desired amount of time at 37 °C, static after which the RNA was isolated, and the Stx-level was determined by ELISA.

3.5 **Bioinformatic analysis**

For RNA sequencing and subsequent transcriptome analysis, the RNA samples were sent to Core Unit SystemMedicin (SysMed), IMIB, Wuerzburg. The following protocol (3.5.1 and 3.5.2) was performed and provided by the members of the Core Unit (Dr Richa Barti).

3.5.1 **RNA library preparation for transcriptome analysis**

Extracted RNA was depleted of ribosomal RNA using the Ribo-Zero rRNA Removal Kit for bacteria (Illumina) according to the manual. Depleted RNA was fragmented for 3 mins at 94°C using the NEBNext Magnesium RNA Fragmentation Module. The RNA ends were repaired with two consecutive T4 PNK incubations (-/+ ATP) and an RppH treatment. Library preparation was performed according to the NEBNext Multiplex Small RNA Library Preparation Guide for Illumina. All adapters and primers were diluted 1:4 and 15 and 16 cycles of PCR were used, respectively. No size selection was performed at the end of the protocol. 12 libraries were pooled and sequenced on a NextSeq 500 with a read length of 75 nt.

3.5.2 Analysis of deep sequencing data

The quality of raw reads (Phred scores, number of duplicates and adapter) were assessed using FastQC (version-0.11.31) (Andrews, 2010). In order to assure a high sequence quality, the Illumina reads in FASTQ format were trimmed with a cut-off phred score of 20 by cutadapt (version-1.15) (Martin, 2011) that also was used to remove the sequencing adapter sequences. The following steps were performed using the subcommand "create", "align" and "coverage" of the tool READemption (version-0.4.3)(Forstner et al., 2014) with default parameters. Reads with a length below 20nt were removed and the remaining reads were mapped to the reference genome sequences (NCBI Reference Sequence: NZ_CP007799.1, [27 June 2014]) using segemehl (Hoffmann et al., 2009). Coverage plots in wiggle format representing the number of aligned reads per nucleotide were generated based on the aligned reads and visualized in the Integrated Genome Browser (Freese et al., 2016). Each graph was normalized to the total number of reads that could be aligned from the respective library. To restore the original data range and prevent rounding of the small error to zero by genome browsers, each graph was then multiplied by the minimum number of mapped reads calculated overall libraries. The differentially expressed genes were identified using DESeq2 (version-1.16.1)(Love et al., 2014). In all cases, only genes with maximum Benjamin-Hochberg corrected p-value (padj) of 0.05, were classified as significantly differentially expressed. The data were represented as MA plots using R. The RNA-Seq data dealing with EcN's transcriptional changes when coincubated with phages (lambda/T4) has been deposited at the NCBI Gene Expression Omnibus (Edgar et al., 2002) and GEO series accession number for the respective projects are provided in the respective result sections.

3.5.3 Functional prediction

Functions of the genes that were significantly up or downregulated in EcN under different conditions were predicted by searching their gene annotations in online databases like Uniprot

(https://www.uniprot.org/) or Ecocyc (https://ecocyc.org/). For those genes annotated as hypothetical proteins in EcN's genome, their sequences were blasted at https://blast.ncbi.nlm.nih.gov/Blast.cgi under nucleotide blast against *E. coli* taxonomic group. By screening the hits with the maximum score and highest query cover, the function of the hypothetical proteins could be predicted.

3.6 **Statistical analysis**

The experiments were performed independently for at least 3 times in triplicates. Data are represented as mean +/- SD. For the statistical analysis of the experimental data, we used GraphPad Prism® version 8. For the simple column graphs, the unpaired t-test was used for the significance tests and the significance are represented in the graphs as ns, *, **, *** and ****. Whereas in the case of grouped column graphs that have more than one variable, the significance was calculated by multiple t-tests.

4 Results

4.1. *E. coli* strain identification

The study aimed to investigate the mechanisms behind the probiotic nature of EcN, which involved comparison with several *E. coli* strains. Therefore, it was vital to assess the purity and identity of *E. coli* strains. *E. coli* strains were analysed for their purity at the single colony-level by plating them on selective *E. coli* coliform agar (ECC) plates. Further identity of each strain and also the EcN mutants used in the study were confirmed by PCR for the strain-specific region and deleted genomic regions, respectively.

4.1.1. Testing the purity of *E. coli* strains with ECC plates

The *E. coli* coliform agar (ECC agar) is a chromogenic selective and differentiation medium that enables the simultaneous detection of different coliforms and *E. coli*. The ECC agar contains two chromogenic substances: X-GLUC and Salmon-GAL, each serving as a substrate for hydrolysis by the bacterial enzymes β-D-glucuronidase (producing blue bacterial colonies) and β-D-galactosidase (producing pink bacterial colonies), respectively. In the case of *E. coli* harbouring both enzymes, bacterial colonies reflected a dark violet phenotype on the ECC plates. ONCs of *E. coli* strains used in this study were serially diluted and 50 µl of 6^{th} dilution were plated on the ECC plate and incubated at 37 ˚C, O/N.

The EcN wildtype (wt) formed blue colonies whereas the K-12 strains MG1655, HB101 formed pink and DH5α formed distinctive light blue colonies on the ECC plates when incubated O/N at 37˚C, O/N (**Figure 4.1. 1**). Interestingly, the pink colonies of MG1655 strain slowly turned into a blue colour in case of longer incubation time (more than 14 h) and hence it was important to document the purity of the strains before 14 h of incubation. The uropathogenic *E. coli* strain CFT073 and the commensal strains SE11 and SE15 formed colonies with violet and dark blue

phenotype, respectively. Furthermore, the pathogenic *E. coli* strain EDL933 produced dark pink colonies (**Figure 4.1. 1**).

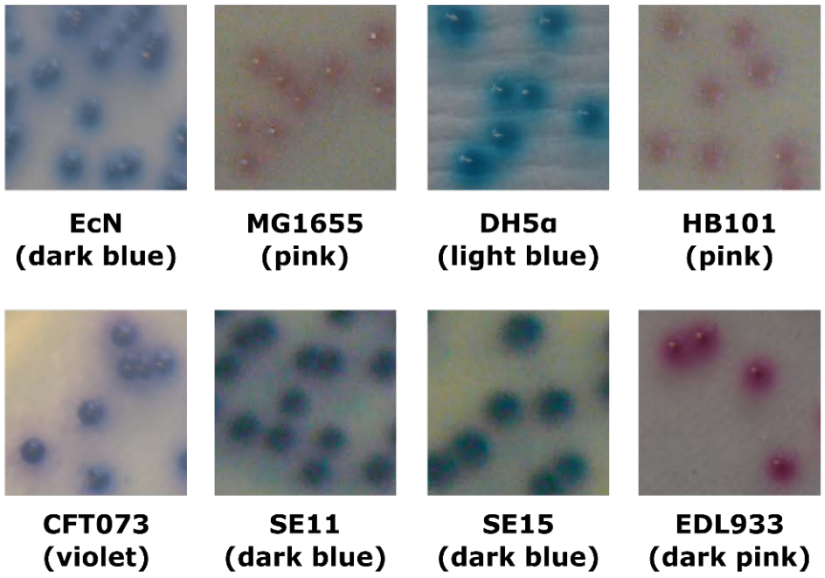

Figure 4.1. 1: *E. coli* strain purity identification on ECC plates. The *E. coli* strains namely, (top panel) EcN, MG1655, DH5α and HB101; (bottom panel) CFT073, SE11, SE15 and EDL933 verified on the ECC plates. Imaging was performed with Canon PowerShot SX260 HS and processed with ImageJ 1.50i.

Altogether, the test with ECC plates assured that there was no contamination of the tested *E. coli* strains detected on a single colony level.

4.1.2. Strain identification by PCR

The identity of the *E. coli* strains was confirmed by strain-specific PCR. For this, 100 µl of ONCs of the *E. coli* strains were boiled at 100 ˚C and 2 µl of samples were used as a template in a PCR reaction. The primers complementary to the strain-specific chromosomal regions were used in the PCR reaction with the 2x PCR Master Mix as mentioned in **Table 3. 2**. Details of the primers used are provided in **Table 2. 6**. The chromosomal regions specific for the EcN strain were amplified with the primer pairs IL2/IR2 (amplicon: 103 bp), IL4/IR4 (amplicon: 186 bp) and IL5/IR5 (amplicon:232 bp) and yielded the expected PCR products. Likewise., the K-12 strains MG1655, DH5α and HB101 screened with the primer pair K-12_F/R

(amplicon:1,684 bp) revealed their identity. In parallel, both the EcN and K-12 strains were also checked for cross-contamination by each other and no cross-contamination was detected (**Figure 4.1. 2**).

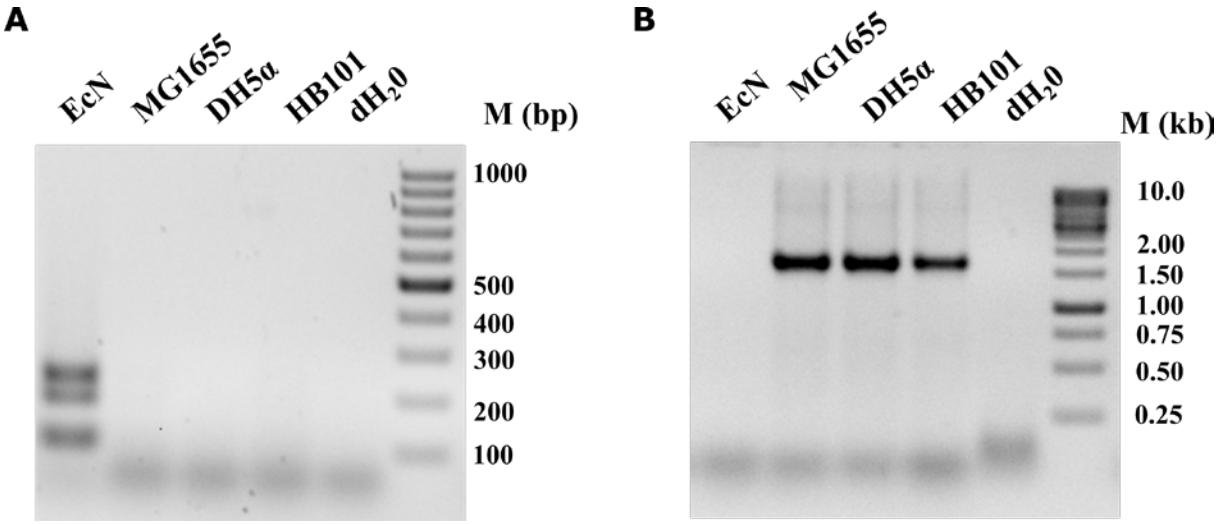

Figure 4.1. 2: PCR screening to confirm the identity of EcN and K-12 strains: The results of **(A)** the multiplex PCR with the EcN specific primer pairs IL2/IR2 (103 bp), IL4/IR4 (186 bp) and IL5/IR5 (232 bp) **; (B)** K-12 specific PCR with the primer pair K-12_F/R (1,684 bp); M – DNA ladder, dH_2O – negative (water) control.

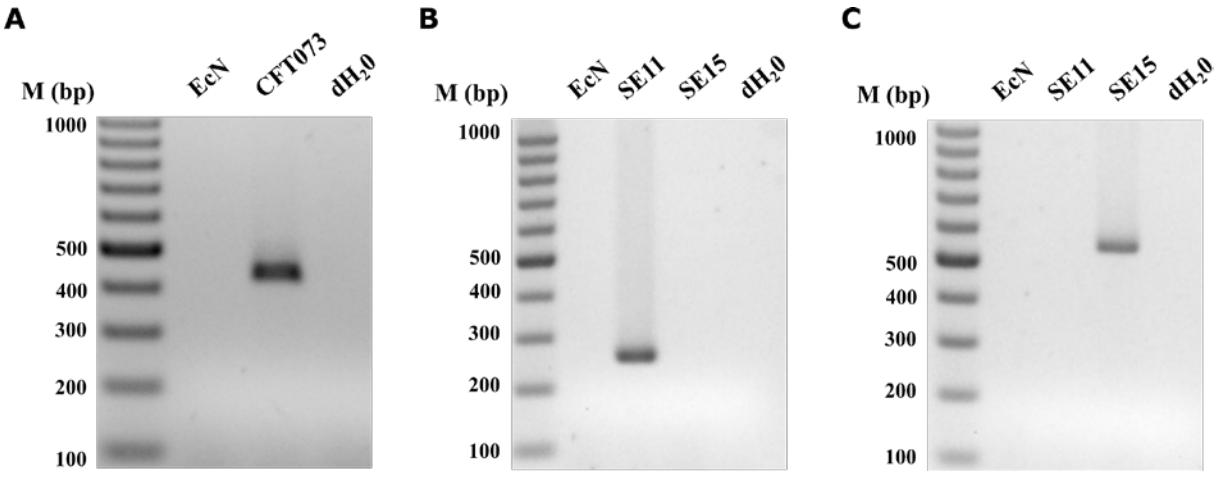

Figure 4.1. 3: PCR screen to confirm the identity of the *E. coli* strains CFT073, SE11 and SE15: The results of PCR with the primer pair **(A)** CFT_F/R (421 bp), **(B)** SE11_F/R (257 bp), and **(C)** SE15_F/R (540 bp); M – DNA ladder, dH_2O – negative (water) control.

In the next step, the identity of the strains CFT073, SE11 and SE15 were analysed by PCR. The hemolysin D (*hlyD*) gene-specific for CFT073 was amplified with *hlyD*- specific primers (CFT_F/R) only in CFT073 but not in EcN. Likewise, SE11_F/R and SE15_F/R primer pairs

were designed to amplify the commensal strains SE11-specific region (ECSE_4549) and SE15-specific fimbrial region, respectively. The use of strain-specific primers yielded expected amplicons only in the presence of the relevant strain (**Figure 4.1. 3**). Thus, the identity of all three strains was confirmed by PCR.

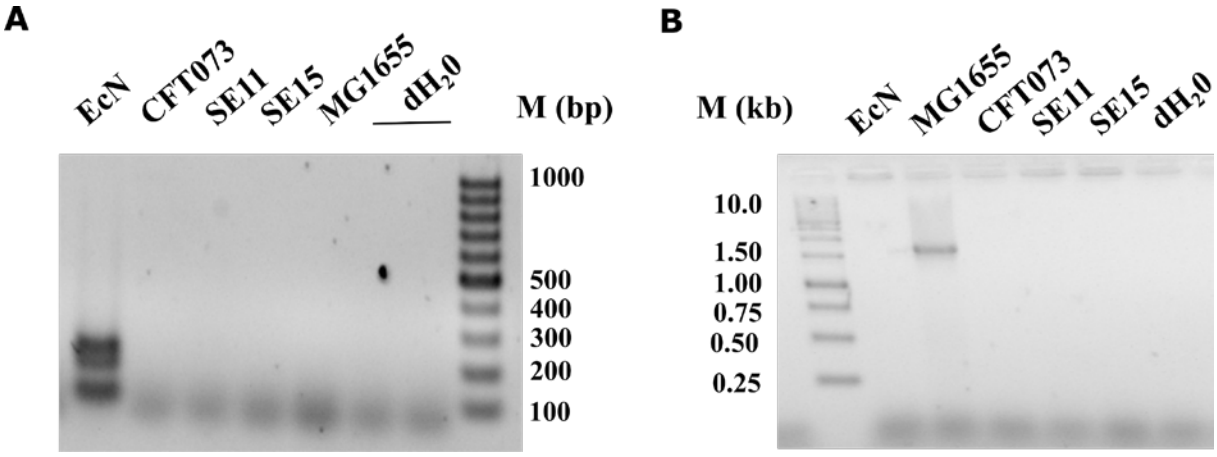

Figure 4.1. 4: PCR screen to check the purity of other *E. coli* strains (CFT073, SE11 and SE15): Results of **(A)** EcN specific multiplex PCR with the primer pairs IL2/IR2 (103 bp), IL4/IR4 (186 bp) and IL5/IR5 (232 bp); **(B)** K-12 specific PCR with the primer pair K-12_F/R (1,684 bp); M – DNA ladder, dH_2O – negative (water) control.

In addition, the above-validated strains were further examined for cross-contamination with EcN or K-12 strains with EcN and K-12 specific primer pairs. The PCR results (**Figure 4.1. 4**) showed that no such contamination was detected in the strains CFT073, SE11 and SE15. The identity of the pathogenic EDL933 strain used in this study was validated by Dr Susanne Bury (Bury, 2018).

4.1.3. EcN mutant verification using PCR

Several EcN deletion mutant strains were employed in the study to examine the possible contribution of those factors in phage resistance of EcN. The details of the deleted regions of all the EcN mutants used in this study are presented in Annexure 1. Previously in the lab, those mutants were screened for their corresponding deletions by amplicon sequencing (Bury, 2018). Further, in this study, the EcN mutants were primarily verified by PCR for their identity for

being EcN and for not being cross-contaminated with K-12 strains. The PCR results (**Figure 4.1. 5**) positively confirmed the identity of the mutant strains as EcN and any contamination with K-12 strains could not be detected.

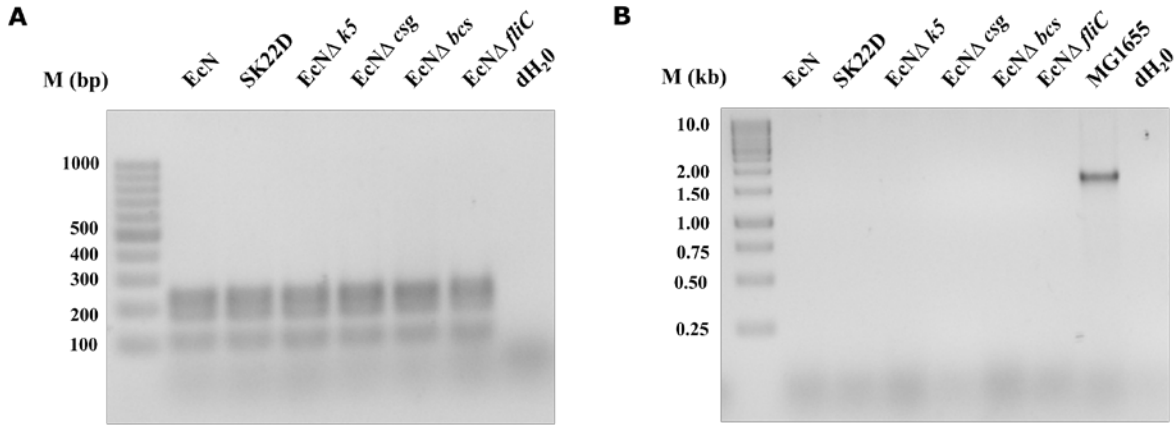

Figure 4.1. 5: PCR screening to confirm the identity of EcN mutants used in this study. The results of **(A)** EcN specific multiplex PCR with the primer pairs namely, IL2/IR2 (103 bp), IL4/IR4 (186 bp) and IL5/IR5 (232 bp); **(B)** K-12 specific PCR with the primer pair K-12_F/R (1,684 bp); M – DNA ladder, dH_2O – negative (water) control.

Secondly, the mutations in these strains which were either loss of few genes or an entire determinant were confirmed by PCR. In the EcN capsule negative mutant (EcNΔ *k5*), the entire K5 capsule determinant spanning from *kps*M to *kps*F (17,523 bp) was deleted. The primer pair complementary either to the flanking sites of the deleted region (K5_ext_F/R) or to the sequences within the deleted region (K5_int_F/R) were employed to verify the deletion. The K5_ext_F/R produced an amplicon of size 1,126 bp with EcNΔ *k5* and failed to yield an amplicon of size 18,651 bp with EcN wildtype (wt) as it was too long to be amplified with the PCR-conditions applied (**Figure 4.1. 6_A (right)**). In the case of K5_int_F/R, an amplicon of size 1,032 bp was observed with EcN wt and as expected no amplicon was obtained with EcNΔ *k5* (**Figure 4.1. 6_A (left)**). Next, the microcin negative mutant of EcN (SK22D) was verified, in which a 3,026 bp region in the microcin gene cluster was deleted. The primer pair mchC_F/R which annealed outside the deleted region produced the expected amplicons of size

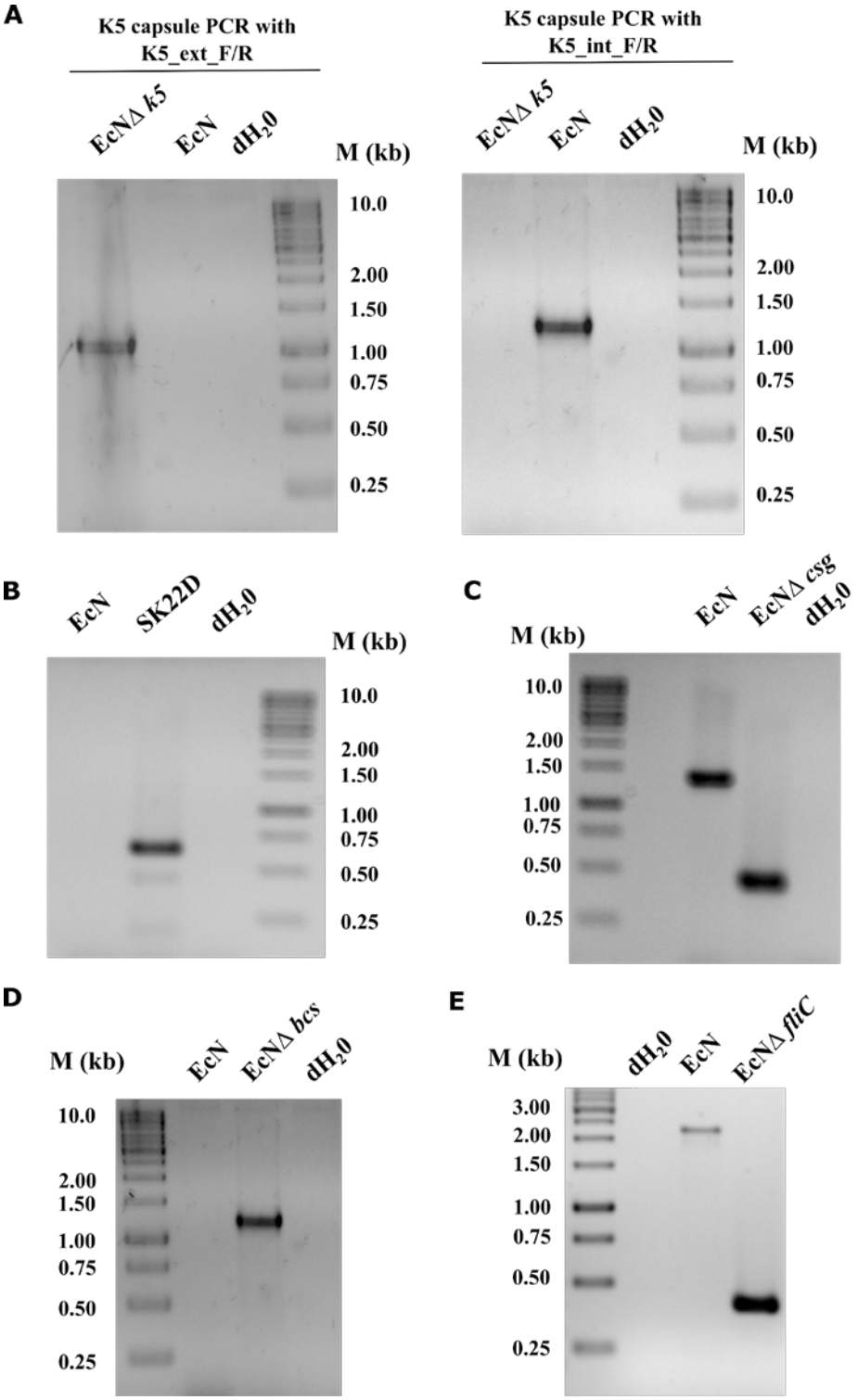

Figure 4.1. 6: PCR screening to confirm the deletions in the EcN mutants: The results of the EcN mutant verification PCR **(A)** EcNΔ *k5* with primer pair K5_ext_F/R (right) and primer pair K5_int_F/R (left), **(B)** SK22D with primer pair mch_F/R, **(C)** EcNΔ *csg* with primer pair csg_F/R, **(D)** EcNΔ *bcs* with primer pair bcs_F/R, and **(E)** EcNΔ *fliC* with primer pair fliC_F/R. All the mutants were screened in parallel with EcN wild type. M – DNA ladder, dH_2O – negative (water) control.

608 bp with SK22D but not with EcN wt as the PCR conditions were not conducive to amplify an amplicon of ~ 3,5 kb (**Figure 4.1. 6_B**). In a similar manner, curli mutant (EcNΔ *csg*), cellulose mutant (EcNΔ *bcs)* and flagellin mutant *(*EcNΔ *fliC)* of EcN were validated as mentioned below. The curli mutant screening primers csg_F/R produced an amplicon of size 1,322 bp with EcN wt and 345 bp with EcNΔ *csg.* Thus, confirming the deletion of *csgB* and *csgA* genes (977 bp) of the curli determinant (**Figure 4.1. 6_C)**. In case of EcNΔ *bcs*, a large region spanning from *yhjQ* to *bcsC* (9,269 bp) was deleted and a PCR with the bcsA_F/R primer pair produced an amplicon of size 1,412 bp only in the EcNΔ *bcs* mutant but not with EcN wt as the amplicon (10,681 bp) was too long to be amplified (**Figure 4.1. 6_D**). Further, the deletion of the *fliC* gene in EcNΔ *fliC* mutant was also confirmed by PCR with the primer pair fliC_F/R and an expected amplicon of size 2,184 bp and 475 bp was obtained with EcN and EcNΔ *fliC*, respectively (**Figure 4.1. 6_E).** To sum up, all the tested EcN mutant strains were clearly demonstrated as EcN and also confirmed for their appropriate genomic deletions.

4.2. **Transcriptomic response of EcN in different culturing conditions**

Mutaflor® is a licensed EcN based probiotic drug that is manufactured and sold by Ardeypharm GmbH, Herdecke, Germany. For the manufacturing purposes, EcN is grown in a fermenter and the timeline of the fermentation process is described in 3.4.1. We were particularly curious in comprehending the gene expression of EcN at the very end of the culturing conditions. Therefore, the samples for transcriptomics were taken from the stationary phase prior to the harvesting point. In the results presented below, the transcriptomes of EcN from two different time points of fermenter-culture conditions namely the start of the stationary phase and the end of the stationary phase were compared to the transcriptome of LB-grown EcN.

4.2.1. **Enhanced expression of fitness factors of EcN in fermenter culture condition**

As mentioned in the introduction, EcN possesses several fitness factors that combinedly said to contribute to the observed probiotic effects of EcN. We were interested to examine the regulation of some of these fitness factors in the EcN fermenter-cultures. Interestingly, one of the most heavily upregulated gene clusters in case of both the fermenter-cultures was the curli fimbrial determinant, responsible for biofilm formation in *E. coli* (Barnhart and Chapman, 2006). The genes *csgB* and *csgA* of the curli determinant were upregulated with highest $\log_2$ fold change of 7.73 and 8.57, respectively at the start of the stationary phase fermenter-culture, and 5.96 and 6.96, respectively at the end of the stationary phase fermenter-culture (**Figure 4.2. 1_A**). Additionally, analysis of the genes belonging to other major fimbrial determinants in

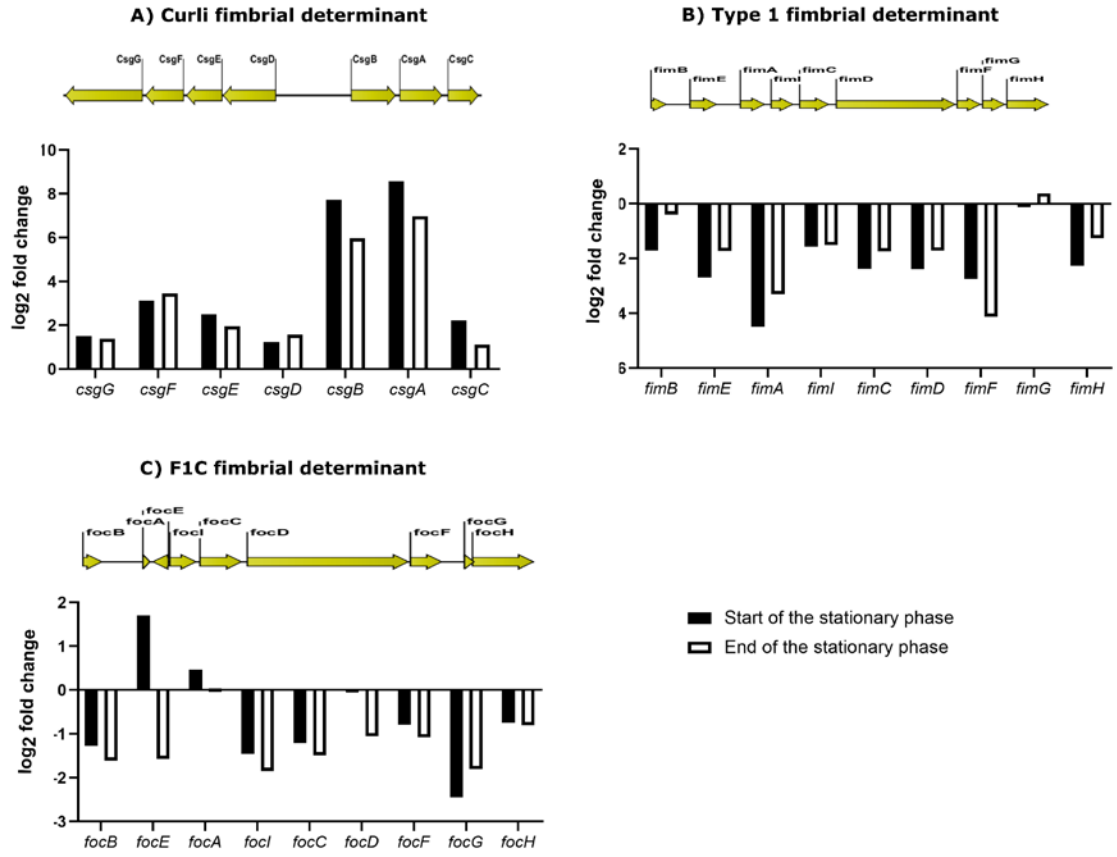

Figure 4.2. 1: Gene regulation of different fimbrial determinants of EcN. The regulation of genes (represented in $\log_2$ fold change) belonging to **(A)** curli fimbrial determinant, **(B)** type 1 fimbrial determinant, and **(C)** F1C fimbrial determinant in EcN fermenter-cultures: start of the stationary phase (black bars) and end of the stationary phase (white bars).

EcN such as Type 1 and F1C fimbrial determinant revealed that most of the genes in these clusters were downregulated (**Figure 4.2. 1_B, C**).

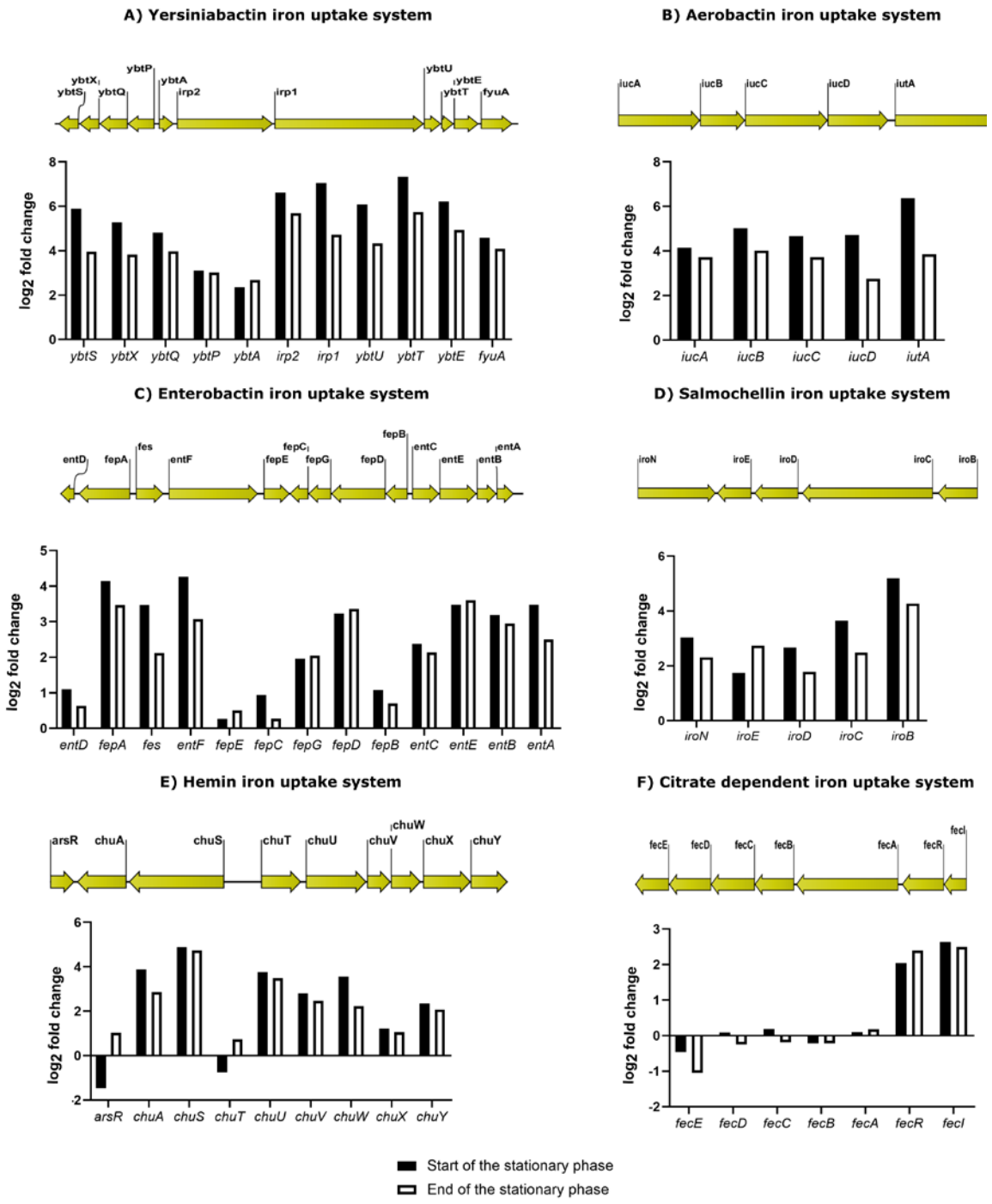

Figure 4.2. 2: Gene regulation of six iron uptake systems in EcN fermenter-cultures. The graphs depict the regulation of genes (represented in $\log_2$ fold change) belonging to the iron uptake systems of EcN in the fermenter-cultures: start of the stationary phase (black bars) and end of the stationary phase (white bars).

Another most intriguing observation was the upregulation of genes belonging to the iron uptake systems present in EcN (**Figure 4.2. 2**). In particular, the genes of the yersiniabactin system (A) were highly upregulated in case of both the fermenter-cultures followed by aerobactin (B), salmochellin (D), enterobactin (C) and hemin (E) iron uptake systems. In contrast, most of the genes of the citrate dependent iron uptake system (F) were downregulated. Apart from the six ferric iron uptake systems, the genes of the ferrous iron transport system (EfeUOB) were also minimally upregulated in the stationary phase cultures (Annexure 2).

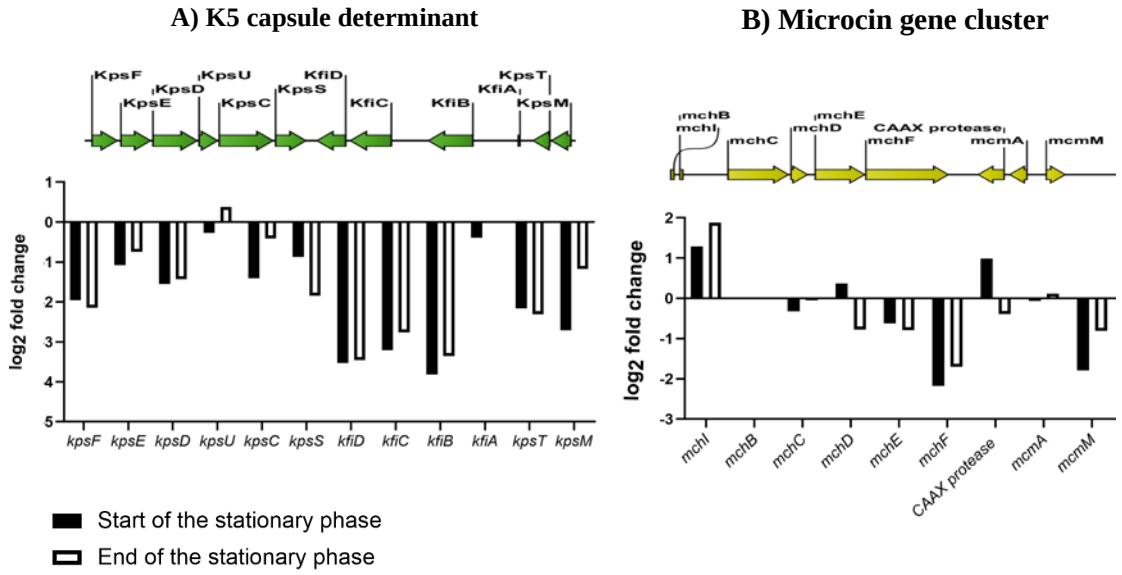

Figure 4.2. 3: Gene regulation of the K5 capsule determinant (A) and the microcin gene cluster (B). The graphs depict the regulation of genes (represented in $\log_2$ fold change) in the EcN fermenter-cultures: start of the stationary phase (black bars) and end of the stationary phase (white bars).

Furthermore, the regulation of genes belonging to the microcin gene cluster producing the two antibacterial compounds: microcin M and H47 involved in the antagonistic effect of EcN (Patzer et al., 2003), the K5 polysaccharide capsule, O6-type LPS and the H1 type flagella associated with immunomodulatory effects of EcN (Grozdanov et al., 2002;Troge et al., 2012;Nzakizwanayo et al., 2015) were analysed. The analysis of microcins and K5 capsule gene clusters revealed a significant downregulation of genes belonging to them (**Figure 4.2. 3**) and the same was observed for the genes involved in flagella production (**Table 4. 1**). Nevertheless,

the genes associated with LPS production showcased a varied expression pattern. The two major clusters attributed to LPS production were *waa* and *wbb* LPS gene clusters, of which the genes of the former presented a reduced expression in general, and the latter showed an increased expression pattern (**Table 4. 1**).

Table 4. 1: Regulation of genes related to flagella and LPS production in EcN

Gene ID	Gene annotation	log_2 fold change	
		Start of the stationary phase	End of the stationary phase
Flagella production-related genes			
EcN1917_0340	Flagellar biosynthesis protein FlhA	-1,151	-0,931
EcN1917_0341	Flagellar motor rotation protein MotB	-2,230	-0,820
EcN1917_1219	Flagellar biosynthesis protein FlgN	-1,036	-0,566
EcN1917_1220	Negative regulator of flagellin synthesis FlgM	-0,156	0,098
EcN1917_1221	Flagellar basal-body P-ring formation protein FlgA	0,072	-1,630
EcN1917_1222	hypothetical protein	-0,073	-0,049
EcN1917_1223	Flagellar basal-body rod protein FlgB	-1,341	-2,492
EcN1917_1224	Flagellar basal-body rod protein FlgC	-1,099	-2,159
EcN1917_1225	Flagellar basal-body rod modification protein FlgD	-0,601	-0,497
EcN1917_1226	Flagellar hook protein FlgE	-1,061	-0,994
EcN1917_1227	Flagellar basal-body rod protein FlgF	-0,872	-0,956
EcN1917_1228	Flagellar basal-body rod protein FlgG	-0,408	-0,647
EcN1917_1229	Flagellar L-ring protein FlgH	-1,357	-1,893
EcN1917_1230	Flagellar P-ring protein FlgI	0,091	-1,236
EcN1917_1231	Flagellar protein FlgJ [peptidoglycan hydrolase]	1,900	1,570
EcN1917_1232	Flagellar hook-associated protein FlgK	-0,639	-0,040
EcN1917_1233	Flagellar hook-associated protein FlgL	-2,418	-1,665
EcN1917_2050	Flagellar protein FlhE	0,770	0,185
EcN1917_2051	Flagellar biosynthesis protein FlhA	-1,512	-2,157
EcN1917_2052	Flagellar biosynthesis protein FlhB	-0,922	-1,814
EcN1917_2063	Flagellar motor rotation protein MotB	-2,000	-1,182
EcN1917_2064	Flagellar motor rotation protein MotA	-2,458	-1,606
EcN1917_2065	Flagellar transcriptional activator FlhC	-1,606	-1,410
EcN1917_2066	Flagellar transcriptional activator FlhD	0,523	-0,050
Lipopolysaccharide gene cluster (*waa*)			
EcN1917_2295	Phosphomannomutase	0,603	-0,733
EcN1917_2296	hypothetical protein	1,957	-1,321
EcN1917_2297	Glycosyltransferase	2,861	0,180

EcN1917_2298	UDP-glucose 4-epimerase	0,405	-2,368
EcN1917_2299	Putative glycosyltransferase	0,427	-1,733
EcN1917_2300	Glycosyl transferase	-0,668	-3,421
EcN1917_2301	Glycosyl transferase	0,123	-0,814
EcN1917_2302	Antigen polymerase O6	-0,354	-2,675
EcN1917_2303	Membrane protein involved in the export of O-antigen 2C teichoic acid lipoteichoic acids	-1,617	-2,019
Lipopolysaccharide gene cluster (*wbb*)			
EcN1917_4044	Lipopolysaccharide heptosyl transferase I	-1,004	-0,713
EcN1917_4045	O-antigen ligase	2,988	1,625
EcN1917_4046	Beta-1,2 C3-glucosyltransferase	2,392	0,457
EcN1917_4047	UDP-galactose:(galactosyl) LPS alpha1,2 C2-galactosyltransferase WaaW	2,370	1,087
EcN1917_4048	Lipopolysaccharide core biosynthesis protein RfaY	3,344	2,105
EcN1917_4049	UDP-glucose:(glucosyl) lipopolysaccharide alpha-1,2 C2-glucosyltransferase	2,324	0,777
EcN1917_4050	UDP-glucose:(glucosyl) lipopolysaccharide alpha-1,2 C3-glucosyltransferase WaaO	1,350	0,048
EcN1917_4051	Lipopolysaccharide core biosynthesis protein WaaP, heptosyl-I-kinase	2,074	1,238
EcN1917_4052	UDP-glucose:(heptosyl) LPS alpha1,2 C3-glucosyltransferase WaaG	2,100	1,216
EcN1917_4053	Lipopolysaccharide heptosyl transferase III	0,956	0,529
EcN1917_4054	3-deoxy-D-manno-octulosonic-acid transferase	-0,022	0,110

Overall, transcriptomic analysis of genes contributing to various fitness factors of EcN in fermenter conditions revealed a strong upregulation of the curli fimbrial determinant (*csg*) and iron uptake systems which were particularly known to play an important role in probiotic properties like efficient colonisation of the gut, biofilm formation and out-competing pathogenic bacteria (Deriu et al., 2013;Carter et al., 2019).

4.3. **Transcriptomic response of EcN coincubated with pathogenic *E. coli* strain EHEC EDL933 and non-pathogenic *E. coli* K-12 strain MG1655**

Transcriptome analysis is an attractive tool to understand the factors in EcN that are influenced by and might influence other *E. coli* strains. In this study, we were interested in characterizing the changes in EcN's genome during coincubation with pathogenic EHEC strain EDL933 (EDL933) and non-pathogenic K-12 strain MG1655 (MG1655). EcN had been reported

reducing the growth and Stx-level of EHEC strains during coculture (Reissbrodt et al., 2009;Rund et al., 2013;Mohsin et al., 2015). However, for the transcriptome analysis, the EcN and EDL933 in the coincubation must be well separated in order to be able to isolate the RNA of EcN for the subsequent transcriptome analysis. Therefore, the coincubation studies were performed in a Transwell system. The Transwell system used in this study had an insert with a membrane pore size of 0.4 μm and this acted as a physical barrier between the EcN in the lower compartment and EDL933/MG1655 in the upper compartment. Although the Transwell system prevented cell-cell contact, it facilitated the diffusion of bacterial secretome and phages from one compartment to the other. Our initial challenge was to investigate if EcN can exert its growth reduction and anti-shiga toxin effect on EDL933 strain in a Transwell system.

4.3.1. Shiga toxin reduction by EcN in a Transwell system

EcN and EDL933 strains were coincubated in a Transwell system as described in the method section 3.4.2. Samples were taken at several time points from insert compartments containing EDL933, which were incubated with or without EcN containing wells of the Transwell setup. Stx-level of the samples were determined with a Verotoxin ELISA kit after sterile filtration (3.1.10). The results clearly indicated that EcN reduced the Stx level of EDL933 strain during coincubation in a Transwell system. The earliest influence of EcN upon EDL933 was observed at 5 h incubation which resulted in ~ 48 % reduction and the reduction reached its maximum of ~ 80 % at 7 and 8 h of incubation and a reduction of the Stx level was observed even after 24 h of incubation (~ 60 % reduction) (**Figure 4.3. 1**).

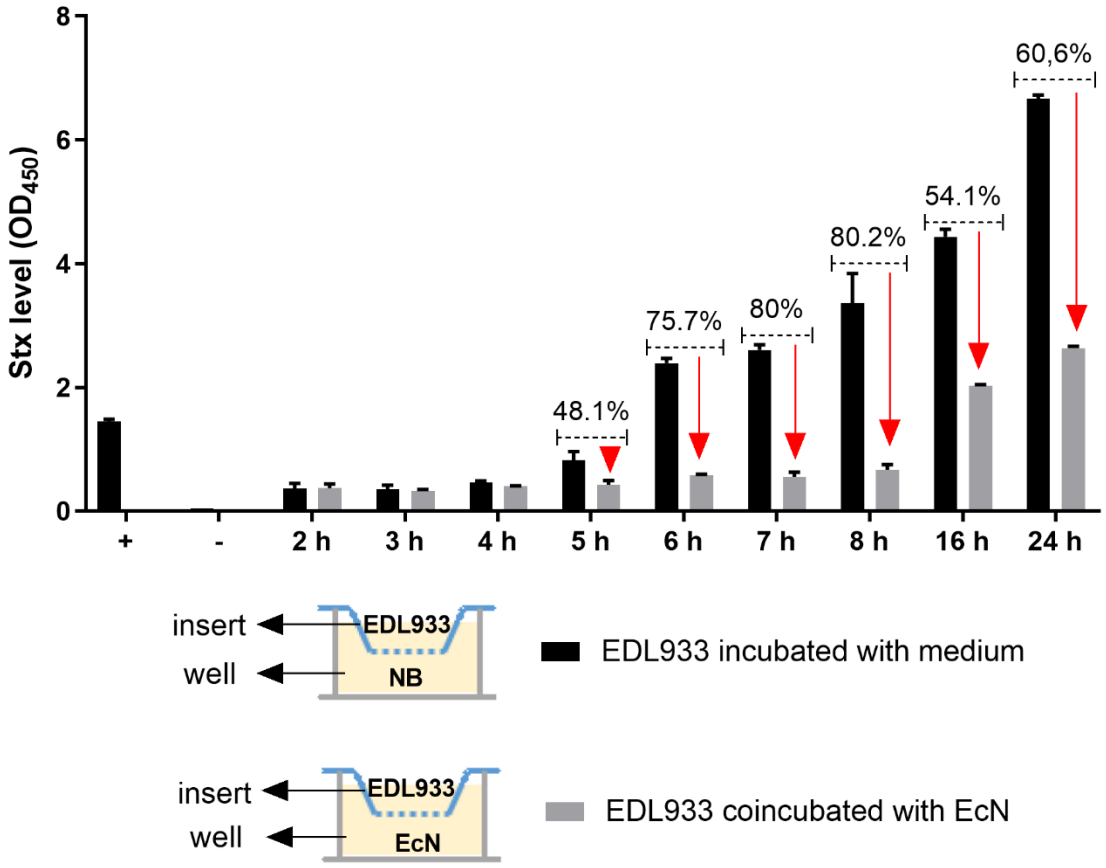

Figure 4.3. 1: Kinetics of Stx reduction by EcN in a Transwell system. The bar graph displays the results of Stx ELISA where the Stx levels were measured at OD_{450}. The black bars represent the Stx level of the EDL933 samples in the insert compartment placed in bacteria-free well (NB – no bacteria) and the gray bars represent the Stx level of the EDL933 samples in the insert compartment located in the well containing EcN. The samples from both the EDL933 compartments were taken for Stx ELISA, after several time points of coincubation in the Transwell system at 37 ˚C, static. "+": positive control from the Verotoxin ELISA kit; "-": negative control (0.9 % saline)

4.3.2. **Time point-based RNA isolation from EcN coincubated with EDL933 and MG1655**

From the results of Stx ELISA in the Transwell system, it was evident that EcN negatively regulated the Stx level of EDL933 and a significant reduction of ~ 48 % was detected as early as 5 h after coincubation. Due to such an early influence of EcN on Stx level, we performed the transcriptomics of EcN at the time points 3 h, 5 h, 7 h and 8 h of coincubation with or without EDL933 in a Transwell system. In order to investigate whether EcN could exhibit a strain-specific transcriptomic change, EcN coincubated with and without MG1655 was also subjected for transcriptomic analysis. The experimental set up is graphically depicted in **Figure 4.3. 2**. For transcriptomic analysis, we isolated RNA from EcN incubated with inserts containing either bacteria-free medium (NB) or EDL933/MG1655.

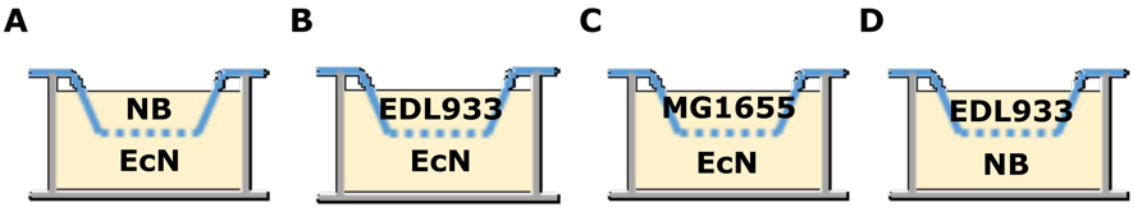

Figure 4.3. 2: Graphical depiction of the Transwell setup for RNA isolation. The Transwell set up consists of cell-impermeable 0.4 µm ThinCert^{TM} cell culture insert placed in a well. The RNA for transcriptomics were isolated from EcN (in the well) incubated **(A)** alone (NB), **(B)** with EDL933 and **(C)** with MG1655. The Transwell set up **(D)** was a control set up to determine the Stx level in EDL933 in the absence of EcN cells. NB – no bacteria.

Along with RNA isolation, the Stx-level in the EDL933 compartments incubated with or without EcN was determined at 3 h, 5 h, 7 h and 8 h after coincubation. The kinetics of Stx reduction further validated our previous finding on the initial drop in Stx level of EDL933 which was observed after 5 h of coincubation with EcN (**Figure 4.3. 3**).

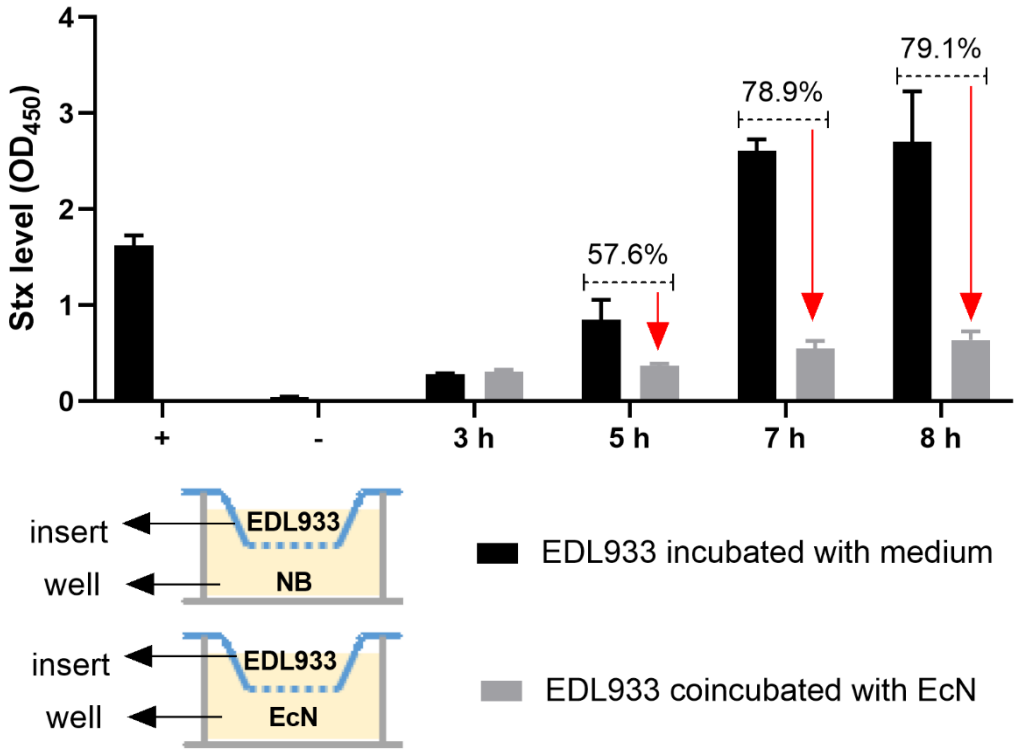

Figure 4.3. 3: Stx reduction in EDL933 by EcN in the Transwell set up. Stx level of EDL933 (in the insert) were determined in the absence of EcN (black bar) and in the presence of EcN (gray bar) after indicated timepoints. "+": positive control from the Verotoxin ELISA kit; "-": negative control (0.9 % saline), NB – no bacteria.

Simultaneously, CFUs/ml of EcN, EDL933 and MG1655 at the specified time points of coincubation were determined by plating 50 µl of the serial dilutions (6^{th} and 7^{th} dilutions) on the ECC plates. In addition, undiluted medium from no bacteria-compartment (NB) was plated on ECC plates and no colonies were detected after 24 h pointing out that the insert served as an efficient barrier for bacterial cells (**Figure 4.3. 4_A, D**). In the Transwell system, the CFUs/ml of EcN were relatively higher than that of other *E. coli* strains in the coincubation. Precisely, in EcN and EDL933 coincubation, the CFUs/ml of EcN was 3.4-fold, 4.25-fold, 5.78-fold and 4.12-fold higher than EDL933 after 3 h, 5 h, 7 h and 8 h of coincubation, respectively. Similarly, in EcN and MG1655 coincubation, the CFUs/ml of EcN cells were 2.09-fold, 3.78-fold, 4.05-fold and 5.50-fold higher than MG1655 after 3 h, 5 h, 7 h and 8 h of coincubation, respectively. On

the other hand, CFUs/ml of EcN and EDL933 did not differ significantly in the presence or absence of another *E. coli* strain in the Transwell setup (**Figure 4.3. 4**).

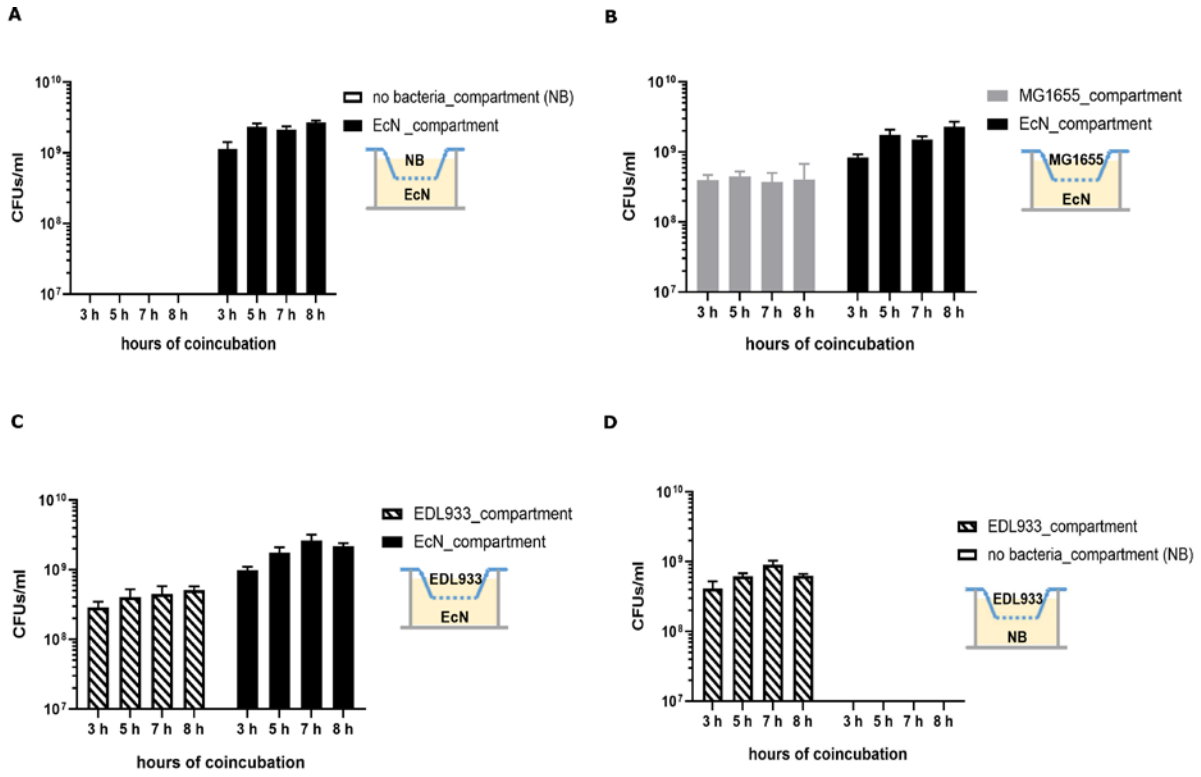

Figure 4.3. 4: Growth kinetics of *E. coli* strains in the Transwell set up for transcriptomics. The CFUs/ml of the *E. coli* strains either alone or in coincubation with another *E. coli* strain at the indicated timepoints at which the RNA was isolated. EcN: black bar, EDL933: black striped lines bar, MG1655: gray bar, (NB) – no bacteria.

4.3.3. Transcriptomic response of EcN towards EDL933 and MG1655

The RNA samples were deep-sequenced and were analysed as explained in method sections 3.5.1 and 3.5.2. As mentioned in the previous section, the transcriptome of EcN coincubated with and without EDL933 in the Transwell system was compared with each other and similar analysis was also performed with and without MG1655. The differentially expressed genes were identified using DESeq2 (version-1.16.1). In all cases, only genes with maximum Benjamin-Hochberg corrected p-value (padj) less than or equal to 0.05, were classified as significantly regulated genes. Gene regulations in EcN coincubated with EDL933 or MG1655 after 3 h, 5 h, 7 h and 8 h were presented as MA plots (**Figure 4.3. 5** & **Figure 4.3. 6**).

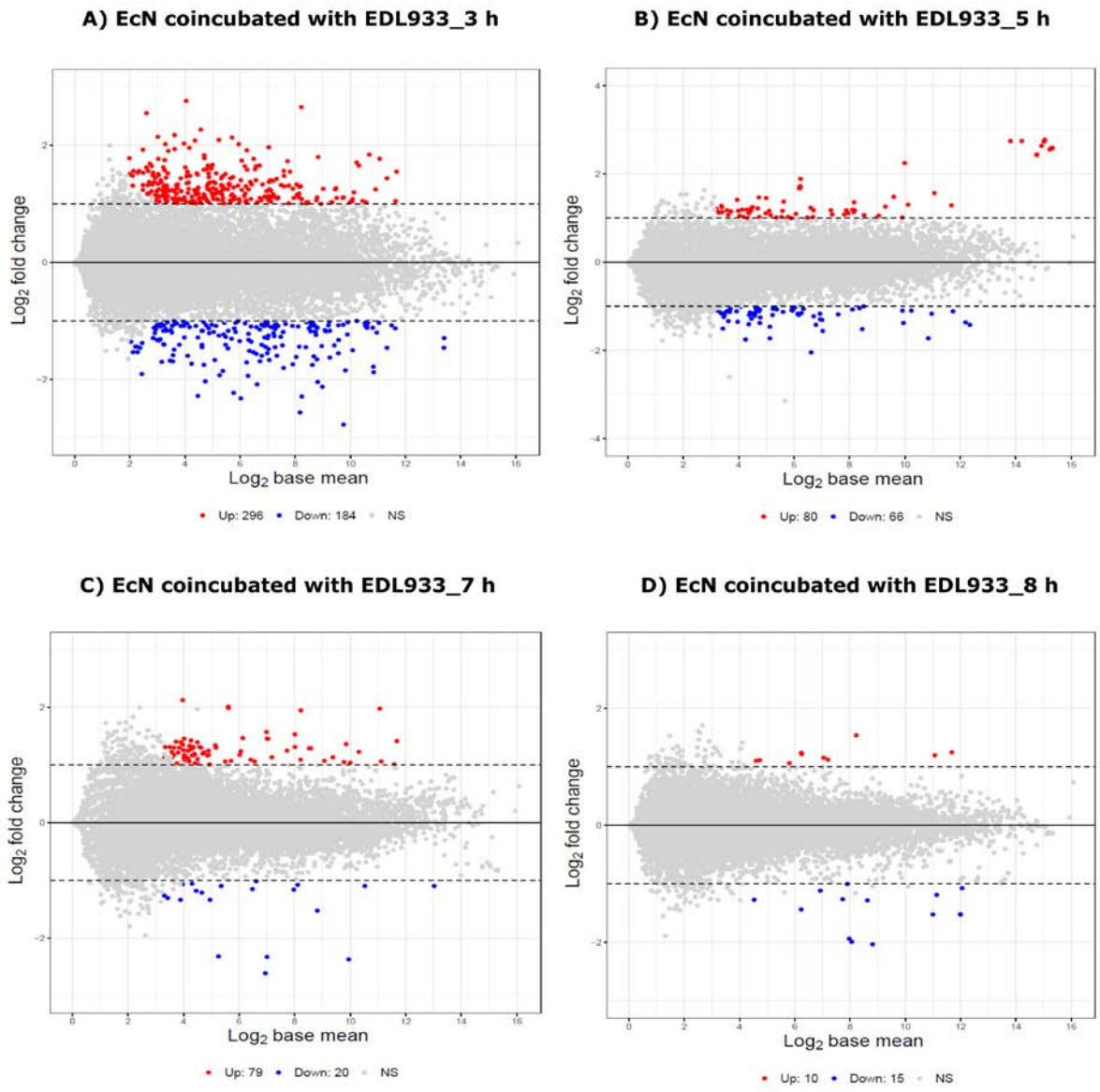

Figure 4.3. 5: MA plots representing the differentially regulated genes in EcN after coincubation with EDL933 for 3 h (A), 5 h (B), 7 h (C) and 8 h (D) in a Transwell system. The expression of each EcN gene was compared for the coincubation with and without EDL933 at each time point. The red dots in the MA plot represent the genes that were significantly upregulated (Up) with $\log_2$ fold change > 1, padj < 0.05 and blue dots represent the genes that were significantly downregulated (Down) with $\log_2$ fold change < -1, padj < 0.05. The gray dots represent the genes which were not significantly regulated in EcN (NS). The horizontal broken lines in the MA plot mark the cut-off value for $\log_2$ fold change as > 1 for (upregulated genes) and < -1 for (downregulated genes). The genes within these lines were not significantly regulated. The gray dots above and below these lines were not significant as their padj value was not less than 0.05. Log_2 fold change: base 2 logarithm of fold-change; Log_2 base mean: base 2 logarithm of mean expression of genes across all the samples.

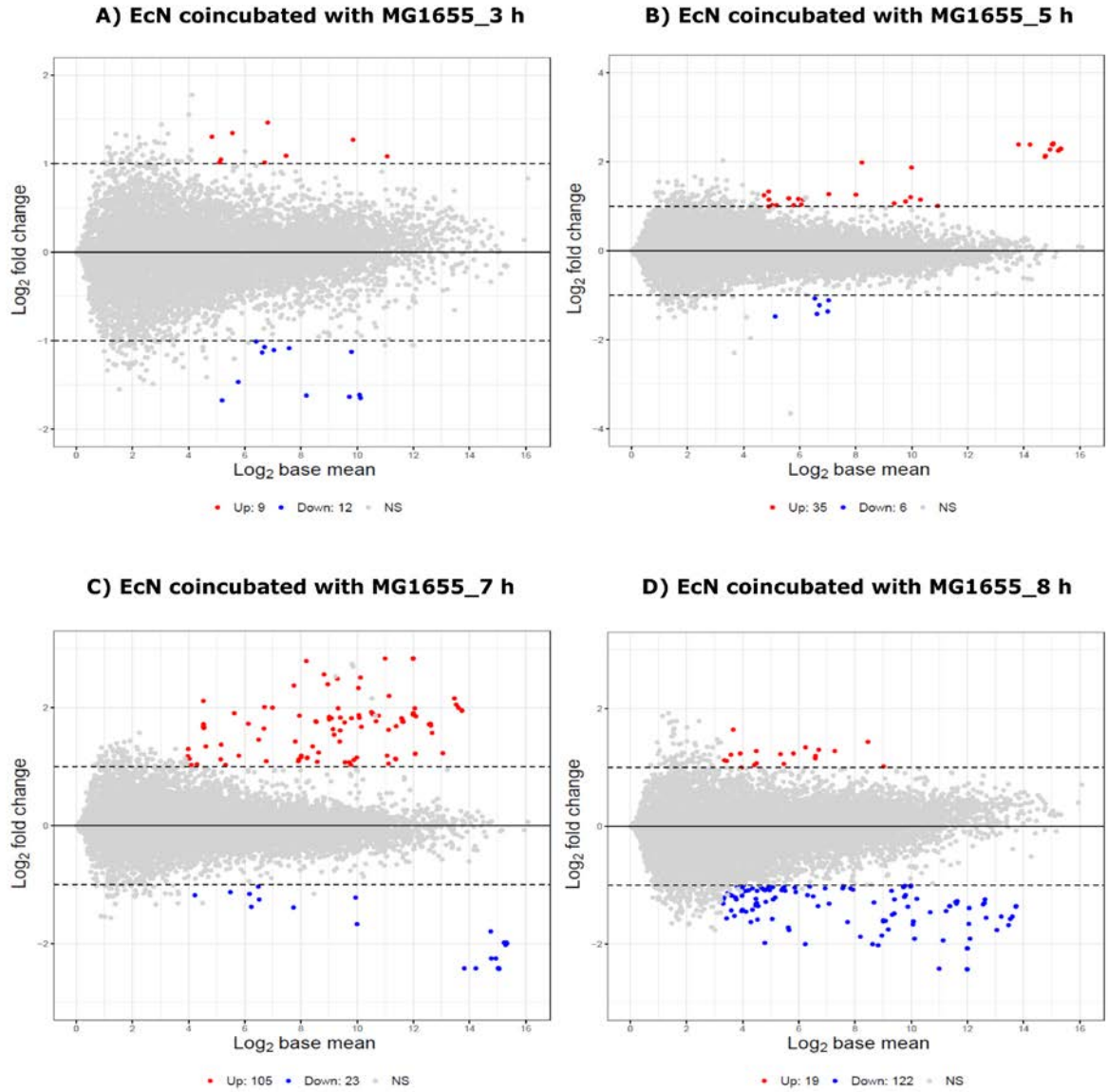

Figure 4.3. 6: MA plots representing the differentially regulated genes in EcN after coincubation with MG1655 for 3 h (A), 5 h (B), 7 h (C) and 8 h (D) in a Transwell system. The expression of each EcN gene was compared for the coincubation with and without MG1655 at each time point. The red dots in the MA plot represent the genes that were significantly upregulated (Up) with $\log_2$ fold change > 1, padj < 0.05 and blue dots represent the genes that were significantly downregulated (Down) with $\log_2$ fold change < -1, padj < 0.05. The gray dots represent the genes which were not significantly regulated in EcN (NS). The horizontal broken lines in the MA plot mark the cut-off value for $\log_2$ fold change as > 1 for (upregulated genes) and < -1 for (downregulated genes). The genes within these lines were not significantly regulated. The gray dots above and below these lines were not significant as their padj value was not less than 0.05. Log_2 fold change: base 2 logarithm of fold-change; Log_2 base mean: base 2 logarithm of mean expression of genes across all the samples.

In addition to MA plots, the regulated genes in EcN coincubated with EDL933 or MG1655, were classified manually using MS Office Excel. The filter option on the fold change column with a number filter command “great than or equal to 1” to categorize the upregulated genes and “less than or equal to -1” for downregulated genes were employed. In both cases, on the padj column a number filter command “less than or equal to 0.05” was provided to sort the significantly regulated genes. The number of genes up and downregulated in EcN when coincubated with EDL933 or MG1655 at different time points were presented in the bar graph (**Figure 4.3. 7**).

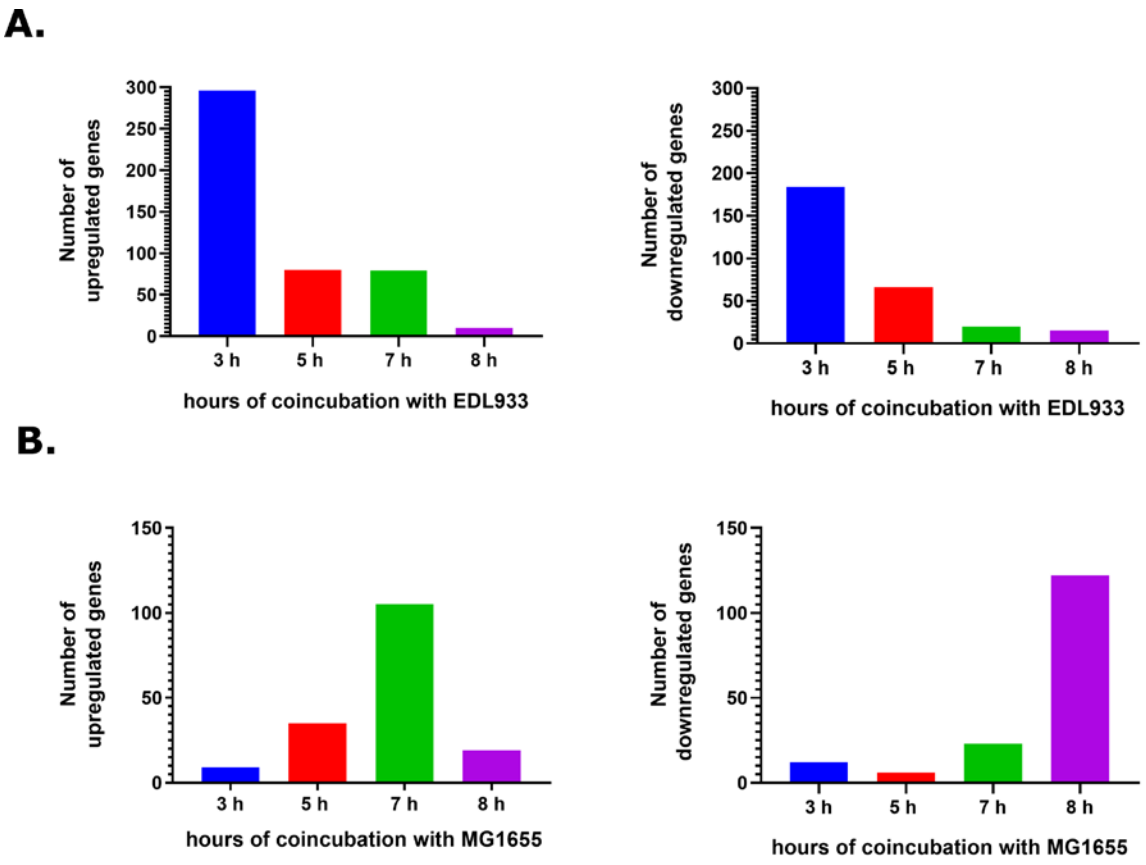

Figure 4.3. 7: Kinetics of differentially regulated EcN genes. The graphs present the number of genes upregulated (left) and downregulated (right) in EcN at the indicated time points when coincubated with either **(A)** EDL933 or **(B)** MG1655 in a Transwell system.

Both MA plots and bar graphs clearly show that at 3 h time point of coincubation with EDL933, the maximum number of genes were regulated (up – 296 genes and down – 184 genes) in EcN, and at the following time points, a gradual decline in the regulated number of genes was observed. Unlike above, EcN coincubated with MG1655 exhibited a differential pattern for the kinetics of the number of genes regulated at different time points. Further, to assess the specificity of EcN's response towards the *E. coli* present in coincubation, Venn diagrams were plotted to quantitatively measure the genes that were specifically regulated in EcN at an indicated time point in response to either EDL933 or MG1655. Venny 2.0 online tool was used to create the Venn diagrams. EcN coincubated with EDL933 elicited the upregulation of genes that were mostly EDL933-specific response at all the investigated time points (**Figure 4.3. 8_A, B, C and D**). The above-analysed data set were employed to generate a bar graph and revealed that the maximum percentage of genes in EcN were uniquely upregulated in response to EDL933 (**Figure 4.3. 8_E**). Similarly, Venn diagrams and a percentage bar graph were also created for the downregulated genes in EcN and illustrated that EcN evoked a similar pattern of response except at 8 h time point at which 67 % of downregulated genes were common to both EDL933 and MG1655 coincubation (**Figure 4.3. 9**).

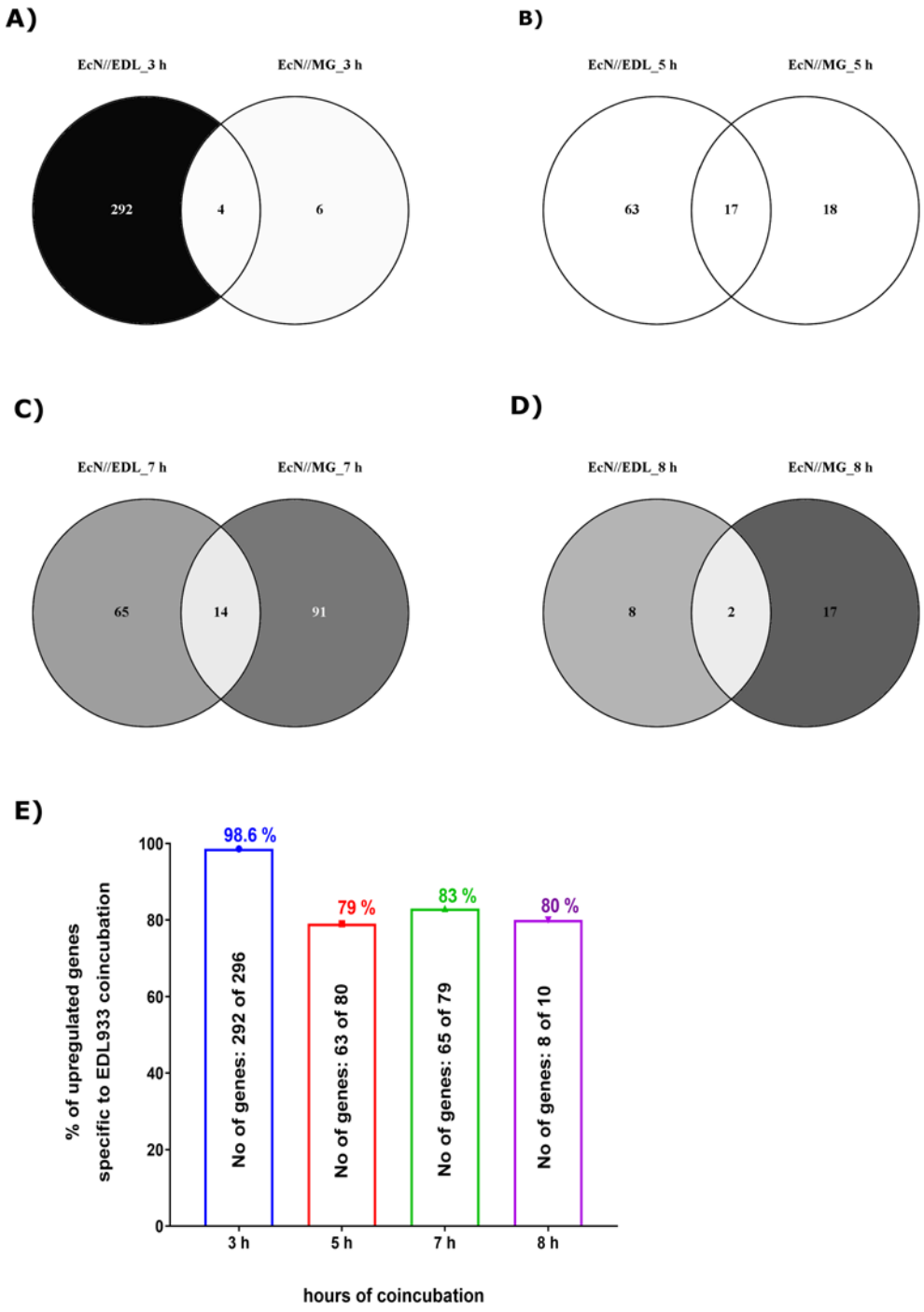

Figure 4.3. 8: Specific upregulation of genes in EcN as a response to EDL933 coincubation. Venn diagrams show the number of genes that were upregulated in EcN specifically to EDL933 (left circle) and MG1655 (right circle) coincubation, the number of genes that were upregulated commonly in EcN for both (EDL933 and MG1655) coincubations are mentioned in the intersection region. Venn diagrams represent genes upregulated after **(A)** 3 h, **(B)** 5 h, **(C)** 7 h and **(D)** 8 h of coincubation. The bar graph **(E)** depicts the percentage of genes that were specifically upregulated in EcN as a response to EDL933 at 3 h (blue), 5 h (red), 7 h (green) and 8 h (magenta) post incubation.

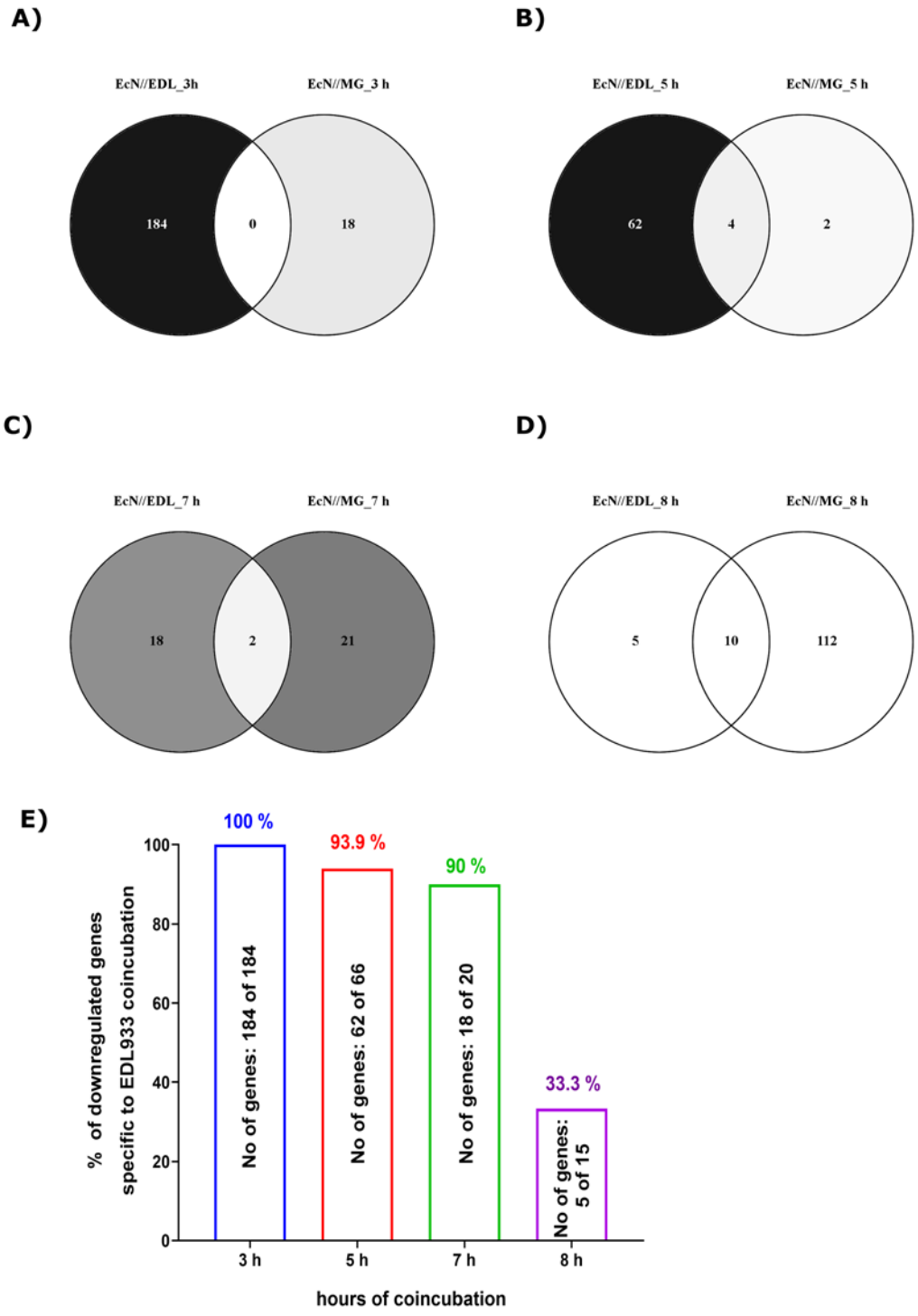

Figure 4.3. 9: Specific downregulation of genes in EcN as a response to EDL933 coincubation. Venn diagrams show the number of genes that were downregulated in EcN specifically to EDL933 (left circle) and MG1655 (right circle) coincubation, the number of genes that were downregulated commonly in EcN for both (EDL933 and MG1655) coincubations are mentioned in the intersection region. Venn diagrams represent genes downregulated after **(A)** 3 h, **(B)** 5 h, **(C)** 7 h and **(D)** 8 h of coincubation. The bar graph **(E)** depicts the percentage of genes that were specifically downregulated in EcN as a response to EDL933 at 3 h (blue), 5 h (red), 7 h (green) and 8 h (magenta) post incubation.

The analysis of transcriptomic results clearly demonstrated a dramatic change in the transcriptome of EcN at 3 h post coincubation with EDL933. Accurately at 3 h time point, 98.6 % of upregulated genes (292 genes out of 296 genes) and 100 % of downregulated genes in EcN were an EDL933 driven specific response. Considering the above finding we attempted to investigate the nature of EcN's genes that were regulated at that time point. Their functions were predicted as described in the methods section 3.5.3. In brief, the functional prediction of genes was performed based on their annotations from EcN's genome. The annotations were further narrowed down to their probable functional role with the help of online databases like Uniprot (https://www.uniprot.org/) or Ecocyc (https://ecocyc.org/). For those genes which were annotated as hypothetical proteins in EcN's genome, their sequences were blasted at https://blast.ncbi.nlm.nih.gov/Blast.cgi under nucleotide blast against *E. coli* taxonomic group to retrieve annotations from their phylogenetically closest members. Finally, genes were sorted into different functional groups based on their predicted functions. The results of functional grouping are presented as column graphs (**Figure 4.3. 10** and **Figure 4.3. 11**). In addition, functional details of up and downregulated genes of EcN when coincubated with EDL933 for 3 h were presented in Annexure 3 (Table 8.1 and Table 8.2).

The functional grouping of upregulated genes revealed that in general, the majority of upregulated genes were metabolism-related genes which included amino acid transport and metabolism (25 genes), nucleotide metabolism (15 genes), carbohydrate transport and metabolism (12 genes), LPS metabolism (9 genes), and cell wall/membrane biogenesis (7 genes). The other most upregulated group of genes were transport-related genes like putative transporters (22 genes), iron uptake and sequestration (22 genes), and efflux systems (9 genes). Besides, genes involved or related to transcription and translation (27 genes), replication and

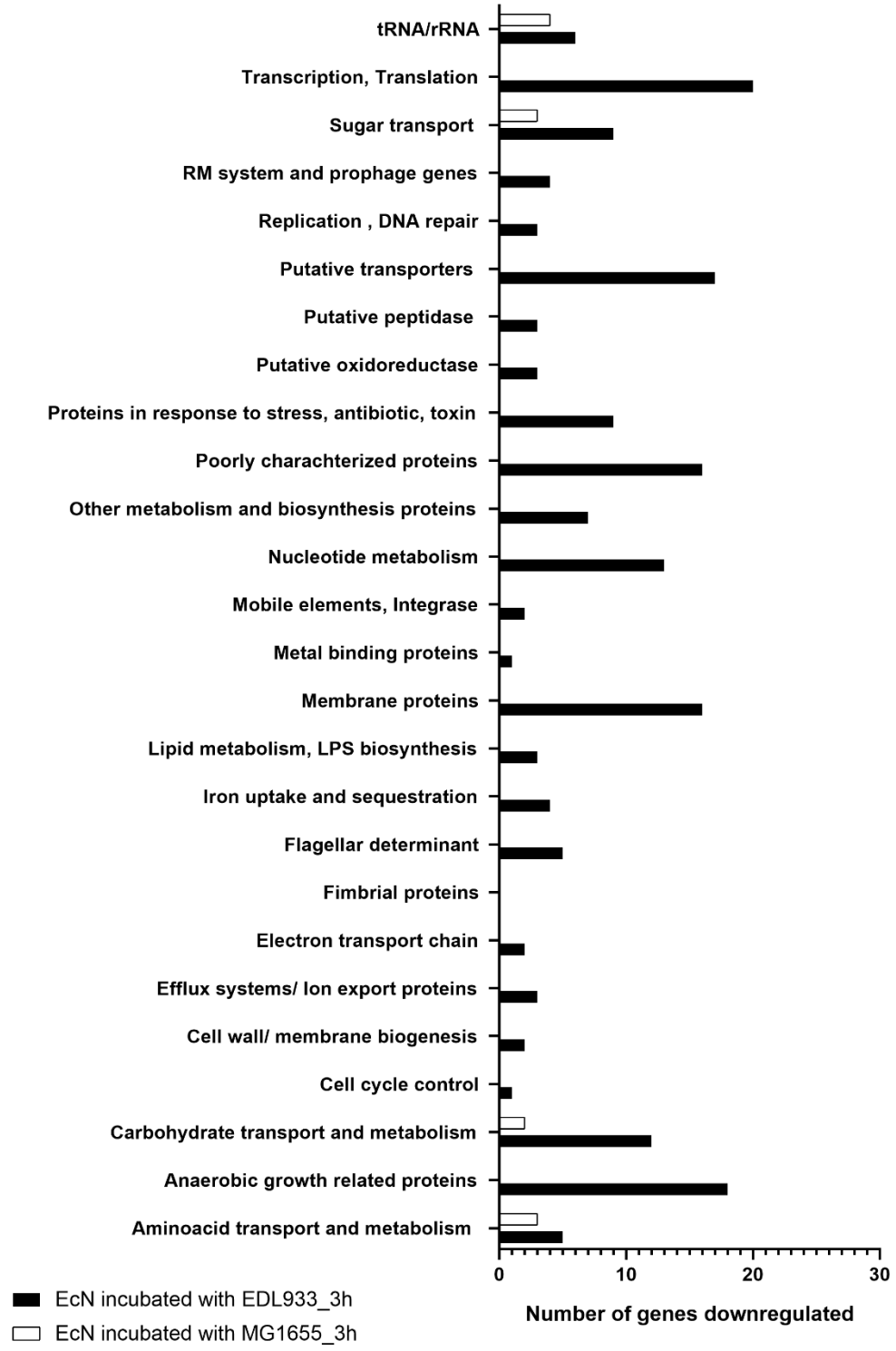

Figure 4.3. 10: Functional grouping of upregulated genes in EcN. The graph displays the number of EcN's genes that were upregulated (log_2 fold change > 1, padj < 0.05) under each functional group when coincubated with EDL933 (black bars) or MG1655 (white bars) for 3 h in a Transwell system.

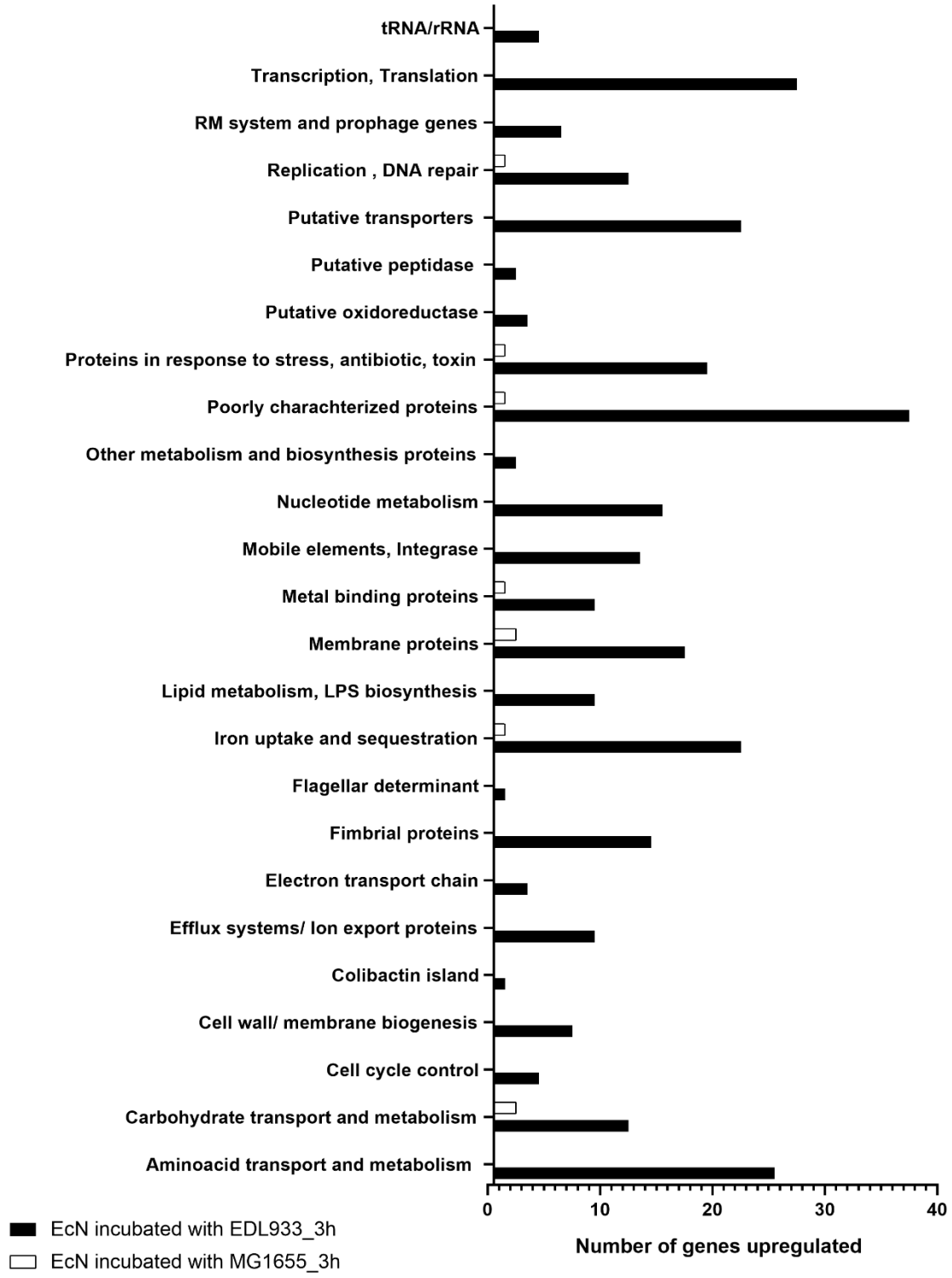

Figure 4.3. 11: Functional grouping of downregulated genes in EcN. The graph displays the number of EcN's genes that were downregulated (log_2 fold change < -1, padj < 0.05) under each functional group when coincubated with EDL933 (black bars) or MG1655 (white bars) for 3 h in a Transwell system.

DNA repair (12 genes), tRNA/rRNA production (4 genes), cell cycle proteins (4 genes) and electron transport chain (3 genes) were also upregulated suggesting an active growth (**Figure 4.3. 10**). Noteworthy were the genes associated with response to stress, antibiotics and toxins (19 genes) and restriction-modification (RM) systems or prophage related genes (7 genes) which were specifically upregulated only in EDL933 coincubation and might be a response driven by *stx*-phages or Stx produced by EDL933. Likewise, fimbrial proteins (13 genes) and one flagellar protein were also specifically upregulated along with 21 membrane proteins, 37 poorly characterized genes and 14 mobile elements (**Figure 4.3. 10**).

The number of downregulated genes in EcN (184 genes) as a response to EDL933 coincubation was 40 % lesser than the upregulated genes. The functional grouping of downregulated genes indicated that the majority of downregulated genes were associated with metabolism which included nucleotide metabolism (13 genes), carbohydrate transport and metabolism (12 genes), amino acid transport and metabolism (5 genes) and LPS metabolism (2 genes). Likewise, membrane-associated proteins (16 genes) and transport-related genes such as putative transporters (17 genes), iron uptake (4 genes) and efflux systems (3 genes) along with genes relating to transcription and translation (20 genes), replication and DNA repair (3 genes) and electron transport chain (2 genes) were also downregulated in EcN as a specific response to EDL933. Unlike most of the functional groups, the genes associated with fimbrial proteins were identified as particularly upregulated but not downregulated in EcN. On the other hand, the genes of anaerobic growth-related proteins (18 genes) and sugar transport-related proteins (9 genes) were exclusively downregulated (**Figure 4.3. 11**).

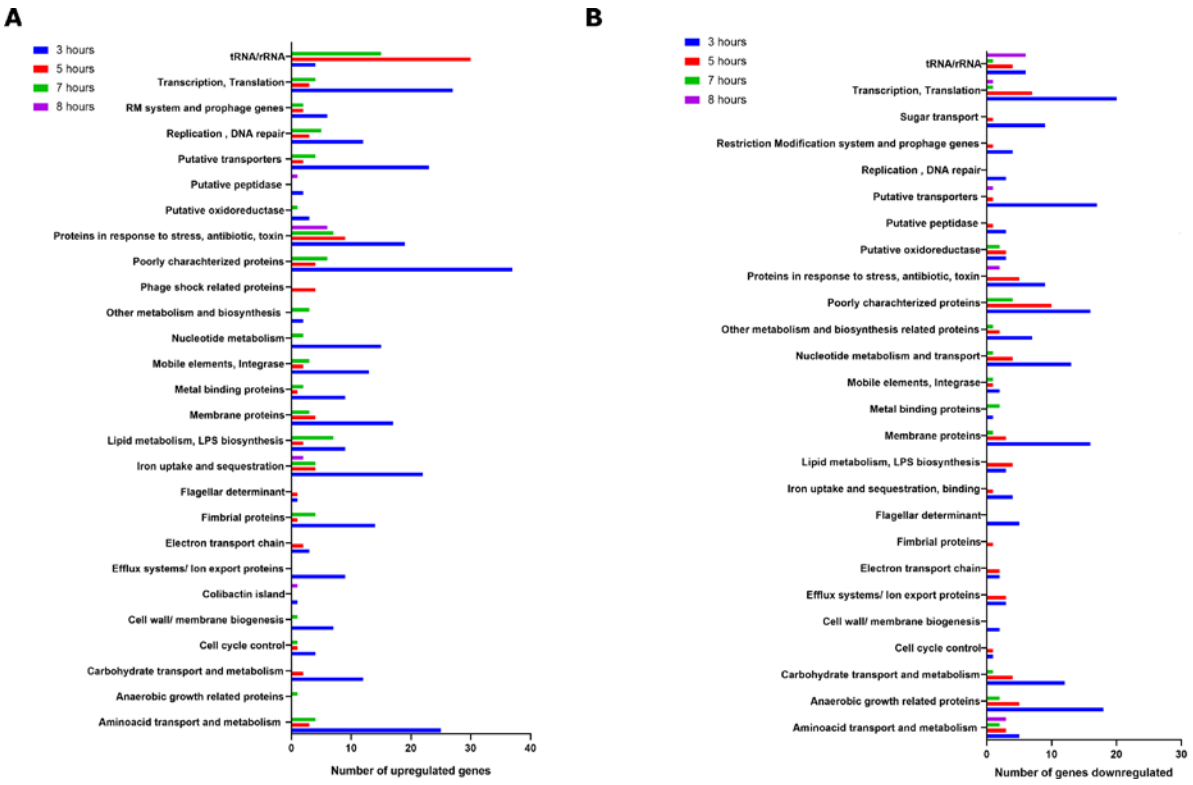

Figure 4.3. 12: Functional grouping of genes up and downregulated in EcN when coincubated with EDL933. The graphs display the result of functional grouping performed for upregulated genes **(A)** with $\log_2$ fold change > 1, padj < 0.05 and downregulated genes **(B)** with $\log_2$ fold change < -1, padj < 0.05 in EcN after coincubated with EDL933 for 3 h (blue), 5 h (red), 7 h (green) and 8 h (magenta) in a Transwell system.

As a next step, the transcriptomic response of EcN incubated with EDL933 for 5 h, 7 h and 8 h was also analysed and a functional prediction was performed for the up and downregulated genes. The transcriptomic analysis revealed that the genes belonging to the functional group iron uptake and sequestration, and genes encoding for proteins in response to stress, antibiotics and toxins were upregulated at all the investigated time points despite the fact the there was a steady decline in the number of genes upregulated over time (**Figure 4.3. 12_A**). Genes of other major functional groups like amino acid transport and metabolism, LPS metabolism, membrane proteins, metal-binding proteins, putative transporters, replication or DNA repair, RM system and prophage genes, transcription and translation, tRNA/rRNA production were upregulated at all the indicated time points except at 8 h after coincubation. Likewise, the EcN genes that were exclusively upregulated during the coincubation (genes associated with fimbrial proteins) were

also upregulated at all time points but not at 8 h (**Figure 4.3. 12_A**). Simultaneously, the functional grouping of EcN's downregulated genes illustrated that the genes related to amino acid transport and metabolism, transcription and translation, tRNA/rRNA production were downregulated at all the investigated time points. Along with them, the expression of genes belonging to functional groups like carbohydrate metabolism, membrane proteins, nucleotide metabolism and proteins in response to stress, antibiotics or toxins was decreased at least at three-time points of the coincubation. The genes related to anaerobic growth-related proteins and sugar transport proteins were exclusively downregulated at three-time points (3, 5 and 7 h) and two-time points (3 h and 5 h) of the coincubation, respectively (**Figure 4.3. 12_B**).

To sum up, with the help of transcriptomic analysis we observed that transcriptomic response exhibited by EcN was specific for the *E. coli* strain present in the coculture.

4.4. Lambdoid phage resistance of EcN

The resistance of EcN towards lysogenic lambda phages propagated from *E. coli* K-12 993 W lysogen was investigated and the results are presented in the following sections.

4.4.1. Testing the lambda lysogeny in EcN cells incubated with lambda phages

As mentioned in the introduction, when a lambda phage infects an *E. coli*, it adopts the lysogenic cycle in which the phage DNA gets integrated into the *E. coli* chromosome as a prophage. The prophage could later switch to lytic cycle upon induction and produce active phage particles. Therefore, to investigate the sensitivity of EcN towards lambda phages, it was inevitable to test both the phage DNA integration and subsequent phage production in EcN. Experiments were performed as described in the method section 3.1.9 to test the lysogeny in EcN when incubated with lambda phages. Firstly, a lambda phage specific PCR was performed with *E. coli* incubated with lambda phages for 24 h as a template. The primer pair λ_Q_F/R

was complementary to part of the lambda phage specific Q gene (a late gene regulator) and could generate an amplicon of size 624 bp.

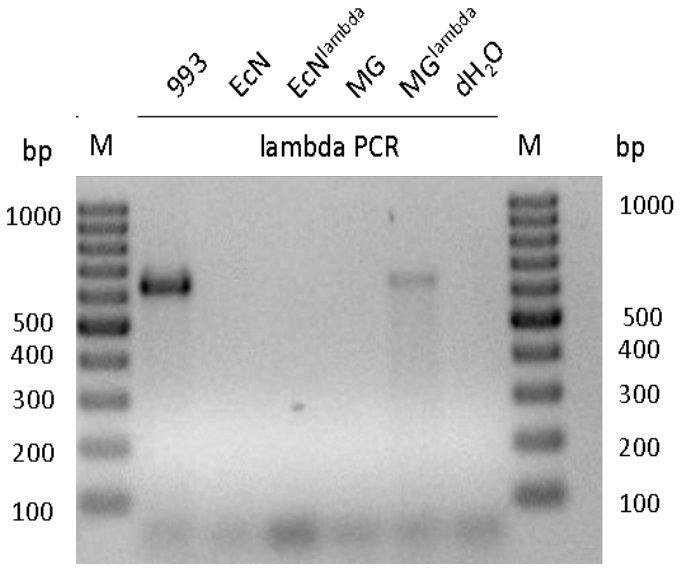

Figure 4.4. 1: PCR to detect the lambda prophage lysogens in EcN and MG1655: EcN or MG1655 was incubated for 24 h with lambda phages (EcN ^{lambda} /MG^{lambda}) or without phages (EcN/MG). The cells were washed twice and plated on LB agar plates after which colonies were collected and screened for the Q gene of the lambda prophage with the primer pair λ_Q_F/R (624 bp). 993: *E. coli* K-12 993 W lysogenic strain that harbours lambda prophage; dH_2O: water control. Images modified from (Bury et al., 2018)

The PCR results showed that the lambda phage specific amplicon was generated with MG1655 incubated with lambda phages as a template but not with EcN incubated with lambda phages as a template, which indicated the absence of any possible lysogeny in EcN (**Figure 4.4. 1**). In another experiment, the *E. coli* strains (EcN or MG1655) were incubated with lambda phages until the phage titer in the supernatant was measured as zero, after which the cells were harvested and incubated with 1 µg/ml MMC for 16 h. These cocultures were sterile filtered and the phage signal was amplified by incubating with fresh MG1655 for 24 h followed by sterile filtration. The PPA of sterile filtrate (**Figure 4.4. 2**) revealed that when EcN was incubated with lambda phages, no single phage plaque was detected on an MG1655 lawn even after prophage induction and phage signal amplification. On the contrary, the MG1655 incubated with lambda phages produced a very high phage titer upon prophage induction. Thus, the results of the PCR

(**Figure 4.4. 1**) and prophage induction (**Figure 4.4. 2**) showcased a complete lambda phage resistance by EcN.

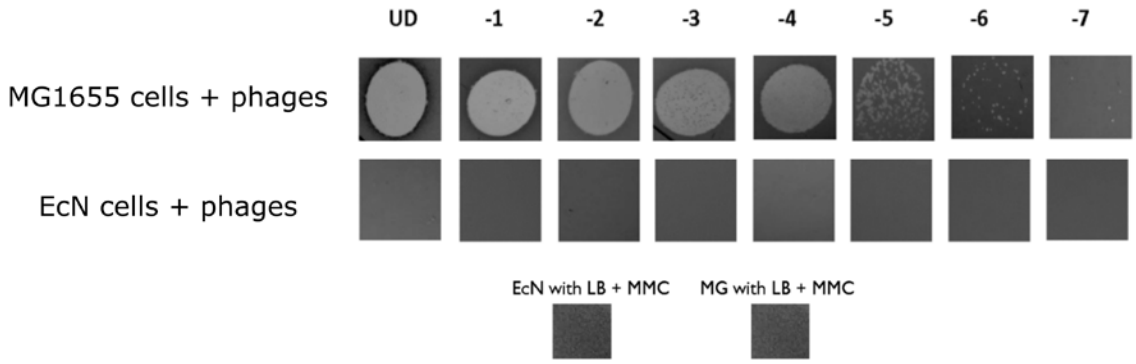

Figure 4.4. 2: Identification of EcN and MG1655 lambda prophage lysogens by PPA: EcN/MG1655 was incubated with lambda phages for 120 h followed by incubation with 1 µg/ml MMC for 16 h and sterile filtration. Phages in the filtrate were amplified by incubation with MG1655 for 24 h after which PFUs/ml were determined with a PPA, UD: undiluted, -1 to -7: tenfold dilutions of the phages in 0.9 % saline. Imaging was performed with Canon PowerShot SX260 HS and processed with ImageJ 1.50i. Images modified from (Bury et al., 2018). Negative controls: EcN/MG with medium (LB) + 1 µg/ml MMC

4.4.2. Role of a lambdoid prophage gene of EcN: the "phage repressor (*pr*)" gene and its role in EcN's lambda phage resistance

As a next approach, we were interested in identifying the factor(s) of EcN that were responsible for its resistance against lambda phages. Earlier in our lab, we observed that EcN was resistant to isolated *stx*-phages from EDL933. This observation was analysed in detail, which involved transcriptomic analysis of EcN in the presence and absence of *stx*-phages (Bury et al., 2018). The experimental design and the results of the transcriptome analysis were elaborately presented in the PhD thesis of Dr Susanne Bury (Bury, 2018). Briefly, EcN was incubated with and without *stx*-phages for 16 h, after which RNA was isolated and subjected to sequencing. The RNA-Seq data have been deposited at the NCBI Gene Expression Omnibus (Edgar et al., 2002) and can be accessed through GEO series accession number: GSE109932 (https://www.ncbi.nlm.nih.gov/geo/query/acc.cgi?acc=GSE109932). The transcriptome analysis revealed strong upregulation of genes corresponding to a lambdoid prophage of EcN

(**Figure 4.3. 3_A)**. By using PHAST – a fast phage search tool (Zhou et al., 2011b) - this prophage was predicted as a complete lambdoid prophage of size 39.8 kb and numbered as prophage 3 in EcN's genome (**Figure 4.3. 3_B**). With the help of literature research, we narrowed down our interest to one of the early genes of prophage 3: EcN_1294, the phage repressor (*pr*) gene which was earlier documented to yield resistance against bacteriophages in *Lactobacillus* when successfully cloned and expressed (Ladero et al., 1998;Alvarez et al., 1999).

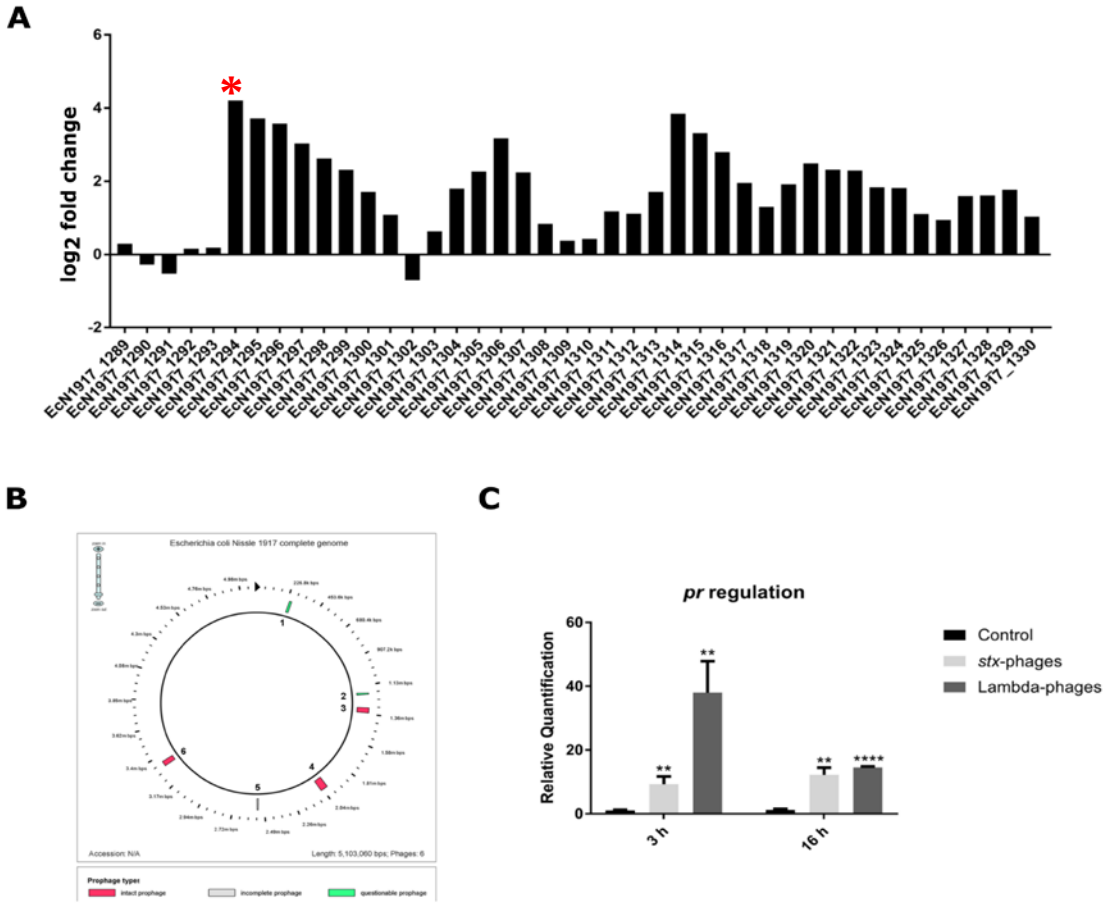

***F*igure 4.4. 3: Regulation of prophage 3 of EcN in the presence of lambdoid phages. (A)** Modulation in expression of genes (in $\log_2$ fold change) belonging to the lambdoid prophage 3 of EcN when incubated with *stx*-phages for 16 h. * highlights the upregulation of *pr* gene (EcN_1294) **(B)** PHAST prediction of EcN's prophages **(C)** Confirmation of the *pr* gene upregulation in EcN incubated with *stx*-phages (light gray bars) and lambda phages (dark gray bars) at the time points 3 h and 16 h by qRT-PCR. The significance was calculated by unpaired t test by comparing to the control (black bars – EcN + LB medium). **p<0.0021, ****p<0.0001. Images modified from (Bury et al., 2018)

The upregulation of EcN's *pr* gene in the presence of lambda and *stx*-phages was validated by qRT-PCR, where relative quantification of *pr* gene was measured with help of the primer pair Pr_RT_F/R after 3 h and 16 h of coincubation (**Figure 4.4. 3_C)**. Followed by confirmation from qRT-PCR, we wanted to examine whether the *pr* gene could directly confer resistance towards lambda phages. To assess this, the *pr* gene was cloned into an inducible pUC19 vector and the lambda phage sensitive MG1655 strain was transformed either with an empty pUC19 plasmid which had no insert (MG1655R) or with pUC19 plasmid harbouring the *pr* gene (MG1655*pr*). PPA was carried out as described in the method section 3.1.8 where 10 µl of serially diluted lambda phages were spotted on 0.7 % LB agar lawn with one of the recombinant MG1655 strains induced with 1 mM IPTG. EcN and MG1655 wildtype strains were used as controls.

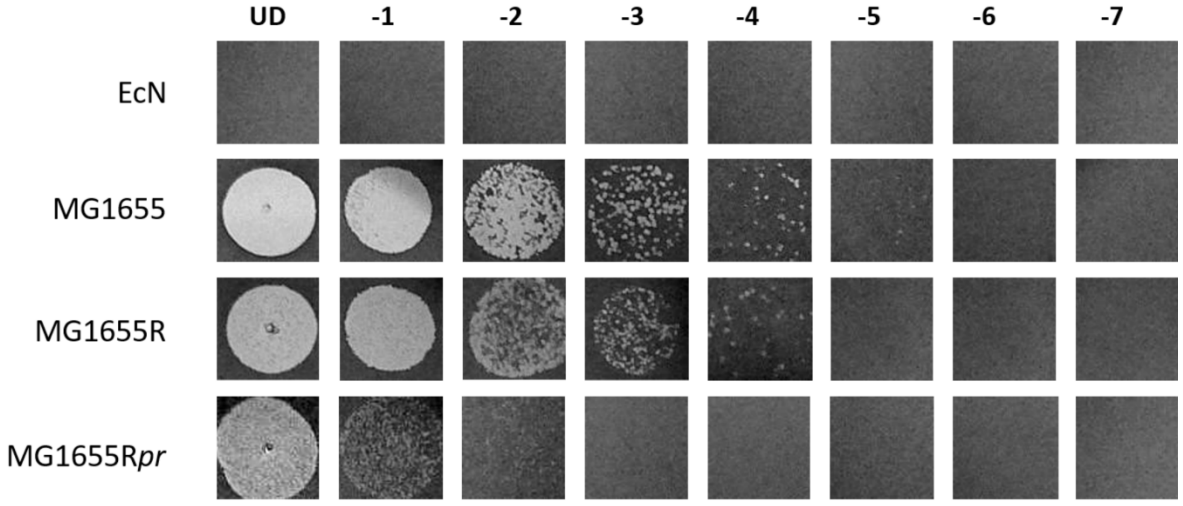

Figure 4.4. 4: Lambda Phage-Plaque-Assay with recombinant MG1655 strains: The image displays the result of PPA performed by dropping serial dilutions of lambda phages (UD: undiluted, -1 to -7: tenfold dilutions of the phages in 0.9 % saline) on the recombinant MG1655 strains. EcN, MG1655 – wildtype strains; MG1655R – recombinant MG1655 strain with an empty pUC19 plasmid; MG1655*pr* – recombinant MG1655 strain with pUC19 plasmid harbouring *pr* gene. Images modified from (Bury et al., 2018)

The PPA clearly showed that the isolated lambda phages could plate on the recombinant MG1655 strain with *pr* gene (MG1655R*pr*) 215- fold less efficiently than on the recombinant MG1655 strain with the pUC19 plasmid that had no insert (MG1655R; vector control) (**Figure**

4.4. 4) and thus demonstrating the significant contribution of EcN's phage repressor (*pr*) gene in its lambda phage resistance.

Apart from the upregulation of EcN's *pr* gene by lambdoid phages (*stx*- and lambda phages), we were intrigued to observe that there was a strong upregulation of antisense transcripts spanning over two early genes of EcN's prophage 3: EcN_1290 (superinfection exclusion protein B (*sieB*)) and EcN_1291 (anti-termination protein N) which were as high as 5.57 and 5.30 $\log_2$ fold change, respectively. Antisense transcripts are defined as transcripts transcribed from the opposite strand of a sense transcript of a protein-coding gene (Pelechano and Steinmetz, 2013). Upon closer analysis with integrated genome browser (IGB) (Freese et al., 2016), a significant upregulation of transcripts (spanning to 1,104 bp) which were mapped to the antisense strand of *sieB* and anti-termination protein N was noted. This upregulation was further confirmed with two-step qRT-PCR performed as described in the method section 3.2.9 with the primer pair 1290_fwd/rev targeting the *sieB* gene. The results showed that in EcN incubated with lambda phages for 3 h, there was a higher upregulation of antisense transcripts of the *sieB* gene than that of its sense transcripts (**Figure 4.4. 5**)

Hence to enquire if the antisense regulation of this transcript was contributing to the phage resistance of EcN, the 1,104 bp sized region was cloned into an inducible pUC19 vector in sense (1290_S) and antisense (1290_AS) orientation. Followed by the transformation of MG1655 strain with either an empty pUC19 plasmid with no insert (MG1655R) or with pUC19 plasmids harbouring, i) *sieB* gene (582 bp) (MG1655*sieB*) or ii) the 1,104 bp region in sense orientation (MG1655_S) or iii) the 1,104 bp region in an antisense orientation (MG1655_AS). PPA was performed by spotting lambda phages on these recombinant MG1655 strains induced with 1 mM IPTG. In parallel, the recombinant MG1655*pr* strain was used as a positive control for phage resistance and the results of PPA are summarized in **Table 4. 2**. The recombinant MG1655*pr* strain showed a significant reduction of about 215-fold in plating efficiency.

However, the other recombinant strains MG1655*sieB*, MG1655_S and MG1655_AS displayed a negligible reduction in plating efficiency when compared to the plating efficiency on MG1655R strain. From these results, we were not able to comprehend the role of the regulation of this antisense transcript in EcN when exposed to lambdoid phages in EcN's lambdoid phage resistance.

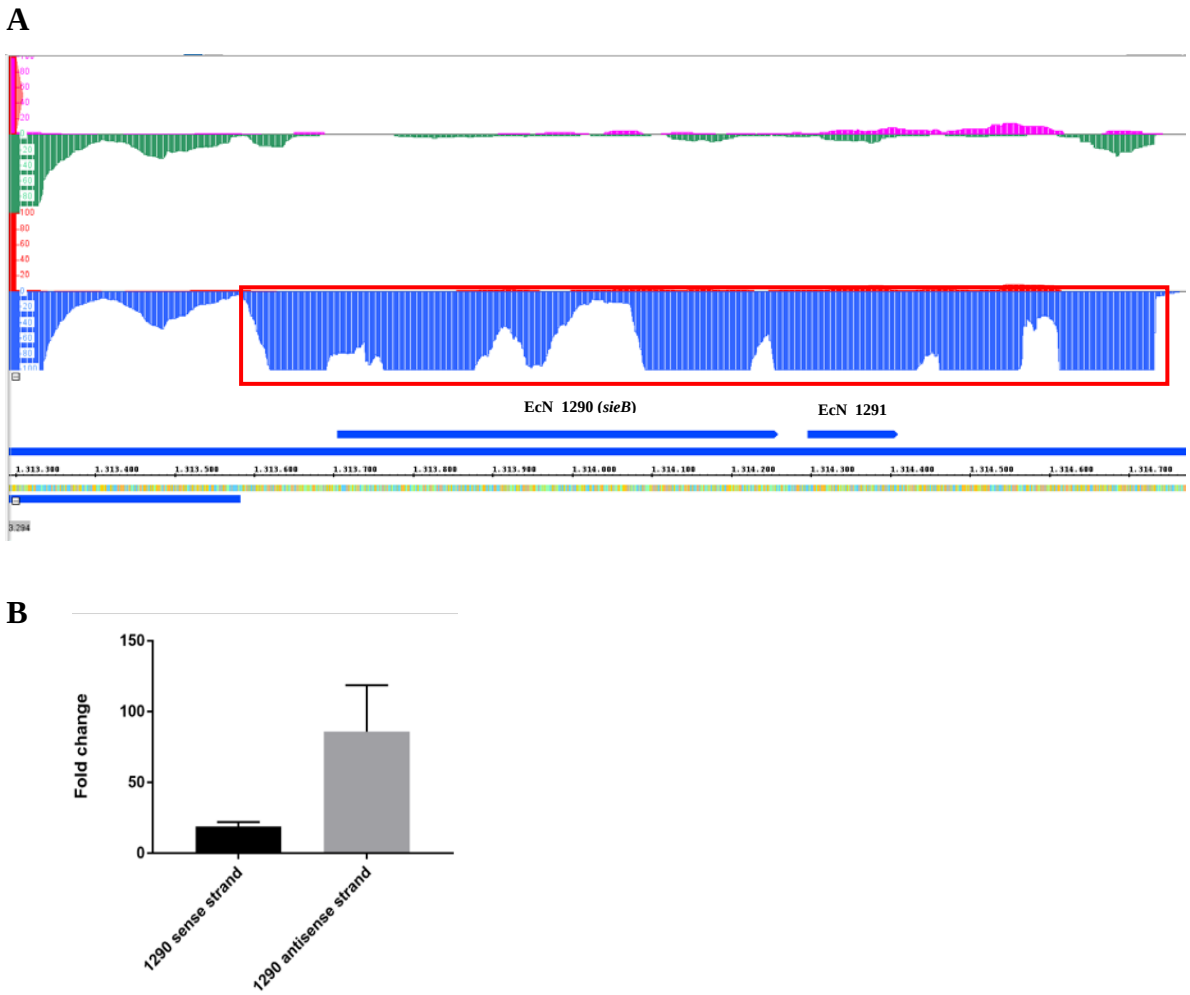

Figure 4.4. 5: Antisense regulation of prophage 3 genes in EcN when incubated with lambdoid phages: (A) Screenshot of gene regulation as viewed in integrated genome browser (IGB). The pink and green colours represent the sense and antisense strands and their respective reads of EcN that was incubated with LB medium for 16 h; red and blue colours represent the sense and antisense strands and their respective reads of EcN that was incubated with *stx*- phages for 16 h. Reads were mapped to EcN genome reference sequence. The red box points out the observed antisense regulation of the 1,104 bp long region that spans over EcN_1290 and EcN_1291. The numbers indicated in y-axis represent number of reads. X-axis represents the co-ordinates of genes in the genome. **(B)** Results of two step RT-PCR presenting the expression (in fold change) of sense and antisense strand of EcN_1290 (*sieB*) gene in EcN when incubated with lambda phages for 3 h.

Table 4. 2: Results of lambda PPA on the recombinant MG1655 strains. The results presented are the mean of three independent trials with at least two replications each.

Recombinant strains	Plasmids	Reduction in plating efficiency when compared to MG1655R
MG1655*pr*	pUC19 *_pr*	~ 215-fold
MG1655*sieB*	pUC19*_sieB*	~ 7.5-fold
MG1655_S	pUC19_S	~ 3-fold
MG1655_AS	pUC19 _AS	~ 2-fold

4.4.3. Determination of lambda phage titer reduction by EcN

In addition to the resistance exhibited by EcN towards lambda phages, we performed experiments to investigate whether EcN can neutralize, destroy or inactivate the lambda phages during coincubation. For this reason, lambda phages were incubated with and without EcN in LB medium. The samples were taken at different time points of coincubation and PFUs/ml were determined by PPA (3.1.8). A striking reduction in lambda phage titer was observed as early as 2 h (~ 11-fold) and 4 h (~ 72-fold) post-incubation with EcN which gradually escalated to ~ 1000-fold at 24 h and remained relatively stable even after 72 h of incubation (**Figure 4.4. 6_A**). Moreover, the CFUs/ml of *E. coli* strains EcN and MG1655 were determined in the presence and absence of lambda phages at the indicated time points. The CFUs/ml of EcN in the presence and absence of phages were comparable and thus confirming the resistance of EcN towards lysis by lambda phages. On the contrary, the CFUs/ml of MG1655 dropped by ~ 214-fold as early as 2 h after incubation inferring the active lysis of MG1655 cells upon phage infection. However, a gradual recovery in the CFUs/ml of MG1655 was observed initially at 4 h where the reduction in CFUs/ml of MG1655 incubated with lambda phages was only about ~ 53-fold compared to that of MG1655 culture without lambda phages **(Figure 4.4. 6_B)**. Further in the course of time (at 48 h and 72 h) only ~ 10-fold difference in CFUs/ml was observed for MG1655 incubated with and without phages. This recovery in CFUs/ml could be hypothesized to the selection of phage resistant MG1655 mutants.

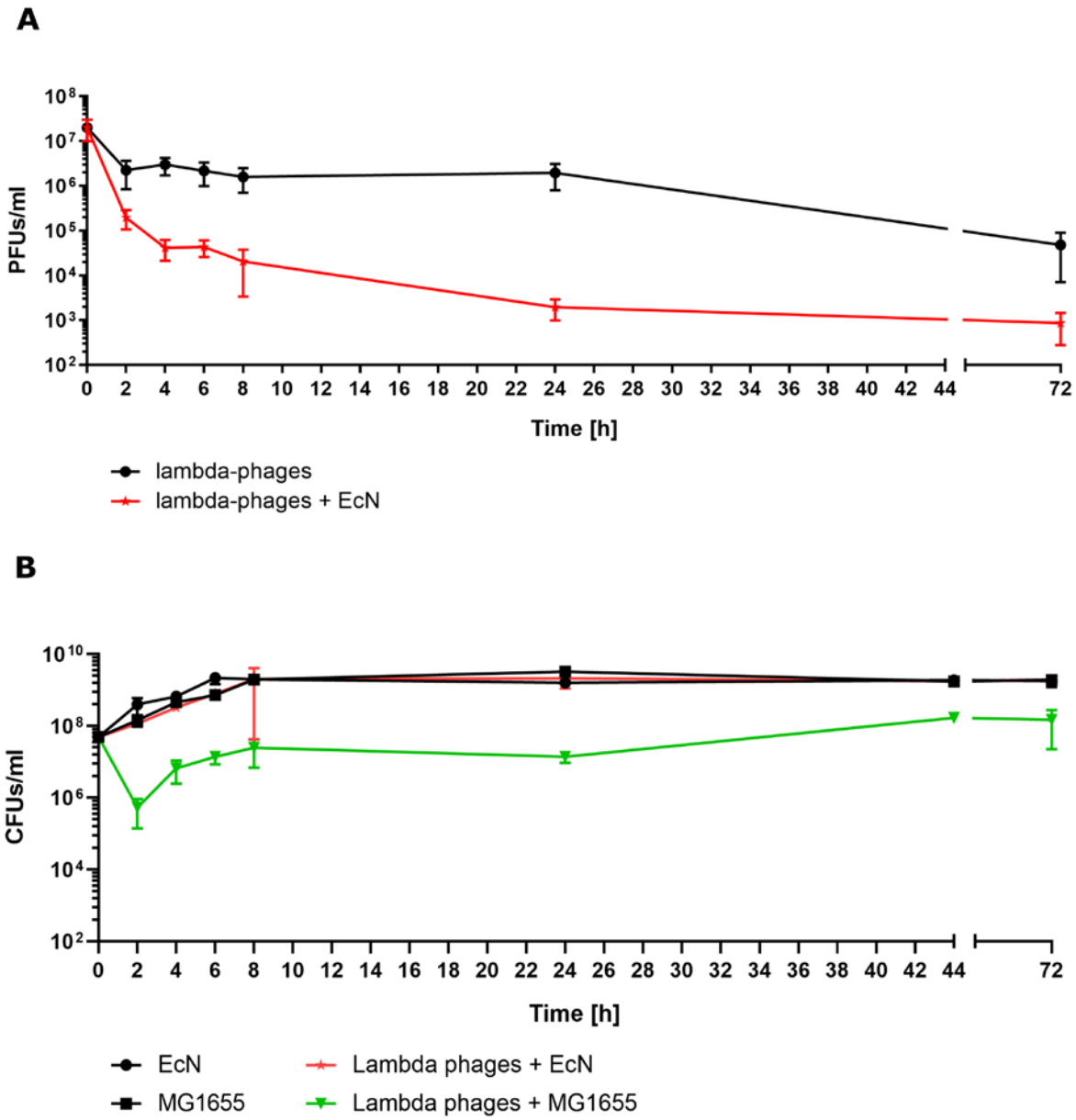

Figure 4.4. 6: Lambda phage titer reduction kinetics and growth kinetics of *E. coli* strains. (A) Kinetics of lambda phage titer reduction (in PFUs/ml) in the presence (red line) and absence (black line) of EcN (lambda:EcN - 1:10) .The samples were taken for PPA at the indicated time points. **(B)** Growth kinetics (in CFUs/ml) of *E. coli* strains (EcN/MG1655) incubated in the presence or absence of lambda phages and CFUs/ml at the specified timepoints were determined by plating them on 1.5 % LB agar containing MG1655.

4.4.4. Impact of EcN mutants on lambda phage inactivation

EcN's membrane-bound components and secretory factors had been reported to contribute to many of its probiotic properties (Hancock et al., 2010a;Troge et al., 2012;Kleta et al., 2014;Nzakizwanayo et al., 2015;Sassone-Corsi et al., 2016;Steimle et al., 2019). We

investigated the participation of these factors in EcN's lambda phage inactivation by employing different deletion mutants of EcN such as SK22D (microcin mutant), EcNΔ *csg* (curli mutant), EcNΔ *K5* (capsule mutant), EcNΔ *fliC* (flagellin mutant) and EcNΔ *bcs* (cellulose mutant) in coincubation studies with lambda phages. The PPA was performed after coincubation and the results indicated that all the EcN mutants used in the study could reduce the lambda phage titer. However, the mutants depicted a differing efficiency in the lambda phage inactivation of about 90-fold for EcN wildtype, 82-fold for SK22D and Δ *bcs*, 16-fold for Δ *csg*, 25-fold for Δ *k5* and 10-fold for Δ *fliC* (**Figure 4.4. 7**). Overall, from the above experiment, we could show that all the tested EcN mutants inactivated the lambda phages with variable efficiency and their reduction ability was not significantly different to that of the EcN wildtype.

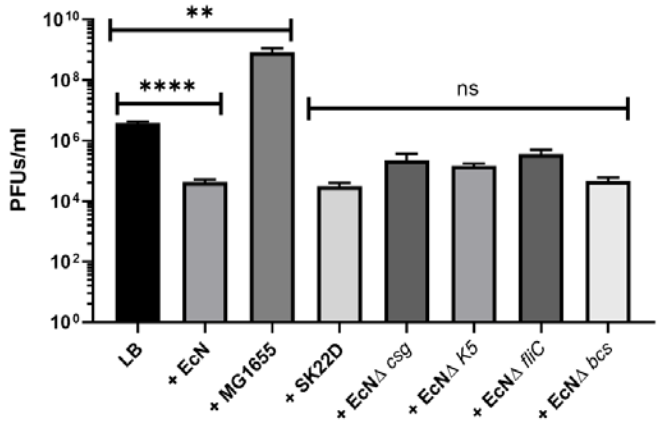

Figure 4.4. 7: **Screening the deletion mutants of EcN to determine their effect on lambda phage titer reduction.** Lambda phages were incubated either alone in LB medium (LB) or with wildtype *E. coli s*trains EcN, MG1655 or with the various deletion mutants of EcN such as SK22D (microcin mutant), EcNΔ *csg* (curli mutant), EcNΔ *k5* (capsule mutant), EcNΔ *fliC* (flagellin mutant) and EcNΔ *bcs* (cellulose mutant) in the ratio of 1:10 for 24 h at 37 ˚C after which the PFUs/ml were determined by PPA. The statistical significance was calculated with unpaired t-test. The significance of EcN and MG1655 were calculated by comparing to medium control (LB) and the EcN mutants were compared to the EcN wildtype. **p<0.0021, ****p<0.0001, ns – not significant.

4.4.5. **Investigation of lambda phage inactivating mechanism(s) of EcN**

Since EcN exhibited a rapid lambda phage titer reduction of about 214-fold after 2 h of incubation with phages (**Figure 4.4. 6_A**) we were interested to find out if this reduction was mediated by binding of the phages to the EcN cells. The lambda phages use the LamB maltoporin in the outer membrane of *E. coli* as a receptor (Randall-Hazelbauer and Schwartz, 1973;Chatterjee and Rothenberg, 2012). Hence, we hypothesized inducing the LamB receptor would, in turn, increase the frequency of lambda phage binding to EcN, which would eventually lead to an enhanced reduction in phage titer. To test this hypothesis, we induced the *lamB* gene expression by incubating EcN in the presence of 0.2 % maltose (Schwartz, 1976). As a proof of concept, the regulation of *lamB* gene expression in EcN incubated in the presence and absence of 0.2 % maltose for 6 h was tested by qRT-PCR. The primer pair lamB_RT_F/R was used to amplify the *lamB* gene and hcaT_F/R primers were used to amplify the reference gene *hcaT*, which was not regulated by maltose. The results of qRT-PCR portrayed a strong upregulation of the *lamB* gene in the presence of maltose **(Figure 4.4. 8_A)**. Consequently, 0.2 % maltose was employed in the coincubation and lambda phage specific PCR was performed with the pellets and supernatants of EcN/MG1655 incubated with lambda phages. The PCR results (**Figure 4.4. 8_B**) revealed that post-incubation, the lambda phage DNA could be detected with the cell pellets of EcN but not with the supernatants. Notably, the intensity of detected phage DNA with the pellets was much more pronounced in the presence of maltose. On the contrary, in the case of MG1655, lambda phage DNA was clearly detected in both pellets and supernatants of coincubation. Like for EcN, the addition of 0.2 % maltose also increased the phage signal associated with the pellets of MG1655. The q-RT PCR and the PCR results clearly indicated a positive correlation between 0.2 % maltose induced *lamB* expression and enhanced phage DNA association with EcN.

The next challenge was to elucidate the influence of the phage binding on the phage titer reduction by EcN, for which we used 0.2 % maltose in *E. coli* and lambda phage coincubation studies. *E. coli* (EcN/MG1655) cells were either killed by treatment with 1 % formaldehyde (FA) or heat (100 ˚C, 1 h) and incubated with lambda phages with or without 0.2 % maltose and PFUs/ml were determined after 24 h by PPA.

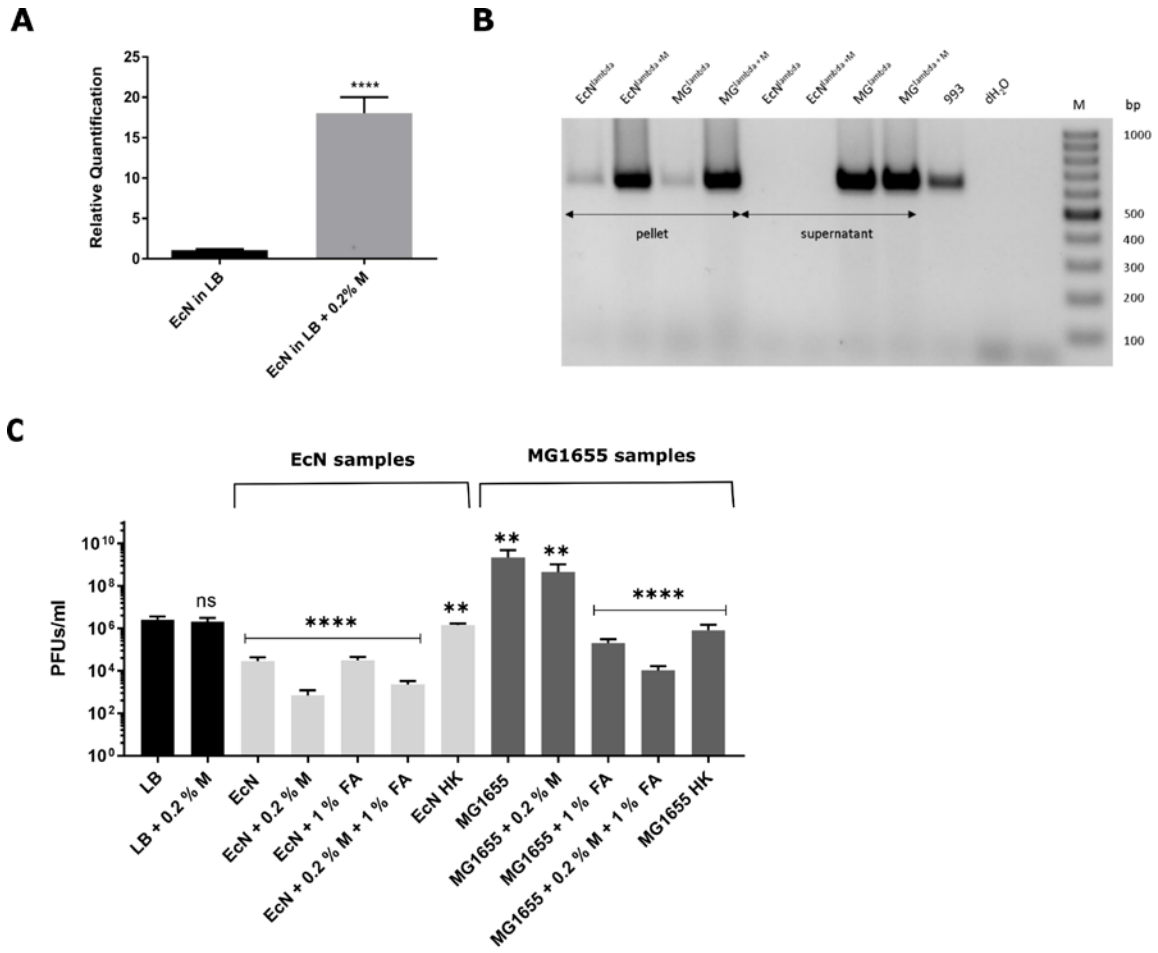

Figure 4.4. 8: Influence of 0.2 % maltose on *lamB* induction and subsequent lambda phage titer reduction in EcN. (A) qRT-PCR results showing the upregulation of *lamB* gene in EcN when incubated in LB medium +/- 0.2 % maltose for 6 h. **(B)** Lambda phage specific PCR was performed with the pellets and the supernatants of *E. coli* (EcN/MG1655) incubated with lambda phages in the presence (lambda + M) or absence (lambda) of 0.2 % maltose for 24 h at 37 ˚C. 993: *E. coli* K-12 strains harboring the lambda prophage used as a positive control for lambda phage specific PCR, dH_2O: negative (water) control. **(C)** Live, heat killed (HK) and 1 % formaldehyde (1 % FA) fixed EcN/MG1655 were incubated with lambda phages in LB medium +/- 0.2 % maltose (0.2 % M) for 24 h at 37 ˚C, after which the PFUs/ml were determined by PPA. ns, not significant, **p < 0.0021 and ****p < 0.0001.

The results (**Figure 4.4. 8_C**) of PPA demonstrated a clear lambda phage titer reduction by EcN, about 87-fold reduction after 24 h and this reduction was further intensified to ~ 2936-fold in the presence of maltose (EcN + 0.2 % M). Comparable to live EcN, the formaldehyde-treated EcN (EcN+ 1 % FA and EcN + 0.2 % M + 1 % FA) showed a similar pattern of phage titer reduction, whereas, the heat-killed EcN (EcN HK) completely lost its ability to reduce the phage titer. As expected, the HK and 1 % FA treated MG1655 did not result in a dramatic change in phage titre, however, the live MG1655 showed an increase in phage titer of about 880-fold after 24 h incubation. Moreover, the addition of maltose also decreased the number of free phages available in the supernatant of MG1655 and thus assuring the increased attachment of phages to *E. coli* in the presence of maltose.

4.4.6. **Impact of other *E. coli* strains on lambda phage inactivation**

Apart from EcN and MG1655, we also tested other *E. coli* strains such as the K-12 strains HB101 and DH5α, commensal strains isolated from healthy individuals such as SE11 and SE15, and the uropathogenic strain CFT073, which is a close relative to EcN, for their ability to reduce the phage titer. The *E. coli* strains named above were incubated with lambda phages at a starting ratio of 10:1 (*E. coli*: phages) for a period of 24 h. Afterwards, the PFUS/ml in the filtered supernatants were detected by PPA. The PPA results (**Figure 4.4. 9**) from the coincubation studies revealed that among the tested *E. coli* strains, only the *E. coli* K-12 strains MG1655, HB101 and DH5α were infected which was evident from a significant increase in the phage titer of about ~ 1350-fold (MG1655), ~ 97-fold (HB101) and ~ 117-fold (DH5α) after 24 h of incubation. While the commensal *E. coli* strains SE11 and SE15 and the uropathogenic strain CFT073 were not only resistant to the lambda phages but were also able to reduce the phage titer after 24 h comparable to EcN (**Figure 4.4. 9**).

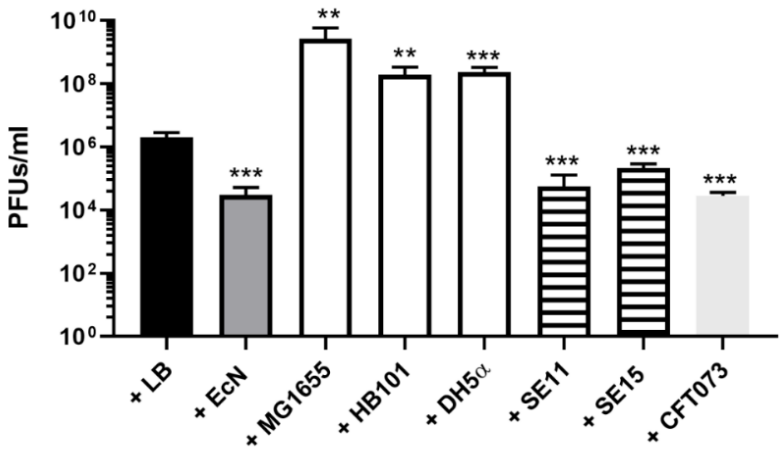

Figure 4.4. 9: Lambda phage titer reduction by other *E. coli* strains: Lambda phages were incubated either alone in medium (LB- black column) or with EcN (dark grey column), *E. coli* K12 strains - MG1655, HB101 and DH5α (white columns), *E. coli* commensal strains - SE11 and SE15 (white columns with black stripes), the uropathogenic strain CFT073 (light grey column) in the ratio of 1:10 for 24 h at 37 ˚C after which the samples were sterile filtered and PFUs/ml were determined by PPA. **p<0.0021, ***p<0.0002.

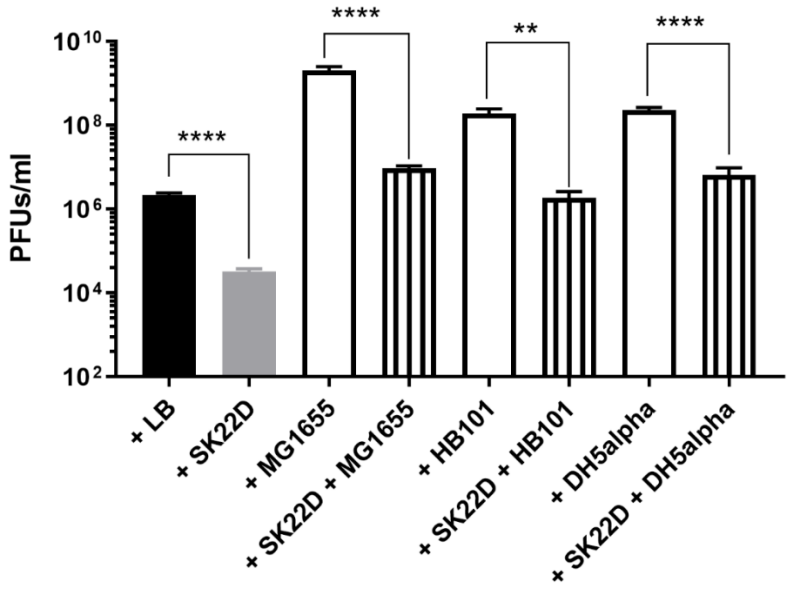

Figure 4.4. 10: EcN's influence on lambda phage infection of K-12 strains: Lambda phages were incubated alone in medium (LB) or in a coculture set up with SK22D (dark greycolumn) / *E. coli* K-12 strains - MG1655, HB101 and DH5α (whitecolumns) / in a triculture set up (white columnswith black vertical stripes) where lambda phages:SK22D:K-12 strains were mixed at a ratio of 1:10:10. The incubation was carried out for 24 h at 37 ˚C after which the samples were sterile filtered and PFUs/ml were determined by PPA. The significance of the triculture set up was calculated by comparing to the coculture with the respective K-12 strain, **p<0.0021, ****p<0.0001.

Following these observations, we were intrigued to investigate whether EcN could interfere with the lambda phage infection of K-12 strains and thereby protecting them from being infected. To test this hypothesis, different K-12 strains were investigated in a triculture set up involving lambda phages:SK22D:K-12 strain as described in 3.1.7. The microcin negative mutant of EcN (SK22D) was used in triculture experiments to avoid the effect of the antibacterial compounds from EcN: microcins M and H47 on the K-12 strains. The experiments with the triculture set up explicitly showed an astounding influence of SK22D on the lambda phage infectivity of K-12 strains. In the absence of SK22D, the K-12 strains were infected by lambda phages and the phage titer was increased by ~ 950-fold (MG1655) and ~ 90-fold (HB101 and DH5α) after 24 h incubation. Nevertheless, in the presence of SK22D the observed phage titer increase was curtailed by ~ 210-fold (MG1655), ~ 105-fold (HB101) and ~ 35-fold (DH5α). Following this, the capacity of the commensal strains SE11 and SE15 to influence the lambda phage infection of MG1655 was tested in a similar triculture coincubation experiment and the results (**Figure 4.4. 11**) demonstrated that these strains were also able to interfere with the lambda phage infection of MG1655 but not as efficient as SK22D. It was implied by a phage titer reduction of ~ 66-fold by SE11 and ~ 177-fold by SE15, compared to that of ~ 210-fold reduction by SK22D in the supernatant after incubation.

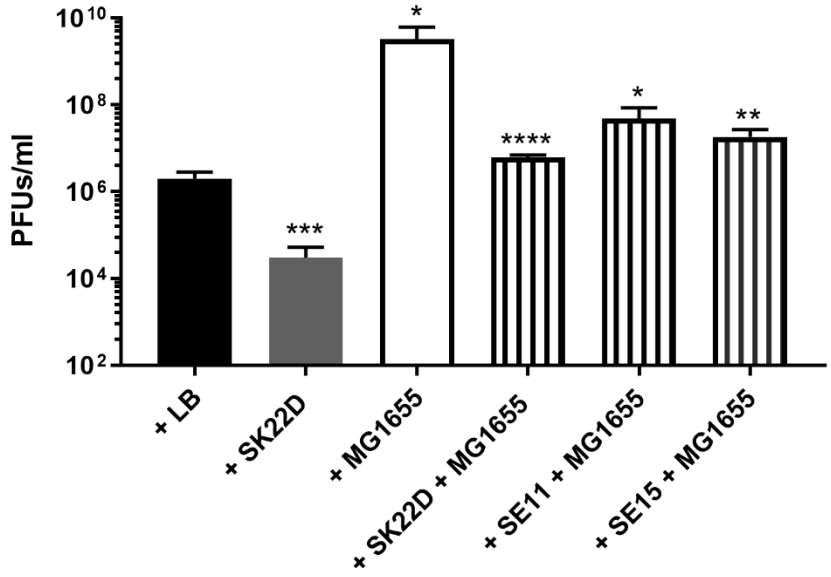

Figure 4.4. 11: Influence of commensal strains on lambda phage infection of MG1655. Lambda phages were incubated either alone in the medium (LB-blackcolumn) or in a coculture set up with SK22D (dark greycolumn) / MG1655 (whitecolumn) or in a triculture set up (white columns with black vertical stripes) where lambda phages:SK22D/SE11/SE15:MG1655 were applied at a of ratio 1:10:10. The incubation was carried out for 24 h at 37 ˚C after which the samples were sterile filtered and PFUs/ml were determined by PPA. The significance of the triculture set up were calculated by comparing to the MG1655 column, *p<0.0332, **p<0.0021, ***p<0.0002 and ****p<0.0001.

In conclusion, from this part of the study, the resistance of EcN towards lambda phages was demonstrated. Phage repressor encoded in EcN's prophage 3 was shown to play an essential role in its resistance against lambda phage infection and could provide partial protection for MG1655 against lambda phages. In addition, EcN was found to inactivate lambda phages during coincubation and the inactivation was mediated by binding to LamB.

4.5. Lytic phage resistance of EcN

The lytic T4 phages belong to one of the most common families of phages present in the gut: *Myoviridae* (Chibani-Chennoufi et al., 2004b;Manrique et al., 2016) and it could be an important challenge for the survival of EcN in the gut. Therefore, we were curious to study the influence of EcN on T4 phages and the initial goal was to determine the sensitivity of EcN to the lytic T4 phages.

4.5.1. T4 phage plaque assay

The resistance of EcN towards lytic T4 phages was determined by PPA. Serial dilutions of the T4 phage lysate were dropped on a PPA plate with either MG1655 or EcN in the soft agar. After incubation at 37 ˚C, no lysis zone or single plaque was detected when T4 phage lysate was added to EcN, whereas with MG1655 lawn, clear lysis zones with higher dilutions and single plaques with lower dilutions of T4 lysate were observed (**Figure 4.5. 1_A)**. Similarly, a liquid culture assay was performed by adding T4 phages into mid-log growing phase EcN or MG1655 cultures. After 4 h of incubation, the MG1655 culture was clear and thus indicating lysis by T4 phages, whereas the EcN culture remained turbid, implying resistance towards lysis by this phage (**Figure 4.5. 1_B)**.

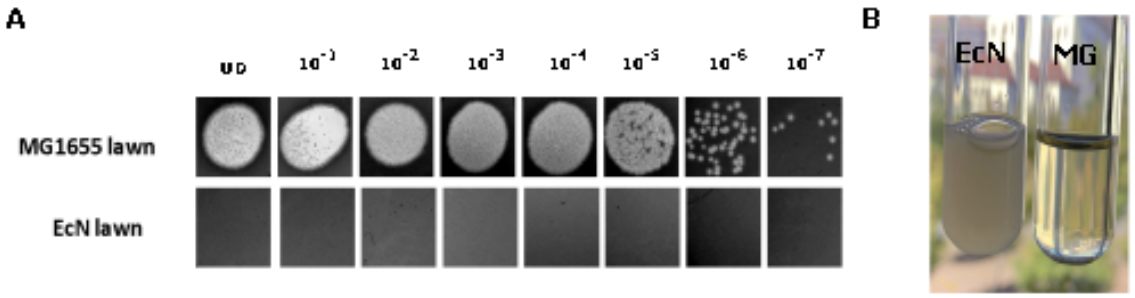

Figure 4.5. 1:T4 phage sensitivity test for *E. coli* strains MG1655/EcN: **(A)** Phage plaque assay: T4 phage lysate was serially diluted [undiluted (UD) to 10^{-7} PFUs/ml] and 10 µl was spotted on the 0.7 % LB agar PPA plates with either MG1655 or EcN and incubated at 37 ˚C, O/N. **(B)** Liquid culture assay: T4 phage lysate (10^6 PFUs/ml) was added to the EcN/MG1655 culture of OD_{600} ~ 0.5 (mid-log growing phase) and incubated at 37 ˚C at 180 rpm for 4 h. Imaging was performed with Canon PowerShot SX260 HS and processed with ImageJ 1.50i. Image modified from (Soundararajan et al., 2019)

4.5.2. Microscopic examination of *E. coli* and T4 phage coincubation

Further, to closely observe the interaction between *E. coli* and T4 phages, the *E. coli* and phage coincubation cultures were analysed by different microscopic techniques.

4.5.2.1. Confocal microscopy of DAPI stained T4 phages incubated with *E. coli*

For the confocal microscopic observation, DAPI (0.5 µg/ml) stained T4 phages were added to the mid-log growing phase EcN or MG1655 cultures (*E. coli* + T4 phages). As a control, LB medium with 0.5 µg/ml DAPI was added to the *E. coli* (*E. coli* – T4 phages). The cocultures were incubated on ice for 30 mins to facilitate the attachment of phages to *E. coli* followed by incubation for 5 mins at 37 ˚C to allow the infection. Finally, the *E. coli* phage incubations were visualized through the 100x objective lens of the Leica microscope-TCS MP5. The confocal microscopic examination revealed that the EcN cells were intact and the DAPI signals were located around the cells (**Figure 4.5. 2**, red arrows). In contrast, in the case of MG1655, apparent cell lysis was evident and the DAPI signals were localized within the cell debris (**Figure 4.5. 2**, green arrows). The results demonstrated that T4 phages could bind to EcN without being able to lyse it and thus proving again the insensitivity of EcN towards T4 phage infection.

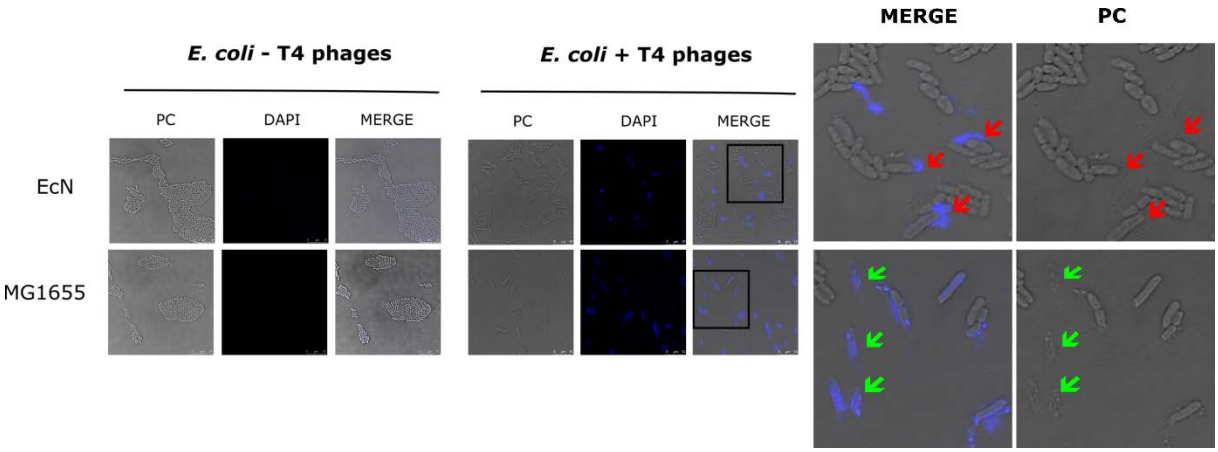

Figure 4.5. 2: Confocal micrograph of *E. coli* incubated with T4 phages: 100 µl of DAPI (0.5 µg/ml) stained T4 phage lysate or medium was added to EcN/MG1655 culture at the ratio of *E. coli*:T4 ~ 1:10. ***E. coli* - T4 phages (left)**: EcN or MG1655 incubated with medium + 0.5 µg/ml DAPI, ***E. coli* + T4 phages (middle)**: EcN or MG1655 cells incubated with T4 phages + 0.5 µg/ml DAPI. PC: phase contrast channel, DAPI: DAPI channel, MERGE: PC + DAPI. **Zoomed-in version (right)**, red arrows point out intact EcN cells, DAPI signal (blue) localized around the cells (top row) and green arrows point out lysed MG1655 cells, DAPI signal (blue) localized within cell debris (bottom row). Image source: (Soundararajan et al., 2019)

4.5.2.2. Observation of T4 phage attachment to EcN by Transmission Electron Microscopy

For electron microscopic examination EcN and T4 phage incubations were negatively stained after 1 h at 37 ˚C and visualized under TEM. The TEM micrographs displayed in **Figure 4.5. 3** clearly established the attachment of T4 phages to EcN (C, D). Specifically, the red arrows point out the T4 phages that were found attached to the intact EcN cells and thereby confirming our observations from the confocal microscopy.

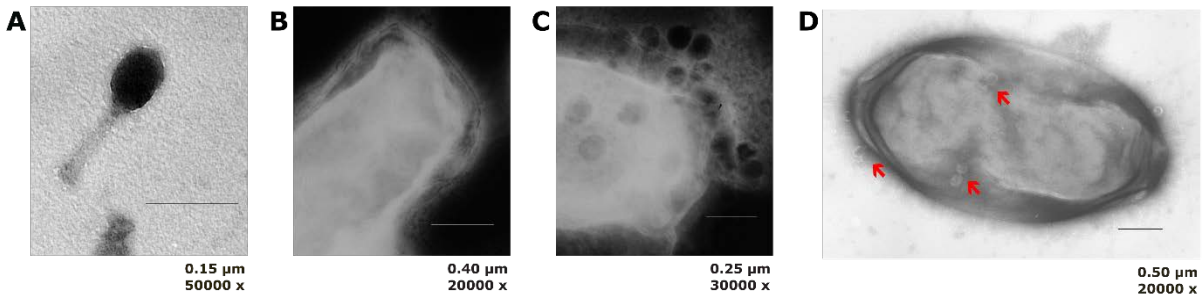

Figure 4.5. 3: TEM micrographs showing the T4 phage attachment to EcN: EcN was incubated with T4 phages (1:100) for 1 h at 37 ˚C and the phage + bacteria mixture was then fixed with 0.5 % glutaraldehyde and stained with 0.5 % uranyl acetate. **(A)** T4 phage in medium, **(B**) EcN incubated in medium, **(C, D)** EcN incubated with T4 phages. Imaging was performed with TEM at different magnifications. The scale bar is shown in each picture. Image modified from (Soundararajan et al., 2019)

4.5.3. T4 phage DNA localization by PCR

Microscopic observations clearly displayed the attachment of T4 phages to EcN and we validated the same with T4 phage specific PCR. By PCR, we aimed to localize the T4 phage DNA following the coincubation with *E. coli* with the primer pair ndd_T4_F/R (580 bp). The cells and supernatants of the *E. coli* (EcN/MG1655) incubated with T4 phage were used as a template and the PCR results revealed that after 24 h of incubation, the T4 phage DNA was found to be predominantly associated with EcN cells (T4_P) rather than cell-free supernatant (T4_S) of the coincubation. In the case of MG1655, the distribution of phage DNA was relatively even between the cells (T4_P) and supernatant (T4_S). An internal control (pKD3

plasmid) was used in the PCR mix which gave an amplicon of 1,098 bp with similar intensity in all the samples and hence excluding the possibility that the difference in the band intensity between EcN cells and supernatant incubated with T4 phages were due to the nature of these samples. Thus, the PCR results substantiated the microscopic findings regarding the attachment of T4 phages to EcN.

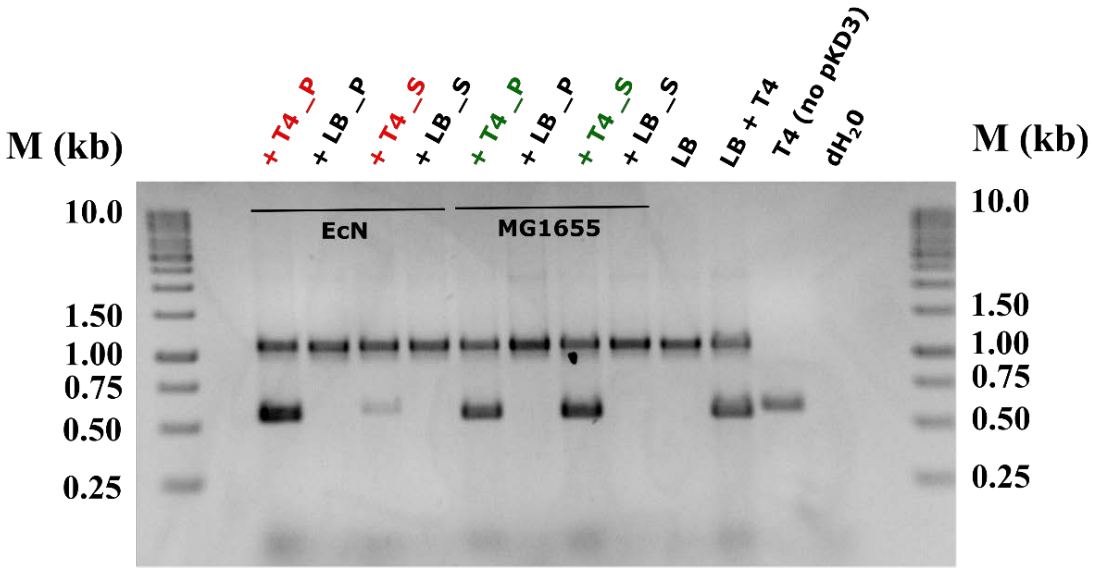

Figure 4.5. 4: Localization of T4 phage DNA with *E. coli* after coincubation: The pellet and the supernatant of EcN/MG1655 incubated with T4 phages for 24 h at 37 ˚C, were used as template in a T4 specific PCR with the primer pair T4_*ndd*_F /R (580 bp). Plasmid pKD3 was used as internal standard along with primer pair pKD3_F/R (1,098 bp). **Lane details:** (**red – EcN**, **green – MG1655**), **+T4_P**: pellet of *E. coli* + T4 phage, **+LB_P**: pellet of *E. coli* + LB medium, **+T4_S**: supernatant of *E. coli* + T4 phage, , **+LB_S**: supernatant of *E. coli* + LB medium, **LB**: LB medium control, **LB + T4**: LB medium + T4 phage, **T4 (no pKD3)**: T4 phage control (no pKD3), **dH$_2$O**: negative control, **M**: GeneRuler 1 kb DNA Ladder

4.5.4. Role of EcN's K5 capsule in its T4 phage resistance

The K5 polysaccharide capsule forms the outermost layer of EcN's cell envelope, therefore we hypothesized, K5 capsule could be a potential target for binding of T4 phages. Hence, to investigate the involvement of the capsule in T4 phage insensitivity, a capsule negative mutant of EcN (EcNΔ *k5*) was employed in our experiments. This mutant lacks the entire K5 capsule determinant in EcN spanning from *kpsM* to *kpsF* which is ~ 17.9 kb in size. The deletion was

confirmed by PCR (**Figure 4.1. 6_A),** and in addition, to further confirm the lack of capsule, a phenotypic verification was performed with the K5 specific phage. This phage bind specifically to the K5 capsule of *E. coli* strains, resulting in an infection and lysis of such strains. When serial dilutions of K5 phages were spotted on a PPA plate with EcN wildtype in the lawn, clear lysis zones were observed indicating a positive infection. On the other hand, with EcNΔ *k5* in the lawn, no lysis zone was observed indicating that the K5 phages could not infect them (**Figure 4.5. 5_left**). These results with K5 phages confirmed the lack of K5 capsule in EcNΔ *k5* strain.

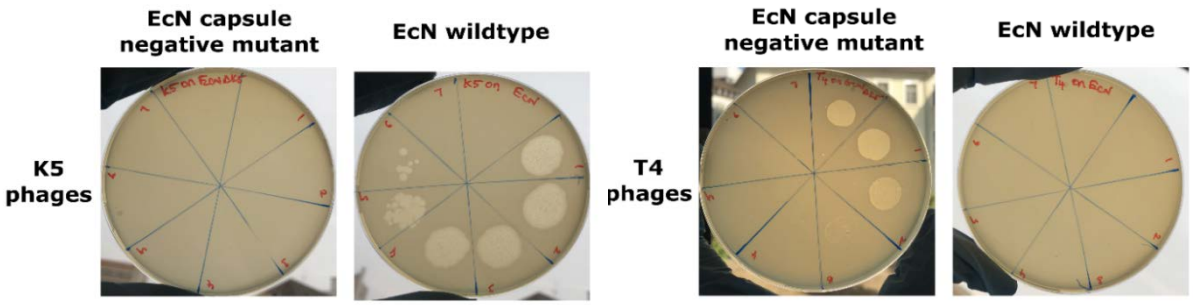

Figure 4.5. 5: Role of K5 capsule in T4 phage resistance of EcN: 200 µl of EcN cultures (EcNΔ *k5*/ EcN wildtype) were mixed with 0.7 % LB agar and poured on a 1.5 % LB agar plate. After solidification, 10 µl of serially diluted K5 capsule specific phages **(Left)** / T4 phages **(right)** were spotted on the lawn and the plates were carefully incubated for 24 h at 37 °C. Imaging was performed with Canon PowerShot SX260 HS and processed with ImageJ 1.50i. Image modified from (Soundararajan et al., 2019)

Similarly the serial dilutions of T4 phages were plated on EcN wildtype and the EcNΔ *k5* lawn, producing lysis zones only on EcNΔ *k5* in contrast to the EcN wildtype lawn where not a single plaque was detected (**Figure 4.5. 5_right**). Thus, with the help of EcNΔ *k5* mutant, we demonstrated a significant role of EcN's K5 capsule in its resistance against T4 phages.

4.5.5. T4 phage inactivation by EcN

In addition to EcN's ability to protect itself from T4 phage infection, we were intrigued to understand whether EcN could also inactivate or destroy the T4 phages in its surrounding. For this purpose, EcN was incubated with T4 phages for 24 h during which the T4 phage titer (in

PFUS/ml) and EcN's growth (in CFUs/ml) were determined by PPA and by plating on LB agar plates, respectively. The results (**Figure 4.5. 6_A)** of phage titer determination established a reduction in phage titer which was ~ 5-fold within 30 mins of incubation and drastically raised to ~ 10-fold and ~ 102-fold after 1 h and 2 h of coincubation. Further, a gradual drop in

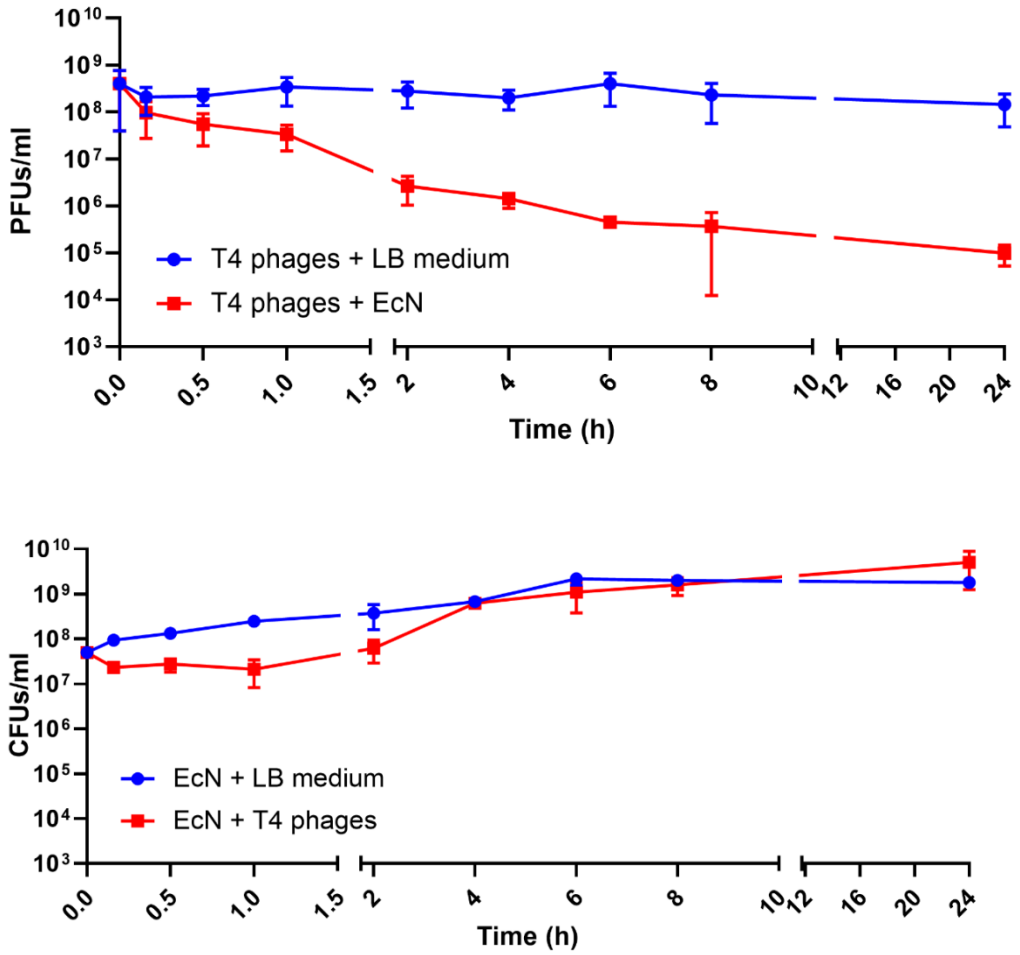

Figure 4.5. 6: T4 phage titer reduction kinetics (A) and EcN's growth kinetics (B) during EcN and T4 phage coincubation. EcN was incubated with T4 phages at a ratio of 1:1 in LB medium at 37 ˚C and samples were taken at indicated time points of coincubation. PFUs/ml **(A)** and CFUs/ml **(B)** were determined for the samples. The blue lines indicate PFUs/ml of T4 phages and CFUs/ml of EcN in LB medium, the red lines indicate PFUs/ml of T4 phages incubated with EcN cells and CFUs/ml of EcN incubated with T4 phages.

PFUs/ml of T4 phages was observed throughout the coincubation and the highest reduction of about ~ 1,470-fold was observed after 24 h. Simultaneously, the graph illustrating the growth kinetics of EcN (**Figure 4.5. 6_B**) displayed a delay in EcN's growth at early time points of coincubation until 1 h. However, after 2 h of coincubation, an elevation in EcN's CFUs/ml was

observed and by 4 h, the growth kinetics of EcN in the presence and absence of T4 phages overlapped each other, displaying no difference in the growth of EcN due to the phages.

Furthermore, to discern the long-term effect of EcN on T4 phages, the coincubation was carried out for a longer time period (120 h) and samples were taken at different time points as mentioned in the graph (**Figure 4.5. 7**) for phage titer (in PFUs/ml) and growth (in CFUs/ml) determination. Surprisingly, after 24 h of coincubation with EcN, instead of a further drop in PFUs/ml as observed in case of lambda phages (**Figure 4.4. 6**), the T4 phage titer raised and at 48 h there was only a 10-fold reduction in phage titer in the presence of EcN when compared to 0 h **(Figure 4.5. 7_A)**. However, the T4 phage titer did not increase more than the number of initial phages added. The results led to speculate that the phage titer increase might be due to the T4 phage infection of EcN cells, nevertheless, the corresponding growth kinetics (CFUs/ml) of EcN (**Figure 4.5. 7_B)** remained stable throughout the coincubation and the CFUs/ml of EcN were comparable in the presence or absence of T4 phages.

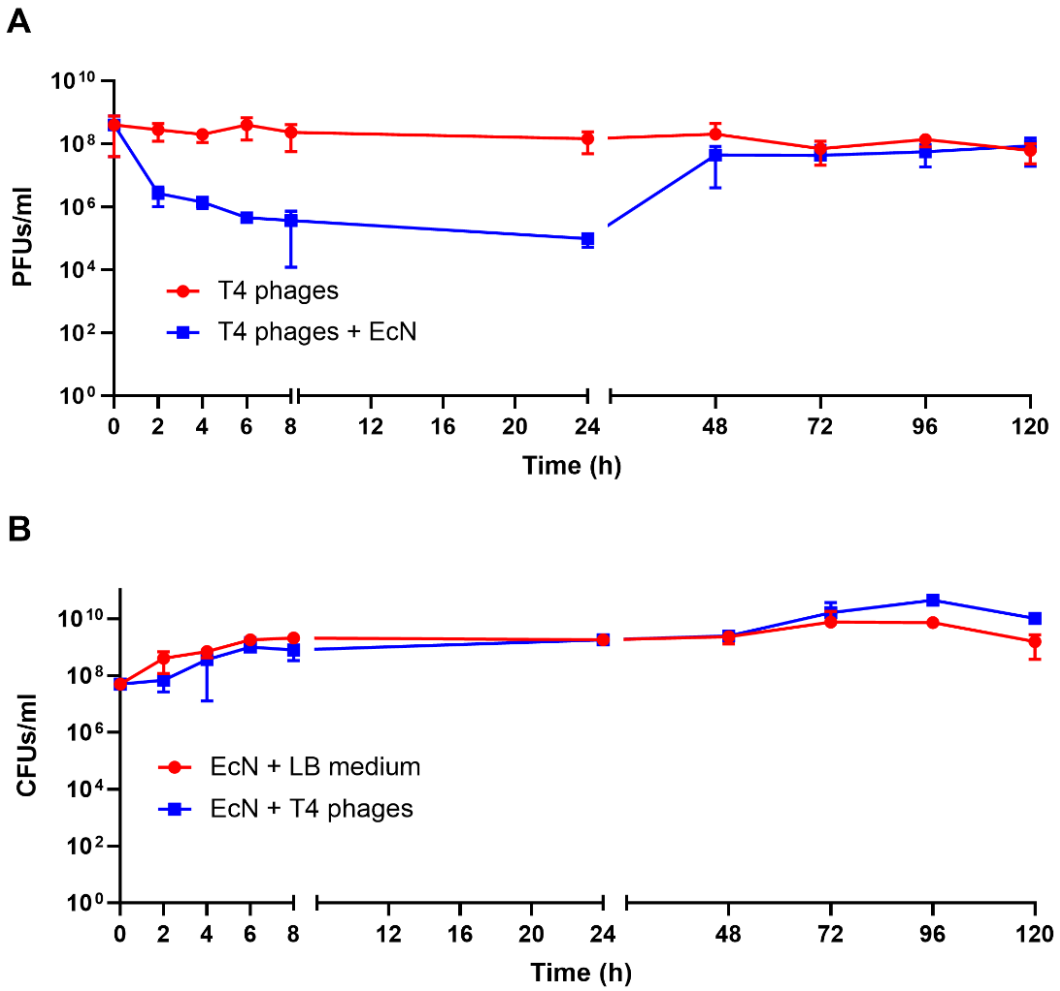

Figure 4.5. 7: Kinetics of T4 phage titer reduction (A) and EcN's growth (B) for 120 h of coincubation. EcN cells were incubated with T4 phages at a ratio of 1:1 in LB medium at 37 ˚C and samples were taken at indicated time points of coincubation. PFUs/ml **(A)** and CFUs/ml **(B)** were determined for the samples and the blue lines indicate PFUs/ml of T4 phages and CFUs/ml of EcN in LB medium, the red lines indicate PFUs/ml of T4 phages incubated with EcN cells and CFUs/ml of EcN incubated with T4 phages.

Hence, we hypothesized that the increase in the phage titer observed after 24 h of coincubation was due to neither the infection nor the subsequent lysis of EcN but rather due to the release of T4 phages that were attached to EcN so far. To apprehend the observed effect, we isolated the T4 phages after 24 h, 48 h and 96 h of coincubation with EcN and serial dilutions of these T4 phages were spotted on the freshly prepared EcN lawn in a PPA and parallelly serial dilutions of fresh T4 phage lysate were also spotted on the lawn prepared with EcN that had been incubated with T4 phages for 24 h, 48 h and 96 h. From this experiment, it was noted that the

T4 phages previously exposed to EcN and the fresh T4 phages failed to plate on EcN lawns no matter if it was freshly prepared EcN or if T4-exposed EcN was employed (**Table 4. 3**).

Table 4. 3: Testing the T4 phage sensitivity of EcN that has been coincubated with T4 phages (A) T4 phages that were incubated with EcN for 24 h/48 h/96 h were serially diluted and spotted on fresh EcN/MG1655 lawn **(B)** EcN incubated with T4 phages for 24 h/48 h/96 h were used to prepare PPA plates on which serial dilutions of freshly prepared T4 phages were spotted. The PPA plates from (A) and (B) were incubated at 37 ˚C, 24 h and the PFUs/ml were determined. The results displayed here are the mean of three independent trials with two replicates each trial. No - No plaques could be detected from the undiluted sample.

Hours of coincubation (exposure)	(A) T4 phages preincubated with EcN spotted on the lawn of		(B) FreshT4 phages on the lawn of EcN preincubated with	
	fresh EcN	fresh MG1655	Medium	T4 phages
24 h	No	7.8×10^5	No	No
48 h	No	9.3×10^6	No	No
96 h	No	1.2×10^7	No	No

Similarly, in another experiment, the EcN cells that were incubated with T4 phages for 96 h were collected and washed thrice with 0.9 % saline. These cells were then incubated at 37 ˚C, 2 h with freshly prepared T4 phage lysate and the PFUs/ml were determined. The results of the

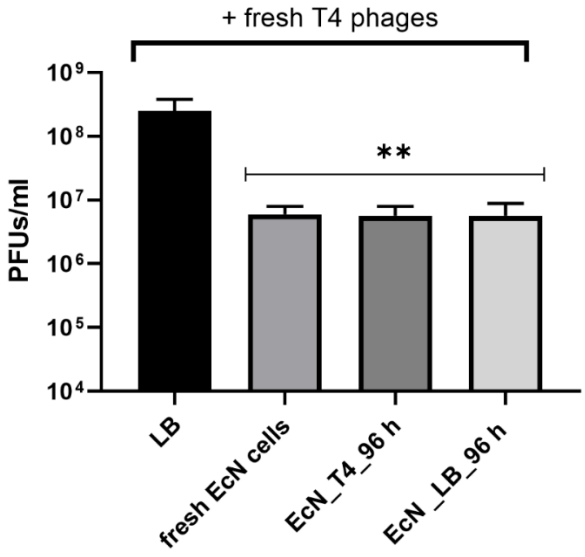

Figure 4.5. 8: T4 phage titer reduction by EcN pre-incubated with T4 phages for 96 h. EcN incubated with either T4 phages (EcN_T4_96 h) or alone in LB medium (EcN_LB_96 h) for 96 h were collected by centrifugation (4,696 x g, 10 mins, RT) and pellets were resuspended in fresh LB medium after washing thrice. 100 µl of freshly prepared T4 phages were added to 100 µl of EcN cells (fresh EcN/ EcN_T4_96 h/ EcN_LB_96 h) in 1 ml LB medium and incubated for 2 h at 37 ˚C after which the PFUs/ml were determined by PPA. LB: T4 + medium control.

PPA (**Figure 4.5. 8**) clearly established that the EcN cells incubated with T4 phages for 96 h (EcN_T4_96 h) reduced the titer of freshly added T4 phages by 100-fold in 2 h which was as efficient as fresh EcN cells. Hence these results collectively eliminated the speculation of EcN becoming sensitive to T4 phages after 24 h of coincubation.

Moreover, an alternative perspective pointing towards the release of attached T4 phages being responsible for the observed increase in phage titer remains open for further investigation. The hypothesis was further affirmed from the results of time point-dependent T4-specific PCR, in which, we could detect more T4 phage DNA in the supernatant of EcN-T4 phage coincubation at 48 h when compared to 24 h time point (**Figure 4.5. 9**).

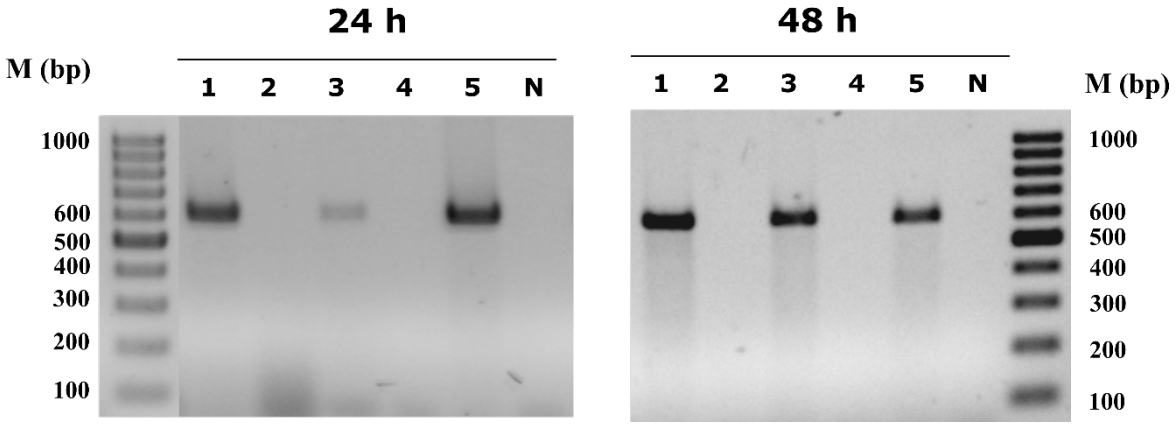

Figure 4.5. 9: Localization of T4 phage DNA with EcN cells/supernatant after coincubation: The pellet and the supernatant of EcN incubated either alone in medium (LB) or with T4 phages for 24 h/ 48 h at 37 ˚C were used as template in a T4 specific PCR with the primer pair T4_*ndd*_F /R (580 bp). **Lane details: 1 -** EcN + T4 _pellet, **2 -** EcN + LB_pellet, **3 -** EcN + T4 _supernatant, **4 -** EcN + LB_supernatant, **5 -** T4 phage control, **N** - (water) negative control, **M** - GeneRuler 100 bp DNA Ladder

4.5.6. Transcriptomic analysis of EcN in the presence of T4 phages

Previously, we observed a dramatic reduction in T4 phage titer after 2 h of incubation with EcN. It is quite likely that the presence of T4 phages might have induced a sea of changes in the transcriptomic profile of EcN. The study aimed to understand if the changes in transcriptome could shed light on possible factors which might contribute to the immunity towards T4 phages in EcN. For the transcriptomic analysis, RNA was isolated from EcN incubated with or without T4 phages for 2 h and their transcriptomic profiles were compared. This RNA-Seq data have been deposited at the NCBI Gene Expression Omnibus (Edgar et al., 2002) and can be accessed through GEO series accession number GSE135946 (https://www.ncbi.nlm.nih.gov/geo/query/acc.cgi?acc=GSE135946). From the results of RNA-seq, it was evident that, the number of genes that were downregulated (123 genes) (log_2 fold change < -2, padj < 0.05) was ~ 4 times higher than the number of genes upregulated (33 genes) (log_2 fold change > 2, padj < 0.05). The function(s) of these genes were predicted as described in 3.5.3 and further assigned into the functional groups as mentioned in the doughnut graphs (**Figure 4.5. 10**). The functional details of the up and down-regulated genes in EcN, when incubated with T4 phages for 2 h, are presented in Annexure 4 (Table 8.3 and Table 8.4). The functional grouping of downregulated genes **(Figure 4.5. 10_B**) clearly indicated that the majority of downregulated genes (58 of 123 genes) belonged to metabolism-related genes. Specifically, ~ 20 % of total downregulated genes were contributing to carbohydrate metabolism and ~ 11 % to amino acid metabolism. Apart from the uncharacterized proteins that corresponded to ~ 16 % of total downregulated genes, the other major downregulated functional groups were stress and growth-related proteins (~ 9 %) and transcription and translation-related proteins (~ 7 %). In general, the observed downregulation of genes associated with metabolism and growth might explain the observed lag in growth kinetics (CFUs/ml) of EcN at early hours (< 2 h) of incubation with T4 phages (**Figure 4.5. 6**). This observation coincides with previous

publications (Winkler and Duckworth, 1971;Fukuma and Kaji, 1972) which reported inhibition in the cellular mechanisms of a host cell when incubated with T4 ghost bacteriophages.

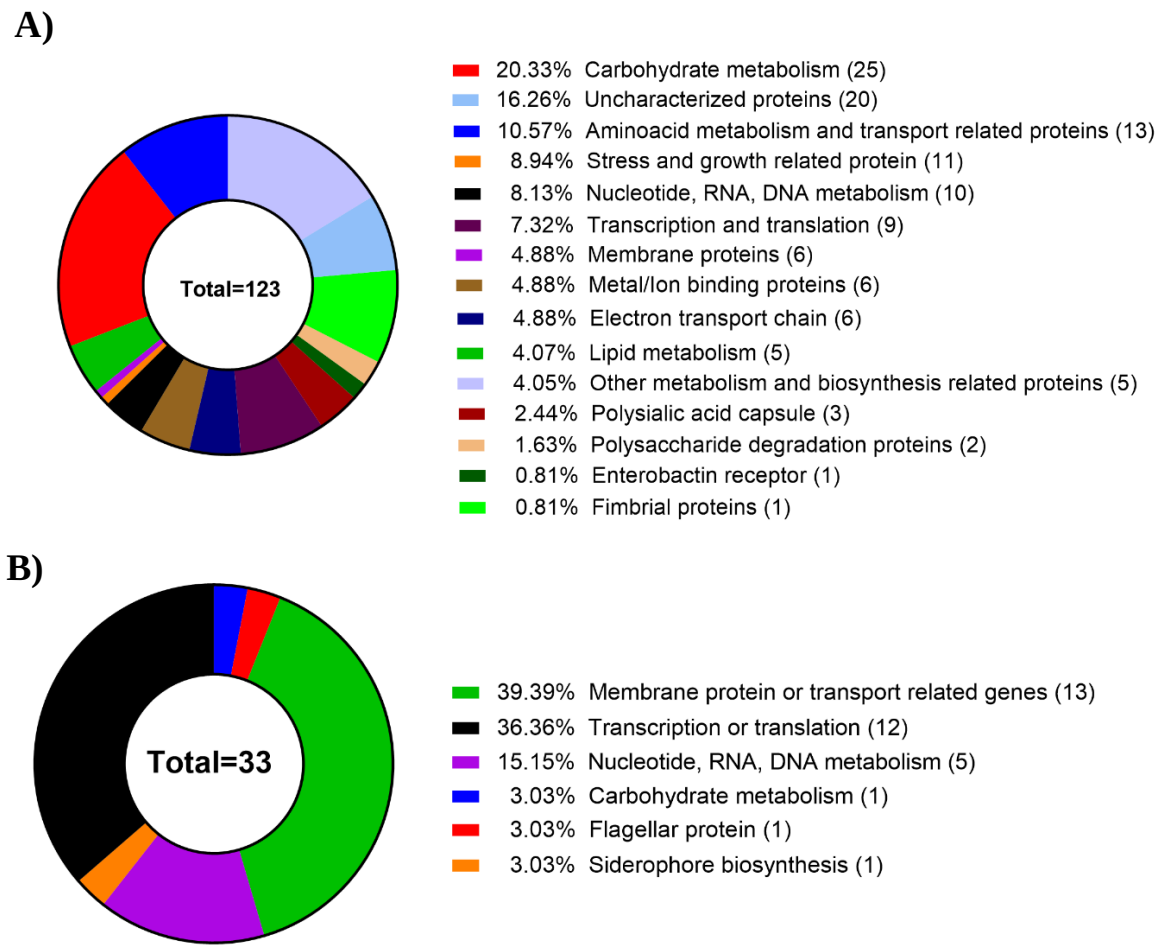

Figure 4.5. 10: Doughnut graphs representing the functional grouping of the genes that were downregulated (i) with log_2 fold change < -2, padj < 0.05 and upregulated (ii) with log_2 fold change > 2, padj < 0.05 in EcN when incubated with T4 phages after 2 h. In the legend of the graph, the numbers in the bracket after the functional groups represents number of genes down or upregulated in the respective group. Image source: (Soundararajan et al., 2019)

The functional grouping of upregulated genes (**Figure 4.5. 10_B**), showcased most of the genes upregulated in EcN after 2 h of incubation with T4 phages, constituted membrane protein or transport-related genes (~ 40 %), followed by transcription or translation-related genes (~ 36 %). The most upregulated gene: *EcN_1772* (log_2 fold change = 4.97) which is a putative inner membrane transport protein. Owing to the literature evidence, that reported certain membrane proteins of bacteria had conferred resistance against phage infections (Biswas et al.,

1992;Labrie et al., 2010;Cumby et al., 2015), we were interested to investigate if *EcN_1772* was responsible for the T4 phage resistance of EcN. For this purpose, the gene was cloned into an inducible pUC19 vector and the T4 phage sensitive MG1655 strain was transformed with the same. However, the successful cloning, followed by induction of expression of this gene was not able to protect the MG1655 strain from getting lysed by T4 phages in PPA (data not shown). Thus, the mere overexpression of *EcN_1772* in MG1655 was insufficient to confer resistance to T4 phages.

4.5.7. Biochemical studies to investigate the T4 phage inactivating factor in EcN

In an approach to elucidate the mechanism(s) of T4 phage inactivation by EcN, we were curious to investigate if any cellular and/or secretory factors of EcN could be responsible for its ability to reduce phage titer. To start with, EcN was tested by incubating with T4 phages at various MOIs and PFUs/ml were determined by PPA. The PPA results exhibited ~ 1,200-fold reduction in the T4 phage titer by EcN after 24 h of incubation at a ratio of 1000:1 (EcN:T4). Similarly, a ~ 98-fold reduction in PFUs/ml was observed, when EcN was incubated with 1000 times more T4 phages (EcN:T4 = 1:1000) (**Figure 4.5. 11_A**). In addition, EcN cells and supernatant were subjected to differential treatments like heat treatment (3.1.11.1) to examine whether the phage inactivating factors were heat sensitive. The PPA results of the coincubation experiments with heat-killed EcN (EcN_HK) and EcN supernatant samples (**Figure 4.5. 11_B**) revealed that not only live EcN cells (EcN) but also EcN supernatant (EcN_S) and supernatant of heat-killed EcN cells (HK_S) were able to reduce the phage titer by ~ 1,000-fold in 24 h. Interestingly, the heat-killed EcN cells (EcN_HK) reduced the phage titer by ~ 16,000-fold, which was ~ 12-fold more efficient than live EcN. The flow-through of EcN_S from the concentration process (EcN_S FT) was not able to reduce the phage titer and therefore excluding the possible participation of lower molecular components of EcN_S (less than 5 KDa) in T4 phage titer reduction. Noteworthy, when the EcN_S was further inactivated by

heat (100 ˚C, 1 h), its ability to reduce phage titer remained intact. Altogether, the heat treatment of either EcN or its supernatant did not result in loss of function demonstrating that

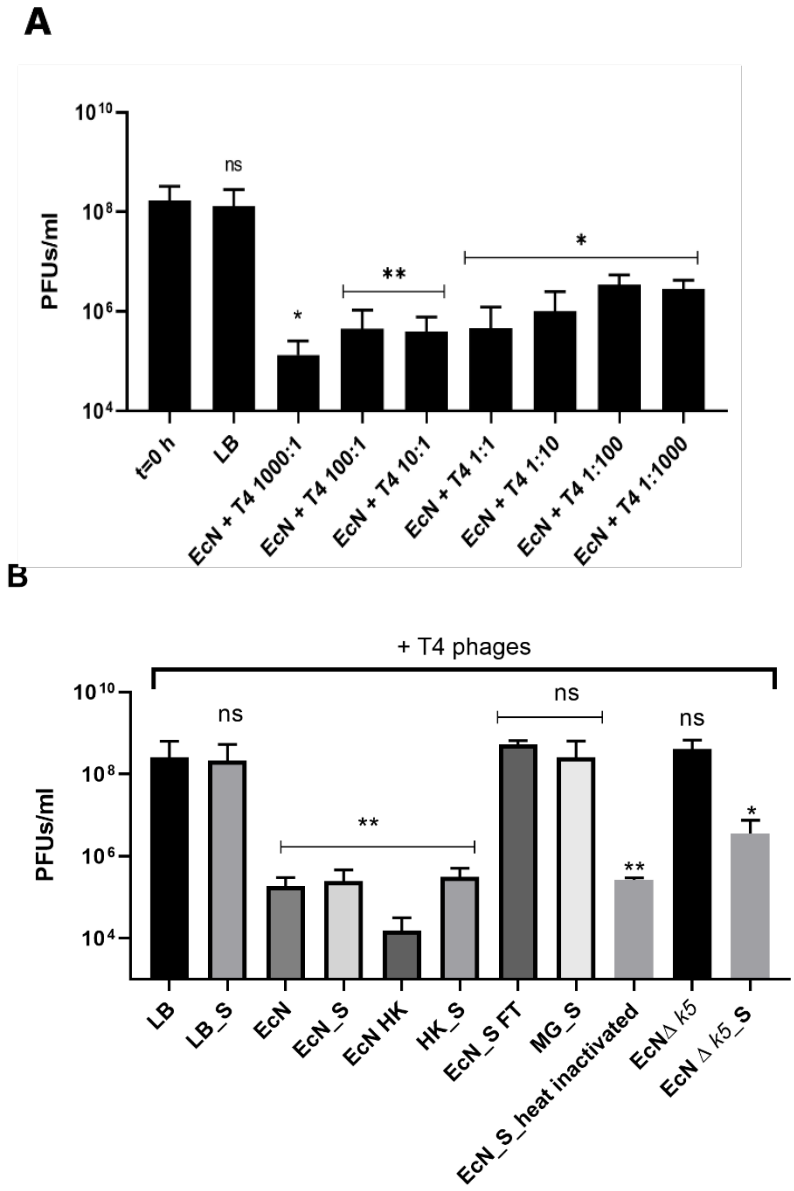

Figure 4.5. 11: Phage titer reduction by EcN and cell-free supernatant (A) EcN was incubated with T4 phages at various MOI at 37 ˚C for 24 h, static after which samples were sterile filtered, and PFUs/ml were determined by PPA. t=0 h: T4 phage titer at time point 0 h, LB: T4 phages + LB (phage titer after 24 h) **(B)** EcN cells were processed as described in 3.1.11 and incubated with T4 phages for 24 h at 37 ˚C, static after which samples were sterile filtered, and PFUs/ml were determined by PPA. The legends of the graph are described in the **Table 3. 1**. Image modified from (Soundararajan et al., 2019)

the factors responsible for T4 phage titer reduction were heat stable. In contrast to EcN, the supernatant of MG1655 (MG_S) was not able to inactivate the T4 phages.

Furthermore, the supernatant of the capsule negative mutant (EcNΔ *k5*) was tested for its ability to inactivate the T4 phages. Owing to its sensitivity towards T4 phages, the capsule negative mutant of EcN did not inactivate the T4 phages as expected. But, the supernatant of EcNΔ *k5* (EcNΔ *k5*_S), was still able to inactivate the phages ~ 100-fold (**Figure 4.5. 11**). Thus, indicating that there must be another factor in the supernatant of EcN responsible for its ability to inactivate the T4 phages.

Further to discern the characteristic features of phage inactivating factors(s), heat-killed cells were subsequently subjected to the treatment either with 40 mM sodium meta periodate (SMP) and/or 1 mg/ml proteinase K (PK) as described in the method section 3.1.11. PK digests peptide bonds between hydrophobic amino acids (aliphatic, aromatic) resulting in degradation of the protein molecules, whereas, SMP cleaves the bond between adjacent carbon atoms that contain hydroxyl groups (cis-glycols) in polysaccharides and thus degrading the carbohydrate molecules in the sample. The results (**Figure 4.5. 12**) indicated that not only the heat-killed EcN cells (EcN HK) but also the heat-killed and PK treated EcN cells (EcN HK+PK) reduced the phage titer after 24 h by ~ 14,000-fold and ~ 22,000-fold, respectively. Intriguingly, when EcN HK or EcN HK+PK were treated with 40 mM SMP and then employed in the coincubation, then the phage titer reduction ability was ~ 420-fold and ~ 1,700-fold less, respectively. From the results of this study, it was concluded that the phage titer reduction ability of EcN was significantly alleviated when the sample was treated with SMP. Thus we devised the hypothesis that the factor in EcN that was responsible for inactivation of T4 phages could be a glycoconjugate and/or a carbohydrate.

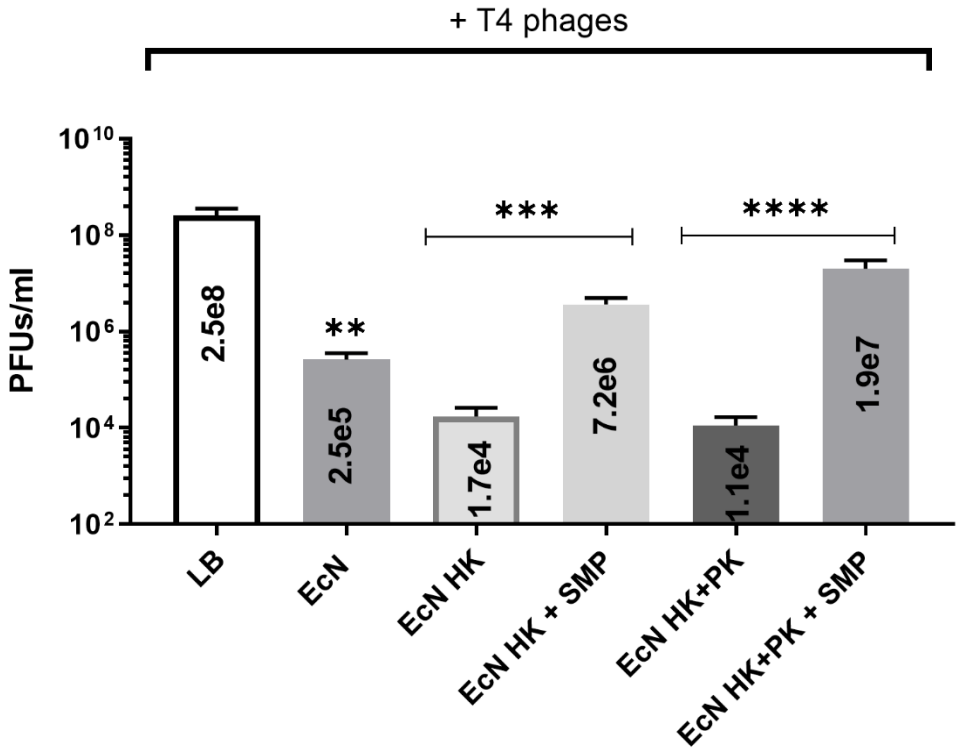

Figure 4.5. 12: Effects of biochemical processing of EcN with SMP and PK on T4 inactivation. The graph displays the results of phage titer reduction by EcN and processed EcN samples. **EcN HK**: heat killed EcN, **EcN HK+ SMP**: EcN HK treated with 40 mM SMP, **EcN HK+ PK**: EcN HK treated with 1 mg/ml PK, **EcN HK + PK + SMP**: EcN HK treated with 40 mM SMP and 1 mg/ml PK. In every case, 100 µl of T4 phages were incubated with 100 µl of LB/ treated or untreated EcN in 1 ml LB medium and incubated at 37 ˚C for 24 h after which the PFUs/ml were determined by PPA

This hypothesis led us to focus on the lipopolysaccharides (LPS) of EcN as a candidate and the *E. coli* supernatant was known to be rich with secreted LPS (Zhang et al., 1998) molecules thus supporting our hypothesis. To fathom the role of LPS in T4 phage inactivation, the antibiotic polymyxin B (PMB) was employed in coincubation studies. PMB could bind to LPS of gram-negative bacteria and it has been previously reported that 25 µg/ml of PMB collapses the structure of LPS by fusing them into an amorphous solid and thereby destroying its T4 phage receptor activity (Koike and Iida, 1971). Hence, we treated EcN samples with 25 µg/ml of PMB and subjected them to coincubation studies. The results (**Figure 4.5. 13_A)** exhibited that addition of PMB clearly inhibited EcN's ability to reduce T4 phage titer. In elaborate, when 25 µg/ml of PMB was added to EcN supernatants namely, EcN_S (supernatant of EcN) and

HK_S (supernatant of heat-killed EcN), their phage inactivation ability was completely abrogated. In case of heat-killed EcN (EcN_HK), the addition of PMB decreased the phage titer reduction ability by ~ 150-fold. Besides, we also demonstrated that when treated with a higher concentration of PMB (5× –125 µg/ml and 10× – 250 µg/ml), heat-killed EcN (EcN HK) did not reduce the phage titer any longer (**Figure 4.5. 13_B**).

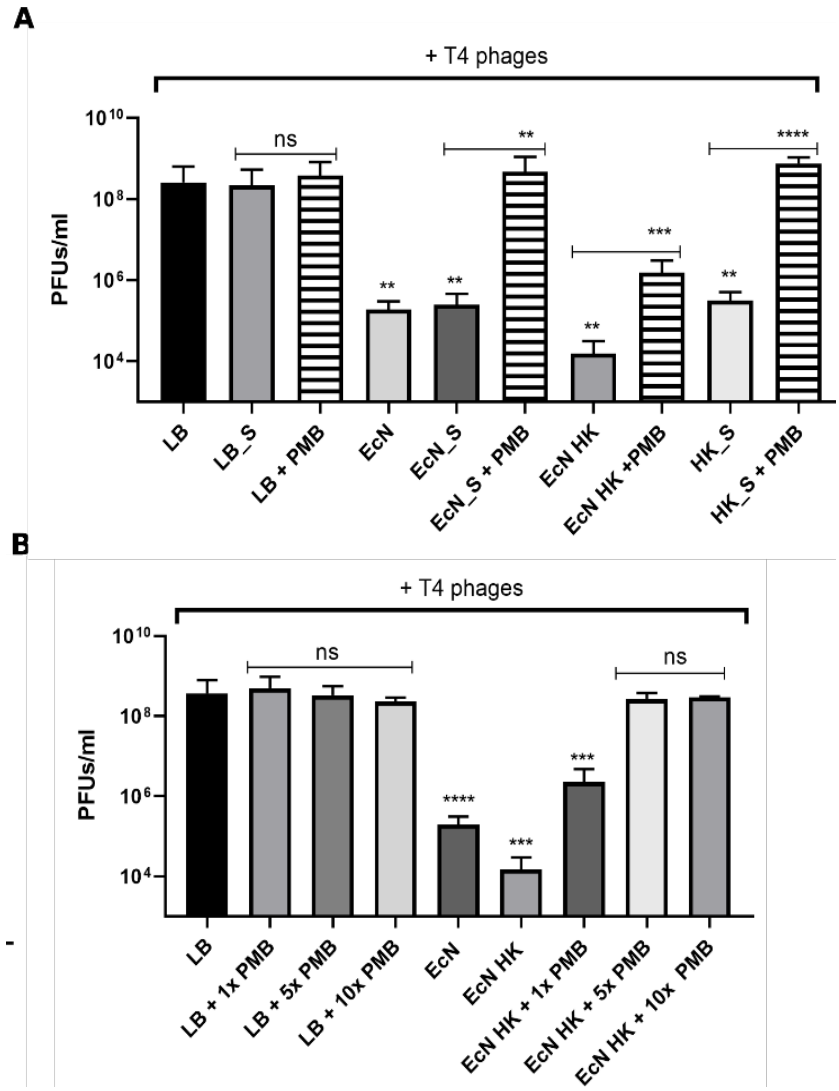

Figure 4.5. 13: T4 phage inactivation by EcN samples treated with PMB. (A) The graph displays the results of phage titer reduction by EcN/ processed EcN samples treated with 25 µg/ml PMB for 1 h at 37 °C after which PFUs/ml were determined by PPA. The legends of the graph are explained in the **Table 3. 1**. **(B)** Phage titer reduction by heat-killed EcN (EcN HK) treated with increasing concentration of PMB: 1× – 25 µg/ml, 5× – 125 µg/ml, 10× – 250 µg/ml. As a control, LB medium was treated with the same concentrations of PMB and used in the incubation. PFUs/ml were determined after 24 h at 37 °C by PPA. ns – not significant, **p<0.0021, ***p<0.0002 and ****p < 0.0001. Image source: (Soundararajan et al., 2019)

The results with PMB suggested that the LPS could be an important factor mediating T4 phage inactivation by EcN. Furthermore, to prove the independent role of EcN's LPS in T4 phage inactivation, LPS was isolated from *E. coli* as described in 3.1.12 and EcN LPS was diluted 1:10, 1:100 and 1:1000 in nuclease-free water and incubated with T4 phages in the presence and absence of PMB for 1 h at 37 ˚C after which the percentage of free phages in the supernatant was determined by PPA. Simultaneously the isolated LPS was also quantified in a 12 % SDS PAGE followed by LPS-specific staining as described in 3.2.11.

The results from the LPS and T4 coincubation studies (**Figure 4.5. 14_A**) presented the ability of isolated EcN LPS (UD; 1:10, 1:100) to inactivate the T4 phages and this ability was completely destroyed in the presence of 25 µg/ml PMB. In line with earlier findings (Beacham and Picken, 1981;Washizaki et al., 2016), we also observed that the LPS of *E. coli* K-12 strains (MG1655, commercially purchased K-12 LPS (0.5 mg/ml)) could not inactivate the T4 phages. Correspondingly, the typical banding pattern of EcN's semi-rough type LPS was visualized on the SDS gel with the lower band referring to the lipid-A-core and the upper band representing single O6-antigen repeating unit (Grozdanov et al., 2002) and on the contrary, in case of *E. coli* K-12 LPS (MG1655, commercial K-12 LPS 0.5 mg/ml) only one band that referred to the LPS core was visible on the gel (**Figure 4.5. 14_B**).

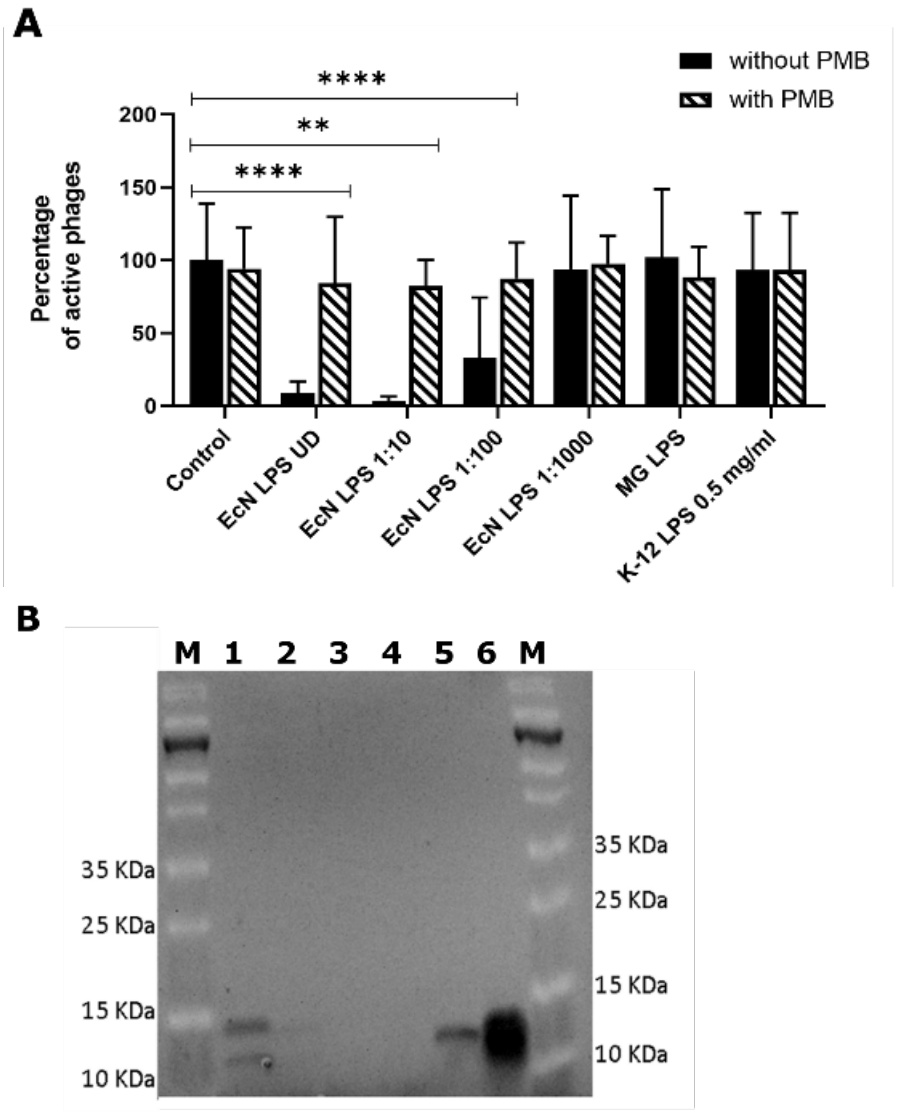

Figure 4.5. 14: T4 phage inactivation by isolated LPS. (A) 100 µl of T4 phages were incubated with 100 µl of LPS isolated from *E. coli* strains (EcN/MG1655) +/- 25 µg/ml PMB for 1 h at 37 °C and percentage of active phages were determined by PPA. **Control**: T4 phages + water, **EcN LPS UD** – undiluted LPS isolated from EcN, **EcN LPS 1:10 or 1:100 or 1:1000** – EcN LPS serially diluted with nuclease free water, **MG LPS** – undiluted LPS isolated from MG1655, **K-12 LPS 0.5 mg/ml** – commercially available K-12 LPS (Cat no: tlrl-eklps, Invivogen). ns – not significant, ∗∗ p<0.0021 and ∗∗∗∗p < 0.0001. **(B)** The isolated LPS was visualized on 12 % TruPAGE precast gels and stained with Pro-Q Emerald 300 LPS gel stain kit. **Lane description** M: Page Ruler prestained protein ladder, 1: EcN LPS UD, 2: EcN LPS 1:10, 3: EcN LPS 1:100, 4: EcN LPS 1:1000, 5: MG1655 LPS, 6: K-12 LPS 0.5 mg/ml. Image source: (Soundararajan et al., 2019)

The long and short tail fibres of T4 phages are known to be involved in its adsorption to receptors at the *E. coli* cell surface (Yu and Mizushima, 1982). Specifically, the initial recognition is performed by the long tail fibres of T4 that reversibly attach to the LPS followed

by the firm attachment of short tail fibres that leads to successful phage infection in a sensitive strain (Washizaki et al., 2016;Brzozowska et al., 2018). In this regard, our next challenge was to identify the molecular component in EcN's LPS that could interact with the tail fibres of T4 phages. We speculated that N-acetylglucosamine (GlcNAc), the terminal molecule in EcN's O6-side chain could be the candidate and hypothesized that if the binding of T4 phages to EcN's LPS was mediated by GlcNAc, then the addition of external GlcNAc should interfere not only with the binding of T4 phages to EcN's LPS but also with the inactivation of T4 phages. To prove the hypothesis, T4 phage adsorption to EcN/MG1655 was investigated in the presence and absence of 0.6 M GlcNAc/Glucose after short intervals of phage addition (1,3,6,9,12 and 30 mins) by PPA. The results **(Figure 4.5. 15_A**) revealed a steady drop in the T4 phage titer of about ~ 100-fold reduction after 30 mins of phage addition to EcN, implying the T4 phage adsorption to EcN. However, in the presence of 0.6 M GlcNAc, as hypothesized, the phage adsorption to EcN and in turn the phage titer reduction was absolutely abolished. In addition, this complete inhibition of phage adsorption to EcN was GlcNAc specific because the presence of glucose at the same concentration did not result in a significant change in phage titer reduction (**Figure 4.5. 15_B**). In contrary to EcN, an increase in T4 phage titer was noticed in the absence of GlcNAc/Glucose after 12 mins of incubation with MG1655 indicating a successful infection and phage propagation. In addition, the presence of both GlcNAc and Glucose inhibited phage adsorption to MG1655. This observation was similar to that of *E. coli* B, where studies reported a range of oligosaccharides inhibited the phage adsorption (Dawes, 1975). Our results collectively suggested that GlcNAc at the terminal end of EcN's O6 antigen could be the effector molecule that mediates the attachment of T4 phages to EcN, thereby neutralizing the T4 phages.

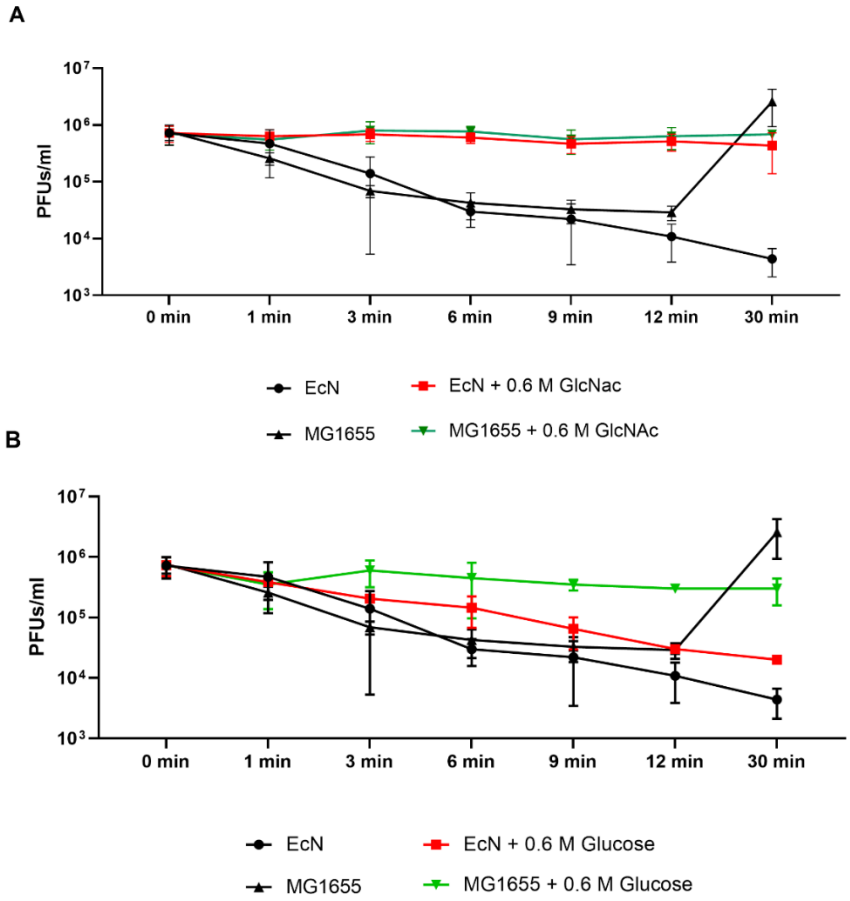

Figure 4.5. 15: T4 phage adsorption to EcN in the presence of 0.6 M GlcNAc. The image displays the kinetics of T4 phage titer reduction after the addition of T4 phages to the *E. coli* cultures in the presence and absence of 0.6 M GlcNAc **(A)** or 0.6 M Glucose **(B)**. In both cases, T4 phages were added to mid-log phase (OD600 = 0.5) EcN or MG1655 culture in the ratio of 1:100 (T4:*E. coli*), PFUs/ml were determined at different time points as mentioned in the graph by PPA. Image modified from (Soundararajan et al., 2019)

4.5.8. Impact of other *E. coli* strains on T4 phages

We were curious to unravel whether the T4 phage inactivation is a unique ability of EcN. To address this, the T4 phage titer reduction ability of other *E. coli* strains such as the uropathogenic strain CFT073 and commensal strains SE11, SE15 and their respective supernatants were investigated. The PPA results (**Figure 4.5. 16**) informed us that only the cells and supernatant of CFT073 were able to reduce the phage titer as efficiently as EcN after 24 h

of incubation, while the incubation with cells/supernatant of SE11 and SE15 did not reduce the phage titer.

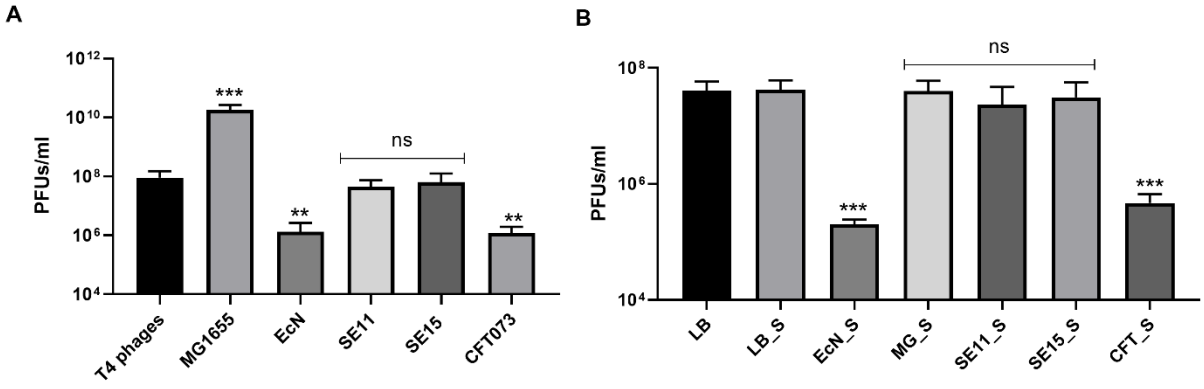

Figure 4.5. 16: Influence of *E. coli* strains and their supernatants on T4 phage titer. The result of coincubation studies performed with **(A)** *E. coli* strains and **(B)** their supernatants. *E. coli* strains or their respective supernatants were incubated with T4 phages for 24 h at 37 °C, static after which the PFUs/ml were determined by PPA. ns – not significant, ∗∗ p<0.0021, ∗∗∗p < 0.001. Image source: (Soundararajan et al., 2019)

Further, to establish the influence of EcN on T4 phage infectivity of the K-12 strains, a triculture set up was made with T4 phage + SK22D + MG1655/HB101/DH5α and the results (**Figure 4.5. 17_A**) demonstrated that the presence of the microcin negative mutant of EcN (SK22D) in the triculture reduced the phage titer increase of the K-12 strains MG1655, DH5α and HB101 by about ~ 5,000-fold, ~ 360-fold and ~ 550-fold, respectively. Moreover, only the CFT073 strain was able to inhibit the MG1655 infection by T4 phages as efficiently as the SK22D strain (**Figure 4.5. 17_B**). Hence, our results, in conclusion, demonstrated that EcN interferes with T4 phage infection of the tested K-12 strains very efficiently and this phenomenon was not commonly observed among the tested commensal strains.

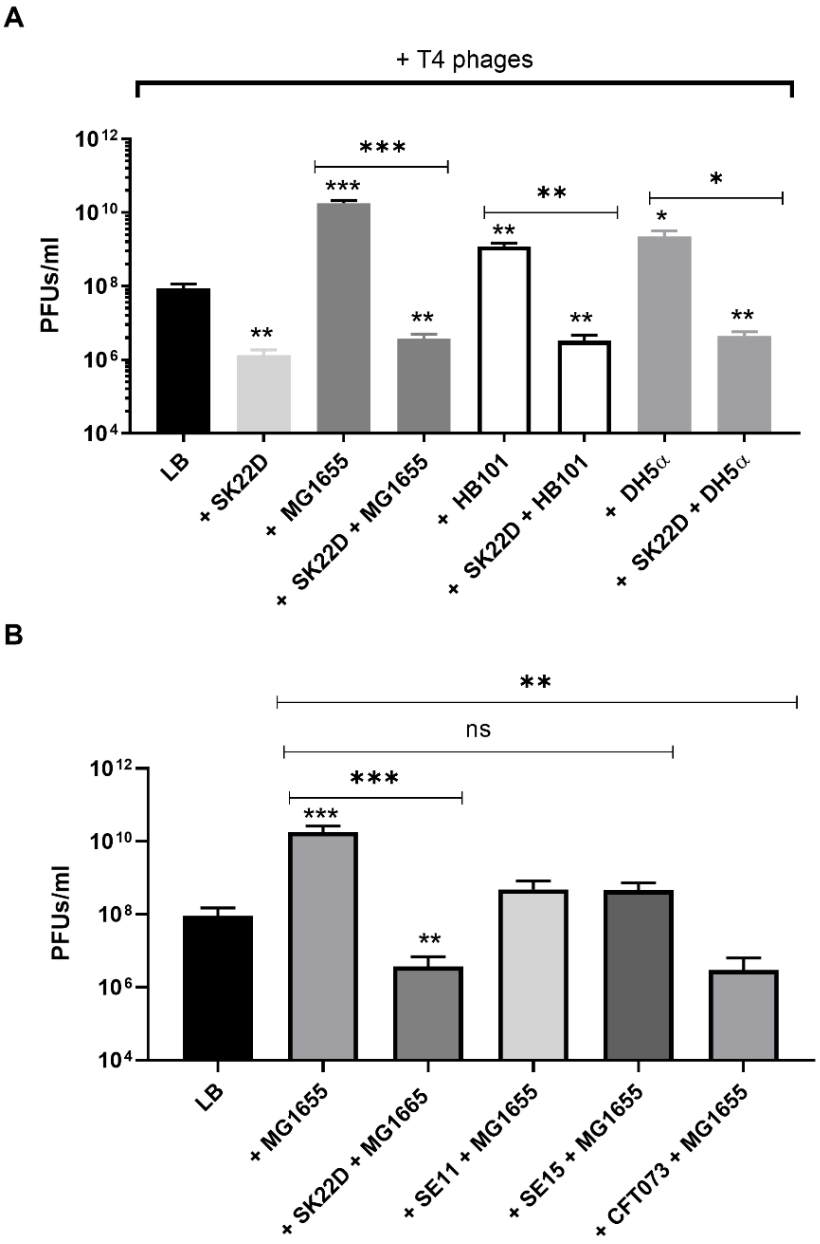

Figure 4.5. 17: Influence on T4 phage infection of K-12 strains by *E. coli* strains:
(A) T4 phages were incubated either alone in LB medium (LB) or in a coculture set up with SK22D/ *E. coli* K12 strains such as MG1655, HB101 and DH5α or in a triculture set up with T4 phages:SK22D:K-12 strains (MOI of 1:1:1) **(B)** Similarly SE11/SE15/CFT073 was employed in triculture set up, T4 phages: SE11/SE15/CFT073:K-12 strains (1:1:1).
In both (A) and (B), the incubation was carried out for 24 h at 37 ˚C after which the PFUs/ml were determined by PPA. The statistical significance was calculated by unpaired t-test. The significance of the triculture set up were calculated by comparing to the respective coculture with the K-12 strains. *p<0.0332, **p<0.0021, ***p<0.0002 and ****p<0.000. Image A was adapted from (Soundararajan et al., 2019)

In summary, from this part of the study, we demonstrated a K5 polysaccharide capsule mediated resistance of EcN towards lytic T4 phage. In addition, EcN also inactivated the T4 phages during coincubation and EcN's O6-type LPS was shown to play a role in the inactivation of T4 phages.

5. Discussion

5.1. Expression of probiotic factors in EcN fermenter culture

More than 100 years since its isolation, EcN is probably the most extensively researched probiotic strain to date (Wassenaar, 2016). Yet, a complete understanding of the molecular mechanism(s) behind EcN's probiotic nature remains deficient. And thus, at the first part of our study, we employed modern transcriptomics based approaches to get insights into the expression of genes in EcN after the fermentation process, as this might closely resemble their gene expression profile in the Mutaflor® capsule. Therefore, the transcriptomes of EcN cultured in the Mutaflor production fermenter were compared to the transcriptome of EcN grown under the laboratory conditions. The regulation of various fitness factors of EcN was analysed in the fermenter cultures as these factors have been reported to contribute to several probiotic traits of EcN (Grozdanov et al., 2004;Sonnenborn and Schulze, 2009). Transcriptomic analysis revealed an astounding upregulation of the curli fimbrial determinant in both tested EcN fermenter cultures. The curli fimbrial determinant of *E. coli* promotes biofilm formation (Barnhart and Chapman, 2006;Beloin et al., 2008) and EcN had been reported to outcompete other intestinal pathogens during biofilm formation (Hancock et al., 2010a). The other major upregulated gene clusters in EcN fermenter cultures corresponded to iron uptake systems of EcN and this was particularly interesting because the iron uptake systems of EcN were reported to be crucial for outcompeting and reducing *S. typhimurium* colonization in mouse models of acute colitis and chronic persistent infection (Deriu et al., 2013). In contrast, we observed the downregulation of other fitness factors of EcN like Type 1 fimbriae, F1C fimbriae, K5 polysaccharide capsule, H1

type flagella and the antibacterial microcins. Particularly, downregulation of microcins could be attributed to the absence of any other non-EcN bacteria in the fermenter. Further, the O6-type LPS of EcN showed a differential expression pattern with an insignificantly regulated *waa* gene cluster and a slightly upregulated *wbb* gene cluster. To sum up, the findings from the study are illustrated in the graphical representation (**Figure 5. 1**) in which red and green arrows indicate the up and downregulation of respective gene glusters.

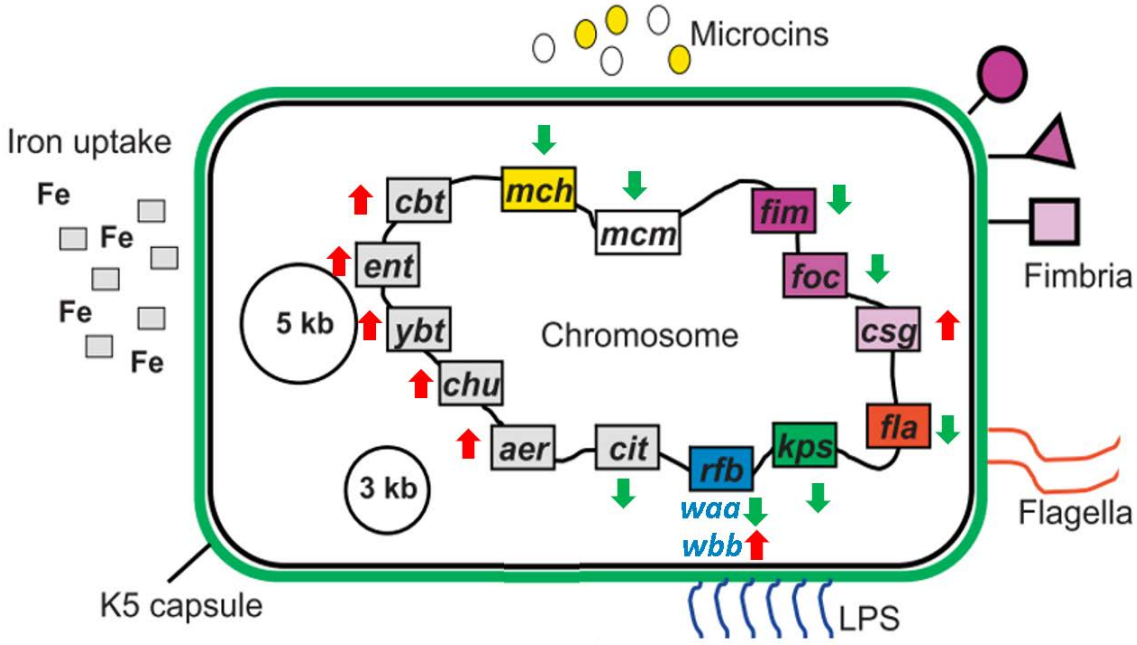

Figure 5. 1: Graphical representation depicting the up/downregulation of various fitness factors of EcN. Gene clusters of EcN's fitness factors were outlined in the chromosome of EcN. Iron uptake systems: *aer* – aerobactin, *chu* – hemin, *ybt*- yersiniabactin, *ent*- enterobactin, *cbt* – salmochellin, *cit*- citrate dependent; *mch* & *mcm* – microcin gene cluster encoding microcins H47 and M; Fimbrial determinants: *fim* – Type 1, *foc* – F1C, *csg* – curli fimbria; *fla* – H1 type flagella; *kps* – K5 capsule; *rfb* – O6 type LPS; Red upward arrows – overall upregulation of the gene cluster, green downward arrows – overall downregulation of the gene cluster.Image adapted from (Jacobi and Malfertheiner, 2011)

From these results, it can be presumed that EcN harvested after the fermentation process was in a metabolic state suitable for biofilm formation and with an increased ability to compete for iron. Both of these traits would aid in its effective temporary colonization of the gut which is

one of the highly acclaimed positive traits of Mutaflor® (Lodinova-Zadnikova and Sonnenborn, 1997;Lodinova-Zadnikova et al., 1998;Barth et al., 2009).

5.2. **EcN shows a discriminative response towards pathogenic and non-pathogenic *E. coli***

The pathogenic EHEC strain EDL933 is associated with the development of gastroenteritis in humans. The major pathogenic factor is Stx, two of which are encoded by two prophages of this strain known as *stx*-phages BP-933W and CP-933V (Herold S1, Siebert J, Huber A, Schmidt H., 2005). These phages can lysogenize commensal *E. coli* and turn them into toxin-producing pathogens (Schmidt, 2001). Antibiotic treatment can be detrimental as it induces the SOS response of the EHEC strains resulting in an increased *stx*-phage production that can worsen the disease progression (Pacheco and Sperandio, 2012). Research for alternative treatment strategies revealed, that the probiotic *E. coli* strain EcN reduced the CFUs/ml of EHEC strains and additionally interfered with the toxin production when being cocultured (Reissbrodt et al., 2009;Rund et al., 2013;Bury et al., 2018). Furthermore, studies have reported that the reduction of toxin can be attributed to the transcriptional repression of the entire *stx*-prophage (Mohsin et al., 2015;Bury, 2018). Increased availability of information on bacterial genomes has now made it possible to understand the individual response of each bacterial strain in the coculture with the help of transcriptome analysis. Therefore, it was critical to keep the EcN separated from other bacterial strains in the coculture to isolate its RNA. To address this, the coculture experiments with EcN and EDL933 strains were performed in a transwell system with an insert of pore-size 0.4 µM that served as an impermeable barrier for bacteria but still allowed the diffusion of the bacterial secretome. The initial reduction in the Stx level of EDL933 compartment was observed after 5 h of incubation with EcN and the reduction was persistent in the following time points investigated (**Figure 4.3. 1**). The results indicated that a direct cell to cell contact was not necessary for EcN to exert its effect on EDL933. In addition, determination of CFUs/ml of *E. coli* strains in the transwell indicated that there was no

significant difference in CFUs/ml of EDL933 between monoculture and cocultures with EcN. The observation was rather contradictory to the already reported coculture results without the Transwell system, in which EcN was in direct contact with EDL933 (Rund et al., 2013;Bury, 2018). The reason for such a contact-dependent growth reduction of EDL933 by EcN could be postulated to be the result of a complete type 6 section system (T6SS) determinant in EcN. Previously, in our lab, it was found that EcN harbours all 13 core components of a T6SS, with the help of T346Hunter (https://omictools.com/t346hunter-tool) – a web-based tool for prediction of section systems in bacterial genomes (Bury, 2018). In addition, genome analysis by Dr Oelschlaeger revealed that EcN has, in fact, the same T6SS determinants as the uropathogenic strain CFT073. In general, T6SS is a pivotal player in mediating the killing of other bacterial strains by direct cell contact and paves way for successful bacterial competition (Journet and Cascales, 2016;Navarro-Garcia et al., 2019). However, studies with T6SS-deletion mutant of EcN are required for proving the involvement of the secretion system in growth inhibition of EDL933.

Further, to unravel the factor(s) in EcN that are responsible for its anti-shiga toxin effect, transcriptomes of EcN were analysed at four different time points of incubation in the presence and absence of a pathogenic strain EDL933 or non-pathogenic strain MG1655. The transcriptome analysis revealed a striking difference in EcN's response based on the *E. coli* that was in the coculture. Especially, a dramatic change in the gene regulation was observed in EcN as early as 3 h after coincubation with EDL933, whereas, EcN showed a very minimal regulation in response to MG1655 (**Figure 4.3. 5** and **Figure 4.3. 6**). Moreover, EcN not only exhibited a remarkable difference in the kinetics of gene regulation over the time points of coincubation but also the nature of genes up and down-regulated between EDL933 and MG1655 coincubation were impressively specific (**Figure 4.3. 7**, **Figure 4.3. 8** and **Figure 4.3. 9**). The functional prediction of up and downregulated genes in EcN aided us to gain a global

outlook on the transcriptomic profile of EcN when cocultured with EDL933/MG1655. The genes belonging to the same functional group were both up and down-regulated in EcN but were absolutely different [Annexure 3 (Table 8.1 and Table 8.2)]. For example, in some of the functional groups, namely, carbohydrate transport and metabolism, membrane proteins, nucleotide metabolism, putative transporters, transcription and translation, an almost similar number of genes were up and down-regulated. However, when examined closer, it was seen that the most upregulated gene of the group: transcription and translation was EcN1917_3132 (Selenium-dependent molybdenum hydroxylase system protein), whereas the most downregulated gene was EcN1917_4649 (Melibiose operon regulatory protein). This was also the case with other functional groups, which was evident from analysing the list of up and downregulated genes in EcN 3 h post-incubation with EDL933 [Annexure 3 (Table 8.1 and Table 8.2)]. In addition, there were some functional groups for which there was a notable difference between the number of genes up and downregulated. For e.g. in the functional group amino acid transport and metabolism, 26 genes were upregulated and only 5 genes were downregulated. Similarly, in the groups like iron uptake and sequestration systems, and LPS metabolism, 23 and 10 genes were upregulated whereas only 4 and 3 genes were downregulated, respectively. Finally, there were also genes belonging to certain functional groups that were exclusively up or downregulated. For instance, genes corresponding to fimbrial proteins were only upregulated, whereas, genes corresponding to sugar transport and anaerobic growth-related proteins were only downregulated. Very often, the *E. coli* transcriptomics studies published focused on studying the transcriptional profile under different monoculture conditions (Snyder et al., 2004;Hancock et al., 2010b;Yung et al., 2016;Hazen et al., 2017;Oladeinde et al., 2018). Rarely have coculture based transcriptomic studies been performed and even then authors have looked only for the regulation of determinants of their interest. For example, in a study by (McCully et al., 2018), the authors have concentrated on studying the nitrogen starvation response of *E. coli* when cultured with phototrophic

Rhodopseudomonas palustris. Hence to our knowledge, we have reported for the first time, a global transcriptomics response of a probiotic *E. coli* strain (EcN) when cocultured with pathogenic or non-pathogenic *E. coli*. However, from these transcriptomics results, it is difficult to be conclusive in addressing our initial goal of identifying the factors in EcN that are responsible for its ability to inhibit Stx production of EDL933. Though the initial inhibition of Stx by EcN in the transwell system was observed at 5 h (**Figure 4.3. 1**), the maximum number of genes up and downregulated in EcN was as early as 3 h post-incubation with EDL933 and the number of genes regulated (both up and down) gradually decreased over time (**Figure 4.3. 7**). Hence, we speculate that the transcriptomic changes in EcN could have occurred already immediately after sensing EDL933, and the time points we chose for transcriptomic analysis were relatively late to notice these changes. Hence in future, analysing the transcriptome of EcN after short exposure with EDL933 (15, 30, 45 and 60 mins post-incubation) could be a probable strategy to unearth the factors or genes that might have been possibly missed at 3 h.

Overall, the specific response of EcN towards the *E. coli* strain EDL933 and MG1655 were particularly startling, given the fact that they share 98.65 % genome identity. This unique trait can be considered as an advantage for its application as a probiotic over the other chemical-pharmaceutical preparations in the market which are known to act identically on all the target *E. coli*. Moreover, one could envisage that EcN might recognise factors of specific bacterial strains or unique factors of different bacterial strains or species which could initiate a specific expression profile. Such a feature would make EcN an attractive therapeutic.

5.3. **Effect of EcN on lysogenic lambda phages**

Infection of bacterial strains by lysogenic phages is one of the main horizontal gene transfer mechanisms in the gut (Chiang et al., 2019;Frazao et al., 2019). The lateral transfer of genes encoding for virulence and antibiotic resistance had been reported as important factors contributing to the emergence of new pathogenic strains and for the global spread of antibiotic

resistance (Cheetham and Katz, 1995;Chen and Novick, 2009;Imamovic et al., 2009;Marinus and Poteete, 2013;Haaber et al., 2016;Colavecchio et al., 2017). Therefore, being resistant to lysogenic phages becomes one of the major safety aspects of a probiotic strain. Initially, the resistance of EcN towards lysogenic lambda phages propagated from lysogenic *E. coli* K-12 strain 993 W was tested. Accordingly, possible lysogeny in EcN incubated with lambda phages was assessed by screening for the lambda phage DNA that could have been integrated into EcN's genome. The PCR screening of EcN, which was incubated with the lambda phages detected no amplicon which indicated that the phage DNA did not integrate into the genome of the probiotic strain. The MG1655 control, on the other hand, was positively determined for the prophage integration (**Figure 4.4. 1**). Similarly, to further confirm the absence of lysogeny, the EcN incubated with lambda phages was induced for prophage production by addition of 1 µg/ml MMC followed by enrichment of phages in the sterile filtrate by incubating with MG1655 (**Figure 4.4. 2**). The PCR results confirmed our finding that no phages were detected in the supernatant of EcN even after forced lytic cycle induction by mitomycin C. In summary, with two different experiments, which particularly confirmed the absence of genome integration of phage DNA and phage propagation, we showed that EcN was not infected by the tested lambda phages.

Phage-bacteria interactions and subsequent fight for survival led to the evolution of bacterial and phage genomes. *E. coli* have continuously evolved many molecular mechanisms, driven by gene expression to prevent phage infections (Labrie et al., 2010;Azam and Tanji, 2019;Mohammed, 2019). An attempt to understand the transcriptional changes in EcN that were resulting in *stx*-phage resistance revealed an upregulation of genes of a lambdoid prophage in EcN (Bury et al., 2018). Further analysis with PHAST – a fast phage search tool - predicted the presence of six prophages in EcN's genome, of which three were predicted as intact. Particularly, upregulated prophage 3 was predicted to be a complete lambdoid prophage of EcN

(**Figure 4.4. 3**). Though EcN was predicted to possess three complete prophages, none of these prophages was induced by MMC, antibiotics or heat. The regulation of the other five predicted prophages in EcN was also analysed and reported as not significantly changed in the presence of *stx*-phages (Bury, 2018). One of the most upregulated genes in the presence of *stx*-phages was EcN_1294, that encoded for the phage repressor gene (*pr*) of prophage 3. For further investigations, the *pr* gene was selected as a candidate since, it was reported in *Lactobacillus* to confer resistance against lytic infection (Ladero et al., 1998;Alvarez et al., 1999). Upregulation of the *pr* gene in EcN incubated with lambda phages for 3 h was also confirmed by qRT-PCR (**Figure 4.4. 3_C**). In line with the previous findings, the successful cloning and overexpression of *pr* gene reduced the plating efficiency of lambda phages by ~ 215-fold on the otherwise, sensitive MG1655 strain (**Figure 4.4. 4**). The phage repressor of lambdoid phages is known to be responsible for lysogeny maintenance (Serra-Moreno et al., 2008;Casjens and Hendrix, 2015), hence it is likely that in the MG1655 cells, the expression of *pr* had reduced the lysis of the cells and promoted the lysogeny. However, in the case of EcN, no lysogens could be detected, even 120 h post-incubation with lambda phages (**Figure 4.4. 2**). Moreover, because the *pr* gene provided only partial protection to the MG1655 strain, presumably, there must be another unidentified additional factor(s) in EcN that contributed to its complete resistance against lambda phages. In this regard, Bury (2018) analysed the presence of prophage 3 of EcN in other *E. coli* strains that were also lambda phage resistant. The analysis revealed that all investigated lambda phage resistant strains harboured all or most of the prophage 3 genes, with 100 % identity in case of uropathogenic strain CFT073 and with slight differences at sequences in case of commensal strains SE11 and SE15. Fascinatingly, only the phage sensitive MG1655 strain lacked most of the prophage 3 genes. With this analysis, we could hypothesize that the presence of the complete prophage 3 was imperative for the complete resistance towards lambda phages (Bury, 2018). For the convenience of the reader, the results of the analysis by Bury are also presented in the following table.

Tabel 5. 1: Presence of EcN's prophage 3 genes in CFT073, the commensal strains SE11 and SE15 and the K-12 strain MG1655. Table modified from (Bury, 2018).

EcN	Description	CFT073	SE11	SE15	MG1655
1289	Mobile element protein	P	-	-	P
1290	putative superinfection exclusion protein	P	-	-	-
1291	hypothetical protein	P	-	-	-
1292	hypothetical protein	P	-	-	-
1293	cI repressor protein	P	P*	P*	-
1294	Phage repressor (pr)	P	P*	P*	-
1295	Origin specific replication initiation factor	P	P	P	-
1296	Replication protein P	P	P	P	-
1297	Phage NinB DNA recombination	P	P	P	-
1298	Phage DNA N-6-adenine methyltransferase	P	-	-	-
1299	Phage NinX	P	P	P	P
1300	Crossover junction endodeoxyribonuclease	P	P	P	P
1301	hypothetical protein	P	P	P	P
1302	Phage antitermination protein Q	P	P	P	P
1303	Outer membrane porin protein NmpC	P	P	P	P
1304	Phage holing	P	P	P	P
1305	Phage tail fibre protein	P	P	P	P
1306	Phage outer membrane lytic protein	P	P	P	P
1307	Lipoprotein Bor	P	P	P	P
1308	hypothetical protein	P	-	-	-
1309	hypothetical protein	P	-	P	-
1310	Terminase small subunit	P	-	P	-
1311	Phage terminase 2C large subunit	P	P	P	-
1312	Phage head-to-tail joining protein	P	P	P	-
1313	Phage portal protein	P	P	P	-
1314	Phage capsid and scaffold	P	P	P	-
1315	Head decoration protein	P	P	P	-
1316	Phage major capsid protein	P	P	P	-
1317	Phage DNA-packaging protein	P	-	P	-
1318	Phage capsid and scaffold	P	P	P	-
1319	Phage tail completion protein	P	P	P	-
1320	Phage minor tail protein	P	P	P	-
1321	Phage tail assembly	P	P	P	-
1322	Phage minor tail protein	P	P	P	-
1323	Phage minor tail protein	P	P	P	-
1324	Phage tail length tape-measure protein 1	P	P	P	-
1325	Phage minor tail protein	P	P	P	-
1326	Phage minor tail protein	P	P	P	-
1327	Phage tail assembly protein	P	P	P	-
1328	Phage tail assembly protein I	P	P	P	-
1329	Phage tail fibre protein	P	P	P	-
1330	Phage tail fibre protein	P	P	P	-

P: gene present in the genome; -: gene not present; *: sequence not identical to EcN.

Transcriptome analysis of EcN coincubated with lambda-phages revealed a strong upregulation of transcripts (1,104 bp) that were transcribed from the antisense strand of genes *sieB* and anti-termination protein N. Strand-specific qRT-PCR performed on EcN incubated with lambda phages for 3 h, demonstrated an upregulation of transcripts from both the strands of *sieB* gene, while expression of transcript was far higher for the antisense (fold change ~ 85) than the sense strand (fold change ~ 19) (**Figure 4.4. 5**). Initially, the expression of antisense transcripts was considered as a gene repression mechanism adopted by the host cell to switch off the gene in response to environmental conditions. However, studies have also pointed out that the pairing of sense and antisense transcripts of a gene is a self-regulatory circuit that controls the dynamics of the expression of the sense transcript (Xu et al., 2011;Pelechano and Steinmetz, 2013). Based on these findings, we can assume that the observed antisense regulation could directly or indirectly regulate the expression of *sieB* gene which was reported to provide resistance against phage infection by blocking the entry of phage DNA (Ranade and Poteete, 1993;McGrath et al., 2002). In future studies, analysing the regulation of sense and antisense strand of *sieB* in EcN at different time points of incubation with lambda phages could shed more light on understanding the dynamics of *sieB* expression. Noteworthy, the cloning of *sieB* gene in MG1655 did not confer resistance against lambda phage infection (**Table 4. 2**). However, this effect could be attributed to lack of proper expression of *sieB* which was not validated in our experimental setup. Anyhow, to clarify the speculations regarding the involvement of the EcN's membrane protein *sieB* in its lambda phage resistance, testing the phage sensitivity of a *sieB* deletion mutant of EcN would be an ideal system.

In summary, we have reported for the first time the involvement of a prophage mediated resistance against lambda phage infection in EcN. Similar prophage genes or prophage mediated resistance mechanisms have been reported in several other bacteria and is termed as superinfection exclusion (Ranade and Poteete, 1993;Hofer et al., 1995;Cumby et al.,

2012;Bondy-Denomy et al., 2016). By preventing the superinfection of similar phages, the prophage 3 of EcN could additionally be involved in maintaining its genome stability.

5.4. **Investigation of EcN's lambda phage resistance/defence mechanism**

The human gut is home to as many phages as bacteria and thus it is inevitable for EcN to battle phages in order to persist and efficiently colonize the gut (Mirzaei and Maurice, 2017). In this regard, apart from being resistant to phage infection, it could be highly beneficial for EcN if it can also neutralize the phages in its surrounding. To address this, EcN was incubated with lambda phages (10:1) and its phage inactivation ability was determined by PPA after several time points of incubation. To our surprise, the inactivation started as early as 2 h after incubation and the phage-titre remained low at all the investigated time points. The corresponding CFUs/ml determination also exhibited the immunity of EcN cells to lysis by lambda phages (**Figure 4.4. 6**). Further, such an early inactivation of lambda phages by EcN prompted the idea of phage binding mediated inactivation by EcN. Lambda phages use the LamB receptor for their binding to the host cell surface (Randall-Hazelbauer and Schwartz, 1973;Schwartz, 1976;Chatterjee and Rothenberg, 2012). Sequence analysis revealed a 97 % sequence identity between the LamB of the phage susceptible MG1655 and resistant EcN strains (Annexure 5). In addition, we found that the LamB of EcN and a K-12 strain functionally complemented each other (i.e.) no difference in lambda phage infection was observed when LamB from EcN was expressed in LamB negative K-12 strain (Soundararajan, 2016). Our hypothesis on binding-mediated phage inactivation was confirmed by PCR and the binding was further intensified in the presence of 0.2 % maltose that was reported to upregulate LamB (Schwartz, 1976;Hoyland-Kroghsbo et al., 2013). Moreover, the phage inactivation ability of EcN was preserved after formaldehyde-treatment, but was lost when the receptor was denaturated by heat-treatment (Mitsuzawa et al., 2006;Matsuura et al., 2015) (**Figure 4.4. 8**).

Conclusively, with these results, we have clearly shown that lambda phages use LamB to attach to the EcN cell surface. However, the phage attachment to EcN's LamB did not progress to a positive infection. Hence, there exist unidentified mechanisms which contribute to phage-inactivation. The unidentified factor(s) that regulates further inactivation could be speculated as to the superinfection exclusion related prophage genes in EcN that were upregulated in the presence of lambda phages. The lambda phage inactivation by other *E. coli* strains that also share the majority of prophage 3 genes fortifies our speculation. Furthermore, EcN exhibited a strong interference with the lambda phage infection of sensitive *E. coli* K-12 strains. The LamB mediated absorption of free lambda phages in the suspension to the EcN cells can possibly be the reason for the observed K-12 protection. This quality can be considered as an added positive attribute of the probiotic strain that might help in weakening the severity and progression of a bacterial disease for a patient, by preventing the infection of other sensitive strains in the gut by virulence gene transmitting phages.

5.5. **Capsule mediated T4 phage defence in EcN**

Extended survival and efficient colonization of the gut are preferred characteristics of a probiotic strain (Fijan, 2014). Consequently, the encounter followed by an infection mediated lysis poses a big threat for EcN's application in prophylaxis or treatment. The sensitivity of EcN to the lytic T4 phages was investigated by phage plaque assay. EcN demonstrated a complete immunity to lysis by T4 phages (**Figure 4.5. 1**). Microscopic examinations and PCR further proved that T4 phages were able to attach to EcN but were not able to infect it, whereas, in case of MG1655, an attachment followed by infection-mediated lysis was clearly evident (**Figure 4.5. 2**, **Figure 4.5. 3** & **Figure 4.5. 4**). Bacteria-phage coexistence and the corresponding evolution of factors contributing to phage resistance are observed widely (Chibani-Chennoufi et al., 2004a;Labrie et al., 2010;Azam and Tanji, 2019). In hunt of probable factors contributing to phage resistance, we initially focussed on the surface structures, as the

attachment of T4 phages to EcN cell surface was clearly established. The K5 polysaccharide capsule forms the outermost layer of EcN cell surface and it is reported to be involved in immunomodulatory effects exerted by EcN in the host (Nzakizwanayo et al., 2015). We aimed to test the participation of K5 capsule in EcN's resistance against T4 phages. For this purpose, the K5 capsule negative EcN mutant was used in our study. The deletion of the K5 determinant in the mutant was confirmed by PCR and the phenotypic loss of capsule in the mutant was verified by phage plaque assay with K5 capsule specific phages. Finally, the T4 phage plaque assay with the capsule negative EcN mutant demonstrated T4 infection, highlighting the importance of the K5 capsule in T4 phage resistance (**Figure 4.5. 5**). Bacterial capsules have been reported previously in several bacteria to provide resistance by masking the phage receptors in the cell membrane and thus preventing the phage adsorption to the receptors, which in general leads to successful infection (Kauffmann, 1945;Scholl et al., 2005;Majkowska-Skrobek et al., 2018).

5.6. **Effect of EcN on lytic T4 phages**

Inactivation of phages in the bacterial environment by binding to surface structures of outer membrane vesicles or to the extracellular matrix e.g. bacterial biofilms are considered as the second line of defence provided by the bacteria apart from protecting itself from phage infection by other means (Manning and Kuehn, 2011;Abedon, 2017;Vidakovic et al., 2018). Correspondingly, our data revealed that EcN also inactivated the T4 phages in coincubation experiments. Determination of phage inactivation kinetics declared a rapid neutralization of T4 phages by EcN, which started as early as 30 mins and was as high as ~ 1,240-fold at 24 h. The corresponding determination of the viability of EcN cells demonstrated an early lag in the growth of EcN. However, after 2 h, the CFUs/ml of EcN in the presence and absence of T4 phages were comparable again (**Figure 4.5. 6**). Transcriptomic analysis disclosed the downregulation of genes belonging to major metabolic pathways and cell growth which was

consistent with previous findings that had reported the inhibition in host cell metabolisms when incubated with T4 ghost bacteriophages (Winkler and Duckworth, 1971;Fukuma and Kaji, 1972;Vallee et al., 1972). These studies have shown that despite the absence of DNA injection, T4 ghosts disrupted the host cellular activities, which are in line with our findings (**Figure 4.5. 7**). Furthermore, from the coincubation experiment, it was observed that there was an increase in the number of free phages available in the supernatant, 48 h post-incubation. This led to the speculation that the T4 phage resistance by EcN might have been lost over a period of time, which could be the probable reason for the increase in phage titer. However, this speculation was eliminated by testing the sensitivity of the EcN from this time point, for infection with fresh T4 phages. Similarly, the possibility of T4 phage adopting a strategy or mechanism to evade EcN's phage resistance was also eliminated, as these pre-incubated T4 phages were still not able to infect the EcN in a lawn (**Table 4. 3**). In addition, EcN incubated with T4 phages up to 96 h were still able to inactivate the freshly added T4 phages as efficient as fresh EcN (**Figure 4.5. 8**). Collectively, from these results, we could exclude the possibility of EcN turning sensitive after 24 h of incubation with T4 phages. The other possible explanation could be the release of attached T4 phages after 24 h, which was supported by T4-specific PCR results (**Figure 4.5. 9**), where the intensity of phage DNA in the supernatant at 48 h was far higher when compared to 24 h. There is also a possibility that a subpopulation of EcN was getting infected and that the number of infected EcN cells was too low to be detected in any of our experiments. However, the above speculation was not supported by the observation that even after 120 h of incubation, the number of available phages in the supernatant was never higher than the number of phages added at time point zero and there was no drop in the number of viable EcN cells until 120 h of incubation. Therefore, the observed increase in phage titer was rather assumed to be due to the release of attached phages. In future, transmission electron microscopic examination of EcN and T4 phage coincubation at these later time points may shed light on our assumption. In addition, quantifying the attachment of T4 phages to EcN at

timepoints like 24 h, 48 h and 72 h would clarify if the phage titer increase in the supernatant is due to release of previously attached phages.

The human gut is a complex environment to sustain and to combat the interminable phage attacks (Mirzaei and Maurice, 2017;De Sordi et al., 2019). Consequently, EcN like probiotics might have acquired multiple weapons or strategies to compete in such an environment. As we already knew that the K5 capsular polysaccharide of EcN is essential for the observed T4 phage resistance, we were curious to examine whether any other factors in EcN could probably mediate phage-inactivation. To this end, cells and supernatants of EcN and of the capsule negative mutant of EcN were investigated for phage-inactivation capacity. The cells and cell-free supernatant of EcN were able to neutralize T4 phages, suggesting that the factor responsible for inactivation of T4 phages in EcN was not only cell-attached but also present in the supernatant (**Figure 4.5. 11**). Noteworthy, though the EcN capsule negative mutant was phage-sensitive, the supernatant of the mutant still inactivated the phages, thereby reassuring our hypothesis on the presence of more than one phage defence associated factor in EcN. Heat and proteinase K treatment of EcN samples disclosed that the phage inactivating factor in EcN was heat stable and proteinase K resistant. Furthermore, heat and proteinase K treatment strangely enhanced the phage reduction ability of the samples and this ability was significantly impaired in the presence of SMP that additionally degraded the carbohydrate molecules in the sample (**Figure 4.5. 12**). From these results, we hypothesized LPS to be the candidate in the EcN cell and in the secretome that inactivated T4 phages (Sharma, 1986;Whitfield and Trent, 2014).

5.7. **EcN's LPS inactivated T4 phages**

The antibiotic polymyxin B (PMB) binds to the LPS of gram-negative bacteria and it has been reported that 25 µg/ml of PMB can destroy the structure of LPS, thereby destroying its phage receptor activity (Koike and Iida, 1971). Coincubation experiments revealed that the phage reduction ability of EcN and supernatant samples were absolutely abolished in the presence of

PMB (**Figure 4.5. 13**). The independent role of EcN's LPS in phage inactivation was established when isolated LPS from EcN inactivated the T4 phages by more than 90 % in 1 h (**Figure 4.5. 14**). It is well-known that LPS of *E. coli* K-12 strains is essential for the adsorption of T4 phages to their cells (Lindberg, 1973;Furukawa et al., 1979;Furukawa and Mizushima, 1982). Nevertheless, in concurrence with previously reported findings (Mutoh et al., 1978;Picken, 1981;Washizaki et al., 2016), we also observed that isolated LPS from *E. coli* K-12 strain MG1655 and commercially purchased *E. coli* K-12 LPS failed to inactivate T4 phages.

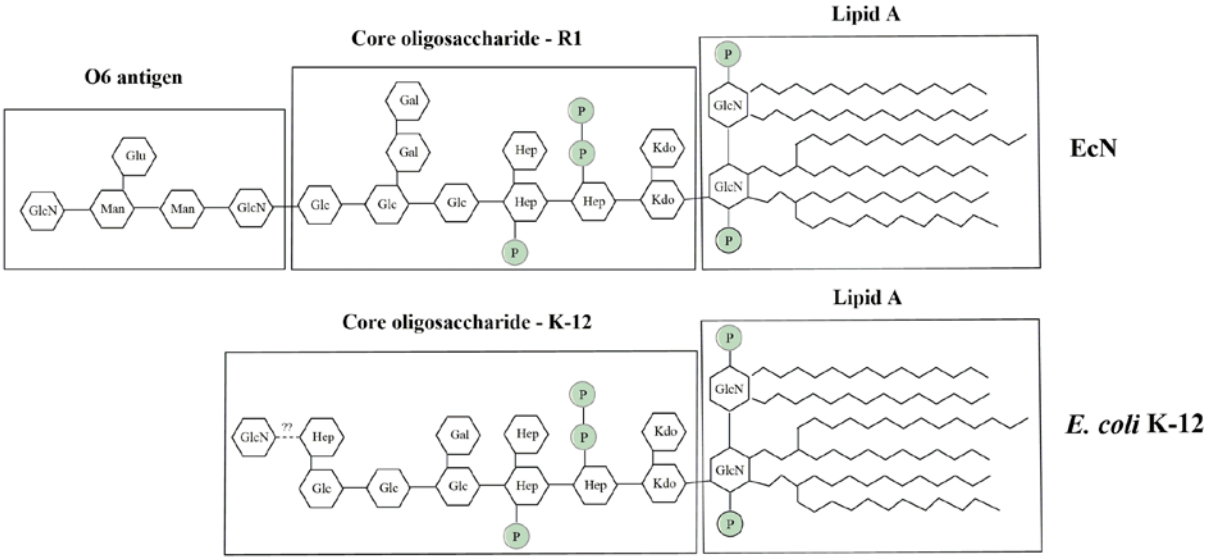

Figure 5. 2: Structural comparison of LPS from EcN and *E. coli* K-12 strain. LPS structures were adapted from (Grozdanov et al., 2002) for EcN. The abbreviations used in this figure are GlcN: N-acetylglucosamine, Man: mannose, Glc: glucose, Gal: galactose, Hep: L-glycero-D-manno heptose, Kdo: 3-deoxy-D-manno-oct-2ulosonic acid, P: phosphate, Gal: N-acetylgalactosamine. The dotted line in the K-12 core between GlcN and Hep indicates GlcN being present only in some *E. coli* K-12 strains (Orskov et al., 1977). Image modified from (Soundararajan et al., 2019)

A closer look at the molecular structures of EcN and generic K-12 LPS (**Figure 5. 2**) depicted the remarkable differences between them. LPS of K-12 strains lack O-antigen and harbour a K-12 type core oligosaccharide whereas EcN possesses O-6 type antigen with R1 core. The terminal molecule of EcN's O6 antigen, N-acetylglucosamine (GlcNAc), was tested for its interaction with T4 phages. Determination of T4 phage adsorption to EcN established that in

the presence of 0.6 M GlcNAc, the adsorption was completely inhibited (**Figure 4.5. 15**). A similar observation was made in *E. coli* B cells, where not only GlcNAc, but also the addition of other monosaccharides like glucosamine, 2-deoxyglucose, 3-O-methyl glucose, and gluconolactone inhibited T4 phage adsorption (Dawes, 1975). On the other hand, in EcN, the inhibition of T4 adsorption was GlcNAc specific, as the addition of 0.6 M Glucose did not inhibit the adsorption as efficiently as in the presence of GlcNAc (**Figure 4.5. 15**). Moreover, the cells and supernatants of other *E. coli* strains were tested for their T4 phage inactivation ability and the results revealed that only the cells and supernatant of the uropathogenic strain CFT073 neutralized the T4 phages as efficiently as EcN.

***E. coli* strains** (O ant:K ant:flagella type)	**O antigen structure**
EcN (O6:K5:H1)	Glc | GlcN - Man - Man - GlcN–
CFT073 (O6:K2:H1)	Glc | – GalN - Man - Man - GlcN–
SE11 (O152:K-:H8)	RhaP | – GlcN - Glc - Glc - GlcN–
SE15 (O150:K-:H5)	Glc | –GlcN(Slac) - Rhap - Rhap - Rhap - GlcN–

Figure 5. 3: The O antigen structures of different *E. coli* strains used in this study. The abbreviations used in this figure are GlcN: N-acetylglucosamine, Man: mannose, Glc: glucose, Gal: galactose, Hep: L-glycero-D-manno heptose, Kdo: 3-deoxy-D-manno-oct-2ulosonic acid, P: phosphate, Gal: N-acetylgalactosamine, Rhap: rhamnopyranose, GlcN(Slac): 2-acetamido-4-O-[(S)-1-carboxy-ethyl]-2-deoxy-D-glucose. LPS structures were adapted from (Grozdanov et al., 2002) for EcN; (Orskov et al., 1977;Washizaki et al., 2016) for *E. coli* K-12 MG1655; (Stenutz et al., 2006) for CFT073, SE11; (Perepelov et al., 2007) for SE15. Image modified from (Soundararajan et al., 2019)

Though the commensal strains SE11 and SE15 were not infected, their cells and supernatant did not inactivate the T4 phages during coincubation (**Figure 4.5. 16**). The analysis of O-antigen structures of all the *E. coli* strains exposed that among the tested *E. coli* strains, only the strains with O6 type LPS inactivated the T4 phages. From these results, we can assume that T4 phage neutralization could be O6 antigen-specific, however, studies with an O-antigen deletion mutant of EcN are required to validate our inference.

Overall, for the first time, we deliver the role of EcN's LPS in its phage defence. Further from our results, we could hypothesize that using its LPS EcN sequesters the T4 phages and inactivates them, thereby not only protecting itself but also the other sensitive bacteria in its surrounding. Triculture experiment with EcN microcin deletion mutant SK22D demonstrated the ability of EcN to protect the K-12 strains from being infected with T4 phages (**Figure 4.5. 17**). As discussed earlier, a similar protective effect by EcN on the K-12 strains was also observed against lambda phages. Hence, in future, it would be worthwhile to focus on the interactions between different players in the tri-culture set up, to elucidate the mechanism of protection.

6. Conclusion

The risk of acquiring gastrointestinal infections and the degree of disease progression might be connected to the balance in the microbiota composition (Bien et al., 2013;Molloy et al., 2013;Pham and Lawley, 2014). Studies have recently discussed the role of gut phages in maintaining the microbial composition and thereby becoming a dominant player (Lepage et al., 2008;Chaffringeon et al., 2019). For centuries, the application of probiotics is known to be of assistance in the treatment of gastrointestinal disorders and microbial dysbiosis (Sonnenborn, 2016). EcN, being one of the most extensively studied probiotic strains, is known for its ability to inhibit Stx production in EHEC strains that are associated with the development of

gastroenteritis in humans (Reissbrodt et al., 2009;Rund et al., 2013;Sahar H. Ali, 2017;Bury et al., 2018).

In the first part of the study, the changes in the transcriptome of EcN were characterised upon exposure to two *E. coli* strains namely, pathogenic EDL933 and non-pathogenic MG1655. For the first time, we demonstrated a strain-specific response by EcN with the help of global transcriptomic analysis. This very character of EcN, to differentiate and uniquely respond to different *E. coli* strains, highlights the safety of using a probiotic strain in a microbiologically rich environment such as gut, rather than chemical-based pharmaceutical preparations that generally act in a relatively similar manner on the whole of bacterial population and thereby posing a great threat for microbiota.

Furthermore, we have established for the first-time the lysogenic and lytic phage resistance as a key probiotic and safety attribute of EcN. Apart from being resistant against tested phages, EcN also drastically reduced the phage numbers during coincubation. In addition, EcN demonstrated a clear interference with the infection of phage susceptible *E. coli* strains. In the case of lambda phages, the presence of prophage-related genes contributed to the resistance. The binding to the phage receptor LamB, which normally would lead to infection, led to the inactivation of the lambda phages.

The K5 polysaccharide capsule-mediated defence was shown for the first time in EcN against T4 phages. In addition, the cell-attached and secreted LPS inactivated the T4 phages. These properties (among others) are most likely important for EcN's survival in the gut and for its ability to execute its probiotic effects.

Our results from *in vitro* studies strongly suggest that the administration of EcN would be an ideal alternative or supportive treatment strategy for gastrointestinal infections. In addition to the already reported antagonistic effects of EcN against various pathogenic bacteria, the

immunity to phage infection observed in this study emphasize the safety of employing EcN in prophylaxis and/or treatment. Phage resistance is an inevitable safety feature of a probiotic that promotes genomic stability and helps to colonize the host's gut despite an established complex microbial community. As an outlook, we strongly propose further *in vivo* studies of EcN to investigate if EcN could exert the above mentioned probiotic traits *in vivo*.

7. References

(2012). "Family - *Siphoviridae*," in *Virus Taxonomy,* eds. A.M.Q. King, M.J. Adams, E.B. Carstens & E.J. Lefkowitz. (San Diego: Elsevier), 86-98.

Abedon, S.T. (2017). Phage "delay" towards enhancing bacterial escape from biofilms: a more comprehensive way of viewing resistance to bacteriophages. *AIMS Microbiol* 3**,** 186-226.

Ali, Y., Koberg, S., Hessner, S., Sun, X., Rabe, B., Back, A., Neve, H., and Heller, K.J. (2014). Temperate *Streptococcus thermophilus* phages expressing superinfection exclusion proteins of the Ltp type. *Front Microbiol* 5**,** 98.

Altenhoefer, A., Oswald, S., Sonnenborn, U., Enders, C., Schulze, J., Hacker, J., and Oelschlaeger, T.A. (2004). The probiotic *Escherichia coli* strain Nissle 1917 interferes with invasion of human intestinal epithelial cells by different enteroinvasive bacterial pathogens. *FEMS Immunol Med Microbiol* 40**,** 223-229.

Alvarez, M.A., Rodriguez, A., and Suarez, J.E. (1999). Stable expression of the *Lactobacillus casei* bacteriophage A2 repressor blocks phage propagation during milk fermentation. *J Appl Microbiol* 86**,** 812-816.

Aminov, R.I. (2010). A brief history of the antibiotic era: lessons learned and challenges for the future. *Front Microbiol* 1**,** 134.

Andrews, S. (2010). FastQC: a quality control tool for high throughput sequence data. .

Armstrong, G.L., Hollingsworth, J., and Morris, J.G., Jr. (1996). Emerging foodborne pathogens: *Escherichia coli* O157:H7 as a model of entry of a new pathogen into the food supply of the developed world. *Epidemiol Rev* 18**,** 29-51.

Arumugam, M., Raes, J., Pelletier, E., Le Paslier, D., Yamada, T., Mende, D.R., Fernandes, G.R., Tap, J., Bruls, T., Batto, J.M., Bertalan, M., Borruel, N., Casellas, F., Fernandez, L., Gautier, L., Hansen, T., Hattori, M., Hayashi, T., Kleerebezem, M., Kurokawa, K., Leclerc, M., Levenez, F., Manichanh, C., Nielsen, H.B., Nielsen, T., Pons, N., Poulain, J., Qin, J., Sicheritz-Ponten, T., Tims, S., Torrents, D., Ugarte, E., Zoetendal, E.G., Wang, J., Guarner, F., Pedersen, O., De Vos, W.M., Brunak, S., Dore, J., Meta, H.I.T.C., Antolin, M., Artiguenave, F., Blottiere, H.M., Almeida, M., Brechot, C., Cara, C., Chervaux, C., Cultrone, A., Delorme, C., Denariaz, G., Dervyn, R., Foerstner, K.U., Friss, C., Van De Guchte, M., Guedon, E., Haimet, F., Huber, W., Van Hylckama-Vlieg, J., Jamet, A., Juste, C., Kaci, G., Knol, J., Lakhdari, O., Layec, S., Le Roux, K., Maguin, E., Merieux, A., Melo Minardi, R., M'rini, C., Muller, J., Oozeer, R., Parkhill, J., Renault, P., Rescigno, M., Sanchez, N., Sunagawa, S., Torrejon, A., Turner, K., Vandemeulebrouck, G., Varela, E., Winogradsky, Y., Zeller, G., Weissenbach, J., Ehrlich, S.D., and Bork, P. (2011). Enterotypes of the human gut microbiome. *Nature* 473**,** 174-180.

Azam, A.H., and Tanji, Y. (2019). Bacteriophage-host arm race: an update on the mechanism of phage resistance in bacteria and revenge of the phage with the perspective for phage therapy. *Appl Microbiol Biotechnol* 103**,** 2121-2131.

Babalova, E.G., Katsitadze, K.T., Sakvarelidze, L.A., Imnaishvili, N., Sharashidze, T.G., Badashvili, V.A., Kiknadze, G.P., Meipariani, A.N., Gendzekhadze, N.D., Machavariani, E.V., Gogoberidze, K.L., Gozalov, E.I., and Dekanosidze, N.G. (1968). [Preventive value of dried dysentery bacteriophage]. *Zh Mikrobiol Epidemiol Immunobiol* 45**,** 143-145.

Baquero, F., Lanza, V.F., Baquero, M.R., Del Campo, R., and Bravo-Vazquez, D.A. (2019). Microcins in *Enterobacteriaceae*: Peptide Antimicrobials in the Eco-Active Intestinal Chemosphere. *Front Microbiol* 10**,** 2261.

Barnhart, M.M., and Chapman, M.R. (2006). Curli biogenesis and function. *Annu Rev Microbiol* 60**,** 131-147.

Barth, S., Duncker, S., Hempe, J., Breves, G., Baljer, G., and Bauerfeind, R. (2009). *Escherichia coli* Nissle 1917 for probiotic use in piglets: evidence for intestinal colonization. *J Appl Microbiol* 107**,** 1697-1710.

Beacham, I.R., and Picken, R.N. (1981). On the receptor for bacteriophage T4 in *Escherichia coli* K12. *Current Microbiology* 6**,** 291-293.

Belizario, J.E., and Faintuch, J. (2018). Microbiome and Gut Dysbiosis. *Exp Suppl* 109**,** 459-476.

Beloin, C., Roux, A., and Ghigo, J.M. (2008). *Escherichia coli* biofilms. *Curr Top Microbiol Immunol* 322**,** 249-289.

Bertozzi Silva, J., Storms, Z., and Sauvageau, D. (2016). Host receptors for bacteriophage adsorption. *FEMS Microbiol Lett* 363.

Bien, J., Palagani, V., and Bozko, P. (2013). The intestinal microbiota dysbiosis and *Clostridium difficile* infection: is there a relationship with inflammatory bowel disease? *Therap Adv Gastroenterol* 6**,** 53-68.

Biswas, S.K., Chowdhury, R., and Das, J. (1992). A 14-kilodalton inner membrane protein of *Vibrio cholerae* biotype e1 tor confers resistance to group IV choleraphage infection to classical vibrios. *J Bacteriol* 174**,** 6221-6229.

Blum-Oehler, G., Oswald, S., Eiteljorge, K., Sonnenborn, U., Schulze, J., Kruis, W., and Hacker, J. (2003). Development of strain-specific PCR reactions for the detection of the probiotic *Escherichia coli* strain Nissle 1917 in fecal samples. *Res Microbiol* 154**,** 59-66.

Bohnlein, C., Kabisch, J., Meske, D., Franz, C.M., and Pichner, R. (2016). Fitness of Enterohemorrhagic *Escherichia coli* (EHEC)/Enteroaggregative *E. coli* O104:H4 in Comparison to That of EHEC O157: Survival Studies in Food and In Vitro. *Appl Environ Microbiol* 82**,** 6326-6334.

Bondy-Denomy, J., Qian, J., Westra, E.R., Buckling, A., Guttman, D.S., Davidson, A.R., and Maxwell, K.L. (2016). Prophages mediate defense against phage infection through diverse mechanisms. *ISME J* 10**,** 2854-2866.

Brzozowska, E., Lesniewski, A., Sek, S., Wieneke, R., Tampe, R., Gorska, S., Jonsson-Niedziolka, M., and Niedziolka-Jonsson, J. (2018). Interactions of bacteriophage T4 adhesin with selected lipopolysaccharides studied using atomic force microscopy. *Sci Rep* 8**,** 10935.

Brzuszkiewicz, E., Thurmer, A., Schuldes, J., Leimbach, A., Liesegang, H., Meyer, F.D., Boelter, J., Petersen, H., Gottschalk, G., and Daniel, R. (2011). Genome sequence analyses of two isolates from the recent *Escherichia coli* outbreak in Germany reveal the emergence of a new pathotype: Entero-Aggregative-Haemorrhagic *Escherichia coli* (EAHEC). *Arch Microbiol* 193**,** 883-891.

Bury, S. (2018). *Molekularbiologische Untersuchungen der antagonistischen Effekte des probiotischen Escherichia coli Stamms Nissle 1917 auf Shiga-Toxin produzierende Escherichia coli Stämme; Molecular biological investigations on the antagonistic effects of the probiotic Escherichia coli strain Nissle 1917 towards Shiga toxin producing Escherichia coli; https://nbn-resolving.org/urn:nbn:de:bvb:20-opus-163401*.

Bury, S., Soundararajan, M., Bharti, R., Von Bunau, R., Forstner, K.U., and Oelschlaeger, T.A. (2018). The Probiotic *Escherichia coli* Strain Nissle 1917 Combats Lambdoid Bacteriophages *stx* and *lambda*. *Front Microbiol* 9**,** 929.

Carding, S.R., Davis, N., and Hoyles, L. (2017). Review article: the human intestinal virome in health and disease. *Aliment Pharmacol Ther* 46**,** 800-815.

Carter, M.Q., Feng, D., and Li, H.H. (2019). Curli fimbriae confer shiga toxin-producing *Escherichia coli* a competitive trait in mixed biofilms. *Food Microbiol* 82**,** 482-488.

Casjens, S.R., and Hendrix, R.W. (2015). Bacteriophage lambda: Early pioneer and still relevant. *Virology* 479-480**,** 310-330.

Chaffringeon, L., De La Cruz, J., Dettling, V., Eme-Scolan, E., and Samain, J. (2019). [The key role of bacteriophages in the defense of the gut epithelium against pathogenic bacteria]. *Med Sci (Paris)* 35**,** 581-583.

Chatterjee, S., and Rothenberg, E. (2012). Interaction of bacteriophage lambda with its *E. coli* receptor, LamB. *Viruses* 4**,** 3162-3178.

Cheetham, B.F., and Katz, M.E. (1995). A role for bacteriophages in the evolution and transfer of bacterial virulence determinants. *Mol Microbiol* 18**,** 201-208.

Chen, J., and Novick, R.P. (2009). Phage-mediated intergeneric transfer of toxin genes. *Science* 323**,** 139-141.

Chen, Y., Yang, F., Lu, H., Wang, B., Chen, Y., Lei, D., Wang, Y., Zhu, B., and Li, L. (2011). Characterization of fecal microbial communities in patients with liver cirrhosis. *Hepatology* 54**,** 562-572.

Chiang, Y.N., Penades, J.R., and Chen, J. (2019). Genetic transduction by phages and chromosomal islands: The new and noncanonical. *PLoS Pathog* 15**,** e1007878.

Chibani-Chennoufi, S., Bruttin, A., Dillmann, M.L., and Brussow, H. (2004a). Phage-host interaction: an ecological perspective. *J Bacteriol* 186**,** 3677-3686.

Chibani-Chennoufi, S., Sidoti, J., Bruttin, A., Dillmann, M.L., Kutter, E., Qadri, F., Sarker, S.A., and Brussow, H. (2004b). Isolation of Escherichia coli bacteriophages from the stool of pediatric diarrhea patients in Bangladesh. *J Bacteriol* 186**,** 8287-8294.

Colavecchio, A., Cadieux, B., Lo, A., and Goodridge, L.D. (2017). Bacteriophages Contribute to the Spread of Antibiotic Resistance Genes among Foodborne Pathogens of the *Enterobacteriaceae* Family - A Review. *Front Microbiol* 8**,** 1108.

Cumby, N., Edwards, A.M., Davidson, A.R., and Maxwell, K.L. (2012). The bacteriophage HK97 gp15 moron element encodes a novel superinfection exclusion protein. *J Bacteriol* 194**,** 5012-5019.

Cumby, N., Reimer, K., Mengin-Lecreulx, D., Davidson, A.R., and Maxwell, K.L. (2015). The phage tail tape measure protein, an inner membrane protein and a periplasmic chaperone play connected roles in the genome injection process of *E. coli* phage HK97. *Mol Microbiol* 96**,** 437-447.

D'herelle, F. (1929). Studies Upon Asiatic Cholera. *Yale J Biol Med* 1**,** 195-219.

D'herelle, F. (2007). On an invisible microbe antagonistic toward dysenteric *Bacilli*: brief note by Mr. F. D'Herelle, presented by Mr. Roux. 1917. *Res Microbiol* 158**,** 553-554.

D'humieres, C., Touchon, M., Dion, S., Cury, J., Ghozlane, A., Garcia-Garcera, M., Bouchier, C., Ma, L., Denamur, E., and E, P.C.R. (2019). A simple, reproducible and cost-effective procedure to analyse gut phageome: from phage isolation to bioinformatic approach. *Sci Rep* 9**,** 11331.

Dawes, J. (1975). Characterisation of the bacteriophage T4 receptor site. *Nature* 256**,** 127-128.

De Sordi, L., Lourenco, M., and Debarbieux, L. (2019). "I will survive": A tale of bacteriophage-bacteria coevolution in the gut. *Gut Microbes* 10**,** 92-99.

Del Cogliano, M.E., Pinto, A., Goldstein, J., Zotta, E., Ochoa, F., Fernandez-Brando, R.J., Muniesa, M., Ghiringhelli, P.D., Palermo, M.S., and Bentancor, L.V. (2018). Relevance of Bacteriophage 933W in the Development of Hemolytic Uremic Syndrome (HUS). *Front Microbiol* 9**,** 3104.

Deriu, E., Liu, J.Z., Pezeshki, M., Edwards, R.A., Ochoa, R.J., Contreras, H., Libby, S.J., Fang, F.C., and Raffatellu, M. (2013). Probiotic bacteria reduce *Salmonella typhimurium* intestinal colonization by competing for iron. *Cell Host Microbe* 14**,** 26-37.

Deveau, H., Garneau, J.E., and Moineau, S. (2010). CRISPR/Cas system and its role in phage-bacteria interactions. *Annu Rev Microbiol* 64**,** 475-493.

Doron, S., Melamed, S., Ofir, G., Leavitt, A., Lopatina, A., Keren, M., Amitai, G., and Sorek, R. (2018). Systematic discovery of antiphage defense systems in the microbial pangenome. *Science* 359.

Doss, J., Culbertson, K., Hahn, D., Camacho, J., and Barekzi, N. (2017). A Review of Phage Therapy against Bacterial Pathogens of Aquatic and Terrestrial Organisms. *Viruses* 9.

Dy, R.L., Przybilski, R., Semeijn, K., Salmond, G.P., and Fineran, P.C. (2014). A widespread bacteriophage abortive infection system functions through a Type IV toxin-antitoxin mechanism. *Nucleic Acids Res* 42**,** 4590-4605.

Eckburg, P.B., Bik, E.M., Bernstein, C.N., Purdom, E., Dethlefsen, L., Sargent, M., Gill, S.R., Nelson, K.E., and Relman, D.A. (2005). Diversity of the human intestinal microbial flora. *Science* 308**,** 1635-1638.

Edgar, R., Domrachev, M., and Lash, A.E. (2002). Gene Expression Omnibus: NCBI gene expression and hybridization array data repository. *Nucleic Acids Res* 30**,** 207-210.

Elespuru, R.K. (1984). "Induction of Bacteriophage Lambda by DNA-Interacting Chemicals. ", in: *Chemical Mutagens.* (Boston, MA: Springer).

Emond, E., Dion, E., Walker, S.A., Vedamuthu, E.R., Kondo, J.K., and Moineau, S. (1998). AbiQ, an abortive infection mechanism from *Lactococcus lactis*. *Appl Environ Microbiol* 64**,** 4748-4756.

Erni, B., Zanolari, B., and Kocher, H.P. (1987). The mannose permease of *Escherichia coli* consists of three different proteins. Amino acid sequence and function in sugar transport, sugar phosphorylation, and penetration of phage lambda DNA. *J Biol Chem* 262**,** 5238-5247.

Ershova, A.S., Rusinov, I.S., Spirin, S.A., Karyagina, A.S., and Alexeevski, A.V. (2015). Role of Restriction-Modification Systems in Prokaryotic Evolution and Ecology. *Biochemistry (Mosc)* 80**,** 1373-1386.

Fang, K., Jin, X., and Hong, S.H. (2018). Probiotic *Escherichia coli* inhibits biofilm formation of pathogenic *E. coli* via extracellular activity of DegP. *Sci Rep* 8**,** 4939.

Fijan, S. (2014). Microorganisms with claimed probiotic properties: an overview of recent literature. *Int J Environ Res Public Health* 11**,** 4745-4767.

Fillol-Salom, A., Martinez-Rubio, R., Abdulrahman, R.F., Chen, J., Davies, R., and Penades, J.R. (2018). Phage-inducible chromosomal islands are ubiquitous within the bacterial universe. *ISME J* 12**,** 2114-2128.

Forstner, K.U., Vogel, J., and Sharma, C.M. (2014). READemption-a tool for the computational analysis of deep-sequencing-based transcriptome data. *Bioinformatics* 30**,** 3421-3423.

Francino, M.P. (2014). Early development of the gut microbiota and immune health. *Pathogens* 3**,** 769-790.

Frank, C., Werber, D., Cramer, J.P., Askar, M., Faber, M., An Der Heiden, M., Bernard, H., Fruth, A., Prager, R., Spode, A., Wadl, M., Zoufaly, A., Jordan, S., Kemper, M.J., Follin, P., Muller, L., King, L.A., Rosner, B., Buchholz, U., Stark, K., Krause, G., and Team, H.U.S.I. (2011). Epidemic profile of Shiga-toxin-producing *Escherichia coli* O104:H4 outbreak in Germany. *N Engl J Med* 365**,** 1771-1780.

Frazao, N., Sousa, A., Lassig, M., and Gordo, I. (2019). Horizontal gene transfer overrides mutation in *Escherichia coli* colonizing the mammalian gut. *Proc Natl Acad Sci U S A* 116**,** 17906-17915.

Freese, N.H., Norris, D.C., and Loraine, A.E. (2016). Integrated genome browser: visual analytics platform for genomics. *Bioinformatics* 32**,** 2089-2095.

Fukuma, I., and Kaji, A. (1972). Effect of bacteriophage ghost infection on protein synthesis in *Escherichia coli*. *J Virol* 10**,** 713-720.

Furukawa, H., Kuroiwa, T., and Mizushima, S. (1983). DNA injection during bacteriophage T4 infection of *Escherichia coli*. *J Bacteriol* 154**,** 938-945.

Furukawa, H., and Mizushima, S. (1982). Roles of cell surface components of Escherichia coli K-12 in bacteriophage T4 infection: interaction of tail core with phospholipids. *J Bacteriol* 150**,** 916-924.

Furukawa, H., Yamada, H., and Mizushima, S. (1979). Interaction of bacteriophage T4 with reconstituted cell envelopes of *Escherichia coli* K-12. *J Bacteriol* 140**,** 1071-1080.

Gareau, M.G., Sherman, P.M., and Walker, W.A. (2010). Probiotics and the gut microbiota in intestinal health and disease. *Nat Rev Gastroenterol Hepatol* 7**,** 503-514.

Garen, A., and Puck, T.T. (1951). The first two steps of the invasion of host cells by bacterial viruses. II. *J Exp Med* 94**,** 177-189.

Gill, S.R., Pop, M., Deboy, R.T., Eckburg, P.B., Turnbaugh, P.J., Samuel, B.S., Gordon, J.I., Relman, D.A., Fraser-Liggett, C.M., and Nelson, K.E. (2006). Metagenomic analysis of the human distal gut microbiome. *Science* 312**,** 1355-1359.

Giulietti, A., Overbergh, L., Valckx, D., Decallonne, B., Bouillon, R., and Mathieu, C. (2001). An overview of real-time quantitative PCR: applications to quantify cytokine gene expression. *Methods* 25**,** 386-401.

Gobin, M., Hawker, J., Cleary, P., Inns, T., Gardiner, D., Mikhail, A., Mccormick, J., Elson, R., Ready, D., Dallman, T., Roddick, I., Hall, I., Willis, C., Crook, P., Godbole, G., Tubin-Delic, D., and Oliver, I. (2018). National outbreak of Shiga toxin-producing *Escherichia coli* O157:H7 linked to mixed salad leaves, United Kingdom, 2016. *Euro Surveill* 23.

Goldfarb, T., Sberro, H., Weinstock, E., Cohen, O., Doron, S., Charpak-Amikam, Y., Afik, S., Ofir, G., and Sorek, R. (2015). BREX is a novel phage resistance system widespread in microbial genomes. *EMBO J* 34**,** 169-183.

Grosse, C., Scherer, J., Koch, D., Otto, M., Taudte, N., and Grass, G. (2006). A new ferrous iron-uptake transporter, EfeU (YcdN), from *Escherichia coli*. *Mol Microbiol* 62**,** 120-131.

Grozdanov, L., Raasch, C., Schulze, J., Sonnenborn, U., Gottschalk, G., Hacker, J., and Dobrindt, U. (2004). Analysis of the genome structure of the nonpathogenic probiotic *Escherichia coli* strain Nissle 1917. *J Bacteriol* 186**,** 5432-5441.

Grozdanov, L., Zahringer, U., Blum-Oehler, G., Brade, L., Henne, A., Knirel, Y.A., Schombel, U., Schulze, J., Sonnenborn, U., Gottschalk, G., Hacker, J., Rietschel, E.T., and Dobrindt, U. (2002). A single nucleotide exchange in the wzy gene is responsible for the semirough O6 lipopolysaccharide phenotype and serum sensitivity of *Escherichia coli* strain Nissle 1917. *J Bacteriol* 184**,** 5912-5925.

Guttsches, A.K., Loseke, S., Zahringer, U., Sonnenborn, U., Enders, C., Gatermann, S., and Bufe, A. (2012). Anti-inflammatory modulation of immune response by probiotic *Escherichia coli* Nissle 1917 in human blood mononuclear cells. *Innate Immun* 18**,** 204-216.

Haaber, J., Leisner, J.J., Cohn, M.T., Catalan-Moreno, A., Nielsen, J.B., Westh, H., Penades, J.R., and Ingmer, H. (2016). Bacterial viruses enable their host to acquire antibiotic resistance genes from neighbouring cells. *Nat Commun* 7**,** 13333.

Hafez, M., Hayes, K., Goldrick, M., Grencis, R.K., and Roberts, I.S. (2010). The K5 capsule of *Escherichia coli* strain Nissle 1917 is important in stimulating expression of Toll-like receptor 5, CD14, MyD88, and TRIF together with the induction of interleukin-8 expression via the mitogen-activated protein kinase pathway in epithelial cells. *Infect Immun* 78**,** 2153-2162.

Halbert, S.P. (1948). The antagonism of coliform bacteria against *Shigellae*. *J Immunol* 58**,** 153-167.

Hancock, V., Dahl, M., and Klemm, P. (2010a). Probiotic *Escherichia coli* strain Nissle 1917 outcompetes intestinal pathogens during biofilm formation. *J Med Microbiol* 59**,** 392-399.

Hancock, V., Vejborg, R.M., and Klemm, P. (2010b). Functional genomics of probiotic *Escherichia coli* Nissle 1917 and 83972, and UPEC strain CFT073: comparison of transcriptomes, growth and biofilm formation. *Mol Genet Genomics* 284**,** 437-454.

Hantke, K. (2020). Compilation of *Escherichia coli* K-12 outer membrane phage receptors - their function and some historical remarks. *FEMS Microbiol Lett*.

Hawrelak, J.A., and Myers, S.P. (2004). The causes of intestinal dysbiosis: a review. *Altern Med Rev* 9**,** 180-197.

Hazen, T.H., Michalski, J., Luo, Q., Shetty, A.C., Daugherty, S.C., Fleckenstein, J.M., and Rasko, D.A. (2017). Comparative genomics and transcriptomics of *Escherichia coli* isolates carrying virulence factors of both enteropathogenic and enterotoxigenic *E. coli*. *Sci Rep* 7**,** 3513.

Henker, J., Muller, S., Laass, M.W., Schreiner, A., and Schulze, J. (2008). Probiotic *Escherichia coli* Nissle 1917 (EcN) for successful remission maintenance of ulcerative colitis in children and adolescents: an open-label pilot study. *Z Gastroenterol* 46**,** 874-875.

Hilborn, E.D., Mermin, J.H., Mshar, P.A., Hadler, J.L., Voetsch, A., Wojtkunski, C., Swartz, M., Mshar, R., Lambert-Fair, M.A., Farrar, J.A., Glynn, M.K., and Slutsker, L. (1999). A multistate outbreak of *Escherichia coli* O157:H7 infections associated with consumption of mesclun lettuce. *Arch Intern Med* 159**,** 1758-1764.

Hofer, B., Ruge, M., and Dreiseikelmann, B. (1995). The superinfection exclusion gene (*sieA*) of bacteriophage P22: identification and overexpression of the gene and localization of the gene product. *J Bacteriol* 177**,** 3080-3086.

Hoffmann, S., Otto, C., Kurtz, S., Sharma, C.M., Khaitovich, P., Vogel, J., Stadler, P.F., and Hackermuller, J. (2009). Fast mapping of short sequences with mismatches, insertions and deletions using index structures. *PLoS Comput Biol* 5**,** e1000502.

Hollister, E.B., Gao, C., and Versalovic, J. (2014). Compositional and functional features of the gastrointestinal microbiome and their effects on human health. *Gastroenterology* 146**,** 1449-1458.

Howard-Varona, C., Hargreaves, K.R., Abedon, S.T., and Sullivan, M.B. (2017). Lysogeny in nature: mechanisms, impact and ecology of temperate phages. *ISME J* 11**,** 1511-1520.

Hoyland-Kroghsbo, N.M., Maerkedahl, R.B., and Svenningsen, S.L. (2013). A quorum-sensing-induced bacteriophage defense mechanism. *mBio* 4**,** e00362-00312.

Hu, B., Margolin, W., Molineux, I.J., and Liu, J. (2015). Structural remodeling of bacteriophage T4 and host membranes during infection initiation. *Proc Natl Acad Sci U S A* 112**,** E4919-4928.

Imamovic, L., Jofre, J., Schmidt, H., Serra-Moreno, R., and Muniesa, M. (2009). Phage-mediated Shiga toxin 2 gene transfer in food and water. *Appl Environ Microbiol* 75**,** 1764-1768.

Jacobi, C.A., and Malfertheiner, P. (2011). *Escherichia coli* Nissle 1917 (Mutaflor): new insights into an old probiotic bacterium. *Dig Dis* 29**,** 600-607.

Journet, L., and Cascales, E. (2016). The Type VI Secretion System in *Escherichia coli* and Related Species. *EcoSal Plus* 7.

Kaiser, G.E. (2014). *Bacteriophage life cycles: The Lytic Life Cycle* [Online]. Available: http://faculty.ccbcmd.edu/courses/bio141/lecguide/unit4/viruses/lytlc.html [Accessed].

Karpman, D., Loos, S., Tati, R., and Arvidsson, I. (2017). Haemolytic uraemic syndrome. *J Intern Med* 281**,** 123-148.

Kauffmann, F.U.G.V. (1945). Über die Bedeutung des serologischen Formenwechsels für die Bakteriophagenwirkung in der Coli-Gruppe. *Acta Path Microbiol Scand A* 22**,** 20.

Kho, Z.Y., and Lal, S.K. (2018). The Human Gut Microbiome - A Potential Controller of Wellness and Disease. *Front Microbiol* 9**,** 1835.

Kleta, S., Nordhoff, M., Tedin, K., Wieler, L.H., Kolenda, R., Oswald, S., Oelschlaeger, T.A., Bleiss, W., and Schierack, P. (2014). Role of F1C fimbriae, flagella, and secreted bacterial components in the inhibitory effect of probiotic *Escherichia coli* Nissle 1917 on atypical enteropathogenic *E. coli* infection. *Infect Immun* 82**,** 1801-1812.

Koike, M., and Iida, K. (1971). Effect of polymyxin on the bacteriophage receptors of the cell walls of gram-negative bacteria. *J Bacteriol* 108**,** 1402-1411.

Kruger, A., and Lucchesi, P.M. (2015). Shiga toxins and *stx* phages: highly diverse entities. *Microbiology* 161**,** 451-462.

Kruis, W., Chrubasik, S., Boehm, S., Stange, C., and Schulze, J. (2012). A double-blind placebo-controlled trial to study therapeutic effects of probiotic *Escherichia coli* Nissle 1917 in subgroups of patients with irritable bowel syndrome. *Int J Colorectal Dis* 27**,** 467-474.

Kruis, W., Fric, P., Pokrotnieks, J., Lukas, M., Fixa, B., Kascak, M., Kamm, M.A., Weismueller, J., Beglinger, C., Stolte, M., Wolff, C., and Schulze, J. (2004). Maintaining remission of ulcerative colitis with the probiotic *Escherichia coli* Nissle 1917 is as effective as with standard mesalazine. *Gut* 53**,** 1617-1623.

Kutter, E., De Vos, D., Gvasalia, G., Alavidze, Z., Gogokhia, L., Kuhl, S., and Abedon, S.T. (2010). Phage therapy in clinical practice: treatment of human infections. *Curr Pharm Biotechnol* 11**,** 69-86.

Labrie, S.J., Samson, J.E., and Moineau, S. (2010). Bacteriophage resistance mechanisms. *Nat Rev Microbiol* 8**,** 317-327.

Ladero, V., Garcia, P., Bascaran, V., Herrero, M., Alvarez, M.A., and Suarez, J.E. (1998). Identification of the repressor-encoding gene of the *Lactobacillus* bacteriophage A2. *J Bacteriol* 180**,** 3474-3476.

Lasaro, M.A., Salinger, N., Zhang, J., Wang, Y., Zhong, Z., Goulian, M., and Zhu, J. (2009). F1C fimbriae play an important role in biofilm formation and intestinal colonization by the *Escherichia coli* commensal strain Nissle 1917. *Appl Environ Microbiol* 75**,** 246-251.

Leatham, M.P., Banerjee, S., Autieri, S.M., Mercado-Lubo, R., Conway, T., and Cohen, P.S. (2009). Precolonized human commensal *Escherichia coli* strains serve as a barrier to *E. coli* O157:H7 growth in the streptomycin-treated mouse intestine. *Infect Immun* 77**,** 2876-2886.

Leiman, P.G., and Shneider, M.M. (2012). Contractile tail machines of bacteriophages. *Adv Exp Med Biol* 726**,** 93-114.

Lepage, P., Colombet, J., Marteau, P., Sime-Ngando, T., Dore, J., and Leclerc, M. (2008). Dysbiosis in inflammatory bowel disease: a role for bacteriophages? *Gut* 57**,** 424-425.

Letarov, A.V., and Kulikov, E.E. (2017). Adsorption of Bacteriophages on Bacterial Cells. *Biochemistry (Mosc)* 82**,** 1632-1658.

Ley, R.E., Turnbaugh, P.J., Klein, S., and Gordon, J.I. (2006). Microbial ecology: human gut microbes associated with obesity. *Nature* 444**,** 1022-1023.

Lievin-Le Moal, V., and Servin, A.L. (2014). Anti-infective activities of *Lactobacillus* strains in the human intestinal microbiota: from probiotics to gastrointestinal anti-infectious biotherapeutic agents. *Clin Microbiol Rev* 27**,** 167-199.

Lindberg, A.A. (1973). Bacteriophage receptors. *Annu Rev Microbiol* 27**,** 205-241.

Lodinova-Zadnikova, R., and Sonnenborn, U. (1997). Effect of preventive administration of a nonpathogenic *Escherichia coli* strain on the colonization of the intestine with microbial pathogens in newborn infants. *Biol Neonate* 71**,** 224-232.

Lodinova-Zadnikova, R., Sonnenborn, U., and Tlaskalova, H. (1998). Probiotics and E. coli infections in man. *Vet Q* 20 Suppl 3**,** S78-81.

Los, J.M., Los, M., Wegrzyn, A., and Wegrzyn, G. (2010). Hydrogen peroxide-mediated induction of the Shiga toxin-converting lambdoid prophage ST2-8624 in *Escherichia coli* O157:H7. *FEMS Immunol Med Microbiol* 58**,** 322-329.

Love, M.I., Huber, W., and Anders, S. (2014). Moderated estimation of fold change and dispersion for RNA-seq data with DESeq2. *Genome Biol* 15**,** 550.

Lu, M.J., and Henning, U. (1989). The immunity (*imm*) gene of *Escherichia coli* bacteriophage T4. *J Virol* 63**,** 3472-3478.

Mackowiak, P.A. (2013). Recycling metchnikoff: probiotics, the intestinal microbiome and the quest for long life. *Front Public Health* 1**,** 52.

Mainil, J. (1999). Shiga/verocytotoxins and Shiga/verotoxigenic *Escherichia coli* in animals. *Vet Res* 30**,** 235-257.

Majkowska-Skrobek, G., Latka, A., Berisio, R., Squeglia, F., Maciejewska, B., Briers, Y., and Drulis-Kawa, Z. (2018). Phage-Borne Depolymerases Decrease *Klebsiella pneumoniae* Resistance to Innate Defense Mechanisms. *Front Microbiol* 9**,** 2517.

Manning, A.J., and Kuehn, M.J. (2011). Contribution of bacterial outer membrane vesicles to innate bacterial defense. *BMC Microbiol* 11**,** 258.

Manrique, P., Bolduc, B., Walk, S.T., Van Der Oost, J., De Vos, W.M., and Young, M.J. (2016). Healthy human gut phageome. *Proc Natl Acad Sci U S A* 113**,** 10400-10405.

Marinus, M.G., and Poteete, A.R. (2013). High efficiency generalized transduction in *Escherichia coli* O157:H7. *F1000Res* 2**,** 7.

Martin, M. (2011). Cutadapt removes adapter sequences from high-throughput sequencing reads. *EMBnet.Journal,* 17**,** 3.

Matsuura, Y., Takehira, M., Joti, Y., Ogasahara, K., Tanaka, T., Ono, N., Kunishima, N., and Yutani, K. (2015). Thermodynamics of protein denaturation at temperatures over 100 degrees C: CutA1 mutant proteins substituted with hydrophobic and charged residues. *Sci Rep* 5**,** 15545.

Maurice, C.F. (2019). Considering the Other Half of the Gut Microbiome: Bacteriophages. *mSystems* 4.

Mccully, A.L., Behringer, M.G., Gliessman, J.R., Pilipenko, E.V., Mazny, J.L., Lynch, M., Drummond, D.A., and Mckinlay, J.B. (2018). An *Escherichia coli* Nitrogen Starvation Response Is Important for Mutualistic Coexistence with *Rhodopseudomonas palustris*. *Appl Environ Microbiol* 84.

Mcgrath, S., Fitzgerald, G.F., and Van Sinderen, D. (2002). Identification and characterization of phage-resistance genes in temperate *Lactococcal* bacteriophages. *Mol Microbiol* 43**,** 509-520.

Melton-Celsa, A.R. (2014). Shiga Toxin (Stx) Classification, Structure, and Function. *Microbiol Spectr* 2**,** EHEC-0024-2013.

Mirzaei, M.K., and Maurice, C.F. (2017). Menage a trois in the human gut: interactions between host, bacteria and phages. *Nat Rev Microbiol* 15**,** 397-408.

Mitsuzawa, S., Deguchi, S., and Horikoshi, K. (2006). Cell structure degradation in *Escherichia coli* and *Thermococcus* sp. strain Tc-1-95 associated with thermal death resulting from brief heat treatment. *FEMS Microbiol Lett* 260**,** 100-105.

Mizoguchi, K., Morita, M., Fischer, C.R., Yoichi, M., Tanji, Y., and Unno, H. (2003). Coevolution of bacteriophage PP01 and *Escherichia coli* O157:H7 in continuous culture. *Appl Environ Microbiol* 69**,** 170-176.

Mohammed, B.O.a.M. (2019). The War between Bacteria and Bacteriophages. *Growing and Handling of Bacterial Cultures*.

Mohsin, M., Guenther, S., Schierack, P., Tedin, K., and Wieler, L.H. (2015). Probiotic *Escherichia coli* Nissle 1917 reduces growth, Shiga toxin expression, release and thus cytotoxicity of enterohemorrhagic *Escherichia coli*. *Int J Med Microbiol* 305**,** 20-26.

Molloy, M.J., Grainger, J.R., Bouladoux, N., Hand, T.W., Koo, L.Y., Naik, S., Quinones, M., Dzutsev, A.K., Gao, J.L., Trinchieri, G., Murphy, P.M., and Belkaid, Y. (2013). Intraluminal containment of commensal outgrowth in the gut during infection-induced dysbiosis. *Cell Host Microbe* 14**,** 318-328.

Monk, M., and Kinross, J. (1975). The kinetics of derepression of prophage lambda following ultraviolet irradiation of lysogenic cells. *Mol Gen Genet* 137**,** 263-268.

Mutoh, N., Furukawa, H., and Mizushima, S. (1978). Role of lipopolysaccharide and outer membrane protein of *Escherichia coli* K-12 in the receptor activity for bacteriophage T4. *J Bacteriol* 136**,** 693-699.

Navarro-Garcia, F., Ruiz-Perez, F., Cataldi, A., and Larzabal, M. (2019). Type VI Secretion System in Pathogenic *Escherichia coli*: Structure, Role in Virulence, and Acquisition. *Front Microbiol* 10**,** 1965.

Nissle, A. (1918). Die antagonistische Behandlung chronischer Darmstörungen mit Colibakterien. *Med. Klinik* 29-30.

Nordstrom, K., and Forsgren, A. (1974). Effect of protein A on adsorption of bacteriophages to *Staphylococcus aureus*. *J Virol* 14**,** 198-202.

Nzakizwanayo, J., Kumar, S., Ogilvie, L.A., Patel, B.A., Dedi, C., Macfarlane, W.M., and Jones, B.V. (2015). Disruption of Escherichia coli Nissle 1917 K5 capsule biosynthesis, through loss of distinct kfi genes, modulates interaction with intestinal epithelial cells and impact on cell health. *PLoS One* 10**,** e0120430.

O'brien, A.D., Newland, J.W., Miller, S.F., Holmes, R.K., Smith, H.W., and Formal, S.B. (1984). Shiga-like toxin-converting phages from *Escherichia coli* strains that cause hemorrhagic colitis or infantile diarrhea. *Science* 226**,** 694-696.

Oelschlaeger, T.A. (2010). Mechanisms of probiotic actions - A review. *Int J Med Microbiol* 300**,** 57-62.

Ofir, G., Melamed, S., Sberro, H., Mukamel, Z., Silverman, S., Yaakov, G., Doron, S., and Sorek, R. (2018). DISARM is a widespread bacterial defence system with broad anti-phage activities. *Nat Microbiol* 3**,** 90-98.

Oladeinde, A., Lipp, E., Chen, C.Y., Muirhead, R., Glenn, T., Cook, K., and Molina, M. (2018). Transcriptome Changes of *Escherichia coli*, *Enterococcus faecalis*, and *Escherichia coli* O157:H7 Laboratory Strains in Response to Photo-Degraded DOM. *Front Microbiol* 9**,** 882.

Olsen, S.J., Miller, G., Breuer, T., Kennedy, M., Higgins, C., Walford, J., Mckee, G., Fox, K., Bibb, W., and Mead, P. (2002). A waterborne outbreak of *Escherichia coli* O157:H7 infections and hemolytic uremic syndrome: implications for rural water systems. *Emerg Infect Dis* 8**,** 370-375.

Orskov, I., Orskov, F., Jann, B., and Jann, K. (1977). Serology, chemistry, and genetics of O and K antigens of *Escherichia coli*. *Bacteriol Rev* 41**,** 667-710.

Oshima, K., Toh, H., Ogura, Y., Sasamoto, H., Morita, H., Park, S.H., Ooka, T., Iyoda, S., Taylor, T.D., Hayashi, T., Itoh, K., and Hattori, M. (2008). Complete genome sequence and comparative analysis of the wild-type commensal *Escherichia coli* strain SE11 isolated from a healthy adult. *DNA Res* 15**,** 375-386.

Pacheco, A.R., and Sperandio, V. (2012). Shiga toxin in enterohemorrhagic *E. coli:* regulation and novel anti-virulence strategies. *Front Cell Infect Microbiol* 2**,** 81.

Patzer, S.I., Baquero, M.R., Bravo, D., Moreno, F., and Hantke, K. (2003). The colicin G, H and X determinants encode microcins M and H47, which might utilize the catecholate siderophore receptors FepA, Cir, Fiu and IroN. *Microbiology* 149**,** 2557-2570.

Pelechano, V., and Steinmetz, L.M. (2013). Gene regulation by antisense transcription. *Nat Rev Genet* 14**,** 880-893.

Penades, J.R., and Christie, G.E. (2015). The Phage-Inducible Chromosomal Islands: A Family of Highly Evolved Molecular Parasites. *Annu Rev Virol* 2**,** 181-201.

Perepelov, A.V., Han, W., Senchenkova, S.N., Shevelev, S.D., Shashkov, A.S., Feng, L., Liu, Y., Knirel, Y.A., and Wang, L. (2007). Structure of the O-polysaccharide of *Escherichia coli* O150 containing 2-acetamido-4-O-[(S)-1-carboxyethyl]-2-deoxy-d-glucose. *Carbohydr Res* 342**,** 648-652.

Pflughoeft, K.J., and Versalovic, J. (2012). Human microbiome in health and disease. *Annu Rev Pathol* 7**,** 99-122.

Pham, T.A., and Lawley, T.D. (2014). Emerging insights on intestinal dysbiosis during bacterial infections. *Curr Opin Microbiol* 17**,** 67-74.

Pharma-Zentrale Gmbh, M. *Phenotypical characteristics of E. coli strain Nissle 1917 and its gene loci in the bacterial chromosome* [Online]. Available: https://www.mutaflor.com/e-coli-strain-nissle-1917-strain-specific-properties-and-mechanisms-of-action/molecular-mechanisms-of-action.html [Accessed].

Picken, I.R.B.a.R.N. (1981). On the Receptor for Bacteriophage T4 in *Escherichia coli* K12 *CURRENT MICROBIOLOGY* 6**,** 3.

Picken, R.N., and Beacham, I.R. (1977). Bacteriophage-resistant mutants of *Escherichia coli* K12. Location of receptors within the lipopolysaccharide. *J Gen Microbiol* 102**,** 305-318.

Podolsky, S.H. (2012). Metchnikoff and the microbiome. *Lancet* 380**,** 1810-1811.

Pruimboom-Brees, I.M., Morgan, T.W., Ackermann, M.R., Nystrom, E.D., Samuel, J.E., Cornick, N.A., and Moon, H.W. (2000). Cattle lack vascular receptors for *Escherichia coli* O157:H7 Shiga toxins. *Proc Natl Acad Sci U S A* 97**,** 10325-10329.

Raman, M., Ambalam, P., Kondepudi, K.K., Pithva, S., Kothari, C., Patel, A.T., Purama, R.K., Dave, J.M., and Vyas, B.R. (2013). Potential of probiotics, prebiotics and synbiotics for management of colorectal cancer. *Gut Microbes* 4**,** 181-192.

Ranade, K., and Poteete, A.R. (1993). Superinfection exclusion (*sieB*) genes of bacteriophages P22 and lambda. *J Bacteriol* 175**,** 4712-4718.

Randall-Hazelbauer, L., and Schwartz, M. (1973). Isolation of the bacteriophage lambda receptor from *Escherichia coli*. *J Bacteriol* 116**,** 1436-1446.

Reissbrodt, R., Hammes, W.P., Dal Bello, F., Prager, R., Fruth, A., Hantke, K., Rakin, A., Starcic-Erjavec, M., and Williams, P.H. (2009). Inhibition of growth of Shiga toxin-producing *Escherichia coli* by nonpathogenic *Escherichia coli*. *FEMS Microbiol Lett* 290**,** 62-69.

Reyes-Robles, T., Dillard, R.S., Cairns, L.S., Silva-Valenzuela, C.A., Housman, M., Ali, A., Wright, E.R., and Camilli, A. (2018). *Vibrio cholerae* Outer Membrane Vesicles Inhibit Bacteriophage Infection. *J Bacteriol* 200.

Riede, I. (1987). Receptor specificity of the short tail fibres (*gp12*) of T-even type *Escherichia coli* phages. *Mol Gen Genet* 206**,** 110-115.

Rossmann, M.G., Arisaka, F., Battisti, A.J., Bowman, V.D., Chipman, P.R., Fokine, A., Hafenstein, S., Kanamaru, S., Kostyuchenko, V.A., Mesyanzhinov, V.V., Shneider, M.M., Morais, M.C., Leiman, P.G., Palermo, L.M., Parrish, C.R., and Xiao, C. (2007). From structure of the complex to understanding of the biology. *Acta Crystallogr D Biol Crystallogr* 63**,** 9-16.

Rostol, J.T., and Marraffini, L. (2019). (Ph)ighting Phages: How Bacteria Resist Their Parasites. *Cell Host Microbe* 25**,** 184-194.

Rund, S.A., Rohde, H., Sonnenborn, U., and Oelschlaeger, T.A. (2013). Antagonistic effects of probiotic *Escherichia coli* Nissle 1917 on EHEC strains of serotype O104:H4 and O157:H7. *Int J Med Microbiol* 303**,** 1-8.

Sahar H. Ali, K.M.a.-J.a.M.T.a.-M. (2017). Impact of probiotic strain of the non-pathogenic *Escherichia coli* "Nissle1917" on gene expression of shiga toxin *E. coli* O157:H7 In vitro and In vivo. *BIOSCIENCE RESEARCH* 14**,** 9.

Samson, J.E., Magadan, A.H., Sabri, M., and Moineau, S. (2013). Revenge of the phages: defeating bacterial defences. *Nat Rev Microbiol* 11**,** 675-687.

Sapelli, R.V., and Goebel, W.F. (1964). The Capsular Polysaccharide of a Mucoid Variant of *E. coli* K 12. *Proc Natl Acad Sci U S A* 52**,** 265-271.

Sashital, D.G. (2017). Prokaryotic Argonaute Uses an All-in-One Mechanism to Provide Host Defense. *Mol Cell* 65**,** 957-958.

Sassone-Corsi, M., Nuccio, S.P., Liu, H., Hernandez, D., Vu, C.T., Takahashi, A.A., Edwards, R.A., and Raffatellu, M. (2016). Microcins mediate competition among *Enterobacteriaceae* in the inflamed gut. *Nature* 540**,** 280-283.

Scanlan, P.D. (2017). Bacteria-Bacteriophage Coevolution in the Human Gut: Implications for Microbial Diversity and Functionality. *Trends Microbiol* 25**,** 614-623.

Schierack, P., Kleta, S., Tedin, K., Babila, J.T., Oswald, S., Oelschlaeger, T.A., Hiemann, R., Paetzold, S., and Wieler, L.H. (2011). *E. coli* Nissle 1917 Affects *Salmonella* adhesion to porcine intestinal epithelial cells. *PLoS One* 6**,** e14712.

Schlee, M., Wehkamp, J., Altenhoefer, A., Oelschlaeger, T.A., Stange, E.F., and Fellermann, K. (2007). Induction of human beta-defensin 2 by the probiotic *Escherichia coli* Nissle 1917 is mediated through flagellin. *Infect Immun* 75**,** 2399-2407.

Schmidt, H. (2001). Shiga-toxin-converting bacteriophages. *Res Microbiol* 152**,** 687-695.

Scholl, D., Adhya, S., and Merril, C. (2005). *Escherichia coli* K1's capsule is a barrier to bacteriophage T7. *Appl Environ Microbiol* 71**,** 4872-4874.

Schwartz, M. (1976). The adsorption of coliphage lambda to its host: effect of variations in the surface density of receptor and in phage-receptor affinity. *J Mol Biol* 103**,** 521-536.

Sender, R., Fuchs, S., and Milo, R. (2016). Revised Estimates for the Number of Human and Bacteria Cells in the Body. *PLoS Biol* 14**,** e1002533.

Serra-Moreno, R., Jofre, J., and Muniesa, M. (2008). The CI repressors of Shiga toxin-converting prophages are involved in coinfection of *Escherichia coli* strains, which causes a down regulation in the production of Shiga toxin 2. *J Bacteriol* 190**,** 4722-4735.

Sharma, S.K. (1986). Endotoxin detection and elimination in biotechnology. *Biotechnol Appl Biochem* 8**,** 5-22.

Shkoporov, A.N., and Hill, C. (2019). Bacteriophages of the Human Gut: The "Known Unknown" of the Microbiome. *Cell Host Microbe* 25**,** 195-209.

Sijtsma, L., Wouters, J.T., and Hellingwerf, K.J. (1990). Isolation and characterization of lipoteichoic acid, a cell envelope component involved in preventing phage adsorption, from *Lactococcus lactis* subsp. *cremoris SK110*. *J Bacteriol* 172**,** 7126-7130.

Snyder, J.A., Haugen, B.J., Buckles, E.L., Lockatell, C.V., Johnson, D.E., Donnenberg, M.S., Welch, R.A., and Mobley, H.L. (2004). Transcriptome of uropathogenic *Escherichia coli* during urinary tract infection. *Infect Immun* 72**,** 6373-6381.

Sonnenborn, U. (2016). *Escherichia coli* strain Nissle 1917-from bench to bedside and back: history of a special *Escherichia coli* strain with probiotic properties. *FEMS Microbiol Lett* 363.

Sonnenborn, U., and Schulze, J. (2009). The non-pathogenic *Escherichia coli* strain Nissle 1917 – features of a versatile probiotic. *Microbial Ecology in Health and Disease* 21**,** 122-158.

Soundararajan, M. (2016). *Molecular studies on safety aspects and probiotic nature of E. coli Nissle 1917*. Masters in Fokus Life Science, Julius Maximilian University of Würzburg.

Soundararajan, M., Von Bunau, R., and Oelschlaeger, T.A. (2019). K5 Capsule and Lipopolysaccharide Are Important in Resistance to T4 Phage Attack in Probiotic *E. coli* Strain Nissle 1917. *Front Microbiol* 10**,** 2783.

Staudova, B., Micenkova, L., Bosak, J., Hrazdilova, K., Slaninkova, E., Vrba, M., Sevcikova, A., Kohoutova, D., Woznicova, V., Bures, J., and Smajs, D. (2015). Determinants

encoding fimbriae type 1 in fecal *Escherichia coli* are associated with increased frequency of bacteriocinogeny. *BMC Microbiol* 15**,** 201.

Steimle, A., Menz, S., Bender, A., Ball, B., Weber, A.N.R., Hagemann, T., Lange, A., Maerz, J.K., Parusel, R., Michaelis, L., Schafer, A., Yao, H., Low, H.C., Beier, S., Tesfazgi Mebrhatu, M., Gronbach, K., Wagner, S., Voehringer, D., Schaller, M., Fehrenbacher, B., Autenrieth, I.B., Oelschlaeger, T.A., and Frick, J.S. (2019). Flagellin hypervariable region determines symbiotic properties of commensal *Escherichia coli* strains. *PLoS Biol* 17**,** e3000334.

Stentebjerg-Olesen, B., Chakraborty, T., and Klemm, P. (1999). Type 1 fimbriation and phase switching in a natural *Escherichia coli fimB* null strain, Nissle 1917. *J Bacteriol* 181**,** 7470-7478.

Stenutz, R., Weintraub, A., and Widmalm, G. (2006). The structures of *Escherichia coli* O-polysaccharide antigens. *FEMS Microbiol Rev* 30**,** 382-403.

Szczepankowska, A. (2012). Role of CRISPR/cas system in the development of bacteriophage resistance. *Adv Virus Res* 82**,** 289-338.

Tanaka, M., and Nakayama, J. (2017). Development of the gut microbiota in infancy and its impact on health in later life. *Allergol Int* 66**,** 515-522.

Tissier, H. (1906). Traitement des infections intestinales par la méthode de la flore bactérienne de l'intestin. *C. R. Soc. Biol.* 60**,** 3.

Toh, H., Oshima, K., Toyoda, A., Ogura, Y., Ooka, T., Sasamoto, H., Park, S.H., Iyoda, S., Kurokawa, K., Morita, H., Itoh, K., Taylor, T.D., Hayashi, T., and Hattori, M. (2010). Complete genome sequence of the wild-type commensal *Escherichia coli* strain SE15, belonging to phylogenetic group B2. *J Bacteriol* 192**,** 1165-1166.

Trafalska, E., and Grzybowska, K. (2004). [Probiotics--an alternative for antibiotics?]. *Wiad Lek* 57**,** 491-498.

Troge, A. (2012). Studien am Flagellensystem des Escherichia coli Stammes Nissle 1917 (EcN) im Hinblick auf seine Funktion als Probiotikum. *Dissertation, Universität Würzburg, Würzburg. Retrieved from urn:nbn:de:bvb:20-opus-74201*.

Troge, A., Scheppach, W., Schroeder, B.O., Rund, S.A., Heuner, K., Wehkamp, J., Stange, E.F., and Oelschlaeger, T.A. (2012). More than a marine propeller--the flagellum of the probiotic *Escherichia coli* strain Nissle 1917 is the major adhesin mediating binding to human mucus. *Int J Med Microbiol* 302**,** 304-314.

Valdebenito, M., Crumbliss, A.L., Winkelmann, G., and Hantke, K. (2006). Environmental factors influence the production of enterobactin, salmochelin, aerobactin, and yersiniabactin in *Escherichia coli* strain Nissle 1917. *Int J Med Microbiol* 296**,** 513-520.

Vallee, M., Cornett, J.B., and Bernstein, H. (1972). The action of bacteriophage T4 ghosts on *Escherichia coli* and the immunity to this action developed in cells preinfected with T4. *Virology* 48**,** 766-776.

Vaughan, R.B. (1965). The Romantic Rationalist: A Study of Elie Metchnikoff. *Med Hist* 9**,** 201-215.

Ventura, M., Sozzi, T., Turroni, F., Matteuzzi, D., and Van Sinderen, D. (2011). The impact of bacteriophages on probiotic bacteria and gut microbiota diversity. *Genes Nutr* 6**,** 205-207.

Vidakovic, L., Singh, P.K., Hartmann, R., Nadell, C.D., and Drescher, K. (2018). Dynamic biofilm architecture confers individual and collective mechanisms of viral protection. *Nat Microbiol* 3**,** 26-31.

Viralzone (2013). *Viral long flexible tail ejection system* [Online]. Swiss Institute of Bioinformatics. [Accessed].

Washizaki, A., Yonesaki, T., and Otsuka, Y. (2016). Characterization of the interactions between *Escherichia coli* receptors, LPS and OmpC, and bacteriophage T4 long tail fibers. *Microbiologyopen* 5**,** 1003-1015.

Wassenaar, T.M. (2016). Insights from 100 Years of Research with Probiotic *E. coli*. *Eur J Microbiol Immunol (Bp)* 6**,** 147-161.
Weitz, J.S., Hartman, H., and Levin, S.A. (2005). Coevolutionary arms races between bacteria and bacteriophage. *Proc Natl Acad Sci U S A* 102**,** 9535-9540.
Whitfield, C., and Trent, M.S. (2014). Biosynthesis and export of bacterial lipopolysaccharides. *Annu Rev Biochem* 83**,** 99-128.
Who (Year). "Guidelines for the Evaluation of Probiotics in Food", in: *Evaluation of Health and Nutritional Properties of Probiotics in Food*: Food and Agriculture Organization and World Health Organization Expert Consultation.).
Who (2011). "Public health review of the enterohaemorrhagic *Escherichia coli* outbreak in germany".).
Willkomm, S., Makarova, K.S., and Grohmann, D. (2018). DNA silencing by prokaryotic Argonaute proteins adds a new layer of defense against invading nucleic acids. *FEMS Microbiol Rev* 42**,** 376-387.
Wilson, J.H., Luftig, R.B., and Wood, W.B. (1970). Interaction of bacteriophage T4 tail fiber components with a lipopolysaccharide fraction from *Escherichia coli*. *J Mol Biol* 51**,** 423-434.
Winkler, H.H., and Duckworth, D.H. (1971). Metabolism of T4 bacteriophage ghost-infected cells: effect of bacteriophage and ghosts on the uptake of carbohydrates in *Escherichia coli* B. *J Bacteriol* 107**,** 259-267.
Xia, P., Zhu, J., and Zhu, G. (2013). *Escherichia coli* Nissle 1917 as safe vehicles for intestinal immune targeted therapy--a review. *Wei Sheng Wu Xue Bao* 53**,** 538-544.
Xu, P., Li, M., Zhang, J., and Zhang, T. (2012). Correlation of intestinal microbiota with overweight and obesity in Kazakh school children. *BMC Microbiol* 12**,** 283.
Xu, Z., Wei, W., Gagneur, J., Clauder-Munster, S., Smolik, M., Huber, W., and Steinmetz, L.M. (2011). Antisense expression increases gene expression variability and locus interdependency. *Mol Syst Biol* 7**,** 468.
Yatsunenko, T., Rey, F.E., Manary, M.J., Trehan, I., Dominguez-Bello, M.G., Contreras, M., Magris, M., Hidalgo, G., Baldassano, R.N., Anokhin, A.P., Heath, A.C., Warner, B., Reeder, J., Kuczynski, J., Caporaso, J.G., Lozupone, C.A., Lauber, C., Clemente, J.C., Knights, D., Knight, R., and Gordon, J.I. (2012). Human gut microbiome viewed across age and geography. *Nature* 486**,** 222-227.
Yu, F., and Mizushima, S. (1982). Roles of lipopolysaccharide and outer membrane protein OmpC of *Escherichia coli* K-12 in the receptor function for bacteriophage T4. *J Bacteriol* 151**,** 718-722.
Yung, P.Y., Grasso, L.L., Mohidin, A.F., Acerbi, E., Hinks, J., Seviour, T., Marsili, E., and Lauro, F.M. (2016). Global transcriptomic responses of *Escherichia coli* K-12 to volatile organic compounds. *Sci Rep* 6**,** 19899.
Zeng, L., and Golding, I. (2011). Following cell-fate in *E. coli* after infection by phage lambda. *J Vis Exp***,** e3363.
Zhang, H., Niesel, D.W., Peterson, J.W., and Klimpel, G.R. (1998). Lipoprotein release by bacteria: potential factor in bacterial pathogenesis. *Infect Immun* 66**,** 5196-5201.
Zhang, X., Mcdaniel, A.D., Wolf, L.E., Keusch, G.T., Waldor, M.K., and Acheson, D.W. (2000). Quinolone antibiotics induce Shiga toxin-encoding bacteriophages, toxin production, and death in mice. *J Infect Dis* 181**,** 664-670.
Zhang, Y., Liao, Y.T., Salvador, A., Sun, X., and Wu, V.C.H. (2019). Complete Genome Sequence of a Shiga Toxin-Converting Bacteriophage, *Escherichia* Phage Lys12581Vzw, Induced from an Outbreak Shiga Toxin-Producing *Escherichia coli* Strain. *Microbiol Resour Announc* 8.

Zhou, K., Zhou, L., Lim, Q., Zou, R., Stephanopoulos, G., and Too, H.P. (2011a). Novel reference genes for quantifying transcriptional responses of *Escherichia coli* to protein overexpression by quantitative PCR. *BMC Mol Biol* 12**,** 18.

Zhou, Y., Liang, Y., Lynch, K.H., Dennis, J.J., and Wishart, D.S. (2011b). PHAST: a fast phage search tool. *Nucleic Acids Res* 39**,** W347-352.

Zmora, N., Zilberman-Schapira, G., Suez, J., Mor, U., Dori-Bachash, M., Bashiardes, S., Kotler, E., Zur, M., Regev-Lehavi, D., Brik, R.B., Federici, S., Cohen, Y., Linevsky, R., Rothschild, D., Moor, A.E., Ben-Moshe, S., Harmelin, A., Itzkovitz, S., Maharshak, N., Shibolet, O., Shapiro, H., Pevsner-Fischer, M., Sharon, I., Halpern, Z., Segal, E., and Elinav, E. (2018). Personalized Gut Mucosal Colonization Resistance to Empiric Probiotics Is Associated with Unique Host and Microbiome Features. *Cell* 174**,** 1388-1405 e1321.

8. Annexure

Annexure 1: Details of deletion mutants of EcN used in this study

The genomic regions (blue arrows) and deletion regions (yellow arrows) of the mutants EcNΔ *mchC-F* (SK22D), EcNΔ *bcs*, EcNΔ *csg*, EcNΔ *k5*, EcNΔ *fliC*, are indicated in this table. The red arrows are the primers used for screening the mutants by amplicon sequencing which was done previously in the lab by Dr Susanne Bury. Source:(Bury, 2018)

A

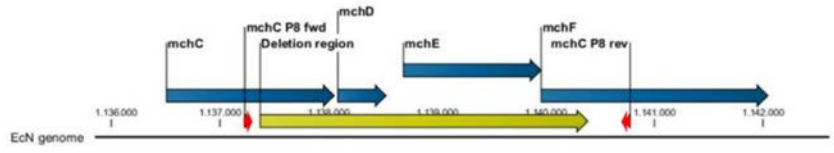

EcN mutant	Microcin genomic region	Deletion region
EcNΔ*mchC-F* (SK22D)	1,136,505 - 1,142,049	1,137,366 - 1,140,391

B

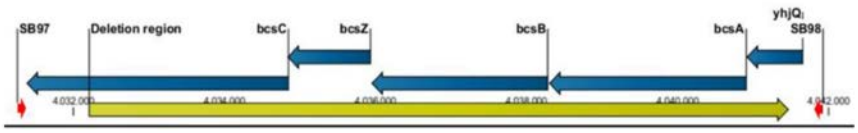

EcN mutant	Cellulose genomic region	Deletion region
EcNΔ*bcs*	4,031,381 - 4,041,666	4,032,204 - 4,041,472

C

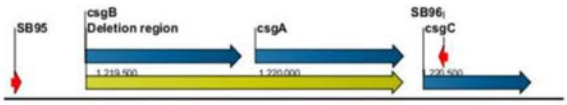

EcN mutant	Curli genomic region	Deletion region
EcNΔ*csg*	1,219,402 - 1,220,774	1,219,405 - 1,220,381

D

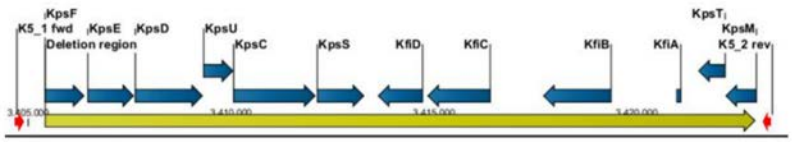

EcN mutant	Capsule genomic region	Deletion region
EcNΔ*k5*	3,405,403 - 3,422,968	3,405,406 - 3,422,928

E

EcN mutant	Flagellin genomic region	Deletion region
EcNΔ*fliC*	2,099,443 - 2,101,230	2,099,435 - 2,101,234

Annexure 2: Regulation of ferrous iron transport system (EfeUOB) in the EcN fermenter cultures

Genes	log_2 fold change in fermenter culture	
	Start of the stationary phase	End of the stationary phase
efeU	1,745	1,485
efeO	1,939	1,631
efeB	1,499	0,812

Annexure 3: Details of up and downregulated genes in EcN when coincubated with EDL933 for 3 h and their functional predictions*

Table 8. 1: List of upregulated genes in EcN (log_2 fold change > 1, padj < 0.05)*

Table 8. 2: List of genes downregulated in EcN (log_2 fold change < -1, padj < 0.05)*

Annexure 4: Functional details of up and down-regulated genes in EcN when incubated with T4 phages for 2 h*

Table 8. 3: Details of the genes downregulated in EcN when incubated with T4 phages after 2 h (log_2 fold change < -2, padj < 0.05)*

Table 8. 4: Details of the genes upregulated in EcN when incubated with T4 phages after 2 h (log_2 fold change>2, padj<0.05)*

***The tables of Annexure 3 and Annexure 4 are provided as the soft copy in the DVD attached to the thesis.**

Annexure 5: Alignment of the amino acid sequence of the lambda phage receptors (LamB) of EcN and MG1655 uising CLC workbench

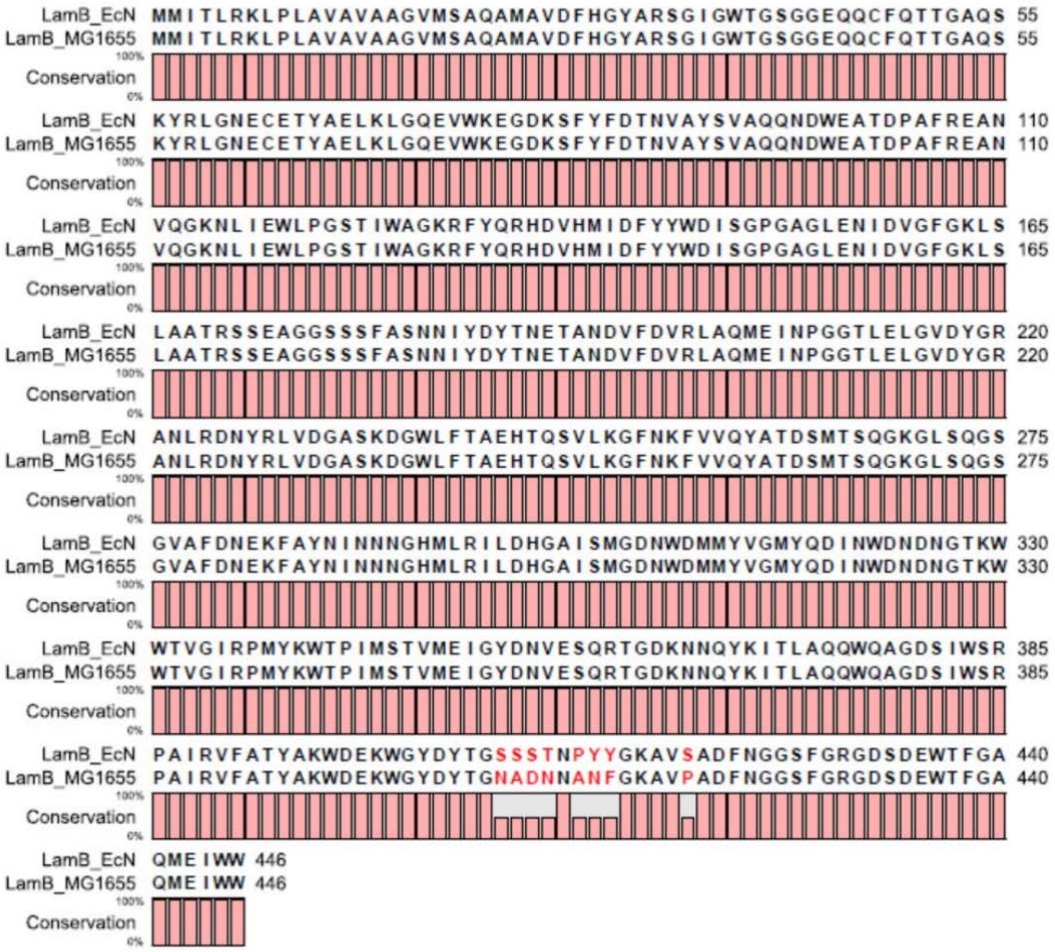

9. Abbreviations

aa	amino acid
abi	abortive infection
Amp	ampicillin
AS	antisense
ATP	adenosine triphosphate
BLAST	basic local alignment search tool
bp	base pair
°C	degree Celsius
CaCl2	calcium chloride
cDNA	complementary DNA
CFUs	colony forming units
cm	centimeter
CRISPR-Cas	Clustered Regularly Interspaced Short Palindromic Repeats
CsCl	Ceasium chloride
DAPI	4′,6-diamidino-2-phenylindole
dH_20	distilled water
dNTP	deoxyribonucleotide triphosphate
DTT	Dithiothreitol
DMSO	dimethylsulfoxide
DNA	deoxyribonucleic acid
ds	double stranded
EAEC	enteroaggregative *E. coli*
ECC	Chromogenic *E. coli* coliform agar
EDTA	Ethylenediaminetetraacetic acid
EcN	*E. coli* Nissle 1917
E. coli	*Escherichia coli*
e. g.	exempli gratia
EHEC	enterohemorrhagic *E. coli*
ELISA	enzyme-linked immunosorbent assay
EtBr	ethidium bromide
EtOH	Ethanol
FA	Formaldehyde
FT	flow through
g	gram
Gb3	Globotriaosylceramide
GI	gastrointestinal tract
GlcNAc	N-acetylglucosamine
h	hour
H	flagellum
HCl	hydrogen chloride
HK	heat-killed
HUS	hemolytic uremic syndrome

IPTG	Isopropyl β-D-1-thiogalactopyranoside
K	capsule
kDa	kilodalton
kb	kilobase
l	liter
LB	Luria-Bertani
LPS	lipopolysaccharide
m	Milli, meter
mRNA	mitochondrial RNA
M	Molar, Marker, maltose
MA	mean average
µ	micro
mins	minutes
MMC	Mitomycin C
MOI	Multiplicity of infection
MUSCLE	multiple sequence alignment
n	nano
Nr.	number
nt	nucleotides
ns	not significant
OD	optical density
O/N	overnight
ONC	overnight culture
OMVs	outer membrane vesicles
PCR	polymerase chain reaction
PFUs	plaque forming units
PHAST	PHAge Search Tool
PPA	phage plaque assay
P. I.	proteinase inhibitor cocktail
PK	proteinase K
PMB	polymyxin B
PPA	Phage-Plaque-Assay
pr	phage repressor
qRT-PCR	Real-Time Quantitative Reverse Transcription PCR
r	ribosomal
R	rough LPS
RKI	Robert Koch Institute
RM	restriction-modification
RNA	ribonucleic acid
rpm	revolutions per minute
RT	room temperature
S	supernatant, sense
SD	standard deviation
sec	second

sie	superinfection exclusion
SMP	sodium meta periodate
sn	supernatant
ss	single stranded
Stx	Shiga toxin
SSIV RT	SuperScript IV Reverse Transcriptase
t	transfer
TAE	Tris-acetate-EDTA
TEM	transmission electron microscope
T6SS	type 6 secretion system
U	units
UD	undiluted
UPEC	uropathogenic *E. coli*
UV	ultraviolet
WHO	World Health Organization
x g	times gravity
%	percentage
*	$p < 0.0332$
**	$p < 0.0021$
***	$p < 0.0002$
****	$p < 0.0001$

10. List of Figures

Figure 1. 1: Schematic representation of various factors in EcN that contribute to the fitness of the strain. 20

Figure 1. 2: Illustration of bacteria and bacteriophage communities in the healthy adult gut..... 23

Figure 1. 3: Lytic and lysogenic cycle of bacteriophages. Stepwise illustration of lysis and lysogenisation of bacteria by virulent and temperate phages. 24

Figure 1. 4: Schematic representation of bacteriophage lambda attachment to *E. coli*. 25

Figure 1. 5: Model depicting the interactions between T4 phage tail and *E. coli* cell surface receptors. 26

Figure 1. 6: Illustration of various stages of bacteriophage life cycle that are targeted by different phage resistance mechanisms. 28

Figure 3. 1: Purified T4 phage band visible after CsCl density centrifugation 43

Figure 3. 2: Schematic representation of the Mutaflor fermentation process…… 59

Figure 3. 3: Illustration of a typical Transwell system used in this study. 60

Figure 4.1. 1: *E. coli* strain purity identification on ECC plates 64

Figure 4.1. 2: PCR screening to confirm the identity of EcN and K-12 strains 65

Figure 4.1. 3: PCR screen to confirm the identity of the *E. coli* strains CFT073, SE11 and SE15..... 65

Figure 4.1. 4: PCR screen to check the purity of other *E. coli* strains (CFT073, SE11 and SE15)..... 66

Figure 4.1. 5: PCR screening to confirm the identity of EcN mutants used in this study. 67

Figure 4.1. 6: PCR screening to confirm the deletions in the EcN mutants. 68

Figure 4.2. 1: Gene regulation of different fimbrial determinants of EcN.. 70

Figure 4.2. 2: Gene regulation of six iron uptake systems in EcN fermenter-cultures..... 71

Figure 4.2. 3: Gene regulation of the K5 capsule determinant (A) and the microcin gene cluster (B). 72

Figure 4.3. 1: Kinetics of Stx reduction by EcN in a Transwell system 76

Figure 4.3. 2: Graphical depiction of the Transwell setup for RNA isolation. 77

Figure 4.3. 3: Stx reduction in EDL933 by EcN in the Transwell set up. 78

Figure 4.3. 4: Growth kinetics of *E. coli* strains in the Transwell set up for transcriptomics. 79

Figure 4.3. 5: MA plots representing the differentially regulated genes in EcN after coincubation with EDL933 for 3 h (A), 5 h (B), 7 h (C) and 8 h (D) in a Transwell system..... 80
Figure 4.3. 6: MA plots representing the differentially regulated genes in EcN after coincubation with MG1655 for 3 h (A), 5 h (B), 7 h (C) and 8 h (D) in a Transwell system. 81
Figure 4.3. 7: Kinetics of differentially regulated EcN genes 82
Figure 4.3. 8: Specific upregulation of genes in EcN as a response to EDL933 coincubation 84
Figure 4.3. 9: Specific downregulation of genes in EcN as a response to EDL933 coincubation 85
Figure 4.3. 10: Functional grouping of upregulated genes in EcN..... 87
Figure 4.3. 11: Functional grouping of downregulated genes in EcN..... 88
Figure 4.3. 12: Functional grouping of genes up and downregulated in EcN when coincubated with EDL933. 90
Figure 4.4. 1: PCR to detect the lambda prophage lysogens in EcN and MG1655..... 92
Figure 4.4. 2: Identification of EcN and MG1655 lambda prophage lysogens by PPA..... 93
*F*igure 4.4. 3: Regulation of prophage 3 of EcN in the presence of lambdoid phages..... 94
Figure 4.4. 4: Lambda Phage-Plaque-Assay with recombinant MG1655 strains 95
Figure 4.4. 5: Antisense regulation of prophage 3 genes in EcN when incubated with lambdoid phages 97
Figure 4.4. 6: Lambda phage titer reduction kinetics and growth kinetics of *E. coli* strains. 99
Figure 4.4. 7: Screening the deletion mutants of EcN to determine their effect on lambda phage titer reduction. 100
Figure 4.4. 8: Influence of 0.2 % maltose on *lamB* induction and subsequent lambda phage titer reduction in EcN. 102
Figure 4.4. 9: Lambda phage titer reduction by other *E. coli* strains. 104
Figure 4.4. 10: EcN's influence on lambda phage infection of K-12 strains. 104
Figure 4.4. 11: Influence of commensal strains on lambda phage infection of MG1655 106
Figure 4.5. 1:T4 phage sensitivity test for *E. coli* strains MG1655..... 107
Figure 4.5. 2: Confocal micrograph of *E. coli* incubated with T4 phages..... 108
Figure 4.5. 3: TEM micrographs showing the T4 phage attachment to EcN 109

Figure 4.5. 4: Localization of T4 phage DNA with *E. coli* after coincubation 110
Figure 4.5. 5: Role of K5 capsule in T4 phage resistance of EcN..... 111
Figure 4.5. 6: T4 phage titer reduction kinetics (A) and EcN's growth kinetics (B) during EcN and T4 phage coincubation.. 112
Figure 4.5. 7: Kinetics of T4 phage titer reduction (A) and EcN's growth (B) for 120 h of coincubation 114
Figure 4.5. 8: T4 phage titer reduction by EcN pre-incubated with T4 phages for 96 h..... 115
Figure 4.5. 9: Localization of T4 phage DNA with EcN cells/supernatant after coincubation..... 116
Figure 4.5. 10: Doughnut graphs representing the functional grouping of the genes that were downregulated in EcN when incubated with T4 phages after 2 h. 118
Figure 4.5. 11: Phage titer reduction by EcN and cell-free supernatant..... 120
Figure 4.5. 12: Effects of biochemical processing of EcN with SMP and PK on T4 inactivation..... 122
Figure 4.5. 13: T4 phage inactivation by EcN samples treated with PMB. 123
Figure 4.5. 14: T4 phage inactivation by isolated LPS. 125
Figure 4.5. 15: T4 phage adsorption to EcN in the presence of 0.6 M GlcNAc 127
Figure 4.5. 16: Influence of *E. coli* strains and their supernatants on T4 phage titer..... 128
Figure 4.5. 17: Influence on T4 phage infection of K-12 strains by *E. coli* strains..... 129
Figure 5. 1: Graphical representation depicting the up/downregulation of various fitness factors of EcN. 131
Figure 5. 2: Structural comparison of LPS from EcN and *E. coli* K-12 strain. 145
Figure 5. 3: The O antigen structures of different *E. coli* strains used in this study. 146

11. List of tables

Table 2. 1: List of laboratory equipment used in this study 30

Table 2. 2: Chemicals used in this study 32

Table 2. 3: DNA and protein ladders used in this study 34

Table 2. 4: List of *E. coli* strains used in this study 35

Table 2. 5: List of the phages used in this study. 36

Table 2. 6: Oligonucleotides used in this study 36

Table 2. 7: Different media composition used in this study 38

Table 2. 8: Kits used in this study 39

Table 2. 9: Column preparation for CsCl density centrifugation 39

Table 3. 1: Description of processed *E. coli* samples 47

Table 3. 2:Taq polymerase-based PCR Master Mix (2x) reaction set up 50

Table 3. 3: Phusion High-Fidelity DNA polymerase -based PCR reaction set up 50

Table 3. 4: PCR conditions for localization of T4 phage DNA by T4 specific PCR 51

Table 3. 5: cDNA synthesis master mix I for step 1 of two-step RT PCR 56

Table 3. 6: cDNA synthesis master mix II for step 1 of two-step RT PCR 56

Table 3. 7: PCR master mix for step 2 of two-step RT PCR 56

Table 4. 1: Regulation of genes related to flagella and LPS production in EcN 73

Table 4. 2: Results of lambda PPA on the recombinant MG1655 strains. 98

Table 4. 3: Testing the T4 phage sensitivity of EcN that has been coincubated with T4 phages 115

Tabel 5. 1: Presence of EcN's prophage 3 genes in CFT073, the commensal strains SE11 and SE15 and the K-12 strain MG1655. 138